Semiconductor-based Photocatalytic Hydrogen Generation

Xiaobo Chen,*,† Shaohua Shen,†,‡ Liejin Guo,‡ and Samuel S. Mao†

Lawrence Berkeley National Laboratory, Berkeley, California 94720, United States, and State Key Laboratory of Multiphase Flow in Power Engineering, Xi'an Jiaotong University, Xi'an, Shaanxi 710049, China

Received May 29, 2010

Contents

* Corresponding author: Xiaobo Chen. E-mail: chenxiaobolbl@gmail.com (Xiaobo Chen); shshen_xjtu@yahoo.com.cn (Shaohua Shen); lj-guo@mail.xjtu.edu.cn (Liejin Guo); SSMao@lbl.gov (Samuel S. Mao).
† Lawrence Berkeley National Laboratory.
‡ Xi'an Jiaotong University.

1. Introduction

Because of its high energy capacity and environmental friendliness, hydrogen has been identified as a potential energy carrier in many low greenhouse gas (GHG) energy scenarios.[1,2] In a proposed hydrogen energy system,[3] hydrogen-containing compounds such as fossil fuels, biomass, or even water are potential sources of hydrogen.[4−11] When hydrogen is derived from hydrocarbons such as fossil fuels or biomass, CO_2 capture and sequestration are requirements in a low GHG scenario.[12−14] On the other hand, hydrogen produced from water does not present the challenge of unwanted emissions at the point of conversion, but it does require that energy be supplied from an external resource.[15] If this energy can be obtained from a renewable energy source such as solar energy, hydrogen can then be considered a green energy alternative capable of powering everything from laptops to submarines. Figure 1 shows a diagram of photocatalytic hydrogen generation in the hydrogen energy system. Such an approach to energy production is one that exhibits due concern for environmental issues and that is becoming increasingly relevant in our world.[16,17] However, the technology to produce hydrogen in a cost-effective, low-GHG manner has not yet been developed.

Since the discovery of hydrogen evolution through the photoelectrochemical splitting of water on n-type TiO_2

10.1021/cr1001645
Published on Web 11/10/2010

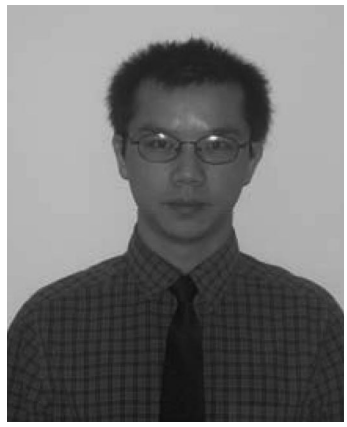

Dr. Xiaobo Chen is at Lawrence Berkeley National Laboratory. He obtained his Ph.D. Degree in Chemistry from Case Western Reserve University. His research interests include materials and devices development, renewable energy science and technology, environmental pollution, and health.

Dr. Shaohua Shen is an assistant professor at Xi'an Jiaotong University, China. He obtained his Ph.D. Degree in Thermal Engineering from Xi'an Jiaotong University in 2010. During 2008−2009, he worked as a guest researcher at Lawrence Berkeley National Laboratory, U.S.A. His research interests include photocatalysis, photoelectrochemistry, and the related materials and devices development.

Dr. Liejin Guo is a professor and the director of the State Key Laboratory of Multiphase Flow in Power Engineering in Xi'an Jiaotong University, China. He obtained his Ph.D. Degree in Engineering Thermophysics from Xi'an Jiaotong University in 1989. His research interest includes multiphase flow, heat transfer, and renewable energy technologies.

electrodes,[18] the technology of semiconductor-based photocatalytic water splitting to produce hydrogen using solar energy has been considered as one of the most important approaches to solving the world energy crisis.[19] Hence, the

Dr. Samuel S. Mao is a career staff scientist at Lawrence Berkeley National Laboratory and an adjunct faculty at The University of California at Berkeley. He obtained his Ph.D. degree in Engineering from The University of California at Berkeley in 2000. He is leading a multidisciplinary research team developing solar-active materials and devices and investigating fundamental energy conversion processes.

development of the necessary semiconductor photocatalysts has undergone considerable research. Over the past 40 years, many photocatalysts reportedly exhibited high photocatalytic activities for splitting water into a stoichiometric mixture of H_2 and O_2 (2:1 by molar ratio) in the ultraviolet (UV) light region. These include La doped $NaTaO_3$,[20] $Sr_2M_2O_7$ (M = Nb, Ta),[21] $La_2Ti_2O_7$,[22] $K_2La_2Ti_3O_{10}$,[23] and β-Ge_3N_4,[24] among others. Of particular note is the NiO/$NaTaO_3$:La photocatalyst, which shows the highest activity with a quantum yield amounting to 56% at 270 nm.[20] However, these oxide photocatalysts are only active under UV irradiation. With respect to the solar spectrum, only a small fraction (ca. 4%) of the incoming solar energy lies in the ultraviolet region, whereas the visible light in the solar spectrum is far more abundant (ca. 46%). It is essential, therefore, as an alternative to UV-active photocatalysts to develop visible-light-driven photocatalysts that are stable and highly efficient for the practical, large-scale production of hydrogen using solar energy. Over the recent years, continuing breakthroughs have been made in the development of novel visible-light-driven photocatalysts, leading to the enhancement of photocatalytic activity for water splitting and inspiring great enthusiasm. A large number of semiconductor materials have been developed as photocatalysts for water splitting to hydrogen under visible-light irradiation.

A significant process has been achieved on semiconductor-based photocatalytic hydrogen generation through water

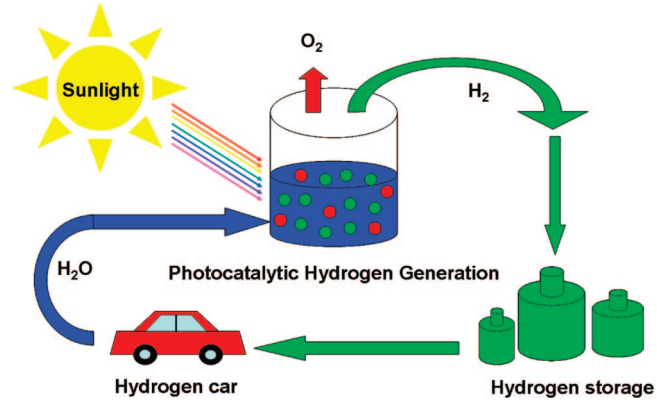

Figure 1. Schematic diagram of photocatalytic hydrogen generation in the hydrogen energy system.

splitting over the past several decades,[25−31] and many excellent reviews have been published.[32−62] In this review, we aim to put together the research effort having been made so far, with a view of providing a good reference and inspiring new ideas for tackling this important challenge. Starting with a brief introduction to semiconductor-based photocatalysts for hydrogen generation from water splitting, we overview the development of high-efficiency, visible-light-driven photocatalysts. A number of synthetic and modification techniques for adjusting the band structure to harvest visible light and improve the charge separation in photocatalysis are discussed. Photocatalytic systems for water splitting are also reviewed and classified into two main kinds: sacrificial reagent-containing water-splitting systems and overall water-splitting systems.

2. Basic Principles of Photocatalytic Hydrogen Generation

2.1. Fundamental Mechanism of Photocatalytic Hydrogen Generation

In Fujishima and Honda's pioneering work, the electrochemical cell they constructed for the decomposition of water into hydrogen and oxygen is shown in Figure 2.[18] When the surface of the TiO_2 electrode was irradiated by UV light, as a result of a water oxidation reaction, oxygen evolution occurred at the TiO_2 electrode. Concomitant reduction led to hydrogen evolution at the platinum black electrode. This concept, which emerged from the use of photoelectrochemical cells with semiconductor electrodes, was later applied by Bard to the design of a photocatalytic system using semiconductor particles or powders as photocatalysts.[63−65]

A photocatalyst absorbs UV and/or visible (Vis) light irradiation from sunlight or an illuminated light source. The electrons in the valence band of the photocatalyst are excited to the conduction band, while the holes are left in the valence band. This, therefore, creates the negative-electron (e^-) and positive-hole (h^+) pairs. This stage is referred to the semiconductor's "photo-excited" state, and the energy difference between the valence band and the conduction band is known as the "band gap". This must correspond to the wavelength of the light for it to be effectively absorbed by the photocatalyst. After photoexcitation, the excited electrons and holes separate and migrate to the surface of photocatalyst. Here, in the photocatalytic water-splitting reaction, they act

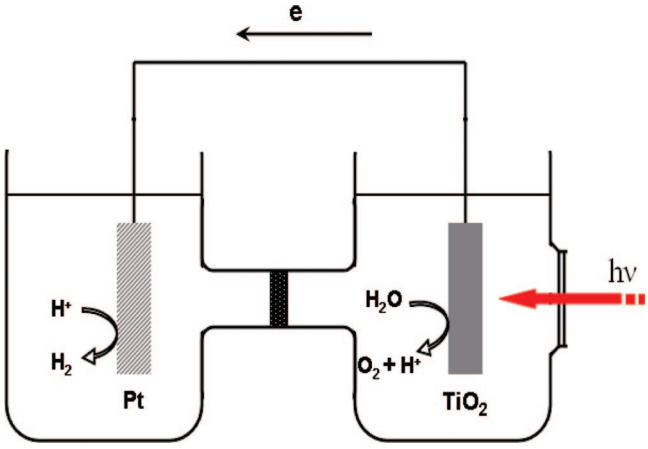

Figure 2. Schematic representation of a photoelectrochemical cell (PEC). Reprinted with permission from ref 18. Copyright 1972 Nature Publishing Group.

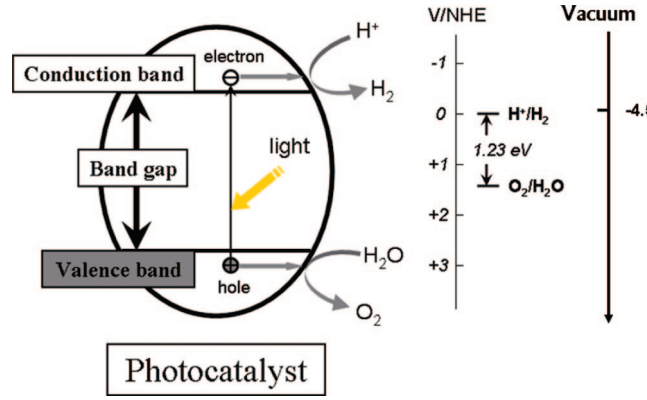

Figure 3. Fundamental principle of semiconductor-based photocatalytic water splitting for hydrogen generation.

as reducing agent and oxidizing agent to produce H_2 and O_2, respectively. A schematic representation of the principle of the photocatalytic system for water is depicted in Figure 3.

Water splitting into H_2 and O_2 is an uphill reaction. It needs the standard Gibbs free energy change ΔG^0 of 237 kJ/mol or 1.23 eV, as shown in eq 1.

$$H_2O \rightarrow \frac{1}{2}O_2 + H_2; \quad \Delta G = +237 \text{ kJ/mol} \qquad (1)$$

Therefore, the band gap energy (E_g) of the photocatalyst should be >1.23 eV (<1000 nm) to achieve water splitting. However, to use visible light, it should be <3.0 eV (>400 nm).

To facilitate both the reduction and oxidation of H_2O by photoexcited electrons and holes, the match of the band gap and the potentials of the conduction and valence bands are important. Both the reduction and oxidation potentials of water should lie within the band gap of the photocatalyst. The bottom level of the conduction band has to be more negative than the reduction potential of H^+/H_2 (0 V vs normal hydrogen electrode (NHE)), whereas the top level of the valence band has to be more positive than the oxidation potential of O_2/H_2O (1.23 V). Parts A and B of Figure 4 show the conduction band edge and valence band edge of some oxide- and sulfide-based semiconductor materials.[66] We can see that there are many semiconductor systems whose electronic structures match well with the redox potential of water into hydrogen and oxygen molecules. The band structure requirement is a thermodynamic requirement for water splitting. Other factors, such as overpotentials, charge separation, mobility, and lifetime of photogenerated electrons and holes, affect the photocatalytic generation of hydrogen from water splitting as well. For example, the band edges of the semiconductor photocatalyst usually vary with the change of pH, as shown in Figure 4C.[66] The phase stability of the semiconductor photocatalyst changes in different pH environments as well.

2.2. Main Processes of Photocatalytic Hydrogen Generation

The processes in the photocatalytic generation of hydrogen are illustrated in Figure 5. They include light absorption of the semiconductor photocatalyst, generation of excited charges (electrons and holes), recombination of the excited charges, separation of excited charges, migration of the charges, trap of excited charges, and transfer of excited

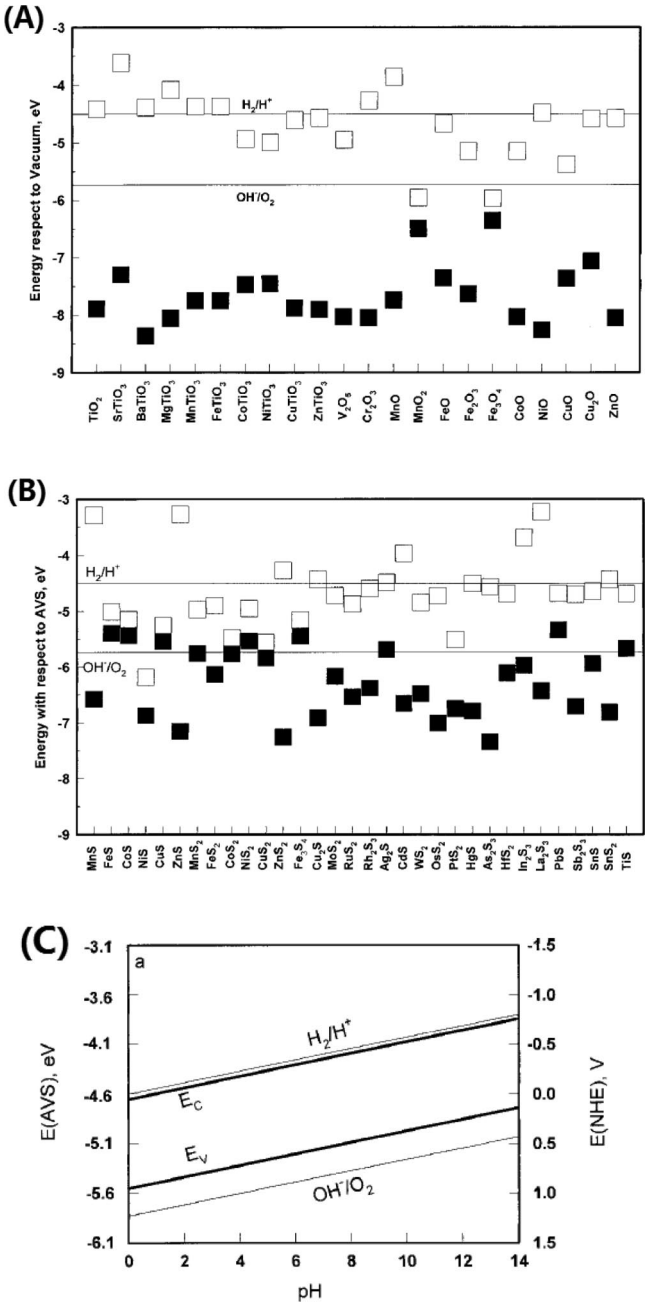

Figure 4. Calculated energy positions of conduction band edges and valence band edges at pH 0 for selected metal oxide (A) and metal sulfide (B) semiconductors. The bottom of open squares represent conduction band edges, and the top of solid squares represent valence band edges. The solid lines indicate water stability limits. (C) pH dependence of the conduction band edge and valence band edge in an aqueous electrolyte solution. Reprinted with permission from ref 66. Copyright 2000 The Mineralogical Society of America.

charges to water or other molecules. All of these processes affect the final generation of hydrogen from the semiconductor photocatalyst system.

The total amount of hydrogen generated is mainly determined by the amount of excited electrons in the water/photocatalyst interface in reducing water. Apparently, any other processes that consume excited electrons should be avoided in order to maximize the efficiency of the hydrogen generation of the photocatalyst system. Any process that generates excited electrons should be considered to act in a possible way to improve the efficiency. Thus, if we look at

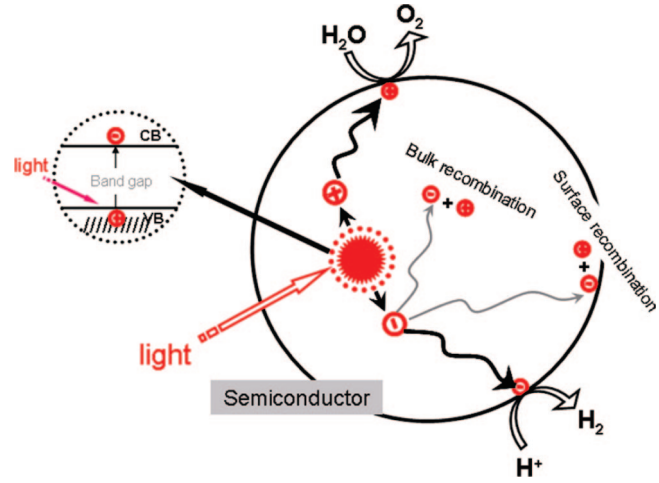

Figure 5. Processes in photocatalytic water splitting. Reprinted with permission from ref 67. Copyright 1995 American Chemical Society.

the charge-generation process, the semiconductor photocatalyst should first have a low band gap to absorb as much light as possible, and reflection or scattering of light by the photocatalyst should be minimized. Second, using the absorbed photons, the semiconductor photocatalyst should have a high efficieny in generating excited charges, instead of generating phonons or heat.

After excited charges are created, charge recombination and separation/migration processes are two important competitive processes inside the semiconductor photocatalyst that largely affect the efficiency of the photocatalytic reaction for water splitting.[67] Charge recombination reduces the excited charges by emitting light or generating phonons. It includes both surface and bulk recombination and is classified as a deactivation process, and it is ineffective for water splitting. The separation of excited electrons and holes sometimes may need to overcome an energy barrier, which is the sometimes binding energy of the excited electron−hole pairs, excitons. Charge separation and migration, on the other hand, is an activation process. This is as a result of the charges being on the surface of the photocatalyst ready for the desired chemical reaction. It is beneficial for hydrogen generation through water splitting. Efficient charge separation and fast charge transport, avoiding any bulk/surface charge recombination avoided, are fundamentally important for photocatalytic hydrogen generation through water splitting. Any approach beneficial to the charge separation and transport should be taken into account such as design of internal-built electric field and use of high photoconductive semiconductor materials.

The reaction of photogenerated H_2 and O_2 to form H_2O on the photocatalyst surface is normally called "surface back-reaction (SBR)". It will inevitably have a negative effect on any enhancement of the photocatalytic activity, because it reduces the amount of H_2 emitted from the photocatalyst. There are two main approaches to suppress SBR: one involves the addition of sacrificial reagents into the photocatalytic reaction environment and the second creates a separation of the photoactive sites on the surface of the photocatalysts. In general, the electron donor and acceptor sacrificial reagents that are added work as an external driving force for the surface chemical reaction and depress the H_2O formation from H_2 and O_2. The separation of the photoactive sites necessary for hydrogen and oxygen evolution, and

which is always accompanied by the surface separation of the photogenerated electrons and holes, has been shown to be greatly affected by the surface properties of the photocatalysts. As well as the surface reaction sites themselves, the surface states and morphology also play an important role.

Taking into consideration the basic mechanism and processes of photocatalytic water splitting, there are two keys to developing a suitable high-efficiency semiconductor for the visible-light-driven photocatalytic splitting of water into H_2 and/or O_2: (1) A photocatalyst should have a sufficiently narrow band gap (1.23 eV < E_g < 3.0 eV) to both harvest visible light and possess the correct band structure. (2) Photoinduced charges in the photocatalyst should be separated efficiently in order to avoid bulk/surface electron/hole recombination. In addition, they must migrate to the photocatalyst surface for hydrogen and/or oxygen evolution at the respective photocatalytic active sites.[58] In summary, it is generally accepted that the correct band structure for efficient visible-light harvesting and effective separation between the photoexcited electrons and the holes is essential to improve the photocatalytic properties of the semiconductor. In addition, with the development of efficient visible-light-driven photocatalysts, it is important that economical, highly efficient photocatalytic systems for light-to-hydrogen energy conversion, in which aqueous solutions containing sacrificial reagents can be used to depress the backward reaction of hydrogen and oxygen to water on the surface of photocatalysts, can be constructed.

2.3. Evaluation of Photocatalytic Water Splitting

There are two apparent indicators that should be paid attention in evaluating the hydrogen generation through photocatalytic water splitting. One is photocatalytic activity, and the other one is photocatalytic stability.

2.3.1. Photocatalytic Activity

The efficiency of photocatalytic hydrogen generation from water splitting can be measured directly on the amount of hydrogen gas evoluted or indirectly on the electrons transferred from semiconductor to water within a certain time period under light irradiation. Different photocatalytic setup configurations, such as inner irradiation type and top irradiation type, and light sources, such as Xe lamp and Hg lamp, are commonly used by different research groups and scientists, which may give different rates of gas evolution when exactly the same photocatalyst is used. This makes it difficult to make direct comparison across the results from different research groups and photocatalytic hydrogen generation systems. Nevertheless, it seems helpful to get approximate correlations between various results if we normalize the rates of gas evolution to the amount of photocatalyst employed within a unit of time. Here, we use the rate of gas (O_2 and H_2) evolution with units such as $\mu mol \cdot h^{-1}$ and $\mu mol \cdot h^{-1} \cdot g^{-1}_{catalyst}$ to make the mensurable comparison between different photocatalysts under similar experimental conditions.

The (apparent) quantum yield, as an extension from the overall quantum yield in a homogeneous photochemical system, becomes important and acceptable to evaluate the photocatalytic activity for water splitting. The overall quantum yield and apparent quantum yield are defined by eqs 2 and 3, respectively.[68]

$$\text{Overall quantum yield (\%)} = \frac{\text{Number of reacted electrons}}{\text{Number of absorbed photons}} \times 100\% \quad (2)$$

$$\text{(Apparent) Quantum yield (QY, \%)} = \frac{\text{Number of reacted electrons}}{\text{Number of incident photons}} \times 100\% = \frac{2 \times \text{Number of evolved } H_2 \text{ molecules}}{\text{Number of incident photons}} \times \frac{1}{100\% \text{ (for } H_2 \text{ evolution)}} = \frac{4 \times \text{Number of evolved } O_2 \text{ molecules}}{\text{Number of incident photons}} \times \frac{1}{100\% \text{ (for } O_2 \text{ evolution)}} \quad (3)$$

The apparent quantum yield is estimated to be smaller than the total quantum yield because the number of absorbed photons is usually smaller than that of incident light. In addition to the quantum yield, the solar energy conversion efficiency that is usually used for evaluation of solar cells is also sometimes reported in the literature. It is defined as

$$\text{Solar energy conversion (\%)} = \frac{\text{Output energy of hydrogen evolved}}{\text{Energy of incident solar light}} \times 100 \quad (4)$$

2.3.2. Photocatalytic Stability

As a good photocatalyst, it should have a good stability for H_2 and/or O_2 production, besides a high photocatalytic activity or quantum yield. To test the photocatalytic stability, a long-time experiment or a repeated experiment is always necessary. Photocorrosion is considered to be the main reason causing the poor stability of photocatalysts, especially the metal sulfide photocatalysts. CdS has frequently been reported to be unstable for photocatalytic H_2 evolution. S^{2-} in CdS rather than water is self-oxidized by photoinduced holes in the valence band of CdS. The photocorrosion reaction occurs as in eq 5,[55]

$$CdS + 2h^+ \rightarrow Cd^{2+} + S \quad (5)$$

3. UV-Active Photocatalysts for Water Splitting

A wide range of semiconducting materials have been developed as photocatalysts for use under UV irradiation. These are shown in Table 1. On the basis of their electronic configuration properties, these UV-active photocatalysts can be typically classified into four groups: (1) d^0 metal (Ti^{4+}, Zr^{4+}, Nb^{5+}, Ta^{5+}, W^{6+}, and Mo^{6+}) oxide photocatalysts, (2) d^{10} metal (In^{3+}, Ga^{3+}, Ge^{4+}, Sn^{4+}, and Sb^{5+}) oxide photocatalysts, (3) f^0 metal (Ce^{4+}) oxide photocatalysts, and (4) a small group of nonoxide photocatalysts.

3.1. d^0 Metal Oxide Photocatalyts

3.1.1. Ti-, Zr-Based Oxides

TiO_2 is the first reported photocatalyst for water splitting under UV irradiation.[69] TiO_2 can produce hydrogen and/or oxygen from water vapor, pure water, and aqueous solutions containing electron donor.[70−77] It was found that, under UV irradiation, colloidal TiO_2 combined with ultrafine Pt and RuO_2 particles generated H_2 with a high quantum yield of $30 \pm 10\%$ and O_2 in stoichiometric proportions from water.[70] The reaction solution had a pH of 1.5, which was adjusted

Table 1. UV-Light-Active Photocatalysts for Water Splitting to Hydrogen and/or Oxygen

photocatalyst	synthetic method	mass (g)	light source	incident light	aqueous reaction solution	activity (μmol·h^{-1}·g^{-1}) co-catal./H_2	activity (μmol·h^{-1}·g^{-1}) co-catal./O_2	QY (%)	reference
TiO_2 (anatase)	MCB TiO_2	0.3	500-W Hg[b]	250−400 nm	water vapor	Rh/1497		29 (340 nm)	74
TiO_2 (anatase)	MCB TiO_2	1	450-W Hg	quartz filter	NaOH	NiO_x/32	NiO_x/14		75
TiO_2 (anatase, 78%)	P25 TiO_2	0.3	400-W Hg	quartz filter	Na_2CO_3	Pt/1893	Pt/957		71
TiO_2 (anatase, 78%)	P25 TiO_2	0.3	250-W Hg	Pyrex filter	pure water	Pt/353	Pt/177	1.4 (300−400 nm)	76
TiO_2	hydrolysis, calcination	0.2	300-W Xe[c]	Pyrex filter	CH_3OH	Pt/∼3300			72
rutile/anatase TiO_2	impregnation, calcination	0.2	300-W Xe	Pyrex filter	CH_3OH	Pt/∼6700			73
colloid TiO_2	hydrolysis reaction	0.025	450-W Hg	Pyrex filter	HCl	Pt−RuO_2/4000		30 (310 nm)	70
mesoporous TiO_2	sol gel method	0.2	300-W Hg	Pyrex filter	CH_3OH	Pt/6925			889, 934, 941
TiO_2 nanowires	electrospinning and sol−gel	1	450-W Hg	Pyrex filter	CH_3OH	54			964, 975
TiO_2 nanotubes	hydrothermal method	1	450-W Hg	Pyrex filter	CH_3OH	285			966
TiO_2 nanosheets	hydrothermal method	1	450-W Hg	Pyrex filter	CH_3OH	117.6			1003
Ni-intercalated $Na_2Ti_2O_5$ nanotubes	hydrothermal method	0.1	450-W Hg		CH_3OH	Pt/∼850			99
TiO_2:Ga	solvothermal method	1.5	UV-lamps	Pyrex filter	Pure water	20.86			79
TiO_2:Ni	hydrothermal method	0.3	300-W Hg	Pyrex filter	CH_3OH	Pt/∼566.7			80
TiO_2:Sc	hydrolysis, calcination	0.1	300-W Hg	Pyrex filter	CH_3OH	Pt/∼7500			82
TiO_2:Y	hydrolysis, calcination	0.1	300-W Hg	Pyrex filter	CH_3OH	Pt/∼7800			82
TiO_2:La	hydrolysis, calcination	0.1	300-W Hg	Pyrex filter	CH_3OH	Pt/∼7680			82
TiO_2:Ce	hydrolysis, calcination	0.1	300-W Hg	Pyrex filter	CH_3OH	Pt/∼4800			82
TiO_2:Pr	hydrolysis, calcination	0.1	300-W Hg	Pyrex filter	CH_3OH	Pt/∼6600			82
TiO_2:Nd	hydrolysis, calcination	0.1	300-W Hg	Pyrex filter	CH_3OH	Pt/∼9300			82
TiO_2:Sm	hydrolysis, calcination	0.1	300-W Hg	Pyrex filter	CH_3OH	Pt/∼10200			82
TiO_2:Gd	hydrolysis, calcination	0.1	300-W Hg	Pyrex filter	CH_3OH	Pt/∼10800			82
TiO_2:Eu	hydrolysis, calcination	0.1	300-W Hg	Pyrex filter	CH_3OH	Pt/∼13200			82
TiO_2:Tb	hydrolysis, calcination	0.1	300-W Hg	Pyrex filter	CH_3OH	Pt/∼4800			82
TiO_2:Dy	hydrolysis, calcination	0.1	300-W Hg	Pyrex filter	CH_3OH	Pt/∼8400			82
TiO_2:Ho	hydrolysis, calcination	0.1	300-W Hg	Pyrex filter	CH_3OH	Pt/∼10200			82
TiO_2:Er	hydrolysis, calcination	0.1	300-W Hg	Pyrex filter	CH_3OH	Pt/∼8400			82
TiO_2:Tm	hydrolysis, calcination	0.1	300-W Hg	Pyrex filter	CH_3OH	Pt/∼8700			82
TiO_2:Yb	hydrolysis, calcination	0.1	300-W Hg	Pyrex filter	CH_3OH	Pt/∼8400			82
TiO_2:Lu	hydrolysis, calcination	0.1	300-W Hg	Pyrex filter	CH_3OH	Pt/∼7200			82
TiO_2:Sn/Eu	polyol method	0.2	288-W F[d]	quartz filter	CH_3OH	Pd/∼92		40.4	81
TiO_2/Cu_xO	impregnation method	1	400-W Hg	quartz filter	CH_3OH	18 500			85−87
TiO_2/SnO_2	polyol method	0.05	288-W F	quartz filter	CH_3OH	Pd/∼83			83
Ag_xO/TiO_2	impregnation method	0.05	solar light	quartz filter	CH_3OH	67 000			88−90
$SrTiO_3/TiO_2$	solid-state reaction	0.1	150-W Hg		HCOOH	560			91
B/Ti oxide	sol−gel method	0.3	400-W Hg	quartz filter	pure water	Pt/73	Pt/36.7		92, 93
meso-TiO_2/ZrO_2	evaporation induced self-assembly process	0.06	500-W Hg	Pyrex filter	CH_3OH	Pt/∼24			84
$CaTiO_3$	Sakai Chemical Industry	0.5	500-W Hg	silica glass	NaOH	Pt/76	Pt/18		120
$SrTiO_3$	Alfa-Ventron	0.5	400-W Hg	Pyrex filter	NaOH	NiO_x/∼70	NiO_x/∼32		109−114
$SrTiO_3$:La	solid-state reaction	0.1	400-W Hg	quartz filter	Na_2CO_3	CoO_x/∼2800	CoO_x/∼1300		116
$SrTiO_3$:Ta	solid-state reaction	0.3	450-W Hg	Pyrex filter	pure water	$Rh_xCr_{2-x}O_3$/∼14 160	$Rh_xCr_{2-x}O_3$/∼7000		117
$SrTiO_3$:Na	solid-state reaction	0.3	450-W Hg	Pyrex filter	pure water	$Rh_xCr_{2-x}O_3$/∼22 220	$Rh_xCr_{2-x}O_3$/∼11 110		117
$Sr_3Ti_2O_7$	polymerized complex method	1	400-W Hg	quartz filter	pure water	NiO_x/144	NiO_x/72		118
$Sr_4Ti_3O_{10}$	polymerized complex method	1	400-W Hg	quartz filter	pure water	NiO_x/170		4.5 (360 nm)	119
$K_2La_2Ti_3O_{10}$	polymerized complex method	1	450-W Hg	quartz filter	KOH	NiO_x/2186	NiO_x/1131		23, 135, 139
$Rb_2La_2Ti_3O_{10}$	solid-state reaction	1	450-W Hg	quartz filter	RbOH	NiO_x/869	NiO_x/430	5 (330 nm)	135
$Rb_{1.5}La_2Ti_{2.5}Nb_{0.5}O_{10}$	solid-state reaction	1	450-W Hg	quartz filter	RbOH	NiO_x/725	NiO_x/358		135
$RbLa_2Ti_2NbO_{10}$	solid-state reaction	1	450-W Hg	quartz filter	RbOH	NiO_x/79	NiO_x/30		135
$Cs_2La_2Ti_3O_{10}$	solid-state reaction	1	450-W Hg	quartz filter	pure water	NiO_x/700	NiO_x/340		135
$Cs_{1.5}La_2Ti_{2.5}Nb_{0.5}O_{10}$	solid-state reaction	1	450-W Hg	quartz filter	pure water	NiO_x/540	NiO_x/265		135
$CsLa_2Ti_2NbO_{10}$	solid-state reaction	1	450-W Hg	quartz filter	pure water	NiO_x/115	NiO_x/50		135
$LaTiO_3$	solid-state reaction	1	450-W Hg	quartz filter	pure water	NiO_x/137			125
La_2TiO_5	solid-state reaction	1	450-W Hg	quartz filter	pure water	NiO_x/442			125
$La_2Ti_3O_9$	solid-state reaction	1	450-W Hg	quartz filter	pure water	NiO_x/386			125
$La_4Ti_3O_{12}$	polymerized complex method	0.5	400-W Hg	quartz filter	pure water	NiO/714	NiO/358		133
$La_2Ti_2O_7$	polymerized complex method	1	450-W Hg	quartz filter	pure water	NiO_x/960	NiO_x/478	27	22, 122−127, 131, 134
$La_2Ti_2O_7$:Sr	solid-state reaction	1	450-W Hg	quartz filter	pure water	NiO_x/1510			125

Table 1. Continued

photocatalyst	synthetic method	mass (g)	light source	incident light	aqueous reaction solution	activity (μmol·h^{-1}·g^{-1}) co-catal./H_2	activity (μmol·h^{-1}·g^{-1}) co-catal./O_2	QY (%)	reference
$La_2Ti_2O_7$:Ca	solid-state reaction	1	450-W Hg	quartz filter	pure water	NiO_x/850			125
$La_2Ti_2O_7$:Ba	solid-state reaction	1	450-W Hg	quartz filter	NaOH	NiO_x/~5000		50	125
$Pr_2Ti_2O_7$	solid-state reaction	1	450-W Hg	quartz filter	pure water	NiO_x/150			127
$PrLaTi_2O_7$	solid-state reaction	1	450-W Hg	quartz filter	pure water	NiO_x/220			127
$Nd_2Ti_2O_7$	solid-state reaction	1	450-W Hg	quartz filter	pure water	NiO_x/99			127
$NdLaTi_2O_7$	solid-state reaction	1	450-W Hg	quartz filter	pure water	NiO_x/131			127
$KaLaZr_{0.3}Ti_{0.7}O_4$	two-step ion-exchange reaction	0.3	450-W Hg	quartz filter	pure water	NiO_x/766.7	NiO_x/386.7	12.5	143
$La_4CaTi_5O_{17}$	solid-state reaction	1	450-W Hg	quartz filter	pure water	NiO_x/499		20 (<320 nm)	134
$CaLa_4Ti_4O_{15}$	polymerized complex method	0.5	400-W Hg	quartz filter	pure water	NiO_x/1186	NiO_x/552		133
$SrLa_4Ti_4O_{15}$	polymerized complex method	0.5	400-W Hg	quartz filter	pure water	NiO_x/2342	NiO_x/1092		133
$BaLa_4Ti_4O_{15}$	polymerized complex method	0.5	400-W Hg	quartz filter	pure water	NiO_x/4600	NiO_x/2308	15 (270 nm)	133
$Ba_3LaNb_3O_{12}$	polymerized complex method	0.5	400-W Hg	quartz filter	pure water	NiO_x/2370	NiO_x/1176		133
$Sr_5Nb_4O_{15}$	polymerized complex method	0.5	400-W Hg	quartz filter	pure water	NiO_x/4400	NiO_x/2200		133
$KTiNbO_5$	polymerized complex method	0.5	450-W Hg	quartz filter	pure water	NiO_x/~60	NiO_x/~20		142
$Na_2Ti_6O_{13}$	solid-state reaction	0.25	400-W Xe	quartz filter	pure water	RuO_2/29.2	RuO_2/14		101−104
$BaTi_4O_9$	solid-state reaction	0.2	400-W Xe	quartz filter	pure water	RuO_2/167	RuO_2/78		104−107, 913, 914
$Gd_2Ti_2O_7$	polymerized complex method	0.5	400-W Xe	quartz filter	pure water	NiO_x/800	NiO_x/396		131
$Y_2Ti_2O_7$	polymerized complex method	0.5	400-W Xe	quartz filter	pure water	NiO_x/~2000	NiO_x/~1000	6 (313 nm)	128, 130, 131
$Bi_4Ti_3O_{12}$	solid-state reaction	1	450-W Hg	Pyrex filter	$CH_3OH/AgNO_3$	Pt/0.6	3		145
$BaBi_4Ti_4O_{15}$	solid-state reaction	1	450-W Hg	Pyrex filter	$CH_3OH/AgNO_3$	Pt/8.2	3.7		145
Bi_3TiNbO_9	solid-state reaction	1	450-W Hg	Pyrex filter	$CH_3OH/AgNO_3$	Pt/33	31		145
$Na_2Ti_3O_7$	solid-state reaction	0.5	500-W Xe		CH_3OH	Pt/38			96
$K_2Ti_2O_5$	solid-state reaction	0.5	500-W Xe		CH_3OH	Pt/69.4			96
$H^+-K_2Ti_2O_5$	solid-state reaction, H^+-exchange	0.5	500-W Xe		CH_3OH	Pt/220		10 (330−360 nm)	96
$K_2Ti_4O_9$	solid-state reaction	0.5	500-W Xe		CH_3OH	Pt/9.6			96
$K_2Ti_6O_{13}$	solid-state reaction	0.5	500-W Xe		CH_3OH	Pt/121.4			96
$Cs_2Ti_2O_5$	solid-state reaction	1	400-W Xe	quartz filter	$CH_3OH/AgNO_3$	500	155		100
$H^+-Cs_2Ti_2O_5$	solid-state reaction, H^+-exchange	1	400-W Xe	quartz filter	CH_3OH	Pt/2512			100
$Cs_2Ti_5O_{11}$	solid-state reaction	1	400-W Xe	quartz filter	CH_3OH	90			100
$Cs_2Ti_6O_{13}$	solid-state reaction	1	400-W Xe	quartz filter	CH_3OH	38			100
$H^+-CsTiNbO_5$	solid-state reaction, H^+-exchange	1	450-W Hg	Pyrex filter	CH_3OH	Pt/320			144
$H^+-CsTi_2NbO_7$	solid-state reaction, H^+-exchange	1	450-W Hg	Pyrex filter	CH_3OH	Pt/87			144
$KBi_3PbTi_5O_{16}$	polymerized complex method	1	450-W Hg	quartz filter	Ce^{3+}/Ce^{4+}	35.21	1.32		146
$SiO_2-K_2Ti_4O_9$	solid-state reaction, stepwise ion-exchange	0.2	450-W Hg	Pyrex filter	CH_3OH	Pt/~2600			98
$SiO_2-K_2Ti_{2.7}Mn_{0.3}O_9$	solid-state reaction, stepwise ion-exchange	0.2	450-W Hg	Pyrex filter	CH_3OH	~1600			98
$Ti_{0.5}Zr_{0.5}PO_4$	sol−gel method	0.5	300-W Xe	>290 nm	Na_2CO_3	Pt/17.7			155
$Zr_2(PO_4)PVX_3$	hydrothermal method	0.025	200-W Hg−Xe	<320 nm	EDTA	Pt/267.8		4 (<320 nm)	156
$CaTi_{0.93}Zr_{0.07}O_3$	polymerized complex method	0.1	500-W Hg	quartz filter	pure water	Pt/1400		1.91 (365 nm)	121
ZrO_2	Soekawa Chemicals	1	400-W Hg	quartz filter	$NaHCO_3$	309	167		78, 147−150
Zr-MCM-41	hydrothermal method	0.1	400-W Hg	quartz filter	pure water	224			151
$BaZrO_3$	Pechini-type process	0.2	400-W Hg	quartz filter	pure water	522.5	131	3.7	152
$BaZr_{0.7}Sn_{0.3}O_3$	Pechini-type process	0.2	400-W Hg	quartz filter	pure water	690	185		153
$La_2Zr_2O_7$	solid-state reaction		500-W Xe	quartz filter	pure water	0.91[a]			154
Nb_2O_5	evaporation-induced self-assembly method	0.1	400-W Hg	quartz filter	CH_3OH	Pt/12315			158
Nb/In mixed oxide	evaporation-induced self-assembly method	0.2	400-W H[e]	quartz filter	CH_3OH	159.3			159
$K_4Nb_6O_{17}$	solid-state reaction	0.5	450-W Hg	quartz filter	pure water	NiO_x/3674	NiO_x/1700	5.3 (330 nm)	157, 160−171
$Rb_4Nb_6O_{17}$	solid-state reaction	1	400-W Hg	quartz filter	pure water	NiO_x/936	NiO_x/451	10 (330 nm)	157, 171
$K_2Rb_2Nb_6O_{17}$	solid-state reaction	1	450-W Hg	quartz filter	pure water	NiO_x/78	NiO_x/39	3.3	171
$K_4Ta_2Nb_4O_{17}$	solid-state reaction	1	400-W Hg	quartz filter	pure water	NiO_x/409	NiO_x/198		157
$NaNbO_3$	polymerized complex method	0.1	400-W Hg	quartz filter	pure water	RuO_2/650	RuO_2/160		172
$KNbO_3$	hydrothermal method	0.2	400-W Hg	quartz filter	methanol	Pt/5170			173
$Ca_2Nb_2O_7$	solid-state reaction	1	450-W Hg	quartz filter	pure water	NiO_x/101		7 (<288 nm)	134
$Sr_2Nb_2O_7$	hydrothermal method	0.2	400-W Hg	quartz filter	pure water	RuO_2/475	RuO_2/220	32 (300 nm)	21, 177, 222, 223
$SrNb_2O_6$	hydrothermal method	0.2	400-W Hg	quartz filter	pure water	RuO_2/435	RuO_2/205	19 (300 nm)	177
$BiNbO_4$	solid-state reaction	1	400-W Hg	quartz filter	pure water	8			200
$BiTa_{0.8}Nb_{0.2}O_4$	solid-state reaction	1	400-W Hg	quartz filter	pure water	41			200
$Sr_2Ta_{0.5}Nb_{1.5}O_7$	solid-state reaction	1	400-W Hg	quartz filter	pure water	NiO_x/280	NiO_x/120		223

Table 1. Continued

photocatalyst	synthetic method	mass (g)	light source	incident light	aqueous reaction solution	activity (μmol·h^{-1}·g^{-1}) co-catal./H_2	activity (μmol·h^{-1}·g^{-1}) co-catal./O_2	QY (%)	reference
$Ba_5Nb_4O_{15}$	polymerized complex method	0.5	400-W Hg	quartz filter	pure water	NiO_x/8042	NiO_x/3922	17 (270 nm)	133, 960
$ZnNb_2O_6$	solid-state reaction	1	450-W Hg		pure water	NiO_x/54	NiO_x/21		194
$NaCa_2Nb_3O_{10}$	solid-state reaction	0.3	450-W Hg	quartz filter	pure water	RuO_2/393.3	RuO_2/186.7		187
$TBA_x[H_{1-x}Ca_2Nb_3O_{10}]$ nanosheet	solid-state reaction, ion-exchange	0.1	750-W Hg	290−600 nm	pure water	Pt/784		7.48	188
$Cs_2Nb_4O_{11}$	solid-state reaction	0.5	400-W Hg	quartz filter	CsOH	NiO_x/3400	NiO_x/1600		175
La_3NbO_7	polymerized complex method	0.5	400-W Hg	quartz filter	pure water	NiO_x/70	NiO_x/34		131, 192
$La_{1/3}NbO_3$	solid-state reaction	0.5	400-W Hg	quartz filter	$CH_3OH/AgNO_3$	Pt/122.1	52.6		193
$RbNbWO_6$	solid-state reaction	0.3	1000-W Hg	quartz filter	RbOH	NiO_x/38	NiO_x/14.3		176
$CsNbWO_6$	solid-state reaction	0.3	1000-W Hg	quartz filter	CsOH	NiO_x/33.7	NiO_x/15.7		176
$BaZn_{1/3}Nb_{2/3}O_3$	solid-state reaction	0.5	400-W Hg	quartz filter	pure water	NiO_x/291.2	NiO_x/145.6		178, 179
In_2BiNbO_7	solid-state reaction	1	400-W Hg	quartz filter	pure water	54.3	26.6		196
Ga_2BiNbO_7	solid-state reaction	1	400-W Hg	quartz filter	pure water	72.6	35.7		196
Bi_2YNbO_7	solid-state reaction	1	400-W Hg	quartz filter	pure water	21			199
Bi_2CeNbO_7	solid-state reaction	1	400-W Hg	quartz filter	pure water	13			199
Bi_2GdNbO_7	solid-state reaction	1	400-W Hg	quartz filter	pure water	10			199
Bi_2SmNbO_7	solid-state reaction	1	400-W Hg	quartz filter	pure water	5			199
Bi_2NdNbO_7	solid-state reaction	1	400-W Hg	quartz filter	pure water	4			199
Bi_2PrNbO_7	solid-state reaction	1	400-W Hg	quartz filter	pure water	2.1			199
Bi_2LaNbO_7	solid-state reaction	1	400-W Hg	quartz filter	pure water	1.8			199
Bi_2AlNbO_7	solid-state reaction	1	400-W Hg	quartz filter	$CH_3OH/Ce(SO_4)_2$	Pt/710	25		197
Bi_2AlNbO_7:La	solid-state reaction	0.1	350-W Hg	quartz filter	CH_3OH	NiO_x/1414			198
Bi_2GaNbO_7	solid-state reaction	1	400-W Hg	quartz filter	$CH_3OH/Ce(SO_4)_2$	Pt/7	10		197
Bi_2InNbO_7	solid-state reaction	1	400-W Hg	quartz filter	$CH_3OH/Ce(SO_4)_2$	Pt/5	7		197
$CaBi_2Nb_2O_9$	solid-state reaction	0.2	350-W Hg	quartz filter	$CH_3OH/AgNO_3$	580	185		195
$SrBi_2Nb_2O_9$	solid-state reaction	0.2	350-W Hg	quartz filter	$CH_3OH/AgNO_3$	3660	530		195
$BaBi_2Nb_2O_9$	solid-state reaction	0.2	350-W Hg	quartz filter	$CH_3OH/AgNO_3$	1130	305		195
$H^+-KLaNb_2O_7$	solid-state reaction, H^+-exchange	1	450-W Hg	quartz filter	$CH_3OH/AgNO_3$	Pt/3800	46		38
$H^+-RbLaNb_2O_7$	solid-state reaction, H^+-exchange	1	450-W Hg	quartz filter	$CH_3OH/AgNO_3$	Pt/2600	2		38
$H^+-CsLaNb_2O_7$	solid-state reaction, H^+-exchange	1	450-W Hg	quartz filter	$CH_3OH/AgNO_3$	Pt/2200	3		38
$H^+-KCa_2Nb_3O_{10}$	solid-state reaction, H^+-exchange	1	450-W Hg	quartz filter	$CH_3OH/AgNO_3$	Pt/19 000	8		38
$H^+-RbCa_2Nb_3O_{10}$	solid-state reaction, H^+-exchange	1	450-W Hg	quartz filter	$CH_3OH/AgNO_3$	Pt/17000	16		38
$H^+-CsCa_2Nb_3O_{10}$	solid-state reaction, H^+-exchange	1	450-W Hg	quartz filter	$CH_3OH/AgNO_3$	Pt/8300	10		38
$H^+-KSr_2Nb_3O_{10}$	solid-state reaction, H^+-exchange	1	450-W Hg	quartz filter	$CH_3OH/AgNO_3$	Pt/43 000	30		38
$H^+-KCa_2NaNb_4O_{13}$	solid-state reaction, H^+-exchange	1	450-W Hg	quartz filter	$CH_3OH/AgNO_3$	Pt/18 000	39		38
$H_{2.33}Sr_{0.67}Nb_5O_{14.335}$	solid-state reaction, stepwise ion-exchange	1	100-W Hg	Pyrex filter	CH_3OH	Pt/6834.4			181
$H_2Ca_4Nb_6O_{20}$	solid-state reaction	1	100-W Hg	Pyrex filter	CH_3OH	928			191
$SiO_2-HCa_2Nb_3O_{10}$	solid-state reaction, stepwise ion-exchange	1	450-W Hg	Pyrex filter	CH_3OH	Pt/10800			189, 190
$K^+-Ca_2Nb_3O_{10}$	solid-state reaction, stepwise ion-exchange	0.1	500-W Xe	Pyrex filter	CH_3OH	Pt/6200			186, 187
$Na^+-Ca_2Nb_3O_{10}$	solid-state reaction, stepwise ion-exchange	0.1	500-W Xe	Pyrex filter	CH_3OH	Pt/9000			186, 187
$HCa_2Nb_3O_{10}$:La	solid-state reaction	1	100-W Hg	Pyrex filter	CH_3OH	Pt/7544			182
$H_2LaNb_2O_7$:In	solid-state reaction	1	100-W Hg	>290 nm	CH_3OH	Pt/5268		1.54 (>290 nm)	183
$H_2LaNb_2O_7$:Mo	solid-state reaction	1	100-W Hg	>290 nm	CH_3OH	Pt/3586			184
Ta_2O_5	solid-state reaction	1	400-W Hg	quartz filter	pure water	NiO_x/1154	NiO_x/529		78, 157, 201, 202
Mg−Ta oxide	sol−gel method	0.3	450-W Hg		pure water	NiO/340	NiO/170		204
Ta_2O_5:Ni	ligand-assisted templating method	0.35	450-W Hg		pure water	194.3	108.6		205
$K_2PrTa_5O_{15}$	solid-state reaction	1	400-W Hg	quartz filter	pure water	NiO/1550	NiO/830		40, 235
$K_2SmTa_5O_{15}$	solid-state reaction	1	400-W Hg	quartz filter	pure water	NiO/623	NiO/272		235
$K_2DyTa_5O_{15}$	solid-state reaction	1	400-W Hg	quartz filter	pure water	NiO/358	NiO/172		235
$K_2TmTa_5O_{15}$	solid-state reaction	1	400-W Hg	quartz filter	pure water	NiO/173	NiO/70		235
$K_3Ta_3Si_2O_{13}$	solid-state reaction	1	400-W Hg	quartz filter	pure water	NiO/368	NiO/188		40, 237
$K_3Ta_3B_2O_{12}$	solid-state reaction	0.5	450-W Hg	quartz filter	pure water	4780	2420	6.5 (254 nm)	238
$LiTaO_3$	solid-state reaction	1	400-W Hg	quartz filter	pure water	430	220		201, 206
$NaTaO_3$	hydrothermal method	0.3	450-W Hg	quartz filter	pure water	NiO/29 333	NiO/14 667		206−209
$KTaO_3$	solid-state reaction	0.5	400-W Hg	quartz filter	pure water	Au/116	Au/50		157, 167, 201, 206
$AgTaO_3$	solid-state reaction	0.15	300-W Xe	Pyrex filter	pure water	NiO/138	NiO/63.3		242
$KTaO_3$:Zr	solid-state reaction	0.1	500-W Xe	Pyrex filter	pure water	NiO_x/935	NiO_x/421		212, 213
$KTaO_3$:Ga	solid-state reaction	0.1	500-W Xe	Pyrex filter	pure water	NiO_x/677	NiO_x/223		213

Table 1. Continued

photocatalyst	synthetic method	mass (g)	light source	incident light	aqueous reaction solution	activity (μmol·h^{-1}·g^{-1}) co-catal./H_2	activity (μmol·h^{-1}·g^{-1}) co-catal./O_2	QY (%)	reference
$KTaO_3$:Hf	solid-state reaction	0.1	500-W Xe	Pyrex filter	pure water	NiO_x/985	NiO_x/398		213
$NaTaO_3$:La	solid-state reaction	1	400-W Hg	quartz filter	pure water	NiO/19 800	NiO/9660	56 (270 nm)	20, 214
$NaTaO_3$:Sr	solid-state reaction	0.5	400-W Hg	quartz filter	pure water	NiO/19 000	NiO/9400		215
$NaTaO_3$:Ba	solid-state reaction	0.5	400-W Hg	quartz filter	pure water	NiO/18 600	NiO/9380		215
$NaTaO_3$:Pr	solid-state reaction	1	400-W Hg	quartz filter	pure water	NiO_x/5290	NiO_x/2580		208, 214
$NaTaO_3$:Nd	solid-state reaction	1	400-W Hg	quartz filter	pure water	NiO_x/5190	NiO_x/2510		208, 214
$NaTaO_3$:Sm	solid-state reaction	1	400-W Hg	quartz filter	pure water	NiO_x/5290	NiO_x/2630		208, 214
$Na_2Ta_2O_6$	hydrothermal method	0.5	450-W Hg	quartz filter	NaOH	NiO/782	NiO/390		218
$K_2Ta_2O_6$	hydrothermal method	0.5	450-W Hg	quartz filter	NaOH	NiO/974	NiO/452		218
$BiTaO_4$	solid-state reaction	1	400-W Hg	quartz filter	pure water	4			200
$CaTa_2O_6$	solid-state reaction	1	400-W Hg	quartz filter	NaOH	NiO/72	NiO/32		208, 220
$SrTa_2O_6$	solid-state reaction	1	400-W Hg	quartz filter	pure water	NiO/960	NiO/490	7 (270 nm)	208, 220
$BaTa_2O_6$	solid-state reaction	1	400-W Hg	quartz filter	pure water	NiO/629	NiO/303		201, 208, 220
$ZnTa_2O_6$	solid-state reaction	1	400-W Hg	quartz filter	pure water	NiO/15	NiO/6		201
$NiTa_2O_6$	solid-state reaction	1	400-W Hg	quartz filter	pure water	11	4		201
$Rb_4Ta_6O_{17}$	solid-state reaction	1	400-W Hg	quartz filter	pure water	NiO_x/92	NiO_x/46		157
$Ca_2Ta_2O_7$	hydrothermal method	0.5	450-W Hg	quartz filter	NaOH	NiO/340	NiO/166		218
$Sr_2Ta_2O_7$	polymerized complex method	0.7	400-W Hg	quartz filter	pure water	NiO/5024	NiO/2476	24 (270 nm)	21, 221−223
$K_2SrTa_2O_7$	solid-state reaction	0.5	400-W Hg	quartz filter	pure water	748	384		226
$H_2SrTa_2O_7$	solid-state reaction	0.5	400-W Hg	quartz filter	pure water	770	358		226
$Rb_2SrTa_2O_7$	solid-state reaction	0.5	400-W Hg	quartz filter	pure water	176	22.8		226
$RbNdTa_2O_7$	solid-state reaction	0.2	400-W Hg	quartz filter	pure water	NiO_x/235	NiO_x/126.5		231−233
$RbLaTa_2O_7$	solid-state reaction	0.2	400-W Hg	quartz filter	pure water	NiO_x/6	NiO_x/3		231−233
$RbSmTa_2O_7$	solid-state reaction	0.2	400-W Hg	quartz filter	pure water	NiO_x/53	NiO_x/28.5		231−233
$H_2La_{2/3}Ta_2O_7$	solid-state reaction, H^+-exchange	0.5	400-W Hg	quartz filter	pure water	NiO/1880	NiO/918		227
$K_2La_{2/3}Ta_2O_7$	solid-state reaction	0.5	400-W Hg	quartz filter	pure water	NiO/292	NiO/132		227
$K_2Sr_{1.5}Ta_3O_{10}$	solid-state reaction	0.5	400-W Hg	Pyrex filter	pure water	RuO_x/200	RuO_x/78.8	2 (252.5 nm)	228
$LiCa_2Ta_3O_{10}$	solid-state reaction, hydrothermal treatment	0.2	400-W Hg	quartz filter	pure water	NiO_x/3540	NiO_x/1665		229
$NaCa_2Ta_3O_{10}$	solid-state reaction	0.2	400-W Hg	quartz filter	pure water	NiO_x/1465	NiO_x/810		229
$KCa_2Ta_3O_{10}$	solid-state reaction	0.2	400-W Hg	quartz filter	pure water	NiO_x/885	NiO_x/405		229
$RbCa_2Ta_3O_{10}$	solid-state reaction	0.2	400-W Hg	quartz filter	pure water	NiO_x/900	NiO_x/455		229
$CsCa_2Ta_3O_{10}$	solid-state reaction	0.2	400-W Hg	quartz filter	pure water	NiO_x/445	NiO_x/265		229
$KBa_2Ta_3O_{10}$	solid-state reaction	1	450-W Hg	quartz filter	pure water	NiO_x/150		8 (<350 nm)	134
$Sr_5Ta_4O_{15}$	polymerized complex method	0.5	400-W Hg	quartz filter	pure water	NiO/2388	NiO/1444		221
$Sr_4Ta_2O_9$	polymerized complex method	0.5	400-W Hg	quartz filter	pure water	NiO/64	NiO/4		221
$Ba_5Ta_4O_{15}$	polymerized complex method	1	450-W Hg	quartz filter	pure water	NiO/7110	NiO/3621		224
$H_{1.8}Sr_{0.81}Bi_{0.19}Ta_2O_7$	solid-state reaction, acid treatment	0.1	350-W Hg	quartz filter	pure water	2460	1110		230
Mg−Ta oxide	sol−gel method	0.3	450-W Hg	quartz filter	pure water	NiO_x/340	NiO_x/170		204
$LaTaO_4$	solid-state reaction	0.2	400-W Hg	quartz filter	pure water	NiO_x/578	NiO_x/257.5		236
$PrTaO_4$	solid-state reaction	0.2	400-W Hg	quartz filter	pure water	NiO_x/23.5	NiO_x/3.5		236
La_3TaO_7	polymerized complex method	0.5	400-W Hg	quartz filter	pure water	NiO_x/328	NiO_x/160		131, 192
$La_{1/3}TaO_3$	solid-state reaction	0.5	400-W Hg	quartz filter	pure water	NiO/70	NiO/15.8		227
$RbTaWO_6$	solid-state reaction	0.3	1000-W Hg	quartz filter	RbOH	NiO_x/232.3	NiO_x/115		176
$CsTaWO_6$	solid-state reaction	0.3	1000-W Hg	quartz filter	CsOH	NiO_x/65.7	NiO_x/29.3		176
Bi_2LaTaO_7	solid-state reaction	1	400-W Hg	quartz filter	pure water	41.8	20.5		239
Bi_2YTaO_7	solid-state reaction	1	400-W Hg	quartz filter	pure water	33.6	16		239
La_2AlTaO_7	solid-state reaction	0.1	350-W Hg	quartz filter	CH_3OH	NiO/1089			240
$Sn_2Ta_2O_7$	solid-state reaction	0.3	300-W Xe	Pyrex filter	CH_3OH	Pt/7			243
$BaNi_{1/3}Ta_{2/3}O_3$	solid-state reaction	0.5	400-W Hg	quartz filter	CH_3OH	Pt/84.4			178, 225
$BaZn_{1/3}Ta_{2/3}O_3$	solid-state reaction	0.5	400-W Hg	quartz filter	CH_3OH	Pt/389.6			178
$CaBi_2Ta_2O_9$	solid-state reaction	0.2	350-W Hg	quartz filter	$CH_3OH/AgNO_3$	1500	300		241
$SrBi_2Ta_2O_9$	solid-state reaction	0.2	350-W Hg	quartz filter	$CH_3OH/AgNO_3$	11 300	600		241
$BaBi_2Ta_2O_9$	solid-state reaction	0.2	350-W Hg	quartz filter	$CH_3OH/AgNO_3$	550	250		241
$PbWO_4$	solid-state reaction	0.25	200-W Hg−Xe	quartz filter	pure water	RuO_2/96	RuO_2/48		244, 245
$Na_2W_4O_{13}$	solid-state reaction	1	400-W Hg	Pyrex filter	$CH_3OH/AgNO_3$	Pt/9	8		247
$Bi_2W_2O_9$	solid-state reaction	1	450-W Hg	Pyrex filter	$CH_3OH/AgNO_3$	Pt/18	218		145
$PbMoO_4$	Morton Thiokol Inc.	0.3	200-W Hg	Pyrex filter	$CH_3OH/AgNO_3$	Pt/98.3	161.7		246
$(NaBi)_{0.5}MoO_4$	solid-state reaction	0.3	300-W Xe	Pyrex filter	$CH_3OH/AgNO_3$	Pt/2	193.3		248
$(AgBi)_{0.5}MoO_4$	solid-state reaction	0.3	300-W Xe	Pyrex filter	$CH_3OH/AgNO_3$	Pt/0	35.7		248
$(NaBi)_{0.5}WO_4$	solid-state reaction	0.3	300-W Xe	Pyrex filter	$CH_3OH/AgNO_3$	Pt/23.3	4.3		248
$(AgBi)_{0.5}WO_4$	solid-state reaction	0.3	300-W Xe	Pyrex filter	$CH_3OH/AgNO_3$	Pt/3.3	19.3		248
Bi_2MoO_6	solid-state reaction	1	450-W Hg	Pyrex filter	$CH_3OH/AgNO_3$	Pt/0.01	2.1		145
CeO_2	air annealing	0.8	550-W Xe	>330 nm	Ce^{4+}		15.9		269
CeO_2:Sr	solid-state reaction	1.1	450-W Hg	quartz filter	pure water	RuO_2/~100	RuO_2/~50		270

Table 1. Continued

photocatalyst	synthetic method	mass (g)	light source	incident light	aqueous reaction solution	activity (μmol·h^{-1}·g^{-1}) co-catal./H_2	activity (μmol·h^{-1}·g^{-1}) co-catal./O_2	QY (%)	reference
Ce-MCM-41	impregnation method	0.05	400-W Hg	quartz filter	pure water	70 800	15 250		271
$BaCeO_3$	polymerized complex method	0.2	400-W Hg		pure water	RuO_2/295	RuO_2/130		272
VO_2	electrodeposition mehtod		500-W Hg	quartz filter	ethanol	20[a]		38.7	250
$NaInO_2$	solid-state reaction	0.25	200-W Hg−Xe	quartz filter	pure water	RuO_2/~3.6	RuO_2/~1.2		258, 260
$CaIn_2O_4$	precipitation, calcination	0.25	200-W Hg−Xe	quartz filter	pure water	RuO_2/~84	RuO_2/~40		259−262
$SrIn_2O_4$	precipitation, calcination	0.25	200-W Hg−Xe	quartz filter	pure water	RuO_2/~28	RuO_2/~12		259−262
$Sr_{0.93}Ba_{0.07}InO_4$	precipitation, calcination	0.25	200-W Hg−Xe	quartz filter	pure water	RuO_2/~28	RuO_2/~12		260
$LaInO_3$	solid-state reaction	0.25	200-W Hg−Xe	quartz filter	pure water	RuO_2/~4.8	RuO_2/~2		259
$Y_xIn_{2-x}O_3$	solid-state reaction	0.25	200-W Hg−Xe	quartz filter	pure water	RuO_2/~32	RuO_2/~14		257
$NaSbO_3$	solid-state reaction	0.25	200-W Hg−Xe	quartz filter	pure water	RuO_2/~26	RuO_2/~8		261, 263
$CaSb_2O_6$	solid-state reaction	0.25	200-W Hg−Xe	quartz filter	pure water	RuO_2/~5.6	RuO_2/~0.8		263
$Ca_2Sb_2O_7$	solid-state reaction	0.25	200-W Hg−Xe	quartz filter	pure water	RuO_2/~12	RuO_2/~4		263
$Sr_2Sb_2O_7$	solid-state reaction	0.25	200-W Hg−Xe	quartz filter	pure water	RuO_2/~30.4	RuO_2/~12		263
Sr_2SnO_4	solid-state reaction	0.25	200-W Hg−Xe	quartz filter	pure water	RuO_2/~16	RuO_2/~6.8		261
$SrSnO_3$	hydrothermal, calcination	0.2	400-W Hg	quartz filter	$CH_3OH/AgNO_3$	Pt/8200	2500		268
$ZnGa_2O_4$	solid-state reaction	0.25	200-W Hg−Xe	quartz filter	pure water	RuO_2/~48	RuO_2/~16		264
Zn_2GeO_4	solid-state reaction	0.25	200-W Hg−Xe	quartz filter	pure water	RuO_2/~84	RuO_2/~40		265
$LiInGeO_4$	solid-state reaction	0.25	200-W Hg−Xe	quartz filter	pure water	RuO_2/~104	RuO_2/~52		266
$Ga_{1.14}In_{0.86}O_3$	solid-state reaction		450-W Hg	>300 nm	$CH_3OH/AgNO_3$	Pt/~30[a]	~25[a]		256
In_2O_3	Kanto Chemicals		450-W Hg	>300 nm	$CH_3OH/AgNO_3$	Pt/0[a]	~60[a]		256
β-Ga_2O_3	rare metallic		300-W Xe	quartz filter	$CH_3OH/AgNO_3$	Pt/~50[a]	~7[a]		256
Ga_2O_3	high-purity chemical	1	450-W Hg	quartz filter	pure water	Ni/338	Ni/171		253, 254
Ga_2O_3:Zn	impregnation, calcination	1	450-W Hg	quartz filter	pure water	Ni/4100	Ni/2200	~20	254
Ga_2O_3:Ca	impregnation, calcination	1	450-W Hg	quartz filter	pure water	Ni/950	Ni/550		254
Ga_2O_3:Sr	impregnation, calcination	1	450-W Hg	quartz filter	pure water	Ni/640	Ni/282		254
Ga_2O_3:Ba	impregnation, calcination	1	450-W Hg	quartz filter	pure water	Ni/765	Ni/348		254
Ga_2O_3:Ta	impregnation, calcination	1	450-W Hg	quartz filter	pure water	Ni/534	Ni/256		254
Bi_2GaVO_7	solid-state reaction	1	400-W Hg	quartz filter	pure water	46.8	22.9		251
Bi_2YVO_8	solid-state reaction	1	400-W Hg	quartz filter	pure water	40.7	20.7	0.628 (>390 nm)	252
Zn−Lu_2O_3/Ga_2O_3	solid-state reaction	0.5	400-W Hg	quartz filter	pure water	NiO_x/100.4	NiO_x/53.4	6.81 (320 nm)	255
Ge_3N_4	NH_3 nitridation	0.5	450-W Xe	>200 nm	H_2SO_4	RuO_2/~3600	RuO_2/~1600	9 (300 nm)	24, 277−279
GaN	NH_3 nitridation	0.3	450-W Xe	>300 nm	H_2SO_4	$Rh_{2-x}Cr_xO_3$/63.3	$Rh_{2-x}Cr_xO_3$/31.7	0.7 (300−340 nm)	275
GaN:Mg	NH_3 nitridation	0.8	450-W Hg	Pyrex filter	pure water	RuO_2/~750	RuO_2/~362.5		276, 759
GaN:Zn	NH_3 nitridation	0.8	450-W Hg	Pyrex filter	pure water	RuO_2/~250	RuO_2/~125		276, 759
GaN:Be	NH_3 nitridation	0.8	450-W Hg	Pyrex filter	pure water	RuO_2/~587.5	RuO_2/~287.5		759
ZnS	precipitation	0.4	200-W Hg	quartz filter	Na_2SO_3	Pt/34 037.5		90 (313 nm)	273, 364
InP	Kojundo Chemical Laboratory	0.2	250-W Hg	quartz filter	Na_2S	Pt/100			274
$AgBr/SiO_2$	Schumann emulsion	0.2	100-W Hg	quartz filter	methanol	650			280
$H_4SiW_{12}O_{40}/SiO_2$	impregnation method	1	450-W Hg	quartz filter	pure water	32.8	16.4		249

[a] The unit of H_2/O_2 evolution rate is μmol·h^{-1}, as the weight of photocatalyst has not been given in the reference. [b] Mercury lamp. [c] Xenon lamp. [d] Fluorescent lamp. [e] Metal halide lamp.

with HCl.[70] The addition of either NaOH or Na_2CO_3 was found to be effective for water splitting using the Pt/TiO_2 photocatalyst.[71,75,78] When TiO_2 was doped with metal ions, the photocatalytic activity for water splitting was effectively enhanced. Chae et al. reported that, whereas Ga doped TiO_2 powder could split pure water stoichiometrically under UV irradiation, pure TiO_2 did not show any activity.[79] The Ni^{2+} doping enhanced the photoactivity of the TiO_2 for hydrogen production from an aqueous methanol solution.[80] Sn/Eu codoped TiO_2 exhibited a high activity for hydrogen generation with a quantum efficiency of ~40% with Pd as the cocatalyst under the irradiation from a fluorescent lamp.[81] Zalas and La studied the effect of lanthanide doping on the photocatalytic activity of TiO_2.[82] The best performance for hydrogen production from an aqueous methanol solution was obtained for the TiO_2 containing 0.5 mol % of Gd oxide as the dopant. The UV-driven photocatalytic activity of TiO_2 was also improved by combining it with a second oxide semiconductor. All of the mixed oxides with heterophase-structures, SnO_2/TiO_2,[83] ZrO_2/TiO_2,[84] Cu_xO/TiO_2,[85−87] Ag_xO/TiO_2,[88−90] and $MTiO_3/TiO_2$ (M = Ca, Sr, Ba),[91] displayed higher rates of photocatalytic hydrogen evolution from aqueous solutions containing electron donors other than TiO_2 alone. With Pt as a cocatalyst, the Ti/B binary oxide stoichiometrically decomposes pure water under UV irradiation.[92,93] When TiO_2 nanoclusters were dispersed in the mesoporous structures of MCM-41 and MCM-48, the formed Ti-MCM-41[94] and Ti-MCM-48[95] showed much higher photocatalytic activity for hydrogen evolution under UV irradiation than bulk TiO_2.

Many white titanates are known to work as efficient photocatalysts for water splitting under UV irradiation. Shibata et al. reported that the layered titanates, $Na_2Ti_3O_7$, $K_2Ti_2O_5$, and $K_2Ti_4O_9$, were active in photocatalytic H_2 evolution from aqueous methanol solutions even without the presence of Pt cocatalyst.[96] These layered titanates, consisting of titanium oxide layers and interlayers, can be modified using ion-exchange reactions.[96,97] Of the materials studied, the H^+-exchanged $K_2Ti_2O_5$ exhibited a high activity with a quantum yield of up to ca. 10%. After being pillared with SiO_2 in the interlayers, $K_2Ti_4O_9$ showed an enhanced photocatalytic acitivity for H_2 evolution from CH_3OH/H_2O mixtures. This is in agreement with an increase in the surface area.[98] The $Na_2Ti_2O_5$ titanate nanotube material with a nickel complex intercalated into the interlayers also showed a high photocatalytic activity for H_2 evolution from water/methanol solutions under UV irradiation.[99] Kudo and Kondo found that a range of Cesium compounds, $Cs_2Ti_nO_{2n+1}$ (n = 2, 5, 6), with layered structures showed photocatalytic activities for H_2 and O_2 evolution from aqueous solutions.[100] The $Cs_2Ti_2O_5$ with a five-coordinate structure consisting of TiO_5 units was more active than $Cs_2Ti_5O_{11}$ and $Cs_2Ti_6O_{13}$ with six-coordinate structures consisting of TiO_6 units. The unsaturated coordination state of the five-coordinate structure worked as the active sites of catalytic reactions and contributed to the photoactivity. The photoactivity of $Cs_2Ti_2O_5$ was also greatly enhanced by the H^+-exchange reaction. Inoue and co-workers investigated a series of alkali-metal titanates with a chemical formula of $M_2Ti_nO_{2n+1}$ (M = Na, K, Rb and n = 2, 3, 4, 6) as photochemical water-splitting catalysts.[101−104] The alkaline metal atoms, M, in $M_2Ti_6O_{13}$ showed a great effect on the photocatalytic activity for water splitting. Interestingly, $RuO_2/M_2Ti_6O_{13}$ (M = Na, K, and Rb) with rectangular tunnel structures showed higher photocatalytic activity than $RuO_2/Cs_2Ti_6O_{13}$ with a layered structure. The activity increased in the order of Na > K > Rb > Cs. Kohno et al. reported that, in a photocatalytic system of ruthenium oxide-deposited barium titanates ($BaTi_4O_9$, $Ba_2Ti_9O_{20}$, $Ba_4Ti_{13}O_{30}$, and $Ba_6Ti_{17}O_{40}$), only $RuO_2/BaTi_4O_9$ was active in water decomposition.[105] The pentagonal prism tunnel structure of $RuO_2/BaTi_4O_9$ gave rise to a higher photocatalytic activity than $RuO_2/K_2Ti_4O_9$ with a zigzag layer structure. It is believed that the tunnel structure was responsible for the high dispersion of the RuO_2 particles.[104,106,107]

The method of catalyst preparation also appears to play a role in the final activity. For example, $BaTiO_3$ synthesized with a polymerized complex method exhibited enhanced photocatalytic activity when compared to the materials prepared by traditional solid-state reaction method.[108] This was due to the larger surface area. Domen and co-workers reported that a NiO-loaded $SrTiO_3$ powder was capable of decomposing pure water as well as water vapor into H_2 and O_2 under UV irradiation.[109−114] The activity of the photocatalyst was increased considerably by a pretreatment in H_2 and using a concentrated NaOH solution for the photocatalytic reaction.[111] The photocatalytic activity of $SrTiO_3$ was also greatly improved by using a modified preparation method[115] or a suitable concentration of metal cations doping (such as La^{3+},[116] Ga^{3+},[117] and Na^+ [117]). Some derivatives, such as $Sr_3Ti_2O_7$ and $Sr_4Ti_3O_{10}$, were also found to be active in water decomposition when loaded with NiO as the cocatalysts.[118,119] Mizoguchi et al. reported that platinized $CaTiO_3$ powder, with band gap of 3.5 eV estimated from optical absorption edge, exhibited a high photocatalytic activity under UV irradiation.[120] By doping with Zr^{4+} to form a $CaTi_{1-x}Zr_xO_3$ solid solution, the activity was further increased. Quantum yields of up to 1.91% and 13.3% for H_2 evolution from pure water and aqueous ethanol solution, respectively, were reported.[121]

Lee and co-workers investigated a series of perovskites whose layers were integrated of the intergrowth with the same elements (La and Ti) but had different layer thicknesses.[122−124] La_2TiO_5, $La_2Ti_3O_9$, and $La_2Ti_2O_7$, which had layered structures made up of slabs of 1, 3, and 4 units, respectively, showed much higher photocatalytic activities under UV irradiation than bulk $LaTiO_3$. Alkaline earth component-doping (Ba, Sr, and Ca) was shown to improve the photoactivities of $La_2Ti_2O_7$. In particular, the NiO-modified Ba-doped $La_2Ti_2O_7$ proved extremely active for overall water splitting with a quantum yield close to 50% on condition that alkaline hydroxide was introduced into the reaction system as an external additive.[125] The activity of $La_2Ti_2O_7$ was highly enhanced by synthesizing the catalyst using the polymerized approach instead of the solid-state reaction method.[22,126] In contrast, $La_2Ti_2O_7$, $Ln_2Ti_2O_7$ (Ln = Pr, Nd) with a layered structure was also active for water splitting but exhibited lower activities, with the activity decreasing in the order $La_2Ti_2O_7 \gg PrLaTi_2O_7 > Pr_2Ti_2O_7 > NdLaTi_2O_7 > Nd_2Ti_2O_7$.[127]

The use of titanate $R_2Ti_2O_7$ (R = Y, Eu−Lu) with pure cubic-pyrochlore structure as water-splitting photocatalysts was first reported in 2004 by Abe's group.[128] Among them, NiO_x-loaded $Y_2Ti_2O_7$ demonstrated the most efficient evolution of H_2 and O_2 in a stoichiometric ratio from pure water under UV irradiation. $Y_2Ti_2O_7$ photocatalysts, with better crystallinity and higher activity, were obtained by the addition of excess Y in the polymerized complex synthetic procedure.[129,130] They also found that the high photocatalytic activ-

ity observed for overall water splitting over $R_2Ti_2O_7$ (R = Y, Gd) was related to the increased mobility of the electrons and holes caused by the corner-shared octahedral TiO_6 network in these materials.[131] Uno et al. also studied the photocatalytic activities for hydrogen evolution using $Ln_2Ti_2O_7$ (Ln = La, Pr, Nd, Sm, Gd, Dy, Ho, Er, and Yb).[132] However, only $La_2Ti_2O_7$ and $Sm_2Ti_2O_7$ showed detectable photocatalytic hydrogen evolution, and even that was a small rate.

Miseki et al. studied the photocatalytic properties of $ALa_4Ti_4O_{15}$ (A = Ca, Sr, and Ba) with a (111) plane-type layered perovskite structure.[133] Of these, NiO_x-modifed $BaLa_4Ti_4O_{15}$ showed the highest activity for water splitting, with a quantum yield of 15% at 270 nm. The highly donor-doped (110) layered perovskite $La_4CaTi_5O_{17}$ was found to be an efficient photocatalyst for overall water splitting with quantum yield as high as 20% under UV irradiation.[134] The spontaneously hydrated layered perovskites with a general formula of $A_{2-x}La_2Ti_{3-x}Nb_xO_{10}$ (A = interlayer cations such as K, Rb, Cs; $x = 0-1$) were found to be efficient photocatalysts for water decomposition under UV irradiation.[135−137] $NiO/Rb_2La_2Ti_3O_{10}$ produced H_2 and O_2 from a RbOH aqueous solution with quantum yield up to 5%. Suitable modification techniques such as cocatalyst loading, using Ni or Au,[138,139] metal-ion doping (Zn^{2+} doping),[140] and alternative synthetic methods[23,141] all led to the enhanced activity of $K_2La_2Ti_3O_{10}$. The polymerized complex synthesis method was also utilized to prepare the high-purity stoichiometric $KTiNbO_5$ photocatalyst, which was demonstrated with increased activity after NiO loading.[142] For $KLaTiO_4$, Zr^{4+} doping had a positive effect on the photocatalytic activity in a water-splitting reaction, giving rise to a quantum yield as high as 12.5%.[143]

Sekine et al. were the first to examine the photocatalytic reactions on the ion-exchangable layered titanoniobate compounds, $CsNbTi_2O_7$ and $CsNbTiO_5$.[144] They found that the H^+-exchanged forms of those compunds work as efficient photocatalysts for H_2 or O_2 evolution from an aqueous solution containing methanol or silver nitrate under UV irradiation. Members of the aurivillius-type layered perovskites $(Bi_2O_2)^{2+}(A_{n-1}B_nO_{3n+1})^{2-}$ (A = Ba, Bi, etc.; B = Ti, Nb, etc.), $Bi_4Ti_3O_{12}$, $BaBi_4Ti_4O_{15}$, and Bi_3TiNbO_9 evolved H_2 and O_2 from aqueous methanol and $AgNO_3$ solutions, respectively.[145] He and Yang investigated the photocatalytic activity for hydrogen production over another layered perovskite $KBi_3PbTi_5O_{16}$ under UV irradiation.[146] It was found that the photocatalyst prepared by the polymerized complex method showed much higher activity than that prepared by the solid-state reaction method. In addition, the rate of hydrogen evolution was greatly improved and affected by the addition of $Ce(SO_4)_2$ in an aqueous suspension.

Sayama and Arakawa were the first to find that the photocatalytic decomposition of pure water proceeded over ZrO_2 powder without any loaded metals as cocatalysts under UV irradiation.[78,147,148] The activity was affected significantly by the pressure of the reaction system, the nature of the additive, and the pH of the solution. Specifically, the addition of Na_2CO_3 or $NaHCO_3$ led to a remarkable increase in the activity and stability of the gas-evolution rate. However, the activity decreased when metals such as Pt, Au, Cu, and RuO_2 were loaded onto the surface of the ZrO_2. It was presumed that the large electronic barrier height of the semiconductor−metal junction prevented the migration of electrons from ZrO_2 to the metal. This would lead to the loaded metals, possibly blocking the reaction sites on the ZrO_2. Reddy et al. revealed that the photocatalytic activity of ZrO_2 prepared by the precipitation method was highly dependent on the hydrolyzing agent used.[149] The highest photocatalytic activity was obtained for the ZrO_2 with the highest surface area when KOH was used as the hydrolyzing agent. Zou et al. reported that a clean and direct metal−support interface of a NiO-loaded ZrO_2 photocatalyst could be obtained using a plasma method.[150] In photocatalytic reactions, this interface proved more efficient for the charge separation and transfer, which in turn led to the higher photocatalytic activity for water splitting using NiO/ZrO_2 by the plasma treatment than that prepared with the traditional thermal treatment. Compared to the conventional bulk ZrO_2, the photocatalytic water-splitting activity was greatly enhanced by the high dispersion of ZrO_2 into the amorphous wall of MCM-41.[151]

$BaZrO_3$ with a cubic perovskite structure produced hydrogen efficiently with a quantum yield up to 3.7% from pure water without the assistance of any cocatalysts under UV irradiation.[152] The high photoactivity of $BaZrO_3$ was attributed to the highly negative potential of the photoinduced electrons, the 180° Zr−O−Zr bond angle, and the large dispersion of the conduction band edge composed of Zr 4d orbitals. When the Zr element was partially substituted by Sn, the photocatalytic activity for water splitting was obviously improved.[153] Uno et al. investigated the photocatalytic activities for hydrogen evolution of a series of lanthanide zirconium oxides, $Ln_2Zr_2O_7$ (Ln = La, Ce, Nd and Sm).[154] Under the illumination of a 500-W Xenon lamp, hydrogen gas was clearly evolved in a distilled water suspension of $La_2Zr_2O_7$, $Sm_2Zr_2O_7$, and $Nd_2Zr_2O_7$. On the other hand, $Ce_2Zr_2O_7$ showed no photocatalytic activity because of its lower conduction band level.

After modification with Pt as a cocatalyst, mesoporous zirconium−titanium phosphates demonstrated considerable activity in photocatalytic water decomposition.[155] The H_2 production rate was gradually increased on the addition of Zr, and the maximum H_2 evolution was observed for the $Zr_{0.5}Ti_{0.5}PO_4$ material. Furthermore, the use of sodium carbonate as a pH adjuster was essential and significant for hydrogen generation and also provided stability for the photocatalytic reaction system. A zirconium phosphate/phosphonate compound with quantum yield of 4% was developed to produce hydrogen photochemically from water. It was based only on the ultraviolet portion of the spectrum in the presence of a sacrificial reductant (EDTA).[156]

3.1.2. Nb-, Ta-Based Oxides

Pure Nb_2O_5, with a band gap of ca. 3.4 eV determined from the threshold of UV−vis absorption, is not active for pure water splitting under UV irradiation.[157] After modification with Pt as a cocatalyst, however, it can efficiently produce H_2 from aqueous solutions containing methanol as an electron donor.[158] Mesoporous Nb_2O_5, synthesized via an evaporation-induced self-assembly method, demonstrated a photocatalytic activity 20 times higher for hydrogen evolution than a bulk Nb_2O_5 without any porosity.[158] Intercalation of In_2O_3 into the mesoporous structure further increased the photoactivity of mesoporous Nb_2O_5 by 2.7 times.[159]

Besides Nb_2O_5, a large number of niobates can produce H_2 and O_2 via water splitting upon UV irradiation. In 1986, Domen and co-workers developed $K_4Nb_6O_{17}$ as the first example of a niobate photocatalyst that showed high and stable activity for H_2 evolution from aqueous methanol

solution without any assistance from other materials such as the noble metals.[160,161] This niobate is composed of layers of niobium oxide sheets, in which potassium ions are located in two different kinds of interlayers. One type of interlayer contains water molecules and potassium ions, and the other contains only potassium ions. The potassium ions between the niobium oxide layers can be exchanged with many other cations including transition metal ions. The activities of catalysts exchanged with H^+, Cr^{3+}, and Fe^{3+} ions were higher than the original $K_4Nb_6O_{17}$. Of particular note is the H^+-exchanged $K_4Nb_6O_{17}$, which showed the highest activity for H_2 evolution from an aqueous methanol solution. Its quantum yield was up to ca. 50% at 330 nm.[160,162] After modification with NiO,[163−166] Au,[167] Pt,[168,169] and Cs[170] as cocatalysts, $K_4Nb_6O_{17}$ was quite efficient for simultaneous hydrogen and oxygen evolution from pure water. Upon the addition of alkaline hydroxide (KOH, NaOH) into the aqueous impregnation solution, the activity of the $NiO/K_4Nb_6O_{17}$ photocatalyst for overall water splitting was enhanced, with a quantum efficiency of 5.3% (330 nm) under optimum conditions.[166] $Rb_4Nb_6O_{17}$, which has the same layered structure, exhibited a high activity for photocatalytic water splitting to form H_2 and O_2 under band gap irradiation. The quantum efficiency at 330 nm was ca. 10% in the initial stage of the reaction over the NiO(0.1 wt %)−$Rb_4Nb_6O_{17}$ photocatalyst.[171] When doped with Ta_2O_5, layered compounds of the type $A_4Ta_xNb_{6-x}O_{17}$ (A = K or Rb, $x = 2$, 3, and 4) were able to decompose water stoichiometrically after the pretreatment of H_2 reduction and O_2 reoxidation at high temperatures. This was possible even in the absence of any loaded metals as cocatalysts.[157] Some other alkaline-metal niobates such as $ANbO_3$ (A = Li, Na, K)[172−174] and $Cs_2Nb_4O_{11}$[175] also catalyzed H_2 and/or O_2 evolution from water under UV irradiation, but only after modification with Pt, RuO_2, or NiO. Ikeda et al. found that tungsten-containing alkaline niobates with a defect pyrochlore structure, $ANbWO_6$ (A = Rb, Cs), and loaded with nickel oxide, showed photocatalytic activity for overall water splitting under UV irradiation.[176] The conduction bands of the materials were thought to be composed of the W5d orbital hybridized with the Nb5d orbital.

Photocatalytic water splitting over the alkaline-earth niobates have been studied by various researchers. The related strontium niobates $SrNb_2O_6$,[177] $Sr_2Nb_2O_7$,[21,134,177] and $Sr_5Nb_4O_{15}$[133] exhibited efficient photocatalytic activities for hydrogen and oxygen production from pure water under UV irradiation. In particular, $Sr_2Nb_2O_7$ with a highly donor-doped (110) layered perovskite structure gave quantum yields as high as 23%.[134] The activity of $Sr_2Nb_2O_7$ was further enhanced to give a quantum yield of 32%, by using a hydrothermal synthetic process that produced a 1D nanostructure with larger Brunauer−Emmett−Teller (BET) surface areas.[177] In comparison, the quantum yield of $Ca_2Nb_2O_7$ was 7%.[134] $Ba_5Nb_4O_{15}$ with a layered perovskite structure was studied by Kudo and co-workers.[133,134] It gave a 17% quantum yield at 270 nm for water splitting when loaded with NiO cocatalysts. Partial substitution of Nb^{5+} with Zn^{2+} gave the resulting $BaZn_{1/3}Nb_{2/3}O_3$ with a distorted perovskite structure, which showed favorable photocatalytic activity under UV irradiation.[178,179]

Domen and co-workers first reported a novel Dion-Jacobsen series of ion-exchangeable niobates, $A(M_{n-1}Nb_nO_{3n+1})$ (A = Na, K, Rb, Cs; M = La, Ca, Sr, etc.), with layered perovskite structures that showed unique photocatalytic activities. This was especially true for the H^+-exchanged forms, for H_2 evolution from aqueous alcohol solutions as well as O_2 evolution from an aqueous silver nitrate solution.[38,180] For example, $KSr_2Nb_3O_{10}$ produced hydrogen at a rate of 0.11 mmol/h/g. After cation exchange with protons, the rate of $HSr_2Nb_3O_{10}$ increased to 43 mmol/h/g.[38] The related layered niobate $K_{2.33}Sr_{0.67}Nb_5O_{14.335}$ was also reported by Wu and co-workers to show much higher photoactivity for hydrogen evolution after a proton-exchange reaction.[181] They further reported that other modifications for proton-exchanged $H(M_{n-1}Nb_nO_{3n+1})$ (M = La, Ca, Sr, etc.), such as metal-ion doping (La^{3+},[182] In^{3+}[183], and Mo^{6+}[184] doped into $HCa_2Nb_3O_{10}$ and $H_2LaNb_2O_7$, respectively), efficiently improved the photocatalytic hydrogen evolution from aqueous methanol solutions. When $H_2LaNb_2O_7$ was synthesized using a polymerized complex method, it showed higher activity for water splitting than the same material prepared by a solid-state reaction.[185]

Ebina and co-workers synthesized a restacked aggregate of exfoliated nanosheets of $[Ca_2Nb_3O_{10}]^-$ by flocculation with NaOH and KOH aqueous solutions. Under UV irradiation, the restacked aggregates, with a 10-fold enhancement of the surface area, showed higher activities for photocatalytic hydrogen evolution than the $KCa_2Nb_3O_{10}$ starting compound;[186] overall photocatalytic splitting of water was achieved when RuO_x was intercalated between the layers during the exfoliation-restacking route.[187] After exfoliation using tetrabutylammonium hydroxide, the restacked $TBA_x[H_{1-x}Ca_2Nb_3O_{10}]$ sheets loaded with Pt cocatalysts produced hydrogen from pure water with a quantum efficiency of 7.5%. However, no oxygen was observed. Transient absorption measurements of the nanosheets revealed charge separation on a nanosecond time scale.[188] SiO_2-pillared $HCa_2Nb_3O_{10}$, prepared from the layered perovskite $KCa_2Nb_3O_{10}$ via alkylammonium ion-intercalated $HCa_2Nb_3O_{10}$, showed much higher photocatalytic activity of H_2 evolution from aqueous solutions of long-chain alcohols.[189,190] This effect was attributed to the expanded interlayer space facilitating the intercalation of such alcohols that could then serve as efficient electron donors. In 2008 a new member of the Dion-Jacobsen perovskites, $H_2Ca_4Nb_6O_{20}$, was reported to be active for H_2 evolution in the presence of methanol as a sacrificial agent under UV irradiation.[191] When Nb was partially substituted by Ta, the resulting $H_2Ca_4Ta_2Nb_4O_{20}$ showed the best photocatalytic activity. The photocatalytic H_2 evolution rate was 8.5 mmol/h/g. Abe and co-workers investigated the effect of crystal structure on water splitting using R_3NbO_7 (R = Y, Yb, Gd, La).[131,192] Only La_3NbO_7, which has an orthorhombic weberite structure and which formed a NbO_6 octahedral network that increased the mobility of both electrons and holes, was active for the photocatalytic water-splitting reaction. On the other hand, $La_{1/3}NbO_3$, crystallizing in an A-site deficient perovskite-type structure instead, catalyzed H_2 evolution with a Pt cocatalyst from CH_3OH/H_2O solution. In addition, O_2 evolution from $AgNO_3$ aqueous solution under UV irradiation was observed.[193]

Kudo et al. reported a new $ZnNb_2O_6$ photocatalyst consisting of d^{10} and d^0 metal ions.[194] Under UV irradiation, the activity of the native $ZnNb_2O_6$ was negligible, whereas NiO-loaded $ZnNb_2O_6$ showed the high activity after a H_2-reduction and O_2-oxidation pretreatment. Chen and co-workers prepared a new series of layered perovskite photocatalysts, $ABi_2Nb_2O_9$ (A = Ca, Sr, Ba), by the conventional

solid-state reaction method.[195] Under UV irradiation, these photocatalysts showed photocatalytic activity for both H_2 and O_2 evolution from aqueous solutions containing sacrificial reagents (methanol and Ag^+). The activities decreased in the order of $SrBi_2Nb_2O_9 > BaBi_2Nb_2O_9 > CaBi_2Nb_2O_9$. Zou and co-workers found that the compounds M_2BiNbO_7 ($M = In^{3+}$, Ga^{3+}) with pyrochlore structures were sensitive to UV irradiation and had the ability to split water stoichiometrically to produce H_2 and O_2.[196] On the other hand, Bi_2MNbO_7 ($M = Al^{3+}$, Ga^{3+}, In^{3+}) with the same pyrochlore structure only evolved H_2 or O_2 in the presence of CH_3OH or $Ce(SO_4)_2$ as sacrificial agents.[197] The photocatalytic hydrogen production over NiO/Bi_2AlNbO_7 was efficiently improved with La^{3+} doping.[198] In comparison, Bi_2MNbO_7 ($M = Y^{3+}$, Ce^{3+}, Gd^{3+}, Sm^{3+}, Nd^{3+}, Pr^{3+}, and La^{3+}) evolved H_2 at only a small rate from pure water under UV irradiation.[199] The increase of ion radius of M^{3+} in Bi_2MNbO_7 led to the decrease in the photocatalytic activity. The narrower band gap formed by the smaller ion radius of M^{3+} suggested easier excitation for an electron from the valence band to the conduction band in the oxide semiconductor. $BiNbO_4$ with a triclinic structure produced only a small amount of hydrogen from pure water under UV irradiation. When doped with Ta, the resulting $BiTa_{0.8}Nb_{0.2}O_4$ had an orthorhombic structure and exhibited much higher activity due to the modified band levels and band gaps.[200]

Ta-based oxides are known to be active photocatalysts for water splitting under UV irradiation. Under band gap (4.0 eV) irradiation, Ta_2O_5 alone can only produce a very small amount of H_2 and no O_2 from pure water.[157,182] After modification with NiO and RuO_2 as the cocatalysts, it displayed great activity for the overall water decomposition.[201] The addition of Na_2CO_3 is also effective for improving the photocatalytic activity of Ta_2O_5, as observed for the TiO_2 photocatalytic system.[78] Mesoporous Ta_2O_5 was found by Domen and co-workers to be an active catalyst for photocatalytic water decomposition after NiO loading.[202] Although the walls of the mesoporous Ta_2O_5 were amorphous, the photocatalytic activity was higher than that of crystallized Ta_2O_5. This was because the small wall thickness of mesoporous Ta_2O_5 favored the migration of excited electron to the surface. When mixed with TiO_2, the mesoporous Ta−Ti mixed oxides formed showed relatively high activities for photocatalytic hydrogen generation from methanol/water mixtures under the irradiation of $\lambda > 300$ nm. However, a higher concentration of TiO_2 in the mixed oxides led to the destruction of the mesoporous structure.[203] In contrast, the introduction of MgO into the mesoporous structure of Ta_2O_5 improved the thermal stability and also gave rise to stable photocatalytic activity for overall water decomposition over Mg−Ta mixed oxides.[204] Ni-mixed mesoporous Ta oxide possessed an incomplete mesoporous structure but exhibited higher photocatalytic activity for overall water decomposition than nonmodified mesoporous Ta oxide under UV irradiation, while Cu-mixed mesoporous Ta oxide evolved H_2 only at a low rate.[205]

In 1998, Kato and Kudo reported that alkali tantalates $ATaO_3$ (A = Li, Na, and K) showed high activities for photocatalytic water splitting into H_2 and O_2 under UV irradiation.[201] The excess of alkali in the synthetic process of the solid-state reaction improved the photocatalytic activities of naked tantalates. The order of the activities was $KTaO_3 \ll NaTaO_3 < LiTaO_3$.[206] Nickel oxide[207,208] and nanosized gold particles[167] were shown to function as efficient cocatalysts for photocatalytic water splitting. Among them, $NiO/NaTaO_3$ was the most photocatalytically active and produced H_2 and O_2 from pure water with a quantum yield of 28% at 270 nm.[207] Compared to the solid-state reaction method, both the hydrothermal method[209,210] and the sol−gel method[211] produced $ATaO_3$ (A = K, Na) with good crystallinity as well as high surface areas. These exhibited higher photocatalytic activity in water splitting than the solid-state produced material. Ishihara and co-workers found for the first time that controlling the charge density in $KTaO_3$ by doping small amounts of acceptors such as tri- or tetravalent cations was effective for improving the photolysis activity of H_2O.[212,213] In particular, $NiO/KTaO_3$ doped with 8 mol % Zr^{4+} exhibited a higher photocatalytic activity than the well-known photocatalyst Pt/TiO_2. The increased activity was brought about by an increase in the lifetime of the photoexcited charge, which in return was caused by a decrease in the charge density.

Kudo and Kato investigated the effects of doping lanthanide (La, Pr, Nd, Sm, Gd, Tb, and Dy)[214] and alkaline-earth metal ions (Ca, Sr, and Ba)[215] into $NaTaO_3$ photocatalysts for efficient water splitting. Lanthanum was the most effective dopant. The apparent quantum yield at 270 nm amounted to 56%,[20] which is the highest quantum yield ever reported for catalysts in pure water splitting. The positive effects on the photocatalytic properties were mainly due to the decrease in the particle size and the ordered surface nanostructure. The many characteristic steps created by the doping affected the electron−hole recombination kinetics as revealed by a time-resolved infrared absorption study of the $NaTaO_3$-based photocatalysts.[216,217] The related photocatalysts $NiO/A_2Ta_2O_6$ (A = K, Na) also worked efficiently for overall water splitting under UV irradiation.[218,219] For the alkaline-earth tantalates ATa_2O_6 (A = Ca, Sr, Ba), the order of photocatalytic activities was $SrTa_2O_6 > BaTa_2O_6 > CaTa_2O_6$. This corresponded to the band gaps and the energy of the photogenerated-electron/hole pairs transferring in the crystal (emission energy).[201,208,220] When the NiO cocatalysts were loaded, $NiO/SrTa_2O_6$ showed the highest activity for overall water splitting. The quantum yield was 7% at 270 nm.[220] In the related series of strontium tantalates $Sr_mTa_nO_{(m+5n/2)}$, the photocatalytic activities for water splitting into H_2 and O_2 decreased in the following order: $Sr_2Ta_2O_7 > Sr_5Ta_4O_{15} > SrTa_2O_6 > Sr_4Ta_2O_9$.[221] The quantum yield of NiO (0.15 wt %)/$Sr_2Ta_2O_7$ prepared by the polymerized complex method was estimated to be ~24% at 270 nm.[21,222] Substitution of Ta for Nb reduced the band gap of $Sr_2Ta_2O_7$ from 4.5 to 3.9 eV.[222,223] Under UV irradiation, all the $Sr_2(Ta_{1-x}Nb_x)_2O_7$ solid solutions loaded with NiO cocatalysts decomposed water into H_2 and O_2 stoichiometrically. But the photocatalytic activity decreased dramatically even when the amount of Nb was small. $Ca_2Ta_2O_7$ with a pyrochlore structure produced H_2 and O_2 in a stoichiometric ratio under UV irradiation. The activity was higher than NiO-loaded niobate pyrochlore, $NiO/Ca_2Nb_2O_7$.[218] Otsuka et al. claimed that, in comparison to $BaTa_2O_6$, $Ba_5Ta_4O_{15}$ prepared under a Ta-rich atmosphere showed a higher photocatalytic activity in the decomposition of H_2O into H_2 and O_2 under UV irradiation.[224] When Ta was partially replaced by Ni or Zn, only H_2 from water was evolved from the resulting $BaM_{1/3}Ta_{2/3}O_3$ (M = Ni, Zn). Methanol was the electron donor, and Pt was the cocatalyst.[178,225]

Shimizu and co-workers first developed $A_2A'Ta_2O_7$ (A = H, K, and Rb; A′ = Sr and $La_{2/3}$) with a hydrated layered perovskite structure. It proved highly efficient for overall

water splitting, even without cocatalysts loading.[226,227] These catalysts showed higher activities than the anhydrous perovskites ($Li_2SrTa_2O_7$, $La_{1/3}TaO_3$, and $KTaO_3$). This was attributed to their hydrated layered structure where the photogenerated electrons and holes can be effectively transferred to the interlayer water. Moreover, as a result of the intercalation of small NiO clusters into the layers of $H_2La_{2/3}Ta_2O_7$ via an ion-exchange reaction, their cocatalyst action remarkably increased the overall activity. This was achieved by shortening the migration distance of the photogenerated charges to the reactive sites. On the other hand, the relatively large NiO particles at the external surface of $H_2SrTa_2O_7$ did not improve the activity. Interestingly, hydration under aqueous conditions changed the crystal structure of $K_2Sr_{1.5}Ta_3O_{10}$ from orthorhombic to a tetragonal symmetry. This was due to water intercalation into the interlayer space.[228] With RuO_x as the cocatalyst, the hydrous $K_2Sr_{1.5}Ta_3O_{10}$ photocatalyst was active in the pure water-splitting process: the quantum yield at 252.5 nm was ~2%. For the layered perovskites $ACa_2Ta_3O_{10}$ (A = Cs, Rb, K, Na, and Li), interlayer hydration was only observed for A = Na and Li.[229] Hydration of the Li phase doubled the rate of photocatalytic gas evolution when loaded with the cocatalyst NiO; this was the highest in the $ACa_2Ta_3O_{10}$ series. Analogously, a quantum yield of 8% was achieved for the Ba-based (100) layered perovskite $KBa_2Ta_3O_{10}$, after modification with NiO.[134]

Li et al. prepared another hydrated layered perovskite, namely, the tantalate $H_{1.81}Sr_{0.81}Bi_{0.19}Ta_2O_7$, from $Bi_2SrTa_2O_9$ using an ion-exchange reaction in hydrochloric acid solution.[230] Under UV irradiation, the $H_{1.81}Sr_{0.81}Bi_{0.19}Ta_2O_7$ photocatalyst showed favorable photocatalytic activity in splitting pure water into H_2 and O_2 even without the assistance of a cocatalyst. Layered lanthanide tantalates and their ion-exchanged phases ($MLnTa_2O_7$, M = Cs, Rb, Na, and H; Ln = La, Pr, Nd, and Sm) were prepared by Machida and co-workers to evaluate their photocatalytic activity for water splitting under UV irradiation.[231−234] The photocatalytic activity was sensitive to not only Ln but also the interlayer cation, M. The highest activity was obtained for M = Rb with the following sequence of Ln: Rb > Nd > Sm > La > Pr. The effects of lanthanide ions on the photocatalytic activities of $LnTaO_4$ (Ln = La, Ce, Pr, Nd, and Sm) with monoclinic structures and $K_2LnTa_5O_{15}$ (Ln = La, Pr, Nd, Sm, Gd, Tb, Dy, and Tm) with tungsten bronze structures were also investigated by Machida's group.[235,236] The photocatalytic activities for water splitting under UV irradiation strongly depended on the particular lanthanide ion. For the $LnTaO_4$ series, $LaTaO_4$ showed the highest rate for the stoichiometric evolution of H_2 and O_2 from pure water; while among the $K_2LnTa_5O_{15}$ series, $K_2PrTa_5O_{15}$ and $K_2SmTa_5O_{15}$ showed relatively high activities for water splitting ($h\nu$ > 3.9−4.1 eV).

The photocatalytic activity of R_3TaO_7 (R = Y, Yb, Gd, La) for water splitting was studied by Arakawa and co-workers.[131,192] They examined the effect of R^{3+} ionic radius on the crystal structure.[131,192] The crystal structures of R_3TaO_7 changed with increasing ionic radius of the R^{3+} ion from a fluorite-type cubic structure to a pyrochloretype cubic structure and finally to a weberite-type orthorhombic structure. In the case of the La_3TaO_7, the photocatalytic activity was greatly increased by the phase transition from cubic to orthorhombic. $K_3Ta_3Si_2O_{13}$ and $K_3Ta_3B_2O_{12}$, which have similar crystal structures, consisting of pillars formed by a corner sharing of three linear TaO_6 chains, were active for water splitting without any cocatalyst.[237,238] The TaO_6 pillars in $K_3Ta_3Si_2O_{13}$ and $K_3Ta_3B_2O_{12}$ are linked by Si_2O_7 ditetrahedral units and BO_3 triangle units, respectively. Thus, the bond angle of O−Ta−O in $K_3Ta_3B_2O_{12}$ (171.5°) is slightly smaller than that in $K_3Ta_3Si_2O_{13}$ (173.1°). The distortion due to the smaller bond angle of $K_3Ta_3B_2O_{12}$ than that found in $K_3Ta_3Si_2O_{13}$ resulted in a wider band gap and higher photocatalytic activity. NiO cocatalyst loading increased the activity of $K_3Ta_3Si_2O_{13}$ drastically but proved ineffective for $K_3Ta_3B_2O_{12}$. In a manner similar to niobates, the tantalates $ATaWO_6$ (A = Rb, Cs) crystallized into a defect pyrochlore structure with a conduction band composed of the W5d orbital hybridized with the Ta4d orbitals.[176] Under UV irradiation, they evolved H_2 and O_2 in a stoichiometric ratio from an aqueous AOH (A = Rb, Cs) solution. It was loaded with NiO as cocatalyst. Even though the pyrochlore-like Bi_2MTaO_7 (M = Y and La) showed a strong optical absorption in the visible region, as photocatalyts these oxides could only produce H_2 and O_2 from pure water under UV irradiation.[239]

Chen and co-workers investigated the photocatalytic water splitting of La_2AlTaO_7 with a view to studying the effect of aluminum on the electronic structure.[240] It was found that instead of the Ta5d state it was the Al3s3p states that acted as the lower conduction band. Under UV irradiation, La_2AlTaO_7 showed photocatalytic activity in splitting pure water into H_2 and O_2 even in the absence of a cocatalyst. In comparison, using $ABi_2Ta_2O_9$ (A = Ca, Sr, Ba), also developed by Chen's group, H_2 or O_2 evolved only from the aqueous solution containing either methanol or $AgNO_3$ as the sacrificial reagent. Simultaneous production of H_2 and O_2 from pure water was not observed.[241] The photocatalytic activities decreased in the order of $SrBi_2Ta_2O_9$ > $CaBi_2Ta_2O_9$ > $BaBi_2Ta_2O_9$. A large range of transition-metal tantalates has been investigated by different researchers with water decomposition as the aim. Under UV irradiation, $NiTa_2O_6$ produced both H_2 and O_2 from pure water without a cocatalyst. On the other hand, with $MnTa_2O_6$, $CoTa_2O_6$, $CrTaO_4$, $PbTa_2O_6$, $FeTaO_4$, and $BiTaO_4$, only traces of H_2 evolved.[200,201] When NiO was loaded as the cocatalyst, $AgTaO_3$ and $ZnTa_2O_6$ were active in water splitting, producing both H_2 and O_2.[201,242] In contrast, in an aqueous methanol solution, $Sn_2Ta_2O_7$ with Pt as the cocatalyst only produced H_2 while $SnTa_2O_6$ was totally inactive.[243]

3.1.3. W-, Mo-Based Oxides

The number of heterogeneous photocatalysts based on either tungstates or molybdates for H_2 or O_2 evolution is quite small. Some were found to be active for water splitting only under UV irradiation even though they showed optical absorption in the visible region. Inoue and co-workers found that $PbWO_4$ incorporating a WO_4 tetrahedron showed high and stable photocatalytic activity for the overall splitting of water. A stoichiometric quantity of H_2 and O_2 was produced under UV irradiation when RuO_2 was loaded onto the metal oxide.[244,245] The photocatalytic performance was attributed to large dispersions in both the valence and conduction bands. This generated very mobile photoexcited holes and electrons. In contrast, a small dispersion in the conduction band was observed for the photocatalytically inactive $CaWO_4$, which has a similar crystal structure. $PbMoO_4$ catalyzed hydrogen evolution from aqueous methanol solution. It also was capable of oxygen evolution from aqueous silver nitrate

solution under UV irradiation, and its oxygen evolution activity was comparable to that observed on TiO_2.[246]

Kudo and co-workers have extensively investigated the photocatalytic activities of tungstates and molybdates.[247,248] Under UV irradiation, $Na_2W_4O_{13}$[247] and $Bi_2W_2O_9$,[145] with layered structures, were active for photocatalytic hydrogen (Pt as cocatalyst) and oxygen evolution in the presence of suitable sacrificial reagents. However, Bi_2MoO_6 with a similar structure evolved only oxygen from $AgNO_3$ aqueous solution at a low rate.[145] They also found that some scheelite-type molybdates and tungstates functioned as photocatalysts for both H_2 or O_2 evolution in the presence of sacrificial reagents.[248] The band gaps (BGs) of scheelite compounds narrowed when they were composed of Ag^+ and Bi^{3+} ions. $(NaBi)_{0.5}MoO_4$ (BG = 3.1 eV), $(AgBi)_{0.5}WO_4$ (BG = 3.2 eV), and $(AgBi)_{0.5}MoO_4$ (BG = 3.0 eV) all showed photocatalytic activity for O_2 evolution from an aqueous solution containing an electron acceptor. On the other hand, $(NaBi)_{0.5}WO_4$ (BG = 3.5 eV) produced H_2 from an aqueous solution containing an electron donor. In comparison, $(AgLn)_{0.5}MoO_4$ (Ln = La, Ce, Eu, Yb) barely produced H_2 or O_2 from aqueous solutions under UV irradiation.

Nguyen et al. developed a novel silicotungstic acid (SWA)−SiO_2 photocatalyst by impregnating of SWA on a silica support.[249] Under UV irradiation, an approximately stoichiometric production ratio of H_2 and O_2 was observed on these SWA−SiO_2 photocatalyts. The role of the photoactive sites in SiO_2 as a donor source for hydrogen formation and that of SWA as an inhibitor for the recombination of photoexcited electrons and holes were appreciable and responsible for the superior photocatalytic performance of the SWA−SiO_2 system.

3.1.4. Other d^0 Metal Oxides

Some other miscellaneous d^0 metal oxides that can catalyze water splitting to H_2 and/or O_2 under UV irradiation are described below. Wang et al. observed that a new crystal structure for nanostructured VO_2, with a body centered-cubic structure (bcc) and a large optical band gap of ~2.7 eV, surprisingly showed excellent photocatalytic activity in hydrogen production from a solution of water and ethanol under UV irradiation.[250] The bcc VO_2 phase exhibited a high quantum efficiency of ~38.7% when synthesized as nanorods. Luan and co-workers first prepared Bi_2GaVO_7 and Bi_2YVO_8 with tetragonal structures by solid-state reactions. These two compounds initiated both H_2 and O_2 evolution from pure water only under UV irradiation. This is in spite of the fact that both of them showed strong optical absorption in the visible region ($\lambda > 420$ nm).[251,252]

3.2. d^{10} Metal Oxide Photocatalyts

Various typical metal oxides with d^{10} (In^{3+}, Ga^{3+}, Ge^{4+}, Sn^{4+}, Sb^{5+}) configurations have all been shown to be effective photochemical water-splitting catalysts under UV irradiation. Of these, Ni-loaded Ga_2O_3 was one of the promising photocatalysts for overall water splitting.[253] Its photocatalytic activity could be effectively improved by the addition of Ca, Cr, Zn, Sr, Ba, and Ta ions.[254] In particular, Zn ion doping remarkably improved the photocatalytic activity, with an apparent quantum yield for Ni/Zn−Ga_2O_3 of ~20%. By combining with Lu_2O_3, the resulting Zn-doped Lu_2O_3/Ga_2O_3 proved to be a novel composite photocatalyst for stoichiometric water splitting under UV irradiation. When the system was loaded with NiO as the cocatalyst, the quantum yield at 320 nm was estimated to be 6.81%.[255] For solid solutions consisting of Ga_2O_3 and In_2O_3, $Ga_{1.14}In_{0.86}O_3$ showed the highest photocatalytic activity for H_2 evolution from aqueous methanol solutions and for O_2 evolution from aqueous silver nitrate solutions.[256] In comparison, the solid solutions of Y_2O_3 and In_2O_3, $Y_{1.3}In_{0.7}O_3$, showed the highest photocatalytic activity for the overall water splitting when combined with RuO_2 as a promoter.[257]

Inoue and co-workers investigated the photocatalytic properties for water decomposition of alkali metal, alkaline earth metal, and lanthanum indates with an octahedrally coordinated In^{3+} d^{10} configuration ion.[258−262] The photocatalytic activity for water decomposition under UV irradiation was considerably large for RuO_2-dispersed $CaIn_2O_4$, $SrIn_2O_4$, and $Sr_{0.93}Ba_{0.07}In_2O_4$ but very poor for RuO_2-dispersed $AInO_2$ (A = Li, Na) and $LnInO_3$ (Ln = La, Nd). The geometric structures of the InO_6 octahedral units for these indates were compared. It was shown that the photocatalytically active indates possessed distorted InO_6 octahedra with dipole moments. The internal fields that arose because of the dipole moment promoted the charge separation in the very initial process of photoexcitation. In addition, the broad sp conduction bands with large dispersions permitted the photoexcited electrons to move to the dispersed promoter RuO_2 particles. A group of p-block metal oxides was reported to have stable activity in decomposing water to H_2 and O_2 under UV irradiation when combined with RuO_2 or Pt as cocatalyt.[261−268] They consist of metal ions with d^{10} configurations and have distorted octahedral and/or tetrahedral structures. For example, the distorted SbO_6 octahedra in $M_2Sb_2O_7$ (M = Ca, Sr),[263] $CaSb_2O_6$,[263] and $NaSbO_3$,[263] the distorted GeO_4 tetrahedra in Zn_2GeO_4,[265] and the distorted InO_6 octahedra and GeO_4 tetrahedra in $LiInGeO_4$[266] were dominantly responsible for photocatalytic activity for water decomposition. Some other metal oxides with d^{10} configuration such as $ZnGaO_4$,[264] Sr_2SnO_4,[261] and $SrSnO_3$[267,268] were also reported to show photocatalytic activity for water splitting.

3.3. f^0 Metal Oxide Photocatalysts

The f-block metal oxides usually combined with other metal oxides as photocatalysts. Pure CeO_2 powder was reported to show a consistent activity toward O_2 production in aqueous solutions containing Fe^{3+} and Ce^{4+} as electron acceptors.[269] Sr^{2+}-doped CeO_2 was an active photocatalyst for overall water splitting when RuO_2 was loaded as a promoter.[270] Ce(III) oxide supported zeolites showed higher photocatalytic activity for pure water splitting.[271] Nonstoichiometric H_2 and O_2 evolution was observed. Photoirradiation of Ce^{3+} species generated electrons ($Ce^{3+} + h\nu \rightarrow Ce^{4+} + e^-$) that were captured effectively by a water molecule for the production of hydrogen. Yuan et al. reported that $BaCeO_3$ produced H_2 and O_2 from aqueous solutions containing CH_3OH and $AgNO_3$ sacrificial reagents, respectively. It also showed some activity under UV irradiation for overall water splitting with the aid of RuO_2 loading.[272]

3.4. Nonoxide Photocatalysts

More than 25 years ago, efficient hydrogen production was achieved by irradiating suspensions of ZnS in SO_3^{2-} solutions under UV irradiation. The quantum yield was determined to be 90% at 313 nm. This was even without any noble metal as cocatalyst.[273] InP, the sole phosphide photocatalyst

developed so far, can also produce H_2 from water containing inorganic sacrificial reducing agents.[274] Aqueous sulfite solutions are particularly efficient.

For the past few years, there have been a few reports on nonoxide photocatalyts capable of decomposing pure water into H_2 and O_2 under UV irradiation. Maeda et al. found that the photocatalytic water-splitting activity of GaN is strongly dependent on the crystallinity of the material and the cocatalyst employed.[275] Modification of well-crystallized GaN with $Rh_{2-y}Cr_yO_3$ nanoparticles as a cocatalyst for H_2 evolution resulted in the stable stoichiometric decomposition of H_2O into H_2 and O_2 under UV irradiation. RuO_2 modification, on the other hand, did not bring about appreciable H_2 and O_2 evolution. However, Zn^{2+}, Mg^{2+}, and Be^{2+} doping of GaN converted it into a remarkably active and stable photocatalyst.[276] Again, the presence of RuO_2 as a cocatalyst was required.[276]

β-Ge_3N_4 was another effective nitride photocatalyst to show efficient activity for splitting water into hydrogen and oxygen when combined with RuO_2 nanoparticles reported by Domen's group.[24,277,278] The photocatalytic activity of RuO_2-loaded β-Ge_3N_4 was strongly dependent on the reaction conditions employed. The highest activity was obtained when the reaction was carried out in 1 M H_2SO_4 aqueous solution. Moreover, treatment of as-prepared β-Ge_3N_4 powder under high-pressure ammonia effectively increased the photocatalytic activity by up to 4 times. This was attributed to a decrease in the density of anion defects in the bulk and surface.[279] The $AgBr/SiO_2$ catalyst prepared from a Schumann emulsion showed a stable and high photocatalytic activity for H_2 generation from CH_3OH/H_2O solution under UV irradiation. The high activity of this $AgBr/SiO_2$ catalyst related to photogenerated Ag species, which could act as the site for H_2 formation.[280]

4. Approaches to Modifying the Electronic Band Structure for Visible-Light Harvesting

With a view to developing photocatalytic applcations using visible-light irradiation, beginning with the photocatalytic splitting of water into H_2 and O_2 using TiO_2 under UV irradiation,[18] prophase studies were also carried out on some narrow band gap semiconductors such as CdS[281,282] and WO_3.[283−285] However, the fact that serious photocorrosion of CdS was observed in the photocatalytic reaction[286−288] and that the relatively positive conduction band of WO_3 proved dissatisfactory for hydrogen production[284] created the major impediments for the efficient performance of these two photocatalysts for use in visible-light-driven water splitting. Some studies were carried out to improve the photocatalytic stability of CdS,[288−292] whereas others used WO_3 as the photoelectrode in the photoelectrochemical cell to satisfy the energy requirement for water splitting with an applied potential.[293−299] To overcome these obstacles, many efforts has been made to develop new visible-light-driven photocatalysts with high water-splitting activities. These are shown in Table 2. On the basis of numerous experimental results from the past 20 years, several common approaches have been adopted in order to make photocatalysts visible-light active for water splitting into hydrogen and/or oxygen: (1) metal or/and nonmetal ions doping for band gap narrowing; (2) developing solid solutions to control the band structure; (3) dye sensitization to make UV-light-active photocatalysts harvest visible light; (4) developing novel single-phase Vis-active photocatalysts through band gap engineering.

4.1. Metal and Nonmetal Doping

4.1.1. Metal Ion Doping

One of the most effective ways to develop visible-light-driven photocatalysts is to create impurity levels in the forbidden band through metal ion doping. This makes the wide band gap photocatalysts active in the visible-light region, and this approach has been known for a long time. Over the past decades, there have been numerous reports on the modification of wide band gap photocatalysts using metal ion doping to make them visible-light active. These include doped TiO_2,[300−303] doped $SrTiO_3$,[303,304] doped $La_2Ti_2O_7$,[305] and doped ZnS,[306,307] among others. Figure 6 depicts the sketch of visible-light-driven photocatalysts by metal ion doping to create active photocatalysts with wide band gaps. In the forbidden band, either a donor level above the original valence band or an acceptor level below the original conduction band is created to make the photocatalysts respond to visible light.

As early as 1982, Borgarello et al. found that Cr^{5+}-doped TiO_2 could produce hydrogen and oxygen via sustained water cleavage under visible-light (400−550 nm) irradiation.[308] Until now, many different metal ions have been doped into TiO_2 to improve the visible-light absorption and photocatalytic activities. These include ions such as V, Ni, Cr, Mo, Fe, Sn, Mn, and so on.[300−314] The electronic structures of TiO_2 compounds doped with the 3d transition metals (V, Cr, Mn, Fe, Co, and Ni) were analyzed by Umebayashi et al. using ab initio band calculations (Figure 7A).[315] They found that the 3d metal doping created an occupied level either in the band gap or in valence band (VB) due to the t_{2g} state of the dopant. The charge-transfer transition between this t_{2g} level and the conduction band (CB) (or VB) of TiO_2 contributed to the photoexcitation under visible light. Using DV-X_α calculations, Nishikawa et al. demonstrated the possibility of shifing the absorption edge of titania to the sunlight region in the case of V-, Cr-, Mn-, Fe-, Co-, Ni-, or Rh-doping and then discussed the relationship between the ionic radius and the change of the band gap (Figure 7B)[316] and found that, of the cations addressed, Ni^{3+} and V^{5+} reduced the band gap most effectively. Cao et al. reported that Sn^{4+}-doped TiO_2 nanoparticle films prepared by the chemical vapor deposition (CVD) method displayed a higher photocatalytic activity than pure TiO_2 under both UV and visible light.[317] The visible-light absorption can be assigned to an electronic transition from the valence band to the doping energy level of the Sn^{4+} ions. This was located 0.4 eV below the conduction band and acted as an electron acceptor level. In contrast, Klosek and Raftery demonstrated that the visible absorption in V^{4+}-doped TiO_2 was indicative of the photoexcitation from the V 3d electron donor level to the TiO_2 conduction band.[318] This brings in a more efficient visible-light-driven activity for ethanol photooxidation over V^{4+}-doped TiO_2 than than of pure TiO_2. The visible-light-driven photocatalytic activity of Fe^{3+}-doped TiO_2 for water splitting was also attributed to the photoexcitation of doping the donor level (i.e., Fe 3d orbitals) to the TiO_2 conduction band.[319−321]

Anpo and co-workers prepared various metal-ion-doped TiO_2 materials using advanced ion implantation.[322−327] They found that the absorption band of metal-ion-implanted TiO_2 (the metals used were V, Cr, Mn, Fe, and Ni) shifted smoothly toward the visible-light region. The extent of the red shift depended on the amount and type of metal ions

Table 2. Visible-Light-Driven Photocatalysts for Water Splitting to Hydrogen and/or Oxygen

Semiconductor photocatalysts for water splitting under visible-light irradiation									
						activity (μmol·h^{-1}·g^{-1})			
photocatalyst	synthetic method	mass (g)	light source	incident light	aqueous reaction solution	cocatal./H_2	cocatal./O_2	QY (%)	reference
TiO_2:Cr	thermal hydrolysis	0.025	450-W Xe	>415 nm	pure water, HCl (pH = 3)	Pt−RuO_2/268	Pt−RuO_2/52		308
TiO_2:Fe	hydrothermal method	0.5	300-W Xe	>400 nm	pure water	3.6			319
TiO_2:Sb/Ni	solid-state reaction	0.5	300-W Xe	>420 nm	methanol/$AgNO_3$	0	25.6		303
TiO_2:Sb/Cr	solid-state reaction	0.5	300-W Xe	>420 nm	methanol/$AgNO_3$	Pt/0.12	63		303
TiO_2:Sb/Rh	solid-state reaction	0.3	300-W Xe	>440 nm	$AgNO_3$		37		332
TiO_2:Ru	solid-state reaction	0.1	500-W Xe	>440 nm	$FeCl_3$		~21.3	0.14 (435 nm)	336
Pt-ionized TiO_2	hydrothermal method	0.5	300-W Xe	>400 nm	pure water	4.6	2.3		337
Ir-ionized TiO_2	hydrothermal method	0.5	300-W Xe	>400 nm	pure water	2.54	1.27		338
Co-ionized TiO_2	hydrothermal method	0.5	300-W Xe	>400 nm	pure water	1.34	0.67		338
TiO_2:Ti^{3+}	radiofrequency magnetron sputtering deposition		500-W Xe	>420 nm	methanol/$AgNO_3$	Pt/0.09	0.5		340
$InTaO_4$:Ni	solid-state reaction	0.5	300-W Xe	>420 nm	pure water	NiO_y/33.2	NiO_y/16.6	0.66 (402 nm)	353
$BiYWO_6$	solid-state reaction	0.3	500-W Xe	>420 nm	pure water	RuO_2/13.7	RuO_2/6.3	0.17 (420 nm)	559
$Bi_{0.5}Dy_{0.5}VO_4$	solid-state reaction	0.2	300-W Xe	>420 nm	pure water	Pt−Cr_2O_3/18.2	Pt−Cr_2O_3/9.6		560
$LiCr(WO_4)_2$	polymer complex method	0.5/0.3	300-W Xe	=420 nm/>420 nm	methanol/$AgNO_3$	Pt/2.4	4.17		660
$NiNb_2O_6$	solid-state reaction	0.5	300-W Xe	>420 nm	pure water	~0.36			661
$NiTa_2O_6$	solid-state reaction	0.5	300-W Xe	>420 nm	pure water	~0.4			661
$InVO_4$	solid-state reaction	0.5	300-W Xe	>420 nm	pure water	NiO_x/5			668
$InNbO_4$	solid-state reaction	0.5	300-W Xe	>420 nm	pure water	NiO_x/3.5			668, 691
$InTaO_4$	solid-state reaction	0.5	300-W Xe	>420 nm	pure water	NiO_x/4.0			668, 691
$CaCo_{1/3}Nb_{2/3}O_3$	solid-state reaction	0.5	300-W Xe	>420 nm	pure water	NiO_x/1.72			680, 681
$SrCo_{1/3}Nb_{2/3}O_3$	solid-state reaction	0.5	300-W Xe	>420 nm	pure water	NiO_x/1.72			680, 681
$BaCo_{1/3}Nb_{2/3}O_3$	solid-state reaction	0.5	300-W Xe	>420 nm	pure water	NiO_x/2.74			680, 681
$SrTiO_3$:Sb/Cr	solid-state reaction	0.5	300-W Xe	>420 nm	methanol/$AgNO_3$	Pt/156	1.8		303
$SrTiO_3$:Ru	solid-state reaction	0.3	300-W Xe	>440 nm	methanol/$AgNO_3$	Pt/5.7	13		344
$InTaO_4$:Ni	solid-state reaction	0.5	300-W Xe	>420 nm	pure water	33.2	16.6	0.66 (402 nm)	353−355
$BiTaO_4$:Cu	solid-state reaction	0.1	350-W Xe	>400 nm	methanol	RuO_2/878			359
$NaNbO_3$:Ir/Sr	solid-state reaction	0.3	300-W Xe	>420 nm	methanol/$AgNO_3$	Pt/36.7	16		361
$NaTaO_3$:Ir/La	solid-state reaction	0.3	300-W Xe	>420 nm	methanol/$AgNO_3$	Pt/36.7	0		361
$Bi_xIn_{1-x}TaO_4$	solid-state reaction	0.5	300-W Xe	>420 nm	methanol/$AgNO_3$	Pt/2.14	24.02		552
$AgNbO_3$	solid-state reaction	0.3	300-W Xe	>420 nm	methanol/$AgNO_3$	Pt/1.7	123.3		242
$BaCr_2O_4$	solid-state reaction	0.5	300-W Xe	>540 nm/>420 nm	methanol/$Ce(SO_4)_2$	Pt/~10	7.5		658
$PbBi_4Ti_4O_{15}$	solid-state reaction	0.3	450-W Xe	>400 nm	methanol/$AgNO_3$	Pt/37.3	1443.3	0.27/21 (>400 nm)	707
$PbBi_2Nb_2O_9$	solid-state reaction	0.3	450-W Xe	>420 nm	methanol/$AgNO_3$	Pt/25.3	1733.3	0.95/29 (>420 nm)	707, 708
$PbTiO_3$	solid-state reaction	0.3	450-W Xe	>400 nm	methanol/$AgNO_3$	Pt/45.3	1743.3	0.33/28 (>400 nm)	707
$SnNb_2O_6$	solid-state reaction	0.3	300-W Xe	>420 nm	methanol/$AgNO_3$	Pt/60	0		243, 709
$SnNbO_2$	solid-state reaction	0.3	300-W Xe	>420 nm	methanol/$AgNO_3$	Pt/48	IrO_2/209.3		710
$In_2O_3(ZnO)_9$	solid-state reaction	1	300-W Xe	>420 nm	methanol/$AgNO_3$	Pt/1.1	1.3		724
$H(Rb)Pb_2Nb_3O_{10}$	solid-state reaction, ion-exchange	1	500-W Xe	>420 nm	methanol/$AgNO_3$	Pt/24	1.1	5/−(420−500 nm)	959
$Sn^{2+}/K_4Nb_6O_{17}$	solid-state reaction, ion-exchange	0.2	300-W Xe	>420 nm	methanol/$AgNO_3$	Pt/115	20		711
$Sn^{2+}/KTiNbO_5$	solid-state reaction, ion-exchange	0.2	300-W Xe	>420 nm	methanol/$AgNO_3$	Pt/270	0		711
$Sn^{2+}/CsTi_2NbO_7$	solid-state reaction, ion-exchange	0.2	300-W Xe	>420 nm	methanol/$AgNO_3$	Pt/90	0		711
$Sn^{2+}/K_2Ti_4O_9$	solid-state reaction, ion-exchange	0.2	300-W Xe	>420 nm	methanol/$AgNO_3$	Pt/115	0		711
$Sn^{2+}/K_2Ti_2O_5$	solid-state reaction, ion-exchange	0.2	300-W Xe	>420 nm	methanol/$AgNO_3$	Pt/25	0		711
$Sn^{2+}/Cs_2Ti_6O_{13}$	solid-state reaction, ion-exchange	0.2	300-W Xe	>420 nm	methanol/$AgNO_3$	Pt/35	0		711
$K_{0.5}La_{0.5}Ca_{0.75}Pb_{0.75}Nb_3O_{10}$	solid-state reaction	0.3	450-W Xe	>400 nm	methanol/$AgNO_3$	Pt/traces	413.3	−/6(>400 nm)	707
$K_{0.5}La_{0.25}Bi_{0.25}Ca_{0.75}Pb_{0.75}Nb_3O_{10}$	solid-state reaction	0.3	450-W Xe	>400 nm	methanol/$AgNO_3$	Pt/traces	560	−/8(>400 nm)	707
Ca_2NiWO_6	solid-state reaction	0.5	300-W Xe	>420 nm	methanol/$AgNO_3$	Pt/0	0.7		664
$BaCrO_4$	solid-state reaction	0.5	300-W Xe	>420 nm	methanol/$AgNO_3$	Pt/1.34	0		657
$SrCrO_4$	solid-state reaction	0.5	300-W Xe	>420 nm	methanol/$AgNO_3$	Pt/0.18	0		657
$SrTiO_3$:Rh	solid-state reaction	0.3	300-W Xe	>440 nm	methanol	Pt/390		5.2 (420 nm)	344
$SrTiO_3$:Ir	solid-state reaction	0.3	300-W Xe	>440 nm	methanol	Pt/28.7			344

Table 2. Continued

Semiconductor photocatalysts for water splitting under visible-light irradiation									
						activity (μmol·h^{-1}·g^{-1})			
photocatalyst	synthetic method	mass (g)	light source	incident light	aqueous reaction solution	cocatal./H_2	cocatal./O_2	QY (%)	reference
$SrTiO_3$:Mn	solid-state reaction	0.3	300-W Xe	>440 nm	$AgNO_3$		9		344
$CaTiO_3$:Rh	solid-state reaction	0.3	300-W Xe	>420 nm	methanol	Pt/28.3			346
$CaTiO_3$:Cu	sol−gel method	0.1	350-W Xe	>400 nm	methanol	NiO_x/22.7			347
$Ca_3Ti_2O_7$:Rh	solid-state reaction	0.3	300-W Xe	>420 nm	methanol	Pt/7			348
$BaNi_{1/3}Nb_{2/3}O_3$	solid-state reaction	0.5	300-W Xe	>420 nm	methanol	Pt/0.74			178, 225
$La_2Ti_2O_7$:Cr	citrate complex method	0.5	500-W Hg	>420 nm	methanol	Pt/30			305, 349
$La_2Ti_2O_7$:Fe	citrate complex method	0.5	500-W Hg	>420 nm	methanol	Pt/20			305, 349
$K_2La_2Ti_3O_{10}$:Fe	solid-state reaction	0.1		visible light	Na_2S/Na_2SO_3	~0.27			350
$K_2La_2Ti_3O_{10}$:W	solid-state reaction	0.1	—	visible light	Na_2S/Na_2SO_3	~0.06			350
$K_4Nb_6O_{17}$:Ni	solid-state reaction	0.2	500-W H	400−800 nm	methanol	144			358
$Bi_4Ti_3O_{12}$:Cr	sol−gel method	0.1	300-W Xe	>400 nm	methanol	58.1			360
$NaTaO_3$:La/Cr	solid-state reaction	0.5	300-W Xe	>420 nm	methanol	Pt/4.4			362
$K_2La_2Ti_3O_{10}$:V	sol−gel method	1	250-W Xe		KI	RuO_2/42.2			351
$K_2La_2Ti_3O_{10}$:Zn	sol−gel method	1	250-W Xe		KI	RuO_2/55.5			140
In_2TiO_5:V	solid-state reaction	0.1	500-W H		pure water	Pt/~50	Pt/~220		352
$Na(Bi_xTa_{1-x})O_3$	hydrothermal method	0.1	350-W Xe	>400 nm	methanol	NiO/75			556
$CsLaSrNb_2NiO_9$	solid-state reaction	0.5	300-W Xe	>420 nm	methanol	Pt/0.6			662
$In_{12}NiCr_2Ti_{10}O_{42}$	solid-state reaction	0.5	300-W Xe	>420 nm	methanol	Pt/16.4			665, 666
Zn/Cr layered double hydroxides	coprecipitation method	0.045	200-W Xe	>400 nm	$AgNO_3$		1073.3	60.9 (410 nm)	667
$Na_{0.9}La_{0.1}Ta_{0.9}Co_{0.1}O_3$	solid-state reaction	0.5	300-W Xe	>420 nm	methanol	Pt/8.68			553
$Nd_2Zr_2O_7$	solid-state reaction	—	500-W Xe	390−520 nm	pure water	0.09			154
$Sm_2Zr_2O_7$	solid-state reaction	—	500-W Xe	390−520 nm	pure water	0.01			154
$K_4Ce_2Ta_{10}O_{30}$	solid-state reaction	0.1	300-W Xe	>420 nm	Na_2SO_3	NiO_x/337.5			714
$K_4Ce_2Nb_{10}O_{30}$	solid-state reaction	0.1	300-W Xe	>420 nm	Na_2SO_3	NiO_x/104			714
Sm_2InTaO_7	solid-state reaction	1	250-W Xe	>400 nm	pure water	NiO_x/4.6			715
Sm_2InNbO_7	solid-state reaction	1	250-W Xe	>400 nm	methanol/$AgNO_3$	Pt/3.75	3.52		716
WO_3	Puratronic WO_3	0.2	900-W Xe	>410 nm	$AgNO_3$		RuO_2/67		284, 929
Cs−WO_3	ion-exchange method	0.4	300-W Xe	>420 nm	Fe^{3+}		490	19 (420 nm)	285
$Ca_{1-x}Bi_xV_xMo_{1-x}O_4$	solid-state reaction	0.5	300-W Xe	>420 nm	$AgNO_3$		201.4	10 (420 nm)	554
$Na_{0.5}Bi_{1.5}VMoO_8$	solid-state reaction	0.5	300-W Xe	>420 nm	$AgNO_3$		144	6.3 (420 nm)	555
$(AgNbO_3)_{0.75}(SrTiO_3)_{0.25}$	solid-state reaction	0.5	300-W Xe	>410 nm	$AgNO_3$		324	16.4 (420.4 nm)	558
$BiVO_4$	precipitation	1	300-W Xe	>420 nm	$AgNO_3$		478	9 (450 nm)	669−671
$Zn_{2.5}VMoO_8$	solid-state reaction	0.5	300-W Xe	>420 nm	$AgNO_3$		~12.6		675
$Mg_{2.5}VMoO_8$	solid-state reaction	0.5	300-W Xe	>420 nm	$AgNO_3$		~5.4		675
$Mg_3V_2O_8$	solid-state reaction	0.5	300-W Xe	>420 nm	$AgNO_3$		7.2	0.23 (420 nm)	676
$Zn_3V_2O_8$	solid-state reaction	0.5	300-W Xe	>420 nm	$AgNO_3$		20.4	0.64 (420 nm)	676
$CaBiVMoO_8$	solid-state reaction	0.5	300-W Xe	>420 nm	$AgNO_3$		105.9		677
$CaBiVWO_8$	solid-state reaction	0.5	300-W Xe	>420 nm	$AgNO_3$		30		677
$AgInW_2O_8$	solid-state reaction	0.5	300-W Xe	>420 nm	$AgNO_3$		7.2		685
$AgLi_{1/3}Ti_{2/3}O_2$	molten reaction	0.2	300-W Xe	>420 nm	$AgNO_3$		165	1.9 (420 nm)	687
$AgLi_{1/3}Sn_{2/3}O_2$	molten reaction	0.2	300-W Xe	>420 nm	$AgNO_3$		120	1.3 (420 nm)	687
$PbMoO_4$:Cr	reflux method	0.5	300-W Xe	>420 nm	$AgNO_3$		143	6 (420 nm)	363
Bi_2WO_6	solid-state reaction	1	300-W Xe	>420 nm	$AgNO_3$		3		145
Bi_2MoO_6	reflux method	0.5	300-W Xe	>420 nm	$AgNO_3$		110		700
$Bi_2Mo_3O_{12}$	solid-state reaction	0.5	300-W Xe	>420 nm	$AgNO_3$		15.2		700
β-$SnWO_4$	solid-state reaction	0.3	300-W Xe	>400 nm	methanol	Pt/1.8			712
Ag_3VO_4	solid-state reaction	0.3	300-W Xe	>420 nm	$AgNO_3$		56.7		684
TiO_2:Rh	impregnation and calcination	0.1	500-W Xe	>440 nm	$FeCl_3 + H_2SO_4$ (pH = 2.4)		7.8	0.14 (435 nm)	336
$BiCu_2VO_6$	solid-state reaction	0.5	300-W Xe	>420 nm	Fe^{3+}		13	1.8 (420 nm)	678
$BiZn_2VO_6$	solid-state reaction	0.8	300-W Xe	>420 nm	Fe^{3+}		2.3	0.76 (420 nm)	679
$Ca_2Fe_2O_5$	sol−gel method	0.1	150-W Xe	visible light	CO_2/H_2O	NiO/1565			683
Nb_2O_5:C	sol−gel method	0.2	300-W Xe	>420 nm	methanol	Pt/7			481
$ZnFe_2O_4$	hydrothermal method	0.1	350-W Xe	>420 nm	pure water	17.03			986
Ag_3PO_4	ion-exchange method	0.5	300-W Xe	>400 nm	$AgNO_3$		1272	80 (480 nm)	717
$Li_9Fe_3(P_2O_7)_3(PO_4)_2$	hydrothermal method	0.1	350-W Xe	>400 nm	KI	3.9			718

Table 2. Continued

Semiconductor photocatalysts for water splitting under visible-light irradiation									
						activity (μmol·h^{-1}·g^{-1})			
photocatalyst	synthetic method	mass (g)	light source	incident light	aqueous reaction solution	cocatal./H_2	cocatal./O_2	QY (%)	reference
CdS	two-step precipitation	0.15	300-W Xe	>420 nm	$Na_2S + Na_2SO_3$	Pt/27333		60 (420 nm)	281, 728, 730, 732, 927, 957
CdS	precipitation	0.1	300-W Xe	>420 nm	lactic acid	MoS_2/5400			782
CdS	precipitation and hydrothermal method	0.3	300-W Xe	>420 nm	$Na_2S + Na_2SO_3$	Pt-PdS/29 233		93 (420 nm)	733
CdS	precipitation	0.1	500-W Hg	>420 nm	$Na_2S + Na_2SO_3$	WC/~1350			786
CdSe	low-temperature solution-phase synthesis	0.01	700-W Hg	>400 nm	$Na_2S + Na_2SO_3$	436	−	13.4 (>400 nm)	974
CdS:Ag	precipitation	0.4	900-W Xe		$Na_2S + Na_2SO_3$	Pt/33480		~25 (450 nm)	282
CdS:In/Cu	hydrothermal method	0.1	300-W W−H[b]	>420 nm	$Na_2S + K_2SO_3$	Pt/2456		26.5 (420 nm)	366
CdS:Mn	hydrothermal method	0.2	500-W Xe	>420 nm	$Na_2S + K_2SO_3$	RuO_x/1935		7 (>420 nm)	367
CdS-ZnS	precipitation	0.1	300-W Hg	>400 nm	$Na_2S + Na_2SO_3$	2007		0.60 (>400 nm)	373, 529, 534, 535
CdS-ZnS	H_2S thermal sulfurization	0.2	350-W Xe	>430 nm	$Na_2S + Na_2SO_3$	900		10.2 (420 nm)	536
$Cd_{0.1}Zn_{0.9}S$:Ni	hydrothermal method	0.2	350-W Xe	>420 nm	$Na_2S + Na_2SO_3$	Pt/585.5		15.9 (420 nm)	374
$Cd_{0.1}Cu_{0.01}Zn_{0.89}S$	precipitation	0.3	350-W Xe	>430 nm	$Na_2S + Na_2SO_3$	1166.7		9.2 (420 nm)	368
$(Zn_{0.95}Cu_{0.05})_{0.67}Cd_{0.33}S$	precipitation	0.3	300-W Xe	>420 nm	$Na_2S + Na_2SO_3$	Pt/3633.3		31.8 (420 nm)	369−371
CdS-ZnS:Ag	precipitation	0.4	900-W Xe		$Na_2S + Na_2SO_3$	Pt/40957.5		37 (450 nm)	282
ZnS:Cu	precipitation	1	300-W Xe	>420 nm	Na_2SO_3	450		3.7 (420 nm)	306
ZnS:Ni	precipitation	1	300-W Xe	>420 nm	$Na_2S + K_2SO_3$	280		1.3 (420 nm)	307
ZnS:Ni	ultrasonic spray pyrolysis	0.1	300-W Xe	>400 nm	$K_2SO_3 + Na_2S$	160		2.1 (430 nm)	365
ZnS:Pb/Cl	precipitation and heat treatment	1	300-W Xe	>420 nm	$K_2SO_3 + Na_2S$	93			527
ZnS:C	solvothermal and calcination	0.1	500-W Hg	>420 nm	$Na_2S + Na_2SO_3$	Pt/~90			501
In_2S_3	hydrothermal method	0.05	300-W Xe	>400 nm	$Na_2S + Na_2SO_3$	Pd/960.2			891
$AgInZn_7S_9$	precipitation and calcination	0.3	300-W Xe	>420 nm	$Na_2S + Na_2SO_3$	Pt/3164.7		20 (420 nm)	537
$Cu_{0.09}In_{0.09}Zn_{1.82}S_2$	precipitation and calcination	0.3	300-W Xe	>420 nm	$Na_2S + Na_2SO_3$	Pt/4090		12.5 (420 nm)	538
$Cu_{0.25}Ag_{0.25}In_{0.5}ZnS_2$	precipitation and calcination	0.3	300-W Xe	>420 nm	$Na_2S + Na_2SO_3$	Ru/7666.7		7.4 (520 nm)	540, 541
$ZnIn_2S_4$	hydrothermal method	0.3	300-W Xe	>420 nm	$Na_2S + Na_2SO_3$	Pt/231			375
$ZnIn_2S_4$	surfactant-assisted hydrothermal method	0.2	300-W Xe	>430 nm	$Na_2S + Na_2SO_3$	Pt/562		18.4 (420 nm)	377, 915
$ZnIn_2S_4$:Cu	surfactant-assisted hydrothermal method	0.2	300-W Xe	>430 nm	$Na_2S + Na_2SO_3$	Pt/757.5		14.2 (420 nm)	378
$AgGaS_2$	solid-state reaction	0.1	500-W Hg	>420 nm	$Na_2S + Na_2SO_3$	Pt/2960		12.4 (>420 nm)	496, 873
$CuGa_3S_5$	solid-state reaction	0.05	300-W Xe	>420 nm	$Na_2S+Na_2SO_3$	NiS/~2800		1.3 (420−520 nm)	498
Ag_2ZnSnS_4	precipitation and calcination	0.3	300-W Xe	>420 nm	$Na_2S + K_2SO_3$	Ru/1607		3 (500 nm)	542
Cu_2ZnGeS_4	precipitation and calcination	0.3	300-W Xe	>420 nm	$Na_2S + K_2SO_3$	Ru/1233			542
$CuGa_2In_3S_8$	solid-state reaction	0.3	300-W Xe	>420 nm	$Na_2S + K_2SO_3$	Rh/10667		15 (560 nm)	543
$AgGa_2In_3S_8$	solid-state reaction	0.3	300-W Xe	>420 nm	$Na_2S + K_2SO_3$	Rh/3433		15 (490 nm)	543
$AgGa_{0.9}In_{0.1}S_2$	solid-state reaction	0.1	500-W Hg	>420 nm	$Na_2S + Na_2SO_3$	Pt/3500			544
$ZnS-In_2S_3-Ag_2S$	hydrothermal method	0.015	300-W Xe	>400 nm	$Na_2S + Na_2SO_3$	220 000		19.8 (420 nm)	545
$ZnS-In_2S_3-CuS$	hydrothermal method	0.01	300-W Xe	>400 nm	$Na_2S+Na_2SO_3$	360 000		22.6 (420 nm)	546
$NaInS_2$	prepicipation and calcination	0.7	300-W Xe	>420 nm	Na_2SO_3	Pt/671.4		6 (440 nm)	500
$CdIn_2S_4$	hydrothermal method	0.5	450-W Xe	>420 nm	$H_2S + KOH$	6960		17.1 (500 nm)	1010
$AgIn_5S_8$	precipitation, calcination	0.3	300-W Xe	>420 nm	$K_2SO_3 + Na_2S$	Pt/200		5.3 (411.2 nm)	497
$CuInS_2$	solvothermal method	0.25	500-W Xe	>420 nm	$Na_2S + Na_2SO_3$	Pt/84			492, 493
$CuIn_5S_8$	precipitation, calcination	0.5	400-W Xe		Na_2SO_3	Pt/~1.4		<0.0002 (460 nm)	492

Table 2. Continued

Semiconductor photocatalysts for water splitting under visible-light irradiation									
						activity (μmol·h^{-1}·g^{-1})			
photocatalyst	synthetic method	mass (g)	light source	incident light	aqueous reaction solution	cocatal./H_2	cocatal./O_2	QY (%)	reference
$Na_{14}In_{17}Cu_3S_{35}\cdot xH_2O$	hydrothermal method	0.5	300-W Xe	>420 nm	Na_2S	18		3.7 (420 nm)	954
$Cu_8Ge_5S_{16}^{4-}$	solvothermal method	0.5	300-W Xe	>400 nm	Na_2SO_3	2.64			956
TiO_2:S	precursor heat-treatment	0.3	500-W Xe	>420 nm	ethanol	Pt/∼0.5			440
$In(OH)_3$:S/Zn	hydrothermal method	0.3	300-W Xe	>420 nm	$Na_2S + Na_2SO_3$	Pt/223.3		0.59 (420 nm)	528
$Sm_2Ti_2S_2O_5$	H_2S thermal sulfurization or solid-state reaction	0.2	300-W Xe	>440 nm	$Na_2S + Na_2SO_3/AgNO_3$	Pt/110	110	0.3/0.7 (440−650 nm)	485, 486, 488
$Gd_2Ti_2S_2O_5$	H_2S thermal sulfurization	0.2	300-W Xe	>440 nm	$Na_2S + Na_2SO_3/AgNO_3$	Pt/105	120	0.1/− (440−650 nm)	488
La−In oxysulfide	solid-state reaction	0.1	300-W Xe	>420 nm	$Na_2S + Na_2SO_3/AgNO_3$	Pt/∼85	IrO_2/∼26	0.2/0.1 (420−600 nm)	489, 490
La−Ga oxysulfide	solid-state reaction	0.1	300-W Xe	>420 nm	$Na_2S + Na_2SO_3/AgNO_3$	Pt/1080	IrO_2/∼10	2.5/0.2 (420−600 nm)	490
$La_{10}OS_{14}$	H_2S thermal sulfurization	0.2	500-W Xe	>500 nm	$Na_2S + Na_2SO_3$	Ru/0.45			491
$La_4In_5S_{13}$	H_2S thermal sulfurization	0.2	500-W Xe	>500 nm	$Na_2S + Na_2SO_3$	Pt/0.5			491
$ZnS_{1-x-0.5y}O_x(OH)_y$	coprecipitation, calcination	0.1	400-W H	>420 nm	$Na_2S + Na_2SO_3$	∼460		3.0 (400−700 nm)	547
ZrW_2O_8:S	hydrothermal method	0.1	300-W Hg−Xe	>400 nm	$AgNO_3$		∼50		484
$(Ga_{0.88}Zn_{0.12})(N_{0.88}O_{0.12})$	NH_3 nitridation, postcalcination	0.3	450-W Hg	>400 nm	pure water + H_2SO_4 (pH = 4.5)	$Rh_{2-y}Cr_yO_3$/2800	$Rh_{2-y}Cr_yO_3$/1400	5.9 (420−440 nm)	563, 564, 567, 569−571, 575, 767−770, 773
$Zn_{1.6}GeN_{1.7}O_{0.5}$	NH_3 nitridation, postcalcination	0.1	450-W Hg	>400 nm	pure water	$Rh_{2-y}Cr_yO_3$/3160	$Rh_{2-y}Cr_yO_3$/1580	2.0 (420−440 nm)	577−580
TaON	NH_3 nitridation	0.4	300-W Xe	>420 nm	ethanol/$AgNO_3$	Ru/300	1650	2.1/34 (420−500 nm)	390, 468, 469, 740
Ta_3N_5	NH_3 nitridation	0.2	300-W Xe	>420 nm	methanol/$AgNO_3$	Pt/∼125	2100	−/10 (420−600 nm)	390, 470, 894
$LaTiO_2N$	NH_3 nitridation	0.2	300-W Xe	>420 nm	methanol/$AgNO_3$	Pt/∼15	51	0.15/1.5 (420−600 nm)	475, 476
$Sr_2Nb_2O_7$:N	NH_3 nitridation	0.1	200-W Xe	>400 nm	methanol/$AgNO_3$	Pt/93	trace		399
$Y_2Ta_2O_5N_2$	NH_3 nitridation	0.3	300-W Xe	>420 nm	ethanol/$AgNO_3$	Pt−Ru/833	467		393
Zr_2ON_2	NH_3 nitridation	0.2/0.05	300-W Xe	>420 nm	methanol/$AgNO_3$	Pt/7	46		396
$Zn_xTiO_yN_z$	NH_3 nitridation	0.2	300-W Xe	>420 nm	methanol/$AgNO_3$	Pt/0.4	400		482
$(SrTiO_3)_{1-x}\cdot(LaTiO_2N)_x$	NH_3 nitridation	0.15	300-W Xe	>420 nm	methanol/$AgNO_3$	Pt/66.7	53.3		562
Ga−Zn−In mixed oxynitride	NH_3 nitridation	0.2	450-W Hg	>400 nm	methanol/$AgNO_3$	Rh/50	CoO_x/∼100		581
$CaTaO_2N$	NH_3 nitridation	0.2	300-W Xe	>420 nm	methanol	Pt/75			42
$SrTaO_2N$	NH_3 nitridation	0.2	300-W Xe	>420 nm	methanol	Pt/100			42
$BaTaO_2N$	NH_3 nitridation	0.2	300-W Xe	>420 nm	methanol	Pt/75			42
$LaTaON_2$	NH_3 nitridation	0.3	300-W Xe	>420 nm	ethanol	Pt−Ru/126.7			394
$Nb_2Zr_6O_{17-x}N_x$	NH_3 nitridation	0.5	450-W Xe	>420 nm	H_2S+KOH	8566		13.5 (550 nm)	398
N-doped Zn−Ga mixed oxide	solid-state reaction	0.02	125-W Hg	visible light	methanol	Rh−Cr_2O_3/37202		5.1%	483
$Zr_xTa_{1-x}O_{1+x}N_{1-x}$	NH_3 nitridation	0.4	300-W Xe	>420 nm	methanol	Ru/∼250			898
TiN film	cathodic arc technique	−	300-W Xe	>400 nm	Na_2S	Pt/∼150[a]			731
TiO_2:N	precursor heat-treatment	0.1	300-W Xe	>400 nm	Na_2SO_3	Pt/∼250			430, 431
TiO_2:N	NH_3 nitridation	1.0	450-W W[c]	>420 nm	$AgNO_3$		221	14 (>420 nm)	708
TiO_2:B/N	sol−gel method	0.15	400-W H	>420 nm	EDTA-2Na	Pt/34.9			465
$TiN_xO_yF_z$	precursor nitridation	0.1	300-W Xe	>420 nm	$AgNO_3$		∼420		460−462
TiO_2:S/N	thermal decomposition	0.35	300-W Xe	>400 nm	methanol	Pt/9.97			463
TiO_2:In/N	polyol method	0.05	288-W F	quartz filter	methanol	Pd/75		0.4 (400 nm)	525
$Ca_{0.25}La_{0.75}TiO_{2.25}N_{0.75}$	NH_3 nitridation	0.2	300-W Xe	>420 nm	$AgNO_3$		IrO_2/500	5 (420−600 nm)	475
$TiSi_2$	Alfa	2	H	310−800 nm	pure water	∼5	∼2.5		719
graphitic C_3N_4	thermal condensation	0.1	300-W Xe	>420 nm	TEA/$AgNO_3$	Pt/107	RuO_2/∼8.3	0.1/−(420−460 nm)	720, 763
$C_3N_{4-x}S_x$	H_2S thermal sulfurization	0.1	300-W Xe	>420 nm	TEA	Pt/∼750			721
barbituric acid modified C_3N_4	copolymerization	0.1	500-W HBO	>420 nm	TEA	Pt/294			722

Table 2. Continued

Semiconductor photocatalysts for water splitting under visible-light irradiation									
						activity (μmol·h^{-1}·g^{-1})			
photocatalyst	synthetic method	mass (g)	light source	incident light	aqueous reaction solution	cocatal./H_2	cocatal./O_2	QY (%)	reference
graphite oxide	modified Hummers' method	0.5	400-W Hg	>400 nm	methanol	4		0.01	723
mesoporous graphitic C_3N_4	silica templated self-polymerization	0.1	500-W Hg	>420 nm	TEA	Pt/1490			952
Cr−$Ba_2In_2O_5$/Cr−In_2O_3	solid-state reaction	0.5	300-W Xe	>420 nm	methanol/$AgNO_3$	Pt/15.8	0.7		819
$Ba_2In_2O_5$/In_2O_3	coprecipitation method	0.3	300-W Xe	>420 nm	methanol	Pt/16.4			820
WO_3/W/$PbBi_2Nb_{1.9}Ti_{0.1}O_9$	solid-state reaction, chemical vapor deposition	0.3	450-W Xe	>420 nm	methanol/$AgNO_3$	Pt/49.3	741	6.06/41 (>420 nm)	877
TaON/ZrO_2	NH_3 nitridation	0.4	300-W Xe	>420 nm	methanol/$AgNO_3$	Ru/∼675	∼312.5		897
HTiNb(Ta)O_5/Fe_2O_3	stepwise intercalation reaction	0.1	500-W Hg	>420 nm	methanol/$AgNO_3$	traces	∼110		839
$HTaWO_6$/(Pt, TiO_2)	stepwise intercalation reaction	1	450-W Hg	>400 nm	methanol	∼670		0.14 (>400 nm)	827
CdS/TiO_2	precipitation, sol−gel method	0.1	350-W Hg	>420 nm	Na_2S + Na_2SO_3	Pt/6400			803−805, 816
Bi_2S_3/TiO_2	hydrothermal method		600-W W		$Na_2S_2O_3$	2900			822
CdS/ZnO	two-step precipitation	0.2	300-W Xe		Na_2S + Na_2SO_3	Pt/3870		3.2 (300−600 nm)	797, 798
CdS/$LaMnO_3$	reverse micelle method	0.1	300-W Xe	>420 nm	Na_2S + Na_2SO_3 + NaOH	375			799
CdS/$KNbO_3$	ion adsorption, precipitation	0.2	500-W Hg−Xe	>400 nm	isopropanol	NiO_x/203.5		8.8 (>400 nm)	800, 801
$TiO_{2-x}N_x$/WO_3	sol−gel	0.05	300-W Hg	>400 nm	Na_2S + Na_2SO_3	Pd/1005		0.45 (>400 nm)	817, 818
MWNT/TiO_2	chemical vapor deposition	1	150-W H	380−780 nm	methanol	Ni/38.1			821
c-CdS/Pt/hex-CdS	direct deposition	0.05	500-W Hg−Xe	>400 nm	Na_2S + Na_2SO_3 + NaOH	13 360			823
CdSe/CdS	colloidal synthesis	0.004	300-W Xe		methanol	Pt/40 000		20 (450 nm)	824
$HLaNb_2O_7$/(Pt, Fe_2O_3)	ion-exchange, photodeposition	1	100-W Hg	>400 nm	methanol	∼372			838
CdS/$K_2Ti_{3.9}Nb_{0.1}O_9$	cation exchange, sulfurization	0.1	300-W Xe		Na_2S	Pt/∼731			840−842
(Pt,$Cd_{0.8}Zn_{0.2}S$)/$HNbWO_6$	cation exchange, sulfurization	1	450-W Hg	>400 nm	Na_2S	∼2678			843
(Pt,$Cd_{0.8}Zn_{0.2}S$)/$HLaNb_2O_7$	cation exchange, sulfurization	1	100-W Hg	>400 nm	Na_2S	∼892.8			845
CdS/ETS-4	ion exchange, sulfurization	0.1	300-W Xe	>420 nm	Na_2S + Na_2SO_3 + NaOH	Pt/175			847
CdS/ETS-10	ion exchange, sulfurization	0.1	300-W Xe	>420 nm	Na_2S + Na_2SO_3 + NaOH	Pt/133			847
CdS/Ti-MCM-41	ion exchange, sulfurization	0.2	350-W Xe	>430 nm	Na_2SO_3	Pt/76		2.6 (420 nm)	849
WS_2/TiO_2	photodeposition	0.2	350-W Xe	>430 nm	Na_2S	Pt/890			850
CdS/$Zr_{0.25}Ti_{0.75}PO_4$	ion exchange, thermal treatment, sulfurization	0.2	300-W Xe	>430 nm	Na_2S + Na_2SO_3	Pt/2300		27.2 (420 nm)	851
Cu_2O/$CuMnO_2$	ion exchange	0.05	500-W H	Pyrex filter	Na_2SO_3 + KOH	424			868
$CuAlO_2$/TiO_2	direct mixing	0.375	200-W W−H	Pyrex filter	Na_2S	21 060			870
$CuFeO_2$/SnO_2	direct mixing		600-W W	Pyrex filter	$Na_2S_2O_3$	11 606		0.5	871
$ZnFe_2O_4$/$SrTiO_3$	solid-state reaction	0.25	600-W W		$Na_2S_2O_3$	410 688			872
CdS/$AgGaS_2$	solid-state reaction, precipitation	0.1	450-W Hg	>420 nm	Na_2S + Na_2SO_3	Pt/4730		19.7 (>420 nm)	873
TiO_2/$AgGaS_2$	solid-state reaction, sol−gel method	0.1	450-W Hg	>420 nm	Na_2S + Na_2SO_3	Pt/4200		17.5 (>420 nm)	874
$CaFe_2O_4$/$MgFe_2O_4$	polymerized complex method	0.3	450-W W	>420 nm	methanol	Pt−RuO_2/82.7		10.1	875
CdS/$Na_2Ti_2O_4(OH)_2$	hydrothermal, ion exchange, sulfurization	0.15	300-W Xe	>420 nm	Na_2S + Na_2SO_3	Pt/2680		43.4 (420 nm)	852−854
Cr_2O_3/$Na_2Ti_2O_4(OH)_2$	hydrothermal, impregnation route	0.1	350-W Xe	>400 nm	Na_2S + Na_2SO_3	36.4			855
$CaFe_2O_4$/$PbBi_2Nb_{0.9}W_{0.1}O_9$	solid-state reaction, hydrothermal method	0.3	450-W Xe	>420 nm	$AgNO_3$		675	38 (>420 nm)	876
Cu_2O/WO_3	electrodeposition	2	400-W Hg	>400 nm	pure water	∼1.9			867

Table 2. Continued

Dye-sensitized semiconductor photocatalysts for water splitting under visible-light irradiation									
						activity (μmol·h^{-1}·g^{-1})			
photocatalyst	synthetic method	mass (g)	light source	incident light	aqueous reaction solution	cocatal./H_2	cocatal./O_2	QY (%)	reference
$K_{0.95}Ta_{0.92}Zr_{0.08}O_3$/Pt/ cyanocobalamin	solid-state reaction	0.1	500-W Xe		pure water + KOH (pH = 11)	575	284	12.2 (300 nm)	633
$K_{0.95}Ta_{0.92}Zr_{0.08}O_3$/Pt/ Cr−tetraphenylporphyrin	solid-state reaction	0.1	500-W Xe		pure water + KOH (pH = 11)	513	257		633
$K_{0.95}Ta_{0.92}Zr_{0.08}O_3$/Pt/ Co-tetraphenylporphyrin	solid-state reaction	0.1	500-W Xe		pure water + KOH (pH = 11)	145	45		633
TiO_2/Pt/$[Ru(dcbpy)_2dpq]^{2+}$	P25-TiO_2	0.04	250-W W−H	visible light	pure water	312.5			611
TiO_2/Pt−RuO_2/ $Ru(bpy)_3^{2+}$	thermal hydrolysis	0.01	450-W Xe	>400 nm	methyl viologen (MV^{2+})	5360		0.06	70, 592, 605−607
TiO_2/Pt/$Ru(dcbpy)_3$	P25 TiO_2	0.002	300-W Xe	>420 nm	EDTA	4000			609
TiO_2/Pt/tetrakis- (4-carboxyphenyl)porphine	TiO-5 standard sample	0.05	500-W Xe	>420 nm	EDTA	134		~0.1 (500−650 nm)	610
TiO_2/Pt/$Ru(bpym)_3^{2+}$	TiO-5 standard sample	0.05	500-W Xe	>420 nm	EDTA	71.6			610
TiO_2/Pt/ merocyanine dye	Ishihara ST-01	0.05	300-W Xe	>410 nm	acetonitrile + NaI	420		1.8 (517 nm)	613, 642−644
TiO_2/Pt/ coumarin dye	Ishihara ST-01	0.05	300-W Xe	>410 nm	acetonitrile + NaI	300		2.5 (440 nm)	613, 642−644
TiO_2/Pt/ N3 dye	Ishihara ST-01	0.05	300-W Xe	>410 nm	acetonitrile + NaI	1080		4.5 (517 nm)	613, 642−644
mesoporous TiO_2/Pt/ $Ru(dcbpy)_2(NCS)_2$	hydrothermal method	0.04	500-W Xe	>420 nm	methanol	310			614, 615
mesoporous TiO_2/Pt/$Ru_2(bpy)_4L_1$-PF_6	hydrothermal method	0.04	500-W Xe	>420 nm	methanol	1020			614, 615
mesoporous TiO_2/ Pt/$Ru(bpy)_2(him)_2$−NO_3	hydrothermal method	0.04	500-W Xe	>420 nm	methanol	695			614, 615
Al_2O_3/TiO_2/ Pt/$Ru(bpy)_3^{2+}$	sol−gel, adsorption method	0.025	300-W Xe	>420 nm	EDTA	1293			616
guanidinium/Nafion/TiO_2/ Pt/$Ru(bpy)_3^{2+}$	adsorption method	0.01	300-W Xe	>420 nm	EDTA	~90			617
Db [NiFeSe]−H/ RuP/TiO_2	adsorption method	0.005	250-W W−H	>420 nm	TEA	712		6.7 (>420 nm)	618
SnO_2/Pt−RuO_2/ $Ru(bpy)_3^{2+}$	Aldrich	0.08	150-W Xe		MV^{2+} + EDTA	685.6		2.4 (350 nm)	619
$K_4Nb_6O_{17}$/ Pt/$Ru(bpy)_3^{2+}$	solid-state reaction	0.005	300-W Xe	>420 nm	EDTA	840		10.5 (450 nm)	604
$H_4Nb_6O_{17}$/ Pt/$Ru(bpy)_2(4,4'$-$(PO_3H_2)_2bpy)^{2+}$	solid-state reaction, ion exchange	0.005	300-W Xe	>420 nm	EDTA	2880		26 (450 nm)	623
$HCa_2Nb_3O_{10}$/Pt/ $Ru(bpy)_2(4,4'$-$(PO_3H_2)_2bpy)^{2+}$	solid-state reaction, ion exchange	0.005	300-W Xe	>420 nm	EDTA	4320		22 (450 nm)	623, 624
$K_{4-x}H_xNb_6O_{17}\cdot nH_2O$/Pt/$RuL_3(PF_6)_2$	solid-state reaction, acid exchange	0.1	200-W Hg−Xe	400−500 nm	KI	1.5		0.3 (400−500 nm)	625, 626
TiO_2/Pt(alizarine)$_2$	P25 TiO_2	0.02	500-W Xe	>430 nm	EDTA			0.5 (500 nm)	627
TiO_2/Pt/zinc porphyrins	thermal hydrolysis	1	1000-W Xe	>520 nm	EDTA	10			630
TiO_2/RuO_2/copper phthalocyanine	commercial anatase TiO_2	0.125	direct sunlight		MV^{2+} + methanol	~568			632
TiO_2/Pt−RuO_2/8- hydroxyquinoline	Montedison TiO_2−U	0.005	450-W Xe	>435 nm	EDTA	8920		0.0034 (457.9 nm)	639
1,1′-binaphthalene-2,2′- diol/Pt/TiO_2	commercial TiO_2	0.05	400-W Hg	>430 nm	TEA	34		0.02 (450 nm)	641
ZnO/Pt/rose bengal	Commercial ZnO	0.03	500-W Xe	>420 nm	TEA + I^-	2700			645
ZnO/Pt/rhodamine B	commercial ZnO	0.03	500-W Xe	>420 nm	TEA + I^-	2560			645
TiO_2/Pt/Eosin-Y	ST-01 TiO_2	0.3	300-W Xe	>460 nm	TEA	1111		10 (520 nm)	646
TiO_2/Rh/Eosin-Y	P25 TiO_2	0.02	200-W H	>420 nm	diethanolamine	1185.5		10.27 (>420 nm)	647, 648, 650
TS-1/Pt/Eosin-Y	hydrothermal method, chemical adsorption	0.04	300-W W−H	>420 nm	TEA	850		9.4 (>420 nm)	651
$Na_2Ti_2O_4(OH)_2$/ Pt/Eosin-Y	hydrothermal method, chemical adsorption	0.04	300-W W−H	>420 nm	TEA	1861.2		14.97 (>420 nm)	649

Table 2. Continued

Dye-sensitized semiconductor photocatalysts for water splitting under visible-light irradiation								
						activity (μmol·h^{-1}·g^{-1})		
photocatalyst	synthetic method	mass (g)	light source	incident light	aqueous reaction solution	cocatal./H_2	cocatal./O_2	QY (%)	reference
Ti-MCM-41/Pt/Eosin-Y	hydrothermal method, chemical adsorption	0.04	300-W W−H	>420 nm	TEA	1027.5		12.01 (>420 nm)	652
titanic acid short nanotubes/Pt/Eosin-Y	hydrothermal method, chemical adsorption	0.02	300-W W−H	>420 nm	TEA	1800		6.65 (>420 nm)	653
titanic acid long nanotubes/Pt/Eosin-Y	hydrothermal method, chemical adsorption	0.02	300-W W−H	>420 nm	TEA	4690		17.36 (>420 nm)	653
titanic acid nanorods/Pt/Eosin-Y	hydrothermal method, chemical adsorption	0.02	300-W W−H	>420 nm	TEA	4060		15.04 (>420 nm)	653
TiO_2/Pt/Fe^{3+}−Eosin-Y	chemical adsoprtion	0.1	400-W H	>420 nm	TEA	2750		19.1 (>420 nm)	654
silica gel/Pt/Eosin-Y	chemical adsorption	0.06	300-W W−H	>420 nm	TEA	716.7		10.4 (>420 nm)	655
multiwalled carbon nanotube/Pt/Eosin-Y	refluxing treatment	0.04	300-W W−H	>420 nm	TEA	3060		12.14 (>420 nm)	656
Co-HPA/Pt/TiO_2	impregnation method	0.075	400-W W	visible light	ethanol	2730			634, 635
Wells-Dawson heteropoly blue/Pt/TiO_2	photocatalytic reduction	0.05	300-W H	>420 nm	glycerol	~62.5		20.0 (670 nm)	637, 638

[a] The unit of H_2/O_2 evolution rate is μmol·h^{-1}, as the weight of photocatalyst has not been given in the reference. [b] Tungsten−halogen lamp. [c] Tungsten-arc lamp.

implanted. The absorption maximum and minimum values stayed constant. Such a shift not only allowed the metal-ion-implanted TiO_2 to use solar irradiation more effectively but also initiated effective photocatalytic reactions, under both UV and visible-light irradiation. It was found that Pt^{4+}- and Ag^+-doped TiO_2 nanoparticles also exhibited improved photocatalytic activities under visible-light or UV irradiation. This was explained as follows: the doping ions in these photocatalysts not only contributed to the visible-light absorption but also served as a recombination inhibitor by trapping electrons or holes, which in return promoted the charge separation required for the photocatalytic reaction.[328,329] However, in some cases, it was found that the metal-ion dopants could also serve as the recombination sites for photoinduced charges and not a recombination inhibitor. This resulted in relatively low photocatalytic activity even under UV irradiation.

In 1994, Choi et al. investigated the effects of metal ion doping on the photocatalytic activity of TiO_2.[330] They found that the photocatalytic activity was related to the electron configuration of the dopant ion. Of the 21 metal-ion dopants studied, Fe, Mo, Ru, Os, Re, V, and Rh ion doping significantly increased the photocatalytic activity, whereas Co and Al ion doping caused detrimental effects. The nature of the metal-ion dopant in the TiO_2 significantly affected the charge recombination and electron transfer rates. An electron paramagnetic resonance (EPR) study of doped TiO_2 colloids showed that Fe- or V-doped TiO_2 caused the growth of the Ti^{3+} signal. These changes were attributed to an inhibition of the hole−electron recombination by Fe^{3+} or V^{4+} dopant. On the other hand, Mo^{6+} dopant behaved as an irreversible electron trap.[331]

Kudo and co-workers reported that Ni^{2+}-, Rh^{3+}-, or Cr^{3+}-doped TiO_2 exhibited virtually no photocatalytic activity, whereas TiO_2 codoped by Ni^{2+}, Rh^{3+}, or Cr^{3+} together with Ta^{5+}, Nb^{5+}, or Sb^{5+} led to efficient O_2 evolution from water.[303,332−335] Reaction conditions required Ag^+ as an electron acceptor and visible-light irradiation. Doping by Ni^{2+}, Rh^{3+}, or Cr^{3+} created donor levels in the forbidden band and made TiO_2 responsive to visible light. The charge balance was maintained by codoping of Ta^{5+}, Nb^{5+}, or Sb^{5+}, which was needed to suppress the recombination between photogenerated electrons and holes. Ohno et al. expanded the effective wavelength of TiO_2 photocatalyst into the visible region by Ru doping.[336] With this particular photocatalyst, the oxygen evolution reaction occurred under the irradiation of visible light at wavelengths longer than 440 nm. Iron(III) ions were used as the electron acceptor. Kahn and co-workers found that Pt-, Ir-, and Co-ionized titania nanotubes prepared by an ion-exchange method were effective photocatalysts for the production of stoichiometric hydrogen and oxygen by water splitting under visible-light irradiation.[337,338] Pt, Ir, and Co ionization all reduced the band gap energy as indicated by UV−vis absorption spectra, resulting in the visible photoresponse ability. Visible-light-responsive TiO_2, obtained by self (Ti^{3+}) doping, was found to decompose water in methanol or silver nitrate solution under visible-light irradiation. The observed absorption and photocatalytic ability in the visible-light region was ascribed to the defect levels present within the band gap of these samples.[339−342]

Attention has also been paid to other oxide semiconductors as host photocatalysts for metal-ion doping. Cr-doped $SrTi_{1-x}Cr_xO_3$ ($x = 0.00, 0.02, 0.05, 0.10$) was prepared by a solvothermal method and showed increasing photocatalytic

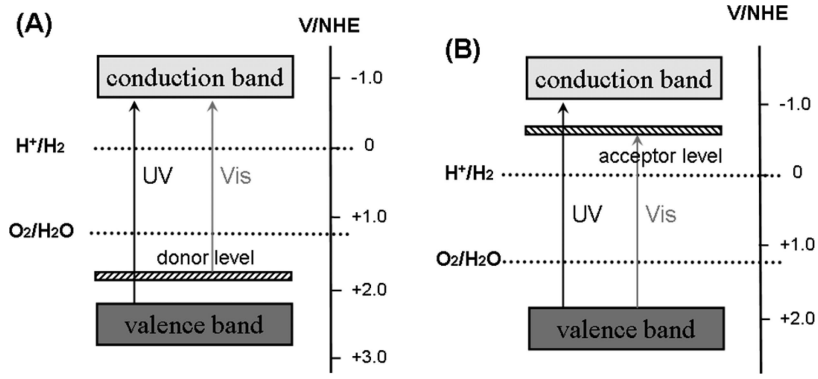

Figure 6. Donor level (A) and acceptor level (B) formed by metal ion doping.

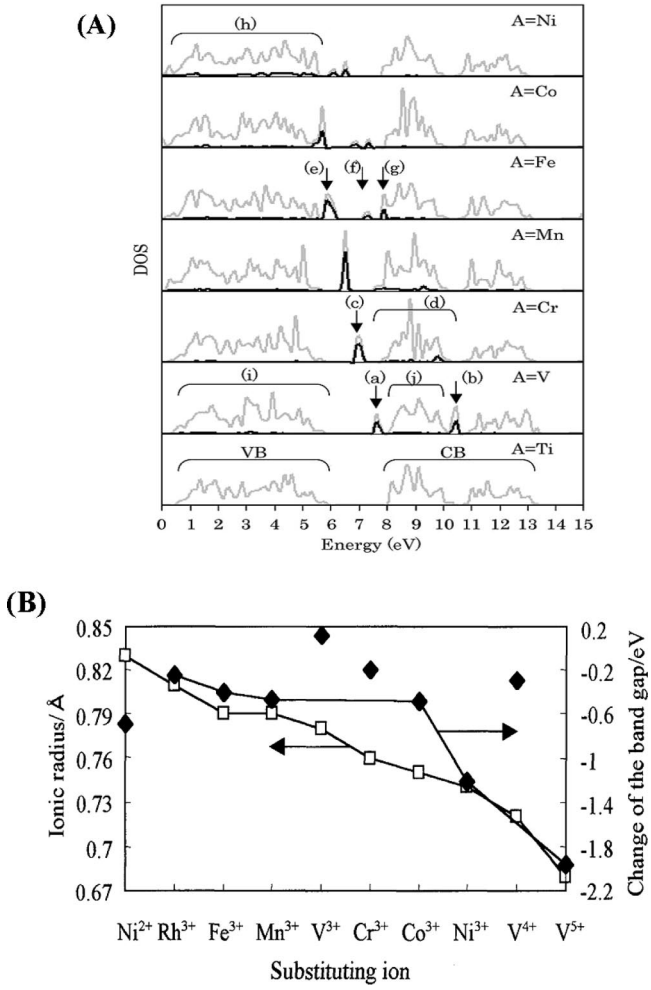

Figure 7. (A) Density of states (DOS) of the metal-doped TiO_2 ($Ti_{1-x}A_xO_2$: A = V, Cr, Mn, Fe, Co, or Ni). Gray solid lines: total DOS. Black solid lines: dopant's DOS. The states are labeled a−j. Reprinted with permission from ref 315. Copyright 2002 Elsevier. (B) The relationship between the ionic radius and the change of the band gap (anatase). Except for some cations, the band gaps decrease with decreasing cation size. Reprinted with permission from ref 316. Copyright 1999 The Chemical Society of Japan.

activities for hydrogen production under both UV and visible light with increasing amounts of chromium. The new band gap in the visible-light range obtained by Cr doping was attributed to the band transition from the Cr 3d to the Cr 3d + Ti 3d hybrid orbital.[304] Wang et al. studied the photophysical and photocatalytic properties of $SrTiO_3$ doped with Cr cations on different sites.[343] Interestingly, $(Sr_{0.95}Cr_{0.05})TiO_3$ with Cr cations (Cr^{3+}) doped at the Sr^{2+} sites showed higher photocatalytic activity of H_2 evolution under visible-light irradiation than $Sr(Ti_{0.95}Cr_{0.05})O_3$ with Cr cations (mixed Cr^3+ and Cr^{6+}) doped at the Ti^{4+} sites. It was concluded that, because the Cr^{6+} cations created the potential level of the empty Cr^{6+} lower than that for H_2 evolution and thus behaved as the trapping center for photoinduced electrons, they should be avoided in Cr-containing visible-light-driven photocatalysts intended for water splitting.

Kudo and co-workers found that Mn- and Ru-doped $SrTiO_3$ showed photocatalytic activities for O_2 evolution from an aqueous silver nitrate solution.[344] Ru-, Rh-, and Ir-doped $SrTiO_3$ loaded with Pt cocatalysts produced H_2 from an aqueous methanol solution under visible-light irradiation ($\lambda > 440$ nm). In particular, the Rh (1%)-doped $SrTiO_3$ gave a quantum yield of 5.2% at 420 nm for H_2 evolution. The visible-light response of Rh-doped $SrTiO_3$ was due to the transition from the electron donor level formed by the Rh ions to the conduction band composed of Ti 3d orbitals. When $SrTiO_3$ was codoped with Sb^{5+}/Cr^{3+}, Ta^{5+}/Cr^{3+}, or Ta^{5+}/Ni^{2+}, all the resulting compounds displayed efficient photocatalytic activities for hydrogen production from aqueous methanol solutions under visible-light irradiation ($\lambda >$ 420 nm).[303,333−345] When Ti^{4+} was replaced by Ni^{2+} or Cr^{3+} in $SrTiO_3$, the results were similar to those for Sb^{5+}/Cr^{3+}-codoped TiO_2. The charge became unbalanced, and recombination centers formed. When a second metal ion such as Ta^{5+} or Sb^{5+} was codoped to compensate for the charge unbalance and suppress the formation of the recombination centers, the visible-light absorption was maintained.

Miyake and co-workers[346] and Chen and co-workers[347] demonstrated that both Rh^{3+}- and Cu^{2+}-doped $CaTiO_3$ were good candidates for visible-light-driven oxide photocatalysis for hydrogen evolution. Reaction occurred under visible-light irradiation with methanol as the electron donor. Miyake and co-workers also found that Rh^{3+}-doped $Ca_3Ti_2O_7$ was active in photocatalytic hydrogen generation under visible light.[348] Moreover, it was found that Rh^{3+}-doped $Ca_3Ti_2O_7$ with a layered structure showed higher stability in air than Rh^{3+}-doped $CaTiO_3$ with a simple perovskite structure. Lee and co-workers studied the effects of both Cr and Fe cation substituion on the photophysical and photocatalytic properties of the layered perovskite $La_2Ti_2O_7$.[305,349] The contribution of these dopants led to the formation of a partially filled 3d band, which served as the electron donor level in the band gap of $La_2Ti_2O_7$. It also caused the excitation of electrons from this localized interband to the conduction band of $La_2Ti_2O_7$ and was responsible for visible-light absorption and the H_2 evolution from water under visible light. Suzuki and co-workers reported that Fe^{3+} and W^{6+} substitution for Ti^{4+} in $K_2La_2Ti_3O_{10}$ resulted in a small activity for hydrogen

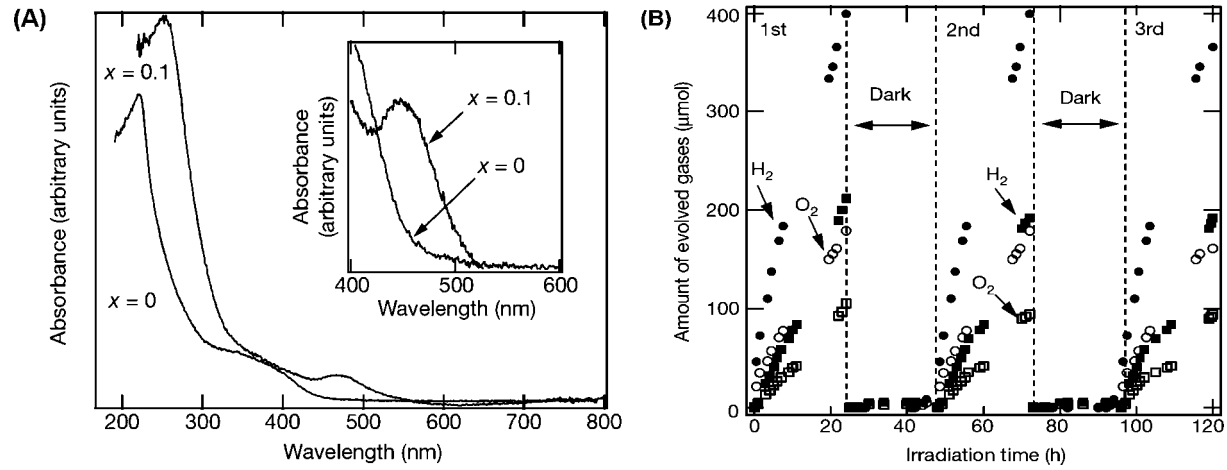

Figure 8. (A) Optical properties of the photocatalyst. The main panel shows the ultraviolet−visible diffuse reflectance spectra of $In_{1-x}Ni_xTaO_4$ ($x = 0$ and 0.1) at room temperature, with the inset providing an expanded view of the spectra in the wavelength region from 400 to 600 nm. (B) Photocatalytic H_2 and O_2 generation. Shown are the evolution of H_2 and O_2 from pure water using as catalyst a suspension of $NiO_y/In_{0.9}Ni_{0.1}TaO_4$ (solid circles, H_2; open circles, O_2) and $RuO_2/In_{0.9}Ni_{0.1}TaO_4$ (solid squares, H_2; open squares, O_2). Experiments were done using 0.5 g of catalyst powder suspended in 250 mL of pure water in a Pyrex glass cell under visible-light irradiation (>420 nm). Light source: 300-W Xe lamp. The gases evolved were determined by thermal conductivity detector (TCD) gas chromatograph. The measurement uncertainties were ~0.05%. Reprinted with permission from ref 353. Copyright 2001 Nature Publishing Group.

production under visible-light irradiation.[350] Under the same condition, pure $K_2La_2Ti_3O_{10}$ showed no activity.

Recently, it was reported that both V-doped and Zn-doped $K_2La_2Ti_3O_{10}$ exhibited high photocatalytic activities of hydrogen production under visible light.[140,351] The hybridization of either V 3d or Zn 3d and O 2p electron orbitals resulted in a new localized energy level. The catalyst was easily excited with lower energy, which in turn improved the photoactivity of $K_2La_2Ti_3O_{10}$ for water splitting. The band gap and photocatalytic activity of In_2TiO_5 also underwent significant changes as a result of V doping. These enabled the absorption of radiation from the entire visible region of 400−800 nm and led to the improvement of photocatalytic hydrogen production under visible light.[352] It is worth mentioning that Zou and co-workers investigated the doping effects of different metal ions (Mn, Fe, Co, Ni, Cu) on the structural and photocatalytic properties of a $InTaO_4$ photocatalyst,[353−357] as shown in Figure 8. Of these, $In_{0.9}Ni_{0.1}TaO_4$ showed the highest photocatalytic activity, which induced direct splitting of water into stoichiometric amounts of oxygen and hydrogen under visible-light irradiation with a quantum yield of ~0.66% at 402 nm. The narrower band gap of Ni-doped $InTaO_4$ was attributed to the Ni 3d donor level formed in the forbidden band.[353] Ni-modified $K_4Nb_6O_{10}$ prepared by a solid-state reaction also exhibited increased visible-light absorption and photocatalytic activity for hydrogen evolution under visible-light irradiation. This was believed to be due to the effect of the Ni^{2+} doping.[358] Cu 3d donor level formed above the valence band of $BiTaO_4$ by Cu^{2+} doping. This contributed to the increased photocatalytic activity for hydrogen evolution under visible light compared to $BiTaO_4$.[359] The strong photoabsorption and good performance of H_2 evolution in the visible-light region shown by Cr^{3+}-doped $Bi_4Ti_3O_{12}$ was largely attributed to the occurrence of the impurity level Cr 3d in both conduction and valence bands.[360]

Kudo and co-workers controlled the oxidation numbers of Ir when it substituted for Nb^{5+} and Ta^{5+} ions in the B sites of a perovskite structure for $NaBO_3$ (B = Nb, Ta).[361] Their strategy consisted of codoping of alkaline earth metal and lanthanum ions for Na^+ ions at the A sites. This contributed to maintaining the charge balance in $NaBO_3$. The resulting $NaNbO_3$:Ir/A (A = Sr, Ba, and La) showed H_2 or O_2 evolution, whereas $NaTaO_3$:Ir/A showed H_2 evolution under visible light. Yang et al. reported that La^{3+}/Cr^{3+}-codoped $NaTaO_3$ showed intense visible-light absorption and H_2 production in the presence of methanol under visible-light irradiation.[362] The photocatalytic activity was much higher than that of monodoped $NaTaO_3$. A high visible-light photocatalytic activity for O_2 evolution from an aqueous solution containing an electron acceptor (quantum yield of 6% at 420 nm) was found for Cr^{6+}-doped $PbMoO_4$. It should be noted that the formation of an electron-acceptor level of Cr 3d orbitals below conduction band as a result of the Cr^{6+} replacement was believed to have given rise to the absorption bands and photocatalytic activity in visible-light region.[363]

Although ZnS is a highly efficient photocatalyst for H_2 evolution because of its high conduction band level, it is only active in the UV light region.[273,364] Hence, it would be quite interesting to see if ZnS becomes visible-light responsive while maintaining its high H_2 evolution activity following some modification. With this in view, a series of Cu- and Ni-doped ZnS photocatalysts were prepared. The results showed high activities for H_2 evolution from the aqueous solutions containing sulfite ions under visible-light irradiation ($\lambda > 420$ nm), even in the absence of a platinum cocatalyst. The visible-light response was a result of the formation of 3d donor levels by the doped Cu^{2+} and Ni^{2+} in the wide band gap of the ZnS host photocatalyst.[306,307,365]

In contrast to the doping modifications described previously, which focused on UV-light-active photocatalysts, some visible-light-driven photocatalysts were also modified by metal-ion doping with the aim of narrowing their band gaps in order to utilize visible light in further longer-wavelength regions to produce more efficient photocatalytic water splitting. Reber and Meier modified the visible-light active photocatalyst CdS by doping it with Ag^+ in order to extend the spectral response up to 620 nm.[282] A significant enhancement in the photocatalytic activity for hydrogen evolution was obtained with CdS powders containing 0.77% Ag^+. Ren et al. reported two series of photocatalysts based on CdS as the base with a little of $MInS_2$ (M = Cu, Ag) as the dopant.[366]

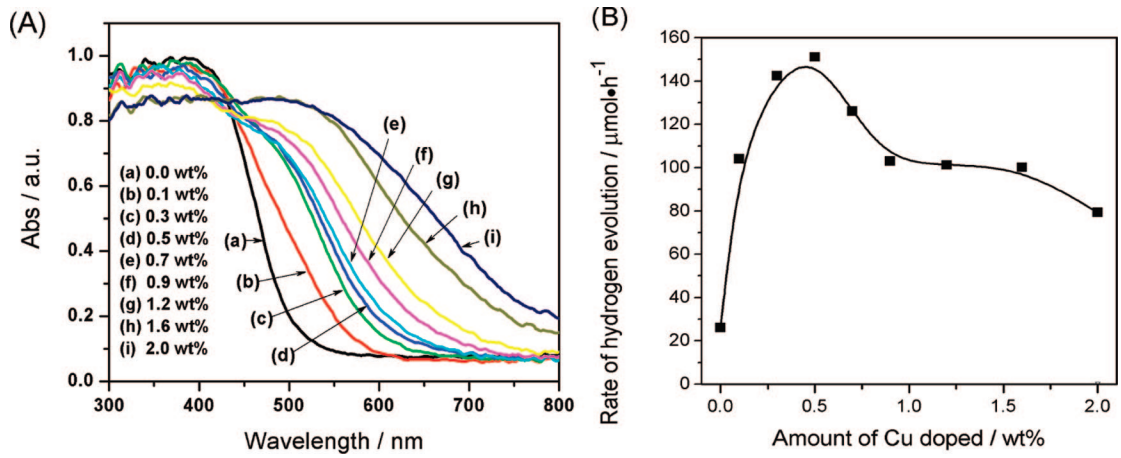

Figure 9. (A) Diffuse reflectance spectra of Cu-doped $ZnIn_2S_4$. (B) Dependence of photocatalytic activity for H_2 evolution over Cu-doped $ZnIn_2S_4$. The concentrations of Cu^{2+} were (a) 0.0 wt %, (b) 0.1 wt %, (c) 0.3 wt %, (d) 0.5 wt %, (e) 0.7 wt %, (f) 0.9 wt %, (g) 1.2 wt %, (h) 1.6 wt %, and (i) 2.0 wt %, respectively. Reprinted with permission from ref 378. Copyright 2008 American Chemical Society.

The resulting compounds had narrower band gaps and higher photocatalytic activities than undoped CdS. More recently, a large degree of Mn doping was discovered to be effective in improving the photocatalytic activity and stability of CdS for visible-light hydrogen production.[367]

In independent studies, Liu et al.[368] and Xu and co-workers[369−371] reported that the Cu-doped $Zn_xCd_{1-x}S$ solid-solution photocatalyst with the absorption edge shifted to a lower energy region displayed higher water-splitting efficiency to produce hydrogen than $Zn_xCd_{1-x}S$, which itself had been shown to be an excellent visible-light-driven photocatalyst.[372,373] Zhang et al. found Ni^{2+} doping also greatly improved the photocatalytic activity of $Zn_xCd_{1-x}S$ for hydrogen production.[374] For some time it has been known that $ZnIn_2S_4$ can efficiently produce hydrogen from some aqueous solutions with sulfite and sulfide ions as the electron donor under visible-light irradiation.[375−377] Shen et al. hydrothermally synthesized a series of Cu-doped $ZnIn_2S_4$ photocatalysts with broader absorptions in the visible-light region than the corresponding undoped $ZnIn_2S_4$.[378] As shown in Figure 9, they found that the photocatalytic activity of $ZnIn_2S_4$ was remarkably enhanced by Cu doping. The 0.5 wt % Cu-doped $ZnIn_2S_4$ photocatalyst showed the highest activity for hydrogen evolution under visible-light irradiation. The surplus doped Cu^{2+} ions served as the recombination sites for the photogenerated electrons and holes.[379]

4.1.2. Nonmetal-Ion Doping

Nonmetal ion doping is another approach used to modify UV-light-active photocatalysts. It has been widely used to narrow the band gap and improve the visible-light-driven photocatalytic activity. Unlike metal-ion dopants, nonmetal-ion dopants are less likely to form donor levels in the forbidden band but instead shift the valence band edge upward. This results in a narrowing of band gap as indicated in Figure 10. The technology of nonmetal-ion doping has been widely used to modify some UV-light-active oxide photocatalysts, such as Ti-based oxides,[380−387] Ta-based oxides,[388−395] Zr-based oxides,[396−398] Nb-based oxides,[398−402] etc.

Various nonmetal ions (such as C, N, S, etc.) were used to dope TiO_2, and the products were studied for their optical and photocatalytic properties. Nonmetal-ion doped TiO_2, in which the absorption spectra were red-shifted to longer wavelengths, exhibited improved photocatalytic activities

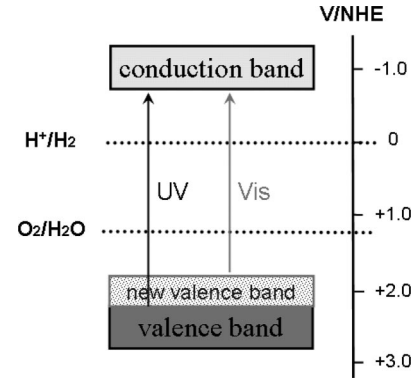

Figure 10. New valence band formation by doping of nonmetal ions.

compared to those for pure TiO_2, especially in the visible-light region.[403−416] Chen and co-workers used X-ray photoelectron spectroscopy (XPS) to show that additional electronic states exist above the valence band edge of pure TiO_2 for C-, N-, and S-doped TiO_2 (Figure 11A).[417,418] This additional electron density of states can explain the red-shifted absorption of these potential photocatalysts, as observed in the "shoulder" and "tail-like" features in the UV−vis spectra (Figure 11B). Asahi et al. studied the substitutional doping of C, N, F, P, and S for O in anatase TiO_2.[419] Using full-potential linearized augmented plane wave (FLAPW) method, they calculated the electronic band structures of anatase TiO_2 with different substitutional dopants as shown in Figure 12. They found that the substitution of N for O, which leads to the mixing of the 2p states of N with the 2p of O, was the most effective. It led to the band gap narrowing by shifting the valence band edge upward, which in return resulted in N-doped TiO_2 having a much higher photocatalytic activity than pure TiO_2 in the visible-light region. Chen et al. found that the ease and degree of nitrogen doping was responsible for the significant increase in photocatalytic activity observed in the TiO_2 nanocolloid versus the nitrided commercial nanopowder.[414] Braun et al. revealed an additional e_g resonance in the valence band of TiO_2 formed by nitrogen doping in the oxygen 1s NEXAFS pre-edge.[420] This extra resonance was found to bear coresponsibility for the photocatalytic performance of N-doped TiO_2 at visible-light wavelengths.

Up until now, N-doped TiO_2 has been both widely investigated and successfully prepared by many different

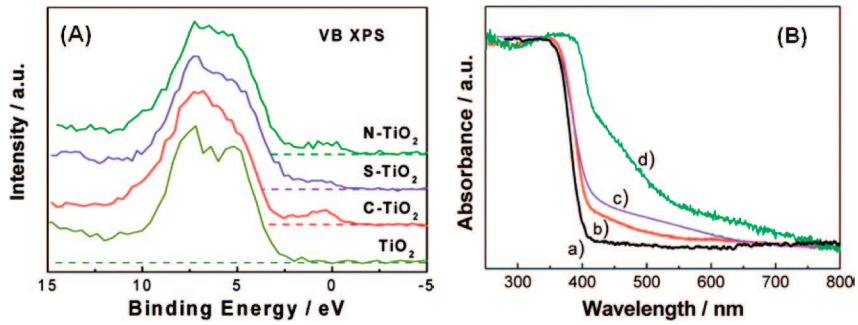

Figure 11. VB XPS spectra (A) and diffuse reflectance spectra (B) of (a) pure TiO_2, (b) C−TiO_2, (c) S−TiO_2, and (d) N−TiO_2. Reprinted with permission from ref 418. Copyright 2008 American Chemical Society.

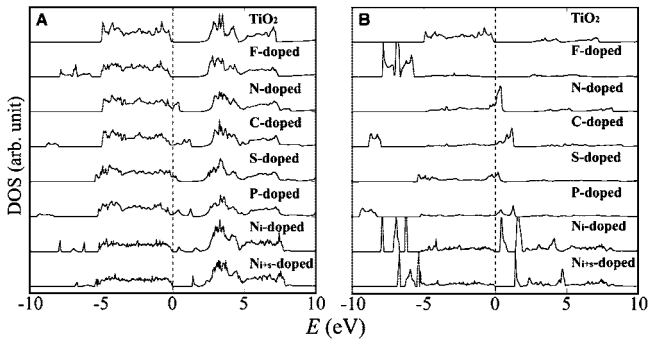

Figure 12. (A) Total DOSs of doped TiO_2 and (B) the projected DOSs into the doped anion sites, calculated by FLAPW. The dopants F, N, C, S, and P were located at a substitutional site for an O atom in the anatase TiO_2 crystal (the eight TiO_2 units per cell). The results for N doping at an interstitial site (N_i-doped) and that at both substitutional and interstitial sites (N_{i+s}-doped) are also shown. Reprinted with permission from ref 419. Copyright 2001 AAAS.

methods. These include physical/chemical vapor deposition,[421,422] the heating of titanium hydroxide and urea,[423] reactive magnetron sputtering,[424,425] a hydrothermal/solvothermal process,[426,427] and treating TiO_2 powder in a NH_3 gas flow.[428,429] Yuan et al. synthesized N-doped TiO_2 by heating a mixture of urea and TiO_2 at 350−700 °C in air.[430] XPS confirmed that both the molecularly chemisorbed N_2 and the substitutional N contributed to the material response to visible light. However, the substitutional N was considered the predominate factor in improving the photocatalytic activity of the water splitting under visible light. Lin et al. demonstrated that the N-doped TiO_2 photocatalyst, synthesized by a two-microemulsion technique, showed favorable photocatalytic hydrogen evolution at neutral pH range in methanol/water solutions.[431] Pillai and co-workers reported that the chemical modification of titanium isopropoxide using different nonmetallic chemical reagents such as urea, sulfuric acid, and trifluoroacetic acid improved both the anatase stability and the photocatalytic activity by doping with nitrogen, sulfur, and fluorine, respectively.[432−434]

The photocatalytic activity of S-doped TiO_2 has also been studied in depth. Using different synthetic methods, anionic sulfur can be doped into TiO_2 to replace the lattice oxygen or as an cation to replace the Ti ion.[407,435−438] It was found that S-doped TiO_2 showed different photocatalytic activities under visible light.[439] In Nishijima and co-workers' study of S-doped TiO_2, a higher activity level for hydrogen evolution than for N-doped TiO_2 photocatalysts under visible light was reported.[440] Kahn et al. prepared C-doped TiO_2 with main rutile structure by pyrolyzing Ti metal in a natural gas flame. The C-doped TiO_2 possessed lower band gap energy and displayed a much higher photoactivity in water splitting than pure TiO_2 with the mixed phase of antanse and rutile.[441] It was found that C-doped TiO_2 nanotubes also displayed a high photoactivity for water splitting.[442] The bandgap reduction and the new intragap band formation in C-doped TiO_2 nanotubes extended its utilization of solar energy up to the visible to infrared region.[442]

To further enhance the visible-light activity, nonmetal codoping of TiO_2 such as F/B-codoping,[443,444] F/N-codoping,[445,446] S/F-codoping,[447] F/C-codoping,[448] C/N-codoping,[449,450] S/N-codoping,[451,452] N/Br-codoping,[453] B/N-codoping,[454,455] N/Si-codoping,[456] C/S-codoping,[457] and P/F-codoping[458] have all been studied. Results suggested that nonmetal-codoped TiO_2 compounds had significant visible photocatalytic activities due to the synergetic effect of the codoping. Luo et al. found that Cl/Br-codoped TiO_2 displayed a much higher photocatalytic activity for water splitting than either Cl- or Br-doped TiO_2.[459] Domen and co-workers found that N/F-codoped TiO_2 had high visible-light photocatalytic activity for water oxidation due to the absorption band of $TiN_xO_yF_z$ in the visible region.[460−462] N/S-codoped TiO_2 showed considerable activity in the photocatalytic water splitting, and under visible light produced H_2. This was attributed to the visible-light photoexcitation of the electrons from the isolated energy levels in the band gap formed by the doped N or S to the conduction band.[463] Liu et al. synthesized B/N-codoped TiO_2 with high visible-light photocatalytic activity.[464] They proposed that the synergistic effects of B/N codoping created visible-light absorption by N doping, and the lifetime of the photoinduced carriers was prolonged by B doping. Subsequently, Li et al. found that the visible-light-driven photocatalytic activity of B/N-codoped TiO_2 for hydrogen evolution increased greatly compared to that of N-doped TiO_2.[465] They believed that the codoping of boron contributed to the excellent activity of B/N-codoped TiO_2, because the doped boron could act as shallow traps for electrons, which prolong the life of photoinduced electrons and holes. Recently, OCN-doped TiO_2 nanoparticles were prepared for photocatalysis in the visible-light region of 380−550 nm as indicated by UV−vis absorption spetra.[466] In this doped TiO_2, the OCN group bonding to titanium atoms produces a weakening of its C═O double bond and a hardening of CN and NO bonds, which enables visible absorption and related photocatalytic activity.[466]

Similar to the case of N-doped TiO_2, N-doping in Ta_2O_5 also caused a valence band upward shift to a higher energy level, which narrows the band gap.[391,467] TaON and Ta_3N_5, prepared from reacting Ta_2O_5 with NH_3, were found to be active for water splitting into hydrogen and oxygen under visible-light irradiation.[390,468−472] In particular, in the presence

of the sacrificial electron acceptor (Ag^+), TaON functioned as a very efficient photocatalyst for the oxidation of water into O_2 (quantum yield of 34%).[468] Recently, nonmetal-ion-doped titanates and tantalates have also been studied for photocatalytic reduction and oxidation under visible-light irradiation. Wang and co-workers found that, in the visible-light range and the near-ultraviolet range, N-doped and N/S-codoped $SrTiO_3$ displayed much higher photocatalytic activities for NO elimination than pure $SrTiO_3$.[473,474] Kasahara and co-workers found that under visible-light irradiation $LaTiO_2N$ reduced H^+ into H_2 and oxidized H_2O into O_2 in the presence of a sacrificial electron donor (methanol) or acceptor (Ag^+) using the band gap transition (2.1 eV).[475,476] Moreover, $LaTiO_2N$ could split water without any sacrificial reagent under visible-light irradiation when used as a photoanode in the photoelectrochemical cell.[477] The visible-light absorption was attributed to the new valence band composed of O 2p orbitals for the lower-energy side and N 2p orbitals for the higher-energy side. Similarly, because of N-doping reducing the band gap energy, N-doped $KTa_{0.92}Zr_{0.08}O_3$ was reported to achieve a complete splitting of water under visible-light irradiation, when Pt was loaded as a cocatalyst.[478] Yamasita and co-workers prepared $MTaO_2N$ (M = Ca, Sr, Ba) by nitriding $M_2Ta_2O_7$ at 1123 K for 15 h. $MTaO_2N$ had small band gap energies (2.5−2.0 eV) and could absorb visible light at 500−630 nm via the N 2p orbitals of the upper regions of the valence bands.[42,395] Under visible-light irradiation, $MTaO_2N$ reduced H^+ into H_2 in the presence of a sacrificial electron donor. These oxynitrides, however, did not function in the oxidation of water due to the fact that the valence band did not have sufficient overpotentials for the oxidation potential of water. Liu et al. reported $Y_2Ta_2O_5N_2$ as a novel photocatalyst with high activity for water splitting into hydrogen and oxygen under visible-light irradiation in the presence of appropriate sacrificial reagents.[393] The smaller bandgap energy of $Y_2Ta_2O_5N_2$ was attributed to the partial replacement of O^{2-} by N^{3-} in $YTaO_4$ and the predominant population of the valence band by a hybrid orbital between N 2p and O 2p.

In addition to Ti-based and Ta-based oxides as the host photocatalysts, some other oxides with wide band gaps were also modified by using nonmetal-ion doping and were found to improve visible-light-driven photocatalytic activities for water splitting. Ji et al. studied photocatalytic water splitting using nitrogen-doped $Sr_2Nb_2O_7$ under visible-light irradiation.[399] After nitrogen doping, the $Sr_2Nb_2O_7$ band gap energy was reduced and subsequently induced photocatalytic activity for hydrogen production from methanol−water mixtures in the visible-light region. Recently, N-doped ZrO_2 and In_2O_3, C-doped In_2O_3, and Nb_2O_5 were also reported to show enhanced photocatalytic activities for water splitting under visible-light irradiation compared to the undoped oxide hosts.[396,479−481] Hisatomi et al. found that the novel spinel-type d^0−d^{10} complex oxynitride photocatalyst $Zn_xTiO_yN_z$ displayed photocatalytic activity for both the reduction and oxidation of water in the presence of either a sacrificial electron donor or acceptor under irradiation at visible wavelengths.[482] Li et al. demonstrated for the first time the development of a simple lamellar-solid acid photocatalyst.[400] N-doped HNb_3O_8 displyed superior visible-light-responsive photocatalytic activity in comparison to N-doped Nb_2O_5 and TiO_2. Kanade et al. reported that N-doped $Nb_2Zr_6O_{17}$ gave a quantum yield of 13.5% for photocatalytic hydrogen production from the decomposition of hydrogen sulfide in KOH aqueous solution under visible-light irradiation.[398] N-doped Ga−Zn mixed oxides with a band gap of 2.6 eV were capable of producing hydrogen from a methanol aqueous solution with an apparent quantum efficiency of 5.1% under visible-light illumination.[483] Rh/Cr_2O_3 was loaded as the cocatalyst.

Some other S^{2-} substituted metal oxides have also received considerable attention as visible-light-responsive photocatalysts for water reduction and/or oxidation. For example, the absorption edge of ZrW_2O_8 was significantly extended to the visible-light region by S doping.[484] H_2 and O_2 were evolved under irradiation of up to 360 and 510 nm, respectively. The visible-light sensitization was attributed to the S 3p states, which increased the width of the valence band itself and caused a decrease in the band gap energy.[484] Ishikawa and co-workers were the first to report a Ti-based oxysulfide, $Sm_2Ti_2S_2O_5$, as a visible-light-driven photocatalyst for hydrogen or oxygen production from aqueous solutions containing a sacrificial electron donor or acceptor.[485−487] It was found that the S 3p orbitals constituted the upper part of the valence band and that these orbitals made an essential contribution to the small band gap energy. Subsequently, it was proposed that the members of the series $Ln_2Ti_2S_2O_5$ (Ln = Pr, Nd, Sm, Gd, Tb, Dy, Ho, and Er) would also function as visible-light-responsive photocatalysts for water splitting. The photocatalytic activity of $[Pr,Nd,Er]_2Ti_2S_2O_5$, containing sulfur defects and Ti as Ti^{3+} was lower than that of the other $Ln_2Ti_2S_2O_5$ forms. It appeared that the electronic band structure was strongly affected by the lanthanoid ions.[488]

Recently, a number of La-based oxysulfides were shown to catalyze H^+ reduction to form H_2 and/or water oxidation to form O_2 under visible irradiation in the presence of a sacrificial electron donor (methanol, Na_2S−Na_2SO_3) and acceptor (Ag^+), respectively. The valence bands of these photocatalysts involved overlap of the O 2p and S 3p orbitals, where the higher-energy region mainly consisted of S 3p orbitals and the lower-energy region was mainly composed of O 2p orbitals.[489−491] Thus, it was deduced that the valence bands of photocatalysts consisting of S 3p orbitals, instead of O 2p orbitals, will result in the formation of narrow band gaps. From the point of view of total substitution of O^{2-} by S^{2-} in oxide semiconductors, some novel ternary sulfide systems, including Zn(Cu)−In−S,[375,376,492−495] Ag−Ga(In)−S,[496,497] Cu−Ga−S(Se),[498,499] and Na−In−S,[500] have been developed as visible-light-driven photocatalysts for hydrogen production from aqueous solution containing a sacrificial reagent, such as Na_2S/Na_2SO_3. In follow-up studies, different modification technologies were used to improve the photocatalytic activities of these single-phase sulfides.

Jang et al. were the first to obtain C-doped ZnS by the calcination of a $ZnS(en)_{0.5}$ complex (en = ethylenediamine), in which carbon interacted with Zn through Zn−C bond formation.[501] The participation of C 2p orbitals in the formation of the upper valence band should be responsible for the reduced band gap and the visible-light absorption of ZnS. This was confirmed by the fact that C-doped ZnS exhibited photoactivity for hydrogen production via water splitting under visible-light irradiation.

4.1.3. Metal/Nonmetal-Ion Codoping

Recently, metal/nonmetal-ion-codoped semiconductor systems have been employed as photocatalysts with the objective

of improving their photocatalytic activity under visible-light irradiation. The modification of TiO_2 by codoping with metal and nonmetal ions was frequently used to improve the photocatalytic activity, especially for pollutant degradation. For instance, (Ce + C, I, N, or B),[502−505] (Fe + N or C),[506,507] (Bi + S, C, or N),[508,509] (Ni + B or N),[510,511] (La + N, I, or S),[512−514] and (Eu, Ta, Mo, Pt, or W + N)[515−519] codoped TiO_2, without exception, exhibited enhanced visible-light photocatalytic activity compared to their undoped counterparts. $SrTiO_3$ codoped with La and N was also reported as having greater visible-light photocatalytic activity than the unmodified $SrTiO_3$.[520−522] However, only a few studies reported metal/nonmetal ion codoped photocatalyst systems with modified conduction and valence band used for visible-light hydrogen production from water. Gai et al. proposed to dope TiO_2 using charge-compensated donor−acceptor pairs such as (N + V), (Nb + N), (Cr + C), and (Mo + C).[523] Among all these systems, TiO_2:(Mo + C) has the highest positive effect on photocatalytic water splitting. This is because it reduces the band gap to the ideal visible-light region. It does not, however, have much effect on the conduction band position. Using density-functional theory (DFT) calculations, Yin et al. predicted that (Mo, 2N) and (W, 2N) were the best donor−acceptor combinations in the low-alloy concentration regime whereas (Nb, N) and (Ta, N) were the best choice of donor−acceptor pairs in the high-alloy concentration regime for solar-driven photoelectrochemical water-splitting.[524]

Sasikala et al. found codoping of TiO_2 with In and N in cationic and anionic sites, respectively, resulted in the narrowing of the band gap of TiO_2 compared to In or N doping alone.[525] As a result, the In- and N-codoped samples exhibited enhanced absorption of visible light and improved photocatalytic activity for hydrogen production. Because of the charge-compensation effect from the donor−acceptor codoping, (N, Al)-codoped ZnO obtained by radio frequency (RF) magnetron sputtering method displayed significantly reduced band gap and enhanced photocurrents under visible-light irradiation, when compared to ZnO and Al-doped ZnO.[526] Tsuji and Kudo synthesized Pb and halogen-codoped ZnS as an active visible-light-driven photocatalyst for H_2 evolution without cocatalysts.[527] Pb doping was responsible for the visible-light absorption, and halogen doping suppressed the formation of nonradiative transition sites in which recombination of photogenerated electrons and holes could occur.

Lei et al. synthesized sulfur-substituted and Zn-doped $In(OH)_3$ in an aqueous solution of ethylenediamine using the hydrothermal method and investigated its photoactivity for H_2 production under visible-light irradiation.[528] As shown in Figure 13, the band gap of $In(OH)_3$ was narrowed by the substitution of S^{2-} for OH^-. The valence band was composed mainly of S 3p orbitals hybridized with O 2p orbitals. Meanwhile, Zn^{2+} doping leveled up the conduction band consisting of In 5s5p and Zn 4s4p orbitals and provided a large thermodynamic driving force for the reduction of water to produce H_2.

4.2. Controlling Band Structure through Solid Solutions

In addition to using foreign elements for doping, forming solid solutions between wide and narrow band gap semiconductors is another promising method for controlling photocatalyst band structure. Both the band gap and position can be adjusted by varying the ratio of the compositions of the narrow and the wide band gap semiconductor in the solid solution. Figure 14 shows the controllable band formation by making a solid solution.

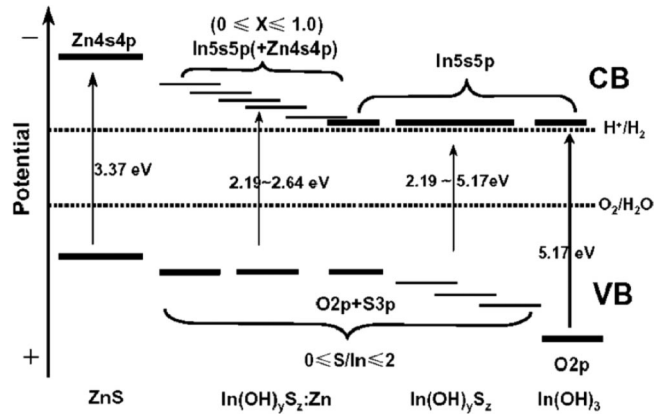

Figure 13. Proposed band structure of $In(OH)_3$, $In(OH)_yS_z$, and $In(OH)_yS_z$:Zn. Reprinted with permission from ref 528. Copyright 2006 Elsevier.

4.2.1. (Oxy)sulfide Solid Solutions

$Cd_xZn_{1-x}S$ ($1 < x < 1$) sulfide solid solutions, formed by combining the wide band gap semiconductor ZnS and the narrow band gap semiconductor CdS, have attracted much research interest for visible-light-driven photocatalysis applications.[529−533] It is known that $Cd_xZn_{1-x}S$ prepared by a coprecipitation method shows quite good photocatalytic activity for hydrogen production from aqueous solutions containing sacrificial reagents S^{2-} and SO_3^{2-} under visible-light irradiation.[534,535] Zhang et al. found that $Cd_{1-x}Zn_xS$ solid solution innovatively prepared by the thermal sulfuration of the corresponding mixed oxide precursors displayed a much higher photoactivity than that prepared by the conventional coprecipitation method.[536] The $Cd_{1-x}Zn_xS$ ($x = 0.2$) solid solution exhibited the highest quantum yield of 10.23% at 420 nm for hydrogen production even without a noble metal as a cocatalyst.

Since 2004, Kudo et al. have focused their attentions on the development of novel photocatalysts from ZnS (wide band gap) and $MInS_2$ (M = Cu, Ag; narrow band gap) sulfide solid solutions.[537−539] The energy structures of the solid solutions were found to be controllable by changing the composition. Taking $ZnS-AgInS_2$ as an example, the diffuse reflectance spectra, as well as the conduction and valence

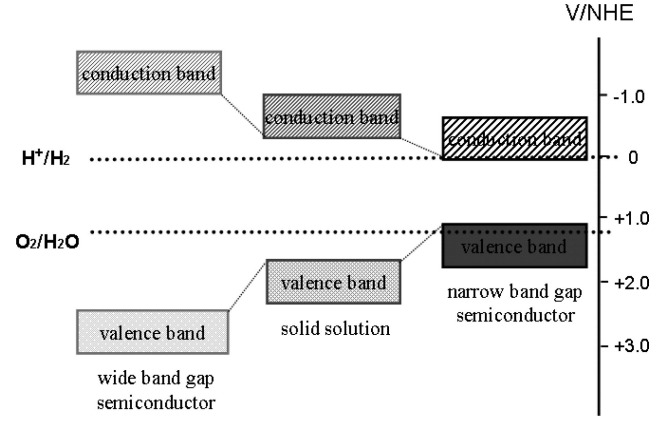

Figure 14. Band structure controlled by making a solid solution.

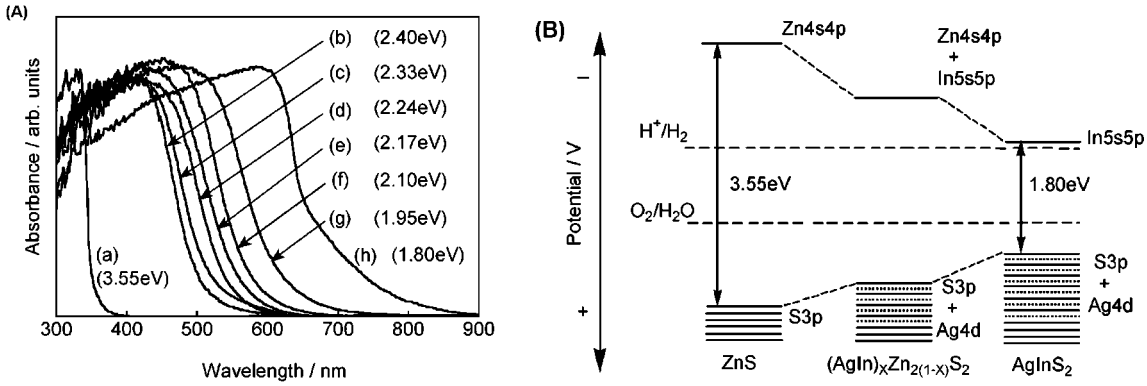

Figure 15. (A) Diffuse reflection spectra of $(AgIn)_xZn_{2(1-x)}S_2$ solid solutions; the values of x are (a) 0, (b) 0.17, (c) 0.22, (d) 0.29, (e) 0.33, (f) 0.40, (g) 0.5, and (h) 1. (B) Band structures of $(AgIn)_xZn_{2(1-x)}S_2$ solid solutions, ZnS, and $AgInS_2$. Reprinted with permission from ref 537. Copyright 2004 American Chemical Society.

band levels, shifted monotonically with the composition of the solid solution as shown in Figure 15.[537] The solid solutions showed high photocatalytic activities for hydrogen evolution under visible-light irradiation. The apparent quantum yields of Pt-loaded $(AgIn)_{0.22}Zn_{1.56}S_2$ (E_g = 2.33 eV) and Pt-loaded $(CuIn)_{0.09}Zn_{1.82}S_2$ (E_g = 2.35 eV) amounted to 20%[537] and 12.5% at 420 nm,[538] respectively. Subsequently, they developed a $ZnS-CuInS_2-AgInS_2$ solid solution, which proved a highly active visible-light-driven photocatalyst. It was demonstrated that the $ZnS-CuInS_2-AgInS_2$ solid solution exhibited an absorption band over a wider wavelength range and a higher photocatalytic activity for hydrogen evolution under the irradiation from a solar simulator compared to the previously reported $ZnS-MInS_2$ (M = Cu or Ag) solid solutions. This was probably due to its narrower band gap ($Cu_{0.25}Ag_{0.25}In_{0.5}ZnS_2$: E_g = 1.77 eV) derived from interactions between the Cu 3d and Ag 4d orbitals involved in the valence band.[540,541]

Another series of novel stannite-type complex sulfide solid solutions with ZnS as the wide band gap semiconductor, $A^I_2-Zn-A^{IV}-S_4$ (A^I = Cu and Ag; A^{IV} = Sn and Ge) was investigated by the same group, also for photocatalytic hydrogen evolution under visible-light irradiation. Among them, Ag_2ZnSnS_4 was the most active, with a quantum yield of ~3% at 500 nm. Cu_2ZnGeS_4 also showed a high activity and had greater stability.[542] The recently reported $AGa_2In_3S_8$ solid solutions formed from AGa_5S_8 and AIn_5S_8 (A = Cu or Ag) gave relatively high quantum yields. They were active for solar H_2 production from aqueous solutions containing electron donors. The apparent quantum yields of Rh(1.5 wt %)/$CuGa_2In_3S_8$ and Rh(0.5 wt %)/$AgGa_2In_3S_8$ were 15% at 560 and 460 nm, respectively.[543] Jang et al. developed novel $AgGa_{1-x}In_xS_2$ solid solutions as visible-light-driven photocatalysts for hydrogen evolution in the presence of an electrolyte (Na_2S/Na_2SO_3).[544] The concentration-dependent band gap tuning was achieved in $AgGa_{1-x}In_xS_2$ ($0 < x < 1$), which was found to vary from 2.6 to 1.9 eV due to the participation of the In 5s5p orbitals in the formation of the lower region of the conduction band. The photocatalytic activity for hydrogen production over $AgGa_{1-x}In_xS_2$ showed the maximum value for $AgGa_{0.9}In_{0.1}S_2$. Chen and co-workers synthesized two nanoporous solid solutions, i.e., $ZnS-In_2S_3-Ag_2S$[545] and $ZnS-In_2S_3-CuS$,[546] using a facile template-free method. Both of them showed relatively high visible-light activities for photocatalytic H_2 evolution from water containing sacrificial reagents of Na_2SO_3 and Na_2S even in the absence of cocatalysts. The quantum yields were 19.8% and 22.6% at 420 nm, respectively.[545,546] Li et al. successfully prepared a zincoxysulfide ($ZnS_{1-x-0.5y}O_x(OH)_y$) solid solution with the valence band formed by S 3p and O 2p hybrid orbitals.[547] It displayed excellent photocatalytic activity for hydrogen evolution, and even without a noble metal cocatalyst, the apparent quantum yield was ca. 3.0% under visible-light irradiation.

4.2.2. Oxide Solid Solutions

The photophysical and photocatalytic properties of oxide semiconductors with similar crystal structures were also studied to explore the possibility of energy structure control using solid solutions.[157,256,548−550] Kudo and Mikami reported the successive changes in absorption, photoluminescence spectra, and conduction band levels of $In_2O_3-Ga_2O_3$ solid solutions.[256] Moreover, they found that both the band gap and conduction band level of the $Sr_2(Ta_{1-x}Nb_x)_2O_7$ solid solution with a layered perovskite structure could be controlled by changing the ratio of niobium to tantalum. All the $Sr_2(Ta_{1-x}Nb_x)_2O_7$ photocatalysts studied had band gaps larger than 3.9 eV and only exhibited photocatalytic activities for water splitting into H_2 and O_2 under UV irradiation.[223] Meanwhile, Zou and co-workers prepared $BiTa_{1-x}Nb_xO_4$ ($0 < x < 1$) solid-solution photocatalysts using solid-state reactions.[200,551] These produced hydrogen both from aqueous CH_3OH/H_2O solutions and from pure water under UV irradiation. Although none of these photocatalysts exhibited visible-light-driven activities, these studies provided some important information for developing novel visible-light-driven photocatalysts derived from oxide solid solutions that could be used for water splitting.

Luan et al. prepared $Bi_xIn_{1-x}TaO_4$ ($0 < x < 1$) solid solutions using a solid-state reaction.[552] The band gaps of the $Bi_xIn_{1-x}TaO_4$ (x = 0.2, 0.5, and 0.8) photocatalysts were estimated at about 2.86, 2.71, and 2.74 eV, respectively. It was suggested that the band structure consisted of a conduction band of mainly Ta 5d, In 5p, and In 5s orbitals, whereas the valence band was principally O 2p, Bi 6s, and Bi 6p orbitals. Under visible-light irradiation ($\lambda > 420$ nm), H_2 and O_2 were evolved from CH_3OH and $AgNO_3$ aqueous solutions, respectively, using the $Bi_xIn_{1-x}TaO_4$ photocatalysts. Yi and Ye prepared $Na_{1-x}La_xTa_{1-x}Co_xO_3$ monophase solid solutions by conventional solid-state reactions.[553] The $Na_{0.9}La_{0.1}Ta_{0.9}Co_{0.1}O_3$ photocatalyst exhibited the highest performance of H_2 evolution (4.34 μmol/h) under visible-light irradiation. The photocatalytic activities of $Na_{1-x}La_x$-$Ta_{1-x}Co_xO_3$ series were mainly attributed to the hybridization of the Co 3d and O 2p orbitals.

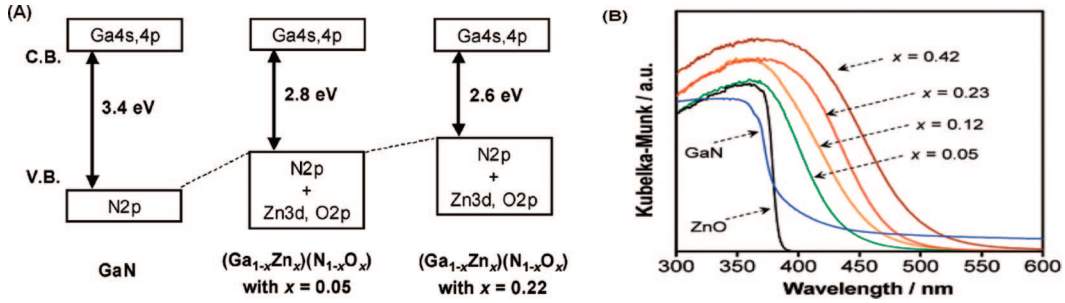

Figure 16. (A) Schematic band structures. Reprinted with permission from ref 569. Copyright 2005 American Chemical Society. (B) UV−visible diffuse reflectance spectra of $(Ga_{1-x}Zn_x)(N_{1-x}O_x)$. Reprinted with permission from ref 51. Copyright 2007 American Chemical Society.

Since the divalent metals in scheelite-type molybdates are easily exchangeable with other elements, Yao and Ye developed new scheelite solid-solution photocatalysts by combining the scheelite molybdates ($CaMoO_4$ and $(Na_{0.5}Bi_{0.5})MoO_4$) with the narrow band gap semiconductor $BiVO_4$.[554,555] These crystallized with similar crystal structures. Both the resulting $CaMoO_4-BiVO_4$ and $(Na_{0.5}Bi_{0.5})MoO_4-BiVO_4$ solid solutions showed high activities for photocatalytic O_2 evolution under visible-light irradiation. In fact, they were even better than that of monoclinic $BiVO_4$, which itself is a well-known efficient visible-light-driven photocatalyst. In the study of Li et al., another series of novel solid-solution photocatalysts $Na(Bi_xTa_{1-x})O_3$ were successfully prepared using a simple hydrothermal method, and $Na(Bi_{0.08}Ta_{0.92})O_3$ showed the highest photocatalytic activity for hydrogen production under visible light.[556] This was attributed to the band structure formed by a hybrid conduction band of the (Bi 6s + 6p + Ta 5d) orbitals.

Wang et al. developed a novel series of solid-solution semiconductors $(AgNbO_3)_{1-x}(SrTiO_3)_x$ $(0 < x < 1)$ as visible-light-active photocatalysts for efficient O_2 evolution and decomposition of organic pollutants.[557,558] The modulation of the band structure (band gap energy, band edge positions, etc.) depends on the extent of the orbital hybridization between both the Ag 4d and O 2p orbitals, as well as that between the Nb 4d and Ti 3d orbitals. As a result of competition between the absorption ability to visible light and the reductive/oxidative abilities, the highest visible-light activities for both O_2 evolution and decomposition of gaseous 2-propanol were realized over $(AgNbO_3)_{0.75}(SrTiO_3)_{0.25}$. The solid solution of Y_2WO_6 and Bi_2WO_6, $BiYWO_6$, was found by Liu et al. to have the photocatalytic ability to completely and stoichiometrically split water into H_2 and O_2 ratio under visible light up to $\lambda < 470$ nm.[559] It was suggested that the Bi 6s and Y 4d orbitals contributed to a new valence band and conduction band, respectively. It was expected that, because of the flexible structure of the solid solution, the activity would be favorably promoted by changing the ratio of Y_2WO_6 and Bi_2WO_6. Soon after, they discovered another $Bi_{0.5}Dy_{0.5}VO_4$ solid solution composed of $BiVO_4$ and $DyVO_4$ that responded to visible light up to 450 nm and completely split water into H_2 and O_2.[560]

4.2.3. Oxynitride Solid Solutions

Starting from the colored oxynitride $LaTiO_2N$, new perovskite-type solid solutions $LaTiO_2N-ATiO_3$ (A = Sr, Ba) were prepared by the thermal ammonolysis method.[561,562] Narrowed band gaps were achieved by both lowering the bottom of the conduction band and raising the top of the valence band as x increased. Thus, $(SrTiO_3)_{1-x}\cdot(LaTiO_2N)_x$ presented suitable band positions for photocatalytic water splitting into hydrogen and oxygen under visible-light irradiation.

Since 2005, Domen's group has systematically investigated on GaN−ZnO solid solutions as potentially new efficient photocatalysts capable of decomposing water into hydrogen and oxygen stoichiometrically under visible-light irradiation.[563−572] The solid solution of GaN and ZnO, $(Ga_{1-x}Zn_x)(N_{1-x}O_x)$, should have band gaps greater than 3 eV, because of the large band gap energies of both GaN and ZnO (>3 eV). However, the p−d repulsion between the N 2p and Zn 3d orbitals shifted the valence-band maximum upward without affecting the conduction-band minimum. This resulted in a narrowing of the band gap of GaN−ZnO solid solution as schematically depicted in Figure 16.[569,573] The result, therefore, was that the band positions of $(Ga_{1-x}Zn_x)(N_{1-x}O_x)$ were suitable for overall water splitting under visible-light irradiation. The quantum efficiency at 420−440 nm was ~2.5%, when $Rh_{2-y}Cr_yO_3$ was loaded as a cocatalyst.[564] The photocatalytic performance of $Rh_{2-y}Cr_yO_3/(Ga_{1-x}Zn_x)(N_{1-x}O_x)$ was due to the fact that the charge recombination was prevented, and there was enhanced reactivity of photoexcited holes in the O_2 evolution reaction.[574] Moreover, the visible-light-driven photocatalytic activity of $Rh_{2-y}Cr_yO_3/(Ga_{1-x}Zn_x)(N_{1-x}O_x)$ was further improved by a postcalcination treatment through reduction of the density of the zinc- and/or oxygen-related defects that functioned as recombination centers for photogenerated electrons and holes in the material. The maximum quantum efficiency obtained by postcalcination treatment is ca. 5.9% at 420−440 nm.[575] This was about an order of magnitude higher than the photocatalytic activity of previously discussed photocatalysts used in overall water splitting under visible light (Ni−$InTaO_4$: 0.66% at 402 nm;[353] $BiYWO_6$: 0.17% at 420 nm[559]). In addition, an appropriate amount of electrolyte (e.g., NaCl and Na_2SO_4) in the photocatalytic reactant solution proved quite effective in enhancing overall water splitting using $Rh_{2-y}Cr_yO_3$-loaded $(Ga_{1-x}Zn_x)(N_{1-x}O_x)$.[576]

Following the development of the $(Ga_{1-x}Zn_x)(N_{1-x}O_x)$ solid solution, $(Zn_{1+x}Ge)(N_2O_x)$,[577−580] the solid solution of $ZnGeN_2$ and ZnO was developed by Domen's group and found to be another active and stable photocatalyst for overall water splitting under visible-light irradiation. Similar to the $(Ga_{1-x}Zn_x)(N_{1-x}O_x)$ solid solution, the band gap narrowing of $(Zn_{1+x}Ge)(N_2O_x)$ was also attributed to the p−d repulsion between the N 2p and Zn 3d orbitals. Thus, the visible-light-driven overall water splitting catalyzed by $(Zn_{1+x}Ge)(N_2O_x)$ proceeded via band gap photoexcitation from the valence band formed by the N 2p, O 2p, and Zn 3d orbitals to the conduction band consisting of Ge 4s and 4p hybridized

orbitals. Instead of the successful formation of the ideal solid solution between $(Ga_{1-x}Zn_x)(N_{1-x}O_x)$ and InN, the obtained Ga−Zn−In mixed oxynitride also behaved as a visible-light-driven photocatalyst for water splitting, but it photocatalyzed H_2 and O_2 evolution only in the presence of an appropriate electron donor or acceptor.[581]

4.3. Dye Sensitization to Harvest Visible Light

Dye sensitization is another powerful strategy to enable the visible-light harvesting of wide band gap semiconductors.[582−584] It has been actively studied in solar energy conversion systems involving dye-sensitized solar cells[585−591] and dye-sensitized photocatalytic reactions.[592−595] Since the breakthrough work by O'Regan and Grätzel in 1991,[596] the dye-sensitized solar cell has attracted much attention, owing to its stability, low cost, and device efficiency. Power-conversion efficiencies of >11% have been achieved.[597−600] The operating principle of dye-sensitizated solar cells usually involves the excitation of the dye and then charge transfer from the dye to the semiconductor.[601] In addition, the application of dye-sensitized solar cells to water splitting has also been achieved.[602] Since the electron-transfer step resembles that in dye-sensitized solar cells, dye-sensitized semiconductors could also function as photocatalysts for water splitting under visible-light irradiation.

Figure 17 illustrates the basic principle of dye-sensitized photocatalytic H_2 production from water. Photoexcitation of the dye adsorbed onto the semiconductor leads to the injection of electrons into the conduction band of the semiconductor. The electrons are consumed by the reduction of water to produce H_2. The oxidized dye molecules are subsequently reduced and then regenerated by accepting electrons from the electron donor.[603,604]

4.3.1. Sensitization Using Ruthenium Complex Dyes

Photocatalytic hydrogen production systems in which ruthenium(II) complex dyes sensitize wide band gap semiconductors to visible light have been the focus of intensive research for many years. In the early 1980s, Grätzel and co-workers[70,592,605−607] succeeded in decomposing water by visible light using $Ru(bpy)_3^{2+}$ and its amphiphilic derivatives as sensitizers. Pt/RuO_2-loaded TiO_2 particles proved particularly effective in those systems, acting as photocatalysts for water-splitting process.

Nakahira et al. found that Pt/TiO_2 sensitized with a polymer-pendant $Ru(bpy)_3^{2+}$ complex was effective in H_2 evolution in the presence of the sacrificial donor (EDTA) under visible-light irradiation.[608] Adsorption of the Ru(dcbpy)$_3$ sensitizer onto platinized TiO_2 particles (Pt/TiO_2) also

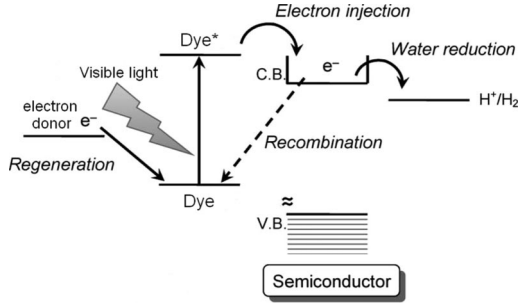

Figure 17. Basic principle of dye-sensitized photocatalytic H_2 production from water. Reprinted with permission from ref 604. Copyright 2008 American Chemical Society.

led to H_2 evolution by visible light, again with a sacrificial donor.[609] Hirano et al. found that, when $Ru(bpym)_3^{2+}$ was used as the visible-light sensitizer, Pt/TiO_2 showed much higher efficiency for H_2 production than $Ru(bpy)_3^{2+}$.[610] This may be due to the greater affinity of $Ru(bpym)_3^{2+}$ on the TiO_2 surface. Dhanalakshmi et al. found that, when TiO_2 and ZnO were sensitized with a new sensitizer ($[Ru(dcbpy)_2(dpq)]^{2+}$), they displayed extremely stable and effcient photocatalytic activity for hydrogen production under visible-light irradiation from water even in the absence of an electron donor.[611] However, interestingly, the photocatalytic activities of $[Ru(dcbpy)_2(dpq)]^{2+}$-sensitized Pt/ZnO and Cu/ZnO were found to be 10 times lower than those of $[Ru(dcbpy)_2(dpq)]^{2+}$-sensitized Pt/TiO_2 and Cu/TiO_2, respectviely. Bae et al. compared the photocatalytic activities and stabilities of two $Ru(bpy)_3^{2+}$-sensitized TiO_2 photocatalysts with different surface-anchoring groups (carboxylate and phosphonate), i.e., c-$Ru(bpy)_3^{2+}$ and p-$Ru(bpy)_3^{2+}$, respectively. Pt/TiO_2/p-$Ru(bpy)_3^{2+}$ anchored through phosphonate groups exhibited higher photocatalytic activity for hydrogen production from water than Pt/TiO_2/c-$Ru(bpy)_3^{2+}$ anchored through carboxylate groups.[612] Because of the more rapid regeneration of p-$Ru(bpy)_3^{2+}$ than c-$Ru(bpy)_3^{2+}$, the phosphonate group seemed to be better than the carboxylate group as a ruthenium sensitizer linkage to the TiO_2 surface in aqueous environment. However, both of them turned out to be unstable in water, not only under visible-light illumination but also in the dark.

Abe et al. studied the effect of the energy gap between the I^{3-}/I^- redox potential and the highest occupied molecular orbital (HOMO) level of the dyes on the photocatalytic activity of Ru complex dye-sensitized Pt/TiO_2 in water−acetonitrile solutions.[613] The system included I^- as an electron donor. It was found that a sufficiently positive HOMO level, compared to the oxidation potential of I^-, was necessary in order to produce a relatively high rate of H_2 evolution over Ru complex dye-sensitized Pt/TiO_2. Peng and co-workers investigated the influence of different ruthenium(II) bipyridyl complexes on the photocatalytic H_2 evolution over TiO_2 under visible light.[614,615] When compared to $Ru(bpy)_2(him)_2-NO_3$- and $Ru(dcbpy)_2(NCS)_2$-sensitized Pt/TiO_2, $Ru_2(bpy)_4L_1-PF_6$-sensitized Pt/TiO_2 displayed higher photocatalytic efficiency and preferable durability for H_2 evolution. This may be related to the dynamic equilibrium between the linkage of the ground dye to TiO_2 and the separation of the oxidized dye from TiO_2. Choi and co-workers investigated the addition of a thin Al_2O_3 overlayer on the $Ru(bpy)_3^{2+}$-sensitized TiO_2 and found that it significantly increased the visible-light-sensitized activity for hydrogen production.[616] As shown in Figure 18, it was proven that the main role of the Al_2O_3 barrier layer was to retard the charge recombination between the electron injected from the excited dye and the oxidized dye. They also found that guanidinium cations adsorbed on nafion-coated $Ru(bpy)_3^{2+}$-sensitized TiO_2 retarded the charge recombination between the electrons injected into the TiO_2 conduction band and the oxidized dye molecules. This resulted in enhanced photocatalytic hydrogen production under visible light.[617]

Reisner et al. constructed a special system consisting of [NiFeSe]−hydrogenase attached to Ru dye-sensitized TiO_2, with triethanolamine (TEA) as the sacrificial electron donor.[618] It showed a high and stable photocatalytic activity for hydrogen generation under visible light. Gurunathan et al. found that the photocatalytic efficiency of SnO_2 could be

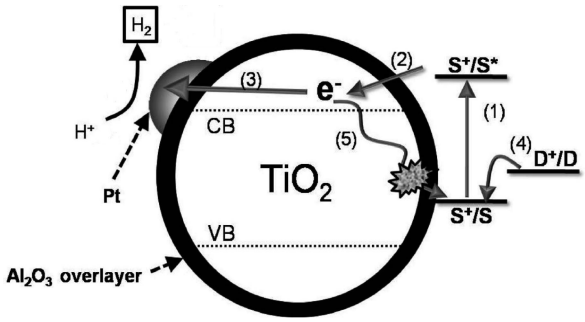

Figure 18. Schematic illustration of electron transfer/recombination processes occurring on a dye-sensitized TiO_2 particle with Al_2O_3 overlayer for H_2 production. The numbered paths indicate the following: (1) dye excitation; (2) electron injection from the excited dye to TiO_2 CB; (3) electron trapping on Pt; (4) regeneration of the oxidized dye by electron donor (D); and (5) back electron transfer to the oxidized dye (recombination). Reprinted with permission from ref 616. Copyright 2009 American Chemical Society.

greatly improved using $Ru(bpy)_3^{2+}$ sensitization.[619] The highest photocatalytic activity for hydrogen evolution, with quantum yield of 2.40% at 350 nm, was observed with the $Pt/SnO_2/RuO_2-Ru(bpy)_3^{2+}-MV^{2+}-EDTA$ system. This may be due to a number of contributing factors, which include the loading of the bifunctional redox catalyst onto SnO_2, electron injection from the excited $Ru(bpy)_3^{2+}$ to the conduction band of SnO_2, electron mediation by MV^{2+}, and electron donation by EDTA to scavenge the valence band holes.

Furube et al. investigated the dynamics of photoexcited $Ru(bpy)_3^{2+}$ intercalated into the $K_4Nb_6O_{17}$ interlayers.[620] Because of the fast and efficient electron transfer between $Ru(bpy)_3^{2+}$ and $K_4Nb_6O_{17}$, the transient bleaching of the $Ru(bpy)_3^{2+}$ band showed fast and nonexponential decay. This differed from the behavior of $Ru(bpy)_3^{2+}$ in water, and led to the photocatalytic hydrogen evolution over $Ru(bpy)_3^{2+}$ intercalated $K_4Nb_6O_{17}$ from aqueous solution containing an electron donor.[621] Later, Mallouk and co-workers studied different layered oxide semiconductors as the building blocks for visible-light H_2 production from water using a ruthenium complex as the photosensitizer.[604,622−626] The $Ru(bpy)_3^{2+}$-sensitized $K_4Nb_6O_{17}$ nanoscrolls exhibited higher photocatalytic activity than $Ru(bpy)_3^{2+}$-sensitized lamellar $K_4Nb_6O_{17}$ and TiO_2. This was primarily due to the high surface area of the nanoscrolls and their excellent ability to bind $Ru(bpy)_3^{2+}$. This led to the facile transfer of electrons from the sensitizer to the Pt catalyst islands via the single-crystalline nanoscrolls. The authors claimed that the platinized $H_4Nb_6O_{17}$ nanoscrolls were a slightly better electron transfer mediator than acid-restacked $HCa_2Nb_3O_{10}$ nanosheets. The apparent quantum yield of visible-light photocatalytic hydrogen production over $Pt/H_4Nb_6O_{17}$ nanoscrolls was ~25% at 450 ± 20 nm, when sensitized by $Ru(bpy)_3^{2+}$ complexes.[623,624]

4.3.2. Sensitization Using Other Transition-Metal Complex Dyes

Many other transition-metal complexes such as polypyridine complexes, alizarine, phthalocyanine, and metalloporphyrins with metal centers including Pt(II), Co(II), Zn(II), and Cr(III) have also been widely used as sensitizers for wide band gap photocatalysts to improve their optical and photocatalytic properties for hydrogen evolution in the visible-light region.

In the study of Zakharenko et al.,[627] the $Pt(alizarine)_2$ complex adsorbed onto the surface of titanium dioxide was found to cause spectral sensitization of TiO_2 and lead to photocatalytic hydrogen production from water in the visible-light region. Two new platinum(II) terpyridyl acetylide complexes were synthesized and used by Jarosz et al.[628] They were used to sensitize platinized TiO_2 for the photogeneration of H_2 using visible light. However, the long-term ability of these complexes to act as sensitizers in this capacity was limited by decomposition after oxidation.

Malinka and co-workers found that H_2 evolved from aqueous suspensions of zinc-porphyrin-sensitized Pt/TiO_2 in the presence of an electron donor, such as EDTA, TEA, and ascorbic and oxalic acids, under irradiation with visible light ($\lambda > 520$ nm).[629,630] Zinc porphyrins displayed increased photostability when absorbed onto the semiconductor surface, and the photocatalytic activity of zinc-porphyrin-sensitized Pt/TiO_2 was greatly affected by factors such as concentrations of platinum, sensitizer and electron donor, the pH and temperature of the suspension. Shimidzu et al. found that the visible-light illumination ($500 < \lambda < 700$ nm) of a water-soluble porphyrin−zinc complex and TEA in aqueous solution with suspended particulate ZnO/Pt resulted in efficient hydrogen production with a quantum yield higher than 3.0% at 548 ± 3 nm.[631]

Nada et al. found that, when copper phthalocyanine was used as a photosensitizer, it was effective for hydrogen production over RuO_2/TiO_2 using UV/solar light irradiation.[632] In fact, copper phthalocyanine exhibited higher efficiency compared to other sensitizers such as ruthenium bipyridyl. Since the splitting of pure water using a dye-sensitized oxide semiconductor has not been achieved previously, it is worth mentioning that Hagiwara et al. were the first to report the sensitizing effects of porphyrinoids on the photocatalytic splitting of H_2O into H_2 and O_2 by $Pt/KTa(Zr)O_3$.[633] The addition of porphyrinoids to $KTa(Zr)O_3$ effectively increased the activity of this compound for pure water splitting. Among the porphyrinoids examined, cyanocobalamin showed the strongest effect on photocatalytic water splitting. Moreover, the metal cation of the porphyrin complex had a large influence on the production rates of H_2 and O_2. For example, $Pt/KTa(Zr)O_3$ sensitized with Cr−tetraphenylporphyrin showed much higher photoactivity than a catalyst sensitized with Co−tetraphenylporphyrin.

Rayalu and co-workers reported that, because of the synergistic effect of Co^{2+} and heteropolyacid (HPA), HPA/Co^{2+} sensitized TiO_2 showed excellent photocatalytic activity for hydrogen evolution under visible light.[634−636] The presence of Co^{2+} not only enhanced the visible-light absorption property but also played a very important role in triggering the overall catalytic efficiency. Recently, a TiO_2 photocatalyst sensitized by grafting surface complexes of lacunary Wells−Dawson W-contained heteropoly blue (HPB) exhibited 20.0% quantum efficiency for H_2 evolution under 670 nm irradiation in the presence of glycerol as the electron donor.[637,638]

4.3.3. Sensitization Using Metal-Free Dyes

Because some transition-metal complexes, especially Ru complexes, are quite expensive, metal-free dyes, such as porphine dyes, xanthene dyes, melocyanine dyes, and coumarin dyes, have all been investigated.

Houlding and Grätzel reported the excellent ability of 8-hydroxyquinoline-sensitized anatase TiO_2 powders to

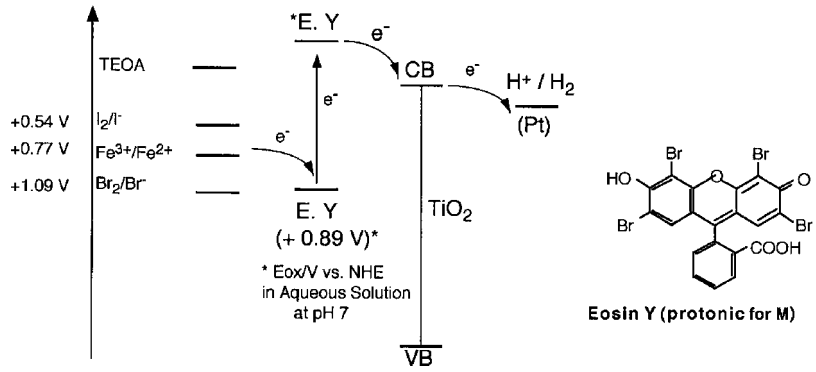

Figure 19. Eosin Y-sensitized TiO_2 for H_2 evolution system in two-step water splitting. Reprinted with permission from ref 646. Copyright 2000 Elsevier.

generate hydrogen in a sacrificial water-reduction system containing EDTA as the electron donor using visible light.[639] Gurunathan et al. investigated the photocatalytic activities for hydrogen production by Pt/SnO_2 sensitized with various metal-free photosensitizers.[619] These included acriflavin, Eosin Blue, rhodamine B, Rose Bengal, and fluorescein. Of all the photosensitizers used, Eosin Blue showed the maximum efficiency to sensitize SnO_2 and evolved a greater amount of hydrogen, even higher than $Ru(bpy)_3^{2+}$. Hirano et al. found that some porphine derivatives, such as tetrakis-(4-carboxyphenyl)porphine (TPPC), tetrakis-(4-sulfonicphenyl)porphine (TPPS), and tetrakis-(4-pyridylphenyl)porphine (TPPPy) were all effective as photosensitizers.[610] It was also found that $TPPC/TiO_2/Pt$ exhibited the highest activity for hydrogen evolution from water in the presence of EDTA as the electron donor. The principal reasons proposed for this enhanced activity include the degree of adsorption onto TiO_2, the different electron densities in excited states, or redox potential. Chatterjee claimed that the efficacy of the photocatalytic system toward hydrogen evolution was quite possibly governed by the excited-state redox properties of the dyes adsorbed onto the surface of the TiO_2 photocatalyst.[640] A binaphthol complex was applied by Ikeda et al. to sensitize TiO_2 for photocatalytic hydrogen evolution from TEA solutions under visible-light irradiation.[641] The photonic efficiency of the photocatalytic reaction at 450 nm was estimated to be 0.02% for the binaphthol-modified TiO_2 loaded with 0.1 wt % Pt.

Abe et al. investigated the significant influence of solvent on hydrogen production over metal-free dye sensitized Pt/TiO_2 photocatalysts from a water−acetonitrile mixed solution containing an iodide electron donor under visible-light irradiation.[613,642−644] The rates of H_2 evolution decreased with increasing water content in the mixed solutions. This was due to the decreasing energy gap between the redox potential of I_3^-/I^- and the HOMO level of the dye. However, when compared to merocyanine sensitized Pt/TiO_2, a relatively high rate of H_2 evolution was still observed over a coumarin-sensitized Pt/TiO_2 photocatalyst even in aqueous solution. This was because coumarin had a sufficiently positive HOMO level compared to the oxidation potential of I^-.

Shimidzu et al. reported extensive studies on visible-light-induced photocatalytic water reduction using some xanthene dye-sensitized particulate Pt-loaded semiconductor catalysts.[645] They found that heavy halogenated xanthene dyes, e.g., Rose Bengal, erythrosine, and eosine bluish, showed high quantum yields of hydrogen production for sensitized platinized semiconductors. However, they tended to photodehalogenate, whereas nonhalogenated xanthene dyes, e.g., uranine and rhodamine B, exhibited high durability against any photodeterioration but only moderate catalytic activities. Interestingly, it was also found that the addition of external halide ions improved the photocatalytic activities of nonhalogenated xanthene dye-sensitized platinized semiconductors. Abe et al. constructed a stable dye-sensitized photocatalyst system in water by a chemical fixation of xanthene dyes onto platinized TiO_2 particles using a silane-coupling reagent.[646] The Eosin Y-fixed $Pt-TiO_2$ exhibited high efficiency and quite steady H_2 production from aqueous TEA solution under visible-light irradiation for long periods. The quantum yield at 520 nm was determined to be ~10%. Figure 19 shows the Eosin Y-sensitized TiO_2 in a two-step water-splitting system for H_2 evolution.

Lu and co-workers systematically studied the Eosin Y-sensitized Ti-based photocatalysts for hydrogen generation from di- or triethanolamine aqueous solution under visible-light irradiation ($\lambda \geq 420$ nm).[647−653] Eosin Y-sensitized Rh/TiO_2,[647] $Pt/Na_2Ti_2O_4(OH)_2$,[649] and Pt/Ti-MCM-41[652] showed relatively excellent photocatalytic activities and long-term stability for hydrogen production. Average quantum yields higher than 10% in the visible-light region were found. In particular, Eosin Y-sensitized $Pt/Na_2Ti_2O_4(OH)_2$, with a quantum yield up to 14.97%, showed good photocatalytic stability for hydrogen production over 100 h after 10 consecutive runs.[649] Subsequently, a much higher quantum yield of 17.36% was obtained over Eosin Y-sensitized Pt-loaded long titanic acid nanotubes. However, the destruction of the nanotube structure after long-time reaction led to a decrease in the hydrogen generation rate.[653]Additionally, the multilayer-Eosin Y-sensitized TiO_2 via Fe^{3+} coupling was found to have a high light harvesting efficiency and photocatalytic activity for hydrogen evolution under visible-light irradiation. The maximum apparent quantum yield for hydrogen evolution is 19.1% from aqueous TEA solution.[654] They also achieved efficient photocatalytic water reduction for hydrogen generation over Eosin Y-sensitized Pt/SiO_2[655] and Pt/MWCNT (multiwalled carbon nanotube)[656] in the presence of TEA as the electron donor. Quantum yields up to 10.4% and 12.14%, respectively, were observed.

4.4. Developing Novel Single-Phase Visible-Light-Responsive Photocatalysts

Even without using the modification technologies discussed above (ion doping, making solid solutions, and dye sensitization), many novel single-phase visible-light-responsive photocatalysts, mostly heterometallic oxides, have been fabricated successfully using metal-mediated band structure

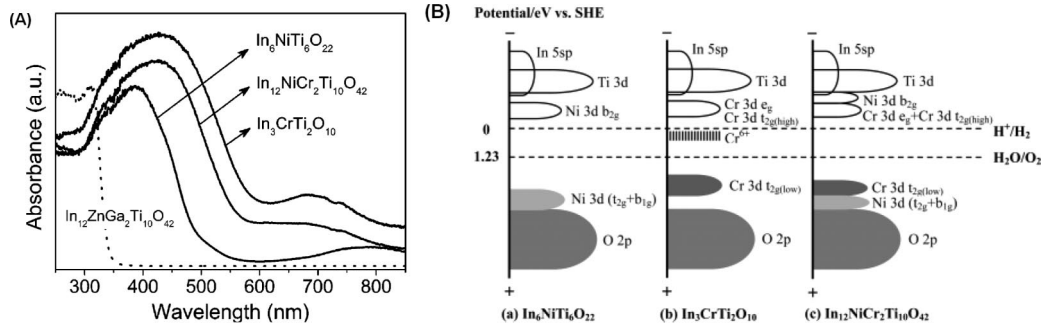

Figure 20. (A) UV−vis absorption spectra of $In_6NiTi_6O_{22}$, $In_3CrTi_2O_{10}$, and $In_{12}NiCr_2Ti_{10}O_{42}$ powder samples at room temperature. The dotted line shows the absorption spectrum of $In_{12}ZnGa_2Ti_{10}O_{42}$. (B) Schematic band structures of (a) $In_6NiTi_6O_{22}$, (b) $In_3CrTi_2O_{10}$, and (c) $In_{12}NiCr_2Ti_{10}O_{42}$. Reprinted with permission from ref 666. Copyright 2007 American Chemical Society.

engineering. In this section, we will focus on recent progress in the design of single-phase heterometallic oxides as novel visible-light-responsive photocatalysts. Of particular interest are materials with band structures mediated and band gap narrowed by d-, s-, and f-orbitals from the outer layer orbital configurations of d-block, p-block, and f-block metal ions, respectively.

4.4.1. d-block Metal Oxides

The versatile features of the d orbitals of some transition metals for band gap narrowing have been demonstrated by doping such d-block transition metals into wide band gap photocatalysts to form a separate donor level in the forbidden band.[353,354,525] The activities of the resulting doped photocatalysts are usually not high because the doping level can also serve as a recombination center for photogenerated electrons and holes. It is expected, therefore, that d-block transition metals could also contribute to the band gap narrowing of single-phase heterometallic oxide photocatalysts.

In the study of Yin et al., the single-phase visible-light-driven photocatalyst $BaCrO_4$, with a band gap determined to be 2.63 eV, was synthesized by a solid-state reaction method.[657] Since the Cr^{6+} 3d orbital was empty, the band structure of $BaCrO_4$ was defined by the 3d level of Cr^{6+} and the O 2p level of the ligand O atom. As a result, the visible-light transition was ascribed to the electronic excitation from the valence band composed of the O 2p orbitals to the conduction band composed of the Cr^{6+} 3d orbitals. Unlike the Cr 3d orbitals in $BaCrO_4$, Cr^{3+} 3d orbitals in $BaCr_2O_4$ were partially filled and split into Cr 3d-t_{2g} and Cr 3d-e_g orbitals. This split in band structure resulted in two cases of electron photoexcitations, namely, the photoexcitation from Cr 3d-t_{2g} to Cr 3d-e_g and the photoexcitation from O 2p to Cr 3d-t_{2g}, evolving H_2 and O_2, respectively.[658] Further reports of Cr-based oxides with different electronic structures of Cr 3d orbitals were conducted by Ouyang et al.[659] In $AgAlO_2$, the valence band and the conduction band were mainly constructed by Ag 4d and O 2p orbitals, and Ag 5s and 5p orbitals, respectively. The band gap was estimated to be 2.95 eV from the UV−vis spectra. When Al element in $AgAlO_2$ was replaced by Cr, both $AgCrO_2$ and Ag_2CrO_4 showed an obvious red shift of the absorption edge. The trivalent Cr ions in $AgCrO_2$ owned three 3d-electrons, which were split to two groups, whereas the hexavalent Cr ions in Ag_2CrO_4 had no 3d-electrons. This was the reason $AgCrO_2$ had double absorption bands and Ag_2CrO_4 only had a single absorption band in the visible-light region. Cr ions with different 3d orbitals had different effects on the band structure. Cr 3d orbitals in Ag_2CrO_4 only contributed to the conduction band, whereas Cr 3d orbitals in $AgCrO_2$ contributed to both valence and conduction bands. This was analogous to the previous reports on $BaCrO_4$[657] and $BaCr_2O_4$.[658]

Lv et al. developed a new photocatalyst, namely, $LiCr(WO_4)_2$, in which the Cr3d level contributed similarly to the formation of both the conduction and valence bands.[660] It showed photocatalytic activity for H_2 evolution under visible-light irradiation. Ye et al. developed a new series of 3d transition metal Ni-containing photocatalysts, NiM_2O_6 (M = Nb, Ta), which proved active for water splitting under visible-light irradiation.[661] For NiM_2O_6, which contains two kinds of octahedra, NiO_6 and MO_6, the valence band energy was assumed to arise from both the O 2p orbitals of the NiO_6 and MO_6 octahedra. The valence band showed a value about 1.0 eV more positive than 2.94 (standard hydrogen electrode (SHE)) of O 2p levels. This resulted in the band gap narrowing of NiM_2O_6. It is believed that the Ni d−d transition between the Ni 3d-t_{2g} and Ni 3d-e_g levels also played an important role in the visible-light photoexicitaion and photocatalytic activity of NiM_2O_6. Similar Ni d−d transitions were also observed in other Ni-containing heterometallic oxides such as $BaNi_{1/3}Nb(Ta)_{2/3}O_3$,[178,225] $MLaSrNb_2NiO_9$ (M = Na, Cs, H),[662,663] and Ca_2NiWO_6.[664] In all these cases, such transitions appeared to be responsible for their visible-light absorption and visible-light-induced photocatalytic activities.

Wang and co-workers systematically investigated the band structures of three oxide semiconductor photocatalysts, $In_6NiTi_6O_{22}$, $In_3CrTi_2O_{10}$, and $In_{12}NiCr_2Ti_{10}O_{42}$.[665,666] They used different 3d transition metals with partially filled 3d orbitals to clarify the effects of the transition metal cations (Ni and/or Cr) on the photophysical and photocatalytic properties. As shown in Figure 20, the split Ni 3d orbitals in $In_6NiTi_6O_{22}$ or the split Cr 3d orbitals in $In_3CrTi_2O_{10}$ formed only a discrete band, whereas the coexistence of both Ni^{2+} and Cr^{3+} in $In_{12}NiCr_2Ti_{10}O_{42}$ enabled the formation of continuous conduction and valence bands through the hybridization of the split Ni 3d and Cr 3d orbitals with the Ti 3d/In 5s5p and O 2p orbitals. The formation of the continuous conduction and valence bands not only decreased the band gap energy but also increased the mobility of the photoinduced charge carriers. Thus, the photocatalytic activity of $In_{12}NiCr_2Ti_{10}O_{42}$ for hydrogen evolution under visible-light irradiation was improved compared to those of $In_6NiTi_6O_{22}$ and $In_3CrTi_2O_{10}$. Silva et al. synthesized a series of Zn/Ti, Zn/Ce, and Zn/Cr layered double hydroxides (LDH) and tested them for the visible-light photocatalytic oxygen generation.[667] Because of the chemical composition and in contrast to the (Zn/M)LDH (M = Ti, Ce), the (Zn/Cr)LDH

containing Cr exhibited much greater light absorption in the visible region. The most active material was found to be the (Zn/Cr)LDH. Its apparent quantum yields for oxygen generation were 60.9% and 12.2% at 410 and 570 nm, respectively.

Ye et al. found that the 3d transition metal V compound, $InVO_4$, was effective for H_2 evolution from pure water under visible-light irradiation.[668] The $InVO_4$ showed photocatalytic activity up to 600 nm, which is a much wider wavelength range than previously reported for In-based oxides such as $InTaO_4$ and $InNbO_4$. This was as expected from the conduction band composed of the less negative V 3d orbitals in $InVO_4$, when compared to the Nb 4d orbitals in $InNbO_4$ and the Ta 5d in $InTaO_4$. It was reported that another vanadate, $BiVO_4$, showed visible-light photocatalytic activity for O_2 evolution from an aqueous solution containing either Ag^+ or Fe^{3+} as electron acceptor.[669−674] However, $BiVO_4$ did not display photocatalytic activity for H_2 evolution. This is because the conduction band composed of the V 3d orbitals was located at less negative potential than for H^+ reduction to H_2. Judging from the above results, it is possible that, depending on the chemical components and crystal structures of different vanadates, the V 3d level is either less negative or more negative than the H_2 evolution potential. Some other V-containing oxide semiconductors, such as $M_{2.5}VMoO_8$ (M = Mg, Zn),[675] $M_3V_2O_8$ (M = Mg, Ni, Zn),[676] $CaBiVMO_8$ (M = W and Mo),[677] Bi_2GaVO_7,[251] Bi_2YVO_8,[252] and BiM_2VO_6 (M = Cu and Zn),[678,679] also displayed efficient visible-light absorption and photocatalytic activities. This is because the V 3d orbitals involved in the band structures act to lower down the conduction band, leading to band gap narrowing of these V-containing oxide photocatalysts.

Yin et al. investigated a new series of visible-light-driven photocatalysts $MCo_{1/3}Nb_{2/3}O_3$ (M = Ca, Sr, and Ba) with an ABO_3-type perovskite structure, in which the B site is occupied by Co^{2+} and Nb^{5+} randomly.[680,681] In these compounds, the Co^{2+} 3d states, which were split into two main peaks, the lower t_{2g} state and the higher e_g state, were strongly hybridized with the O 2p states to form the valence bands. As a result, the observed visible-light absorption for $MCo_{1/3}Nb_{2/3}O_3$ was ascribed to the electronic excitations from the Co^{2+} t_{2g} state to the Nb^{5+} 4d state. Sun et al. reported that, in $Bi_5FeTi_3O_{15}$, the Fe 3d band split into two main parts, corresponding to the Fe t_{2g} and the Fe e_g, respectively.[682] The photoexcitation from the hybridized O 2p + Fe t_{2g} + Bi 6s orbitals to the Fe e_g orbitals were most probably responsible for the visible-light absorption of $Bi_5FeTi_3O_{15}$. Because of the Fe 3d orbitals involved in the band structure, $Ca_2Fe_2O_5$ was sensitive to visible light. Its band gap was estimated to be ~1.86 eV from opitical absorption spectra. This could split pure water to generate H_2 under visible-light irradiation, after $Ca_2Fe_2O_5$ was loaded with NiO.[683]

Kato et al. found that the band gaps of $AgTaO_3$ and $AgNbO_3$ were 0.6 eV smaller than those of $NaTaO_3$ and $NaNbO_3$, respectively, although their crystal structures of $AgMO_3$ (M = Ta, Nb) were similar to those of $NaMO_3$.[242] DFT calculations showed that a hybrid Ag 4d and O 2p orbital formed a valence band at a higher energy level than O 2p orbitals, and this resulted in the decrease in the band gaps of $AgMO_3$ (M = Ta, Nb). These findings made it possible to develop $AgNbO_3$ as a good visible-light-driven photocatalyst with the ability to evolve H_2 or O_2 from water in the presence of sacrificial reagents. Similarly, the contribution of Ag^+ to the valence band formation for α-$AgVO_3$ led to a smaller band gap than in α-$NaVO_3$, which was responsible for the unnegligible photocatalytic activity for O_2 evolution under visible-light irradiation.[684] Keeping in mind the valence bands consisting of hybridized Ag 4d and O 2p orbitals, some noval Ag-based metal oxides, such as $AgInW_2O_8$,[685] α-$AgGaO_2$,[686] Ag_2ZnGeO_4,[687] and $AgLi_{1/3}M_{2/3}O_2$ (M = Ti and Sn),[688] were developed as visible-light-driven photocatalysts. The valence bands of these metal oxides are located at higher energy levels than those consisting of only O 2p orbitals. This is what leads to the narrowed band gaps and hence to the proposed visible-light-driven photocatalytic activities.

4.4.2. p-block Metal Oxides

In addition to the d-block transition metals, s-orbitals from the outer layer-orbital configurations of p-block metal ions are also effective to mediate the band structures. Tang and co-workers synthesized MIn_2O_4 (M = Ca, Sr, Ba) semiconductors as potential visible-light-photoactive materials containing the InO_6 octahedral structure.[689,690] For these In-containing oxides, the highest occupied band was composed of O 2p orbitals, which corresponded to the valence band. The lowest unoccupied band which was mainly composed of the In 5s orbitals, which corresponds to the conduction band. Taking this into consideration, the visible-light absorption was attributed to the photoexcition from the O 2p orbital to the In 5s orbital. However, for $InMO_4$ (M = Ta, Nb), which contains two kinds of octahedra, InO_6 and MO_6, the valence band was assumed to be a combination of both the O 2p levels of InO_6 and NbO_6 octahedrons. It showed ~1.1 eV more positive than that of the O 2p levels.[691−693] This is quite similar to the case in which the valence band of $NiNb_2O_6$ containing NiO_6 and NbO_6 octahedra was attributable to both the O 2p levels of NiO_6 and NbO_6 octahedra.[661,694] The relatively positive valence band energy suggested that both $InTaO_4$ and $InNbO_4$ had suitable band structures and could respond to visible light. This was quite different from the visible-light photoexcition from O 2p orbital to In 5s orbital in MIn_2O_4 (M = Ca, Sr, Ba).

Zhou et al. prepared a visible-light-responsive polycrystalline $Bi_{12}TiO_{20}$ photocatalyst using a simple solid-state reaction between Bi_2O_3 and TiO_2 powders.[695] Its band gap was narrowed to be 2.78 eV through the introduction of the p-block transition metal Bi. The band structure of $Bi_{12}TiO_{20}$ originated from the Ti 3d band as well as the Bi 6s and O 2p hybridized band. This hybridization shifted the valence band upward, causing the band gap of $Bi_{12}TiO_{20}$ to be narrowed. Similarly, for some other Bi(III)-containing oxides, such as $CaBi_2O_4$,[696,697] Bi_2WO_6,[145,698,699] Bi_2MoO_6,[700] $BiSbO_4$,[701] and Bi_2MNbO_7 (M = Al, Ga, In),[702,703] the proposed band structure of the valence bands also involved the hybridized orbitals between the Bi 6s and the O 2p orbitals. These played an important role in their visible-light absorption and photocatalytic activities. Kako et al. investigated the photophysical properties and band structure of $NaBiO_3$ as a visible-light-driven oxide Bi (V) photocatalyst.[704] They found that the band structure of the valence band in $NaBiO_3$, mainly composed of the O 2p orbitals, was quite different from that of Bi(III)-containing oxides. The latter was composed of hybridized orbitals between the Bi 6s and the O 2p orbitals at the top of the valence band. This situation arose because the contribution of the empty Bi^{5+} 6s orbitals in $NaBiO_3$ to the valence band was much smaller than the filled Bi^{3+} 6s orbitals in the Bi (III)-containing oxides.

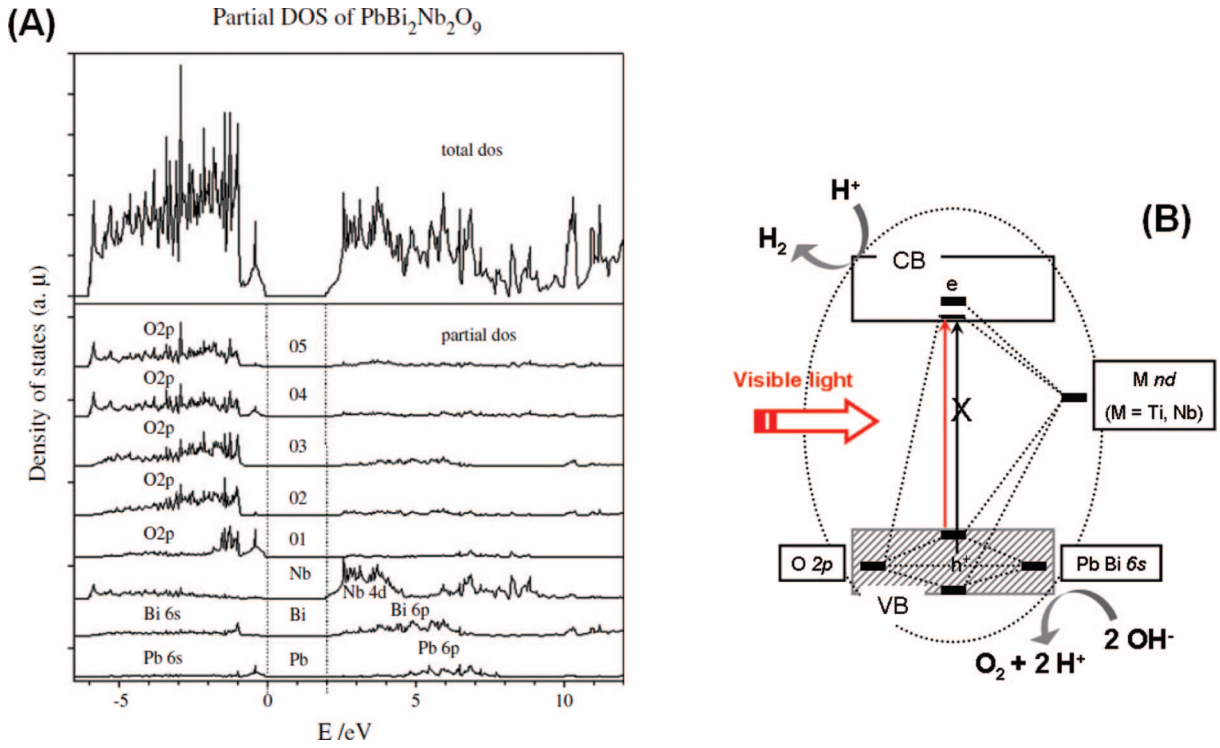

Figure 21. (A) Calculated total and partial density of states (DOS) of $PbBi_2Nb_2O_9$. The conduction and valence bands of the compound consist of empty Nb 4d and occupied O 2p orbital, with the latter hybridized with Pb6s and/or Bi6s, giving the smaller band gap compared to compounds that do not contain Pb and Bi in their structure. (B) Schematic band energy diagram of lead- or bismuth-substituted perovskite-related oxides. Reprinted with permission from ref 707. Copyright 2006 Elsevier.

Li and co-workers developed the two binary lead niobates, $Pb_3Nb_2O_8$ and $Pb_3Nb_4O_{13}$, as visible-light-sensitive photocatalysts.[705,706] Compared to pure Nb_2O_5, the hybridization of the Pb 6s and O 2p orbitals in these lead niabates raised the position of the valence band edge and narrowed the band gap, leading to the observed visible-light responses. Kim and co-workers investigated the substitution effects of lead on the photophysical and photocatalytic properties of a range of UV-light-active photocatalysts: $CaBi_4Ti_4O_{15}$, $CaBi_2Nb_2O_9$, $K_{0.5}La_{0.5}Ca_{1.5}Nb_3O_{10}$, and $Sr_3Ti_2O_7$.[707,708] They found that their lead-containing analogues ($PbBi_4Ti_4O_{15}$, $PbBi_2Nb_2O_9$, $K_{0.5}La_{0.5}Ca_{0.75}Pb_{0.75}Nb_3O_{10}$, $K_{0.5}La_{0.25}Bi_{0.25}Ca_{0.75}Pb_{0.75}Nb_3O_{10}$, and $PbTiO_3$) absorbed visible light and exhibited good photocatalytic activities for water decomposition under visible-light irradiation. This was attributed to the additional hybridization of the occupied Pb 6s and O 2p orbitals in such lead-containing compounds. This pushed up the position of the valence band, giving a smaller band gap compared to their respective lead-free counterparts as shown in Figure 21.

Hosogi and co-workers found that $SnNb_2O_6$[243,709] and $SnNbO_2$,[710] which contain Sn^{2+} with a $5s^2$ electron configuration, showed the photocatalytic activity under visible-light irradiation for H_2 or O_2 evolution from an aqueous solution containing methanol or $AgNO_3$. The valence band level formed from a hybrid orbital of Sn 5s and O 2p was higher than that consisting of only O 2p orbitals. This made $SnNb_2O_6$ responsive to visible light. Furthermore, they developed a novel series of Sn^{2+}-exchanged layered metal oxides, $Sn^{2+}/KTiNbO_5$, $Sn^{2+}/K_4Nb_6O_{17}$, $Sn^{2+}/CsTi_2NbO_7$, $Sn^{2+}/K_2Ti_4O_9$, $Sn^{2+}/K_2Ti_2O_5$, and $Sn^{2+}/Cs_2Ti_6O_{13}$. These Sn^{2+}-exchanged layered metal oxides had visible-light absorption bands and showed activities for H_2 or O_2 evolution from an aqueous solution containing a sacrificial reagent under visible-light irradiation.[711] This was due to the electronic transition from an electron donor level consisting of Sn 5s orbitals to conduction bands consisting of Ti 3d and Nb 4d orbitals. Of particular note is the contribution of the Sn 5s filled orbitals to the valence band structure of β-$SnWO_4$, which causes a decrease in the band gap, leading to a novel visible-light active photocatalyst for H_2 evolution from an aqueous methanol solution under visible-light irradiation.[712]

4.4.3. f-block Metal Oxides

The introduction of rare earth 4f orbitals with a view to tuning the electronic structure has also been investigated for developing new visible-light-driven photocatalysts. Zou et al. investigated the effects of the rare earth elements on the band structures and photophysical properties of Bi_2RNbO_7 (R = Y, rare earth).[199,713] They found that the R 4f orbitals of the R^{3+} ions were very important for the band structures of these photocatalysts. The visible-light absorption was found to be based on the R 4f and Nb 4d band transition between the R^{3+} and Nb^{5+} ions. That is to say, the partly filled R 4f level in the rare earths could form a new energy level in the band structure, and the 4f−d transition resulted in the narrowed band gaps of these photocatalysts. Hwang et al. also found that the 4f band of rare earths greatly contributed to the band structures of $R_2Ti_2O_7$ (R = rare earth: La, Pr, Nd).[127] The R 4f level in $R_2Ti_2O_7$ was shifted to a lower energy as the number of 4f electrons increased. This decreased the band gap energy of both $Pr_2Ti_2O_7$ and $Nd_2Ti_2O_7$. A similar phenomenon was also discovered by Uno and co-workers for the $R_2M_2O_7$ (R = La, Pr, Nd, Sm, Gd, Dy, Ho, Er, and Yb; M = Ti, Zr) photocatalysts.[132,154] Because of the effect of the 4f orbital electrons, $Sm_2M_2O_7$ (M = Ti, Zr) and $Nd_2Zr_2O_7$ were considered possible

candidates capable of responding to visible light for photocatalytic hydrogen production from water.

Tian et al. developed a series of Ce-containing metal oxide photocatalysts $K_4Ce_2M_{10}O_{30}$ (M = Ta, Nb), capable of evolving H_2 and O_2 from aqueous solutions, under visible-light irradiation ($\lambda > 420$ nm), containing a sacrificial electron donor and acceptor, respectively.[714] It was demonstrated that the conduction bands of $K_4Ce_2M_{10}O_{30}$ (M = Ta, Nb) were mainly attributed to the Ta 5d (or Nb 4d) orbitals, while the valence bands were composed of hybridized O 2p + Ta 5d (or Nb 4d) and occupied Ce 4f orbitals. The latter made an essential contribution to the small band gap energy of these photocatalysts. The pyrochlore-type compound Sm_2InMO_7 (M = Ta, Nb), with a $4f-d^{10}-d^0$ configuration, was found to be a new stable visible-light-responsive photocatalyst for H_2 evolution from water. The $4f-d^{10}-d^0$ configuration was also proven useful for visible-light photocatalysis from the viewpoint of both the crystal and electronic structure.[715,716]

4.4.4. Miscellaneous Photocatalysts

Recently, some phosphate semiconductors were reported to show good photocatalytic activity for water splitting under visible-light irradiation. For example, Ag_3PO_4 showed an extremely high quantum yield of ca. 80% at wavelengths less than ~480 nm for O_2 evolution from an aqueous silver nitrate solution.[717] It was significantly higher than previously reported values.[667] $Li_9Fe_3(P_2O_7)_3(PO_4)_2$, prepared by a hydrothermal method, was proven to be active for photocatalytic H_2 evolution under visible-light irradiation, where I^- was used as the electron donor.[718]

$TiSi_2$, with a band gap range from 3.4 to 1.5 eV, was reported as a promising semiconducting catalyst for visible-light-driven overall water splitting. The evolution of oxygen and hydrogen was facilitated with the formation of the catalytic centers on the surface of $TiSi_2$ by photooxidation. Moreover, the reversible photoadsorption of oxygen onto the $TiSi_2$ catalyst allowed the convenient separation of the hydrogen and oxygen products.[719]

A metal-free polymeric photocatalyst, carbon nitride (g-C_3N_4), was developed by thermal condensation for efficient hydrogen or oxygen production from water under visible-light irradiation with the assistance of a sacrificial reagent. By varying the thermal condensation conditions, the fine adjustment of the electronic and optical properties was possible. The band gap of the fully condensed graphitic carbon nitride was estimated to be 2.7 eV. Whereas the valence band was a combination of the HOMO levels of the melem monomer derived from the nitrogen p_z orbitals, the conduction band was similarly connected to the LUMO of the melem monomer predominantly from the carbon p_z orbitals.[720] Homogeneous substitution of sulfur for lattice nitrogen within g-C_3N_4 gave rise to an increased valence bandwidth in combination with an elevated conduction band minimum and a slightly reduced absorbance. The resulting $C_3N_{4-x}S_x$ showed a H_2 evolution rate 8.0 times higher than C_3N_4 under the irradiation of $\lambda > 420$ nm.[721] The optical absorption of g-C_3N_4 was extended into the visible region up to about 750 nm after being copolymerized with barbituric acid.[722] The modified g-C_3N_4 showed a remarkable improvement in H_2 evolution activity compared to g-C_3N_4 under both UV and visible-light irradiation.[722]

A graphite oxide semiconductor photocatalyst was reported to steadily produce H_2 under visible-light irradiation from an aqueous methanol solution, even in the absence of Pt as the cocatalyst.[723] The band gap energy of graphite oxide was dependant on the number of oxygenated sites and was estimated from optical absorption spectra to be 2.4−4.3 eV. The valence band edge of graphite oxide was mainly composed of the O 2p orbitals. The conduction band edge was mainly formed by the antibonding π^*-orbitals and had a higher energy level than that needed for H_2 generation.

5. Approaches for Efficient Photogenerated Charge Separation

While visible-light-driven photocatalysts with proper band structures are currently developed using some modification technology or band engineering approaches as discussed above, the issue of photogenerated charge separation is another key factor strongly affecting the efficiency of the photocatalytic water-splitting process. Clearly, in order to increase the utilization rate of the photogenerated charges and obtain high photocatalytic water-splitting activities, the photogenerated charges must be efficiently separated to avoid bulk/surface charge recombination and transfer to the separated active sites on the surface of the photocatalysts. This is to ensure depression of the backward reaction of hydrogen and oxygen to form water. In this section, we will review the primary approaches and achievements to date for the efficient separation of photogenerated charges in the water-splitting process. We aim to present the numerous experimental and theoretical research results that have appeared over the past decades.

5.1. Cocatalyst Loading

Transtition metals, especially the noble metals, are widely used as effective cocatalysts for photocatalytic water splitting. Taking Pt as an example, the processes of charge transfer between cocatalyst and host photocatalyst are described in Figure 22. When the noble metal is loaded onto the surface of the photocatalyst, the photogenerated electrons migrate to the surface of the host photocatalyst and are entrapped by the noble metal cocatalyst, because the Fermi energy level of noble metal is always lower than that of the semiconductor photocatalyst. Meanwhile, the photogenerated holes stay at the host photocatalyst and migrate to its surface. This results in the efficient separation of the photogenerated electrons and holes. Subsequently, the separately localized electrons and holes become involved in their roles as the reducer and oxidizer, respectively, in the photocatalytic reaction. Overall, the role played by the cocatalysts dispersed on the surface of the photocatalysts is extremely important. It improves the

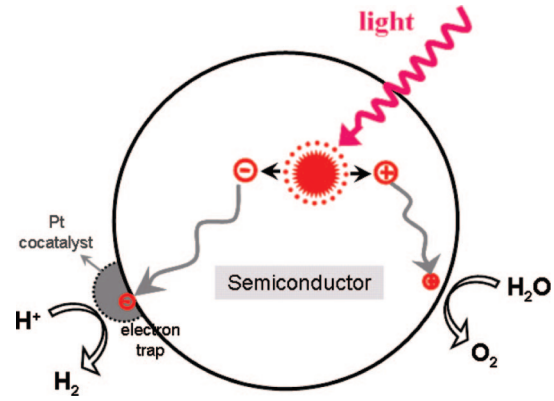

Figure 22. Processes of charge transfer between host photocatalyst and cocatalyst, taking Pt as the example of cocatalyst.

overall photocatalytic activity of the water splitting because it helps to promote charge separation, which in return reduces both bulk and surface electron/hole recombination. It also accelerates the surface chemical reaction by inhibiting the backward reaction.

5.1.1. Noble Metal Cocatalysts

As one of the noble metals, Pt has been widely used as the cocatalyst in photocatalytic water splitting over many different kinds of semiconductors: oxides,[71,80,92,186,724−726] (oxy)sulfides,[489,490,727−730] and (oxy)nitrides.[390,430,468,476,731] All have been shown to greatly enhance the photocatalytic activity for hydrogen evolution. Up until now, the highest photocatalytic activities for hydrogen production from water using visible-light irradiation are from photocatalysts loaded with Pt as the cocatalyst.[732,733] Some other noble metals, such as Au,[734−739] Ru,[540,541,740−742] Pd,[735,743−745] Ag,[746−750] and Rh,[751−754] have also been reported as efficient cocatalysts.

Iwase et al. found that fine gold nanoparticles played an important role in the creation of active sites for H_2 evolution and the enhancement of charge separation.[167] In addition, the back-reaction between H_2 and O_2 to produce water on the Au cocatalyst was negligible in comparison to that on a Pt cocatalyst. This ultimately led to improved photocatalytic activities of some titanate, niobate, and tantalate photocatalysts for overall water splitting. Hara et al. reported the unusual enhancement of H_2 evolution by Ru on a TaON photocatalyst under visible-light irradiation.[740] It should be noted that, under identical conditions, other noble metals, such as Pt, Ir, and Rh, were ineffective in promoting any evolution of H_2. The authors deduced that the electronic structure of the interface between the Ru particles and TaON possibly facilitated electron transfer from TaON to Ru. This ultimately gave an impetus to charge separation.

Wu et al. investigated H_2 production with low CO selectivity from the photocatalytic reforming of glucose in water on metal/TiO_2 catalysts (metal = Pt, Rh, Ru, Ir, Au, Ni, and Cu).[755] The loaded metals, in particular Rh, were found to greatly enhance the rate of H_2 production. This was attributed to the fact that the Schottky barrier formed at the metal and TiO_2 interface could serve as an efficient electron trap, thus preventing photogenerated electron−hole recombination. The effect of the nature of the metal cocatalyst was interpreted in terms of different electronic interactions between the metal nanoparticles and the TiO_2 surface.[756] It was also reported that the smaller the Schottky barrier height at the metal/semiconductor junction, the greater was the electron flow from semiconductor to metal, thus leading to higher photocatalytic activity for hydrogen production.[757] On the other hand, the synergistic enhancement effect of the Pt and Ru coloading on hydrogen evolution compared to that of either Pt or Ru alone was observed by Liu and co-workers.[393,394] They considered that the superior activity of Pt/Ru-loaded $LaTaON_2$ (or $Y_2Ta_2O_5N_2$) for H_2 evolution was related to enhanced electron transfer from the conduction band of the photocatalyst to the Pt/Ru cocatalysts. This retards the possibility of electron−hole recombination in the valence band and improves the charge separation efficiency. When cocatalysts consisting of Au/Pd bimetallic nanoparticles with core/shell structures were loaded onto the TiO_2 surface, selective H_2 permeability by the Pd shell was believed to contribute to the selective donation of the photogenerated electrons to the protons. The result is greatly enhanced photocatalytic production of H_2 from aqueous ethanol solutions.[758]

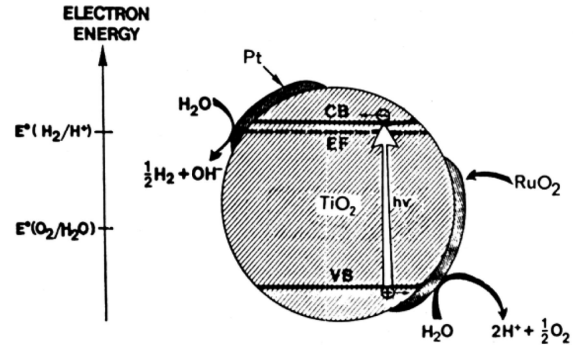

Figure 23. Schematic illustration of the photoinduced events leading to water decomposition on Pt/RuO_2−TiO_2 composite catalyst. Reprinted with permission from ref 70. Copyright 1981 American Chemical Society.

5.1.2. Transition-Metal Oxide Cocatalysts

Some transition-metal oxides such as RuO_2[187,244,257,277,577,759,760] and NiO[109,110,175,206,761,762] are also well-known as efficient cocatalysts in water splitting. Domen and co-workers found that β-Ge_3N_4 alone exhibited little photocatalytic activity for water decomposition.[24,277] However, when loaded with RuO_2, the material became photocatalytically active under UV irradiation ($\lambda > 200$ nm). Maeda et al. found that the presence of RuO_2 cocatalysts loaded on the g-C_3N_4 surface was indispensable not only for enhancing O_2 evolution activity but also for suppressing the oxidative decomposition of the nitride catalyst.[763] Similarly, IrO_2 was also found to act as a water oxidation cocatalyst for water splitting.[622,764,765]

Borgarello and co-workers noted a pronounced synergistic effect in catalytic activity when both RuO_2 and Pt are codeposited onto the TiO_2 particles.[308,606,766] Figure 23 depicts the photosplitting of water on Pt/RuO_2−TiO_2. It has been proposed that Pt is likely to yield an ohmic contact whereas a Schottky barrier may be formed by RuO_2. This would direct the electron flow to the Pt sites while the holes would be trapped by RuO_2,[70] resulting in efficient charge separation and improved photocatalytic activity. Moreover, Teramura et al. found that the high dispersion of RuO_2 nanoclusters on the catalyst surface was essential for improving the photoactivity for H_2 and O_2 evolution in overall water splitting.[767] It was demonstrated that both Ru(IV) species and bulk RuO_2 exhibited less activity for overall water splitting, whereas with RuO_2 nanoclusters as cocatalyst, $(Ga_{1-x}Zn_x)$-$(N_{1-x}O_x)$ displayed an improvement of H_2 and O_2 evolution.

In a series of studies using $(Ga_{1-x}Zn_x)(N_{1-x}O_x)$, Maeda and co-workers loaded Cr−M (M being one of the transition metals, Fe, Co, Ni, Cu, Ru, Rh, Pd, Ag, Ir, or Pt) as a mixed-oxide cocatalyst onto $(Ga_{1-x}Zn_x)(N_{1-x}O_x)$ using a coimpregnation method.[768−771] The largest improvement in activity was obtained by loading the Rh−Cr mixed oxide (1 wt % Rh and 1.5 wt % Cr) with calcination at 623 K. It was proposed that loading the Cr−Rh mixed oxide facilitated the charge transfer from the host photocatalyst to the cocatalyst. It is also possible that, in addition, the loading promoted the creation of active sites for hydrogen evolution, which resulted in inhibited charge recombination and enhanced photocatalytic activity.[772] Maeda and co-workers also developed noble metal/Cr_2O_3 core/shell nanoparticles as a cocatalyst for overall photocatalytic water splitting.[773−775] Figure 24 shows

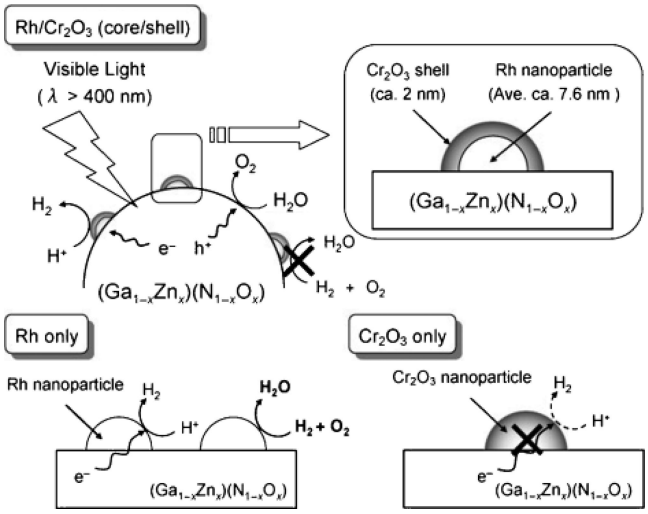

Figure 24. Schematic reaction mechanism of overall water splitting on Rh/Cr_2O_3-core/shell-loaded $(Ga_{1-x}Zn_x)(N_{1-x}O_x)$ and the corresponding processes on supported Rh nanoparticles and Cr_2O_3 nanoparticles. The impregnation of GaN:ZnO with Cr_2O_3 nanoparticles alone does not promote overall water splitting. H_2 evolution occurs on Rh nanoparticles loaded on GaN:ZnO; however, in the presence of O_2, this H_2 reacts immediately with O_2 on the Rh nanoparticles to form H_2O. For Rh/Cr_2O_3-core/shell-loaded $(Ga_{1-x}Zn_x)(N_{1-x}O_x)$, H_2 evolution occurs on the Cr_2O_3 shell, and O_2 evolution occurs on the surface of GaN:ZnO bulk, thereby preventing water formation from H_2 and O_2 on Rh nanoparticles. Reprinted with permission from ref 773. Copyright 2006 Wiley-VCH.

a schematic reaction mechanism for overall water splitting on Rh/Cr_2O_3-core/shell-loaded $(Ga_{1-x}Zn_x)(N_{1-x}O_x)$. The mode of operation is quite different to cocatalysts such as the Rh−Cr mixed oxide, in which at least two roles are played simultaneously. In the Rh/Cr_2O_3 core/shell cocatalyst, the Rh core and the Cr_2O_3 shell worked independently. The Rh core promotes charge separation in $(Ga_{1-x}Zn_x)(N_{1-x}O_x)$ as well as tunneling electron transfer to the Cr_2O_3 shell, whereas the Cr_2O_3 shell provides catalytic active sites for H_2 production, thereby preventing water formation from H_2 and O_2 on the Rh. The Rh core could be further replaced by other noble metals (Pd, Pt) as well as metal oxides (NiO_x, RuO_2, Rh_2O_3). This also resulted in enhanced photocatalytic activity for overall water splitting under visible-light irradiation.[776] This enhancement in activity was primarily due to the suppression of undesirable reverse reactions (H_2-O_2 recombination and/or O_2 photoreduction) and possibly the protection of the core component from chemical corrosion. This depended on the core type. Among the core materials examined, Rh species exhibited relatively high performance. Interestingly, with assistance of Mn_3O_4 nanoparticles coloading, the photocatalytic activity for overall water splitting was improved for $(Ga_{1-x}Zn_x)(N_{1-x}O_x)$, which was modified with core/shell-structured Rh/Cr_2O_3 nanoparticles. The Mn_3O_4 nanoparticles functioned as O_2 evolution sites, and Rh/Cr_2O_3 nanoparticles hosted H_2 evolution sites.[777]

When NiO acts as the cocatalyst for photocatalytic water splitting, an activation pretreatment is generally necessary for NiO-loaded photocatalysts in order to obtain high activities.[175,353,778] A reduction−reoxidation treatment produces a double-layered NiO/Ni structure on the surface of the photocatalyst. Because NiO has a lower Fermi level in comparison to metallic Ni, this double-layered structure facilitates the electron transfer from the photocatalyst material to the Ni layer and then onto the NiO layer of the H_2 evolution sites. The result is the efficient charge separation for water splitting and the suppression of the backward reaction of water splitting on the metallic Ni surface.

Tian et al. investigated the effects of nanosized Pt, RuO_2, and NiO_x loading onto the visible-light-driven photocatalysts $K_4Ce_2M_{10}O_{30}$ (M = Ta, Nb) for hydrogen evolution from water.[779] The photocatalytic activities of evolving H_2 were markedly promoted by cocatalysts loading, in particular, the NiO_x loading with the formation of the NiO/Ni double-layered structure. This was attributable to enhanced electron migration from the conduction band of the photocatalyst to the NiO/Ni cocatalyst. Hwang et al. prepared a series of metal oxide (MO_x, M = Ni, Pt, Cs, Bi, Fe, Pb, Ce)-loaded $Sr_2Nb_2O_7$ photocatalysts using the impregnation method and following reduction−oxidation treatment.[780] Of these metal oxides, the NiO_x cocatalyst showed the highest activity for water splitting. The reduction−oxidation pretreatment for the formation of a double-layered structure was important to achieve the high activity especially for NiO_x-loaded catalysts. This could be ascribed to the more efficient electron−hole separation as a result of the role of nickel played in the p-type/n-type junction between NiO_x and $Sr_2Nb_2O_7$ as formed in the reduction−oxidation pretreatment. However, this marked dependence of photocatalytic activity on pretreatment conditions was not observed for any other metal oxides in this study. To improve the photocatalytic activity of H_2O decomposition, various kinds of metal oxides (MO_x: M = Cr, Mn, Fe, Co, Cu, Ru, Ag, Ce, Sm, and Pb) were introduced into the $NiO_y-K_2La_2Ti_3O_{10}$ catalyst as a second component of the cocatalyst together with NiO_y. Only the $CrO_x-NiO_y-K_2La_2Ti_3O_{10}$ catalyst showed higher photocatalytic activity and durability for longer periods of irradiation than the parent $NiO_y-K_2La_2Ti_3O_{10}$.[781]

5.1.3. Nonmetal-Oxide Cocatalysts

In addition to the noble metals and the transition-metal oxides, some other compounds, such as the transition-metal sulfides, have also been developed as novel cocatalysts. Zong and co-workers developed MoS_2 as a novel cocatalyst for photocatalytic hydrogen evolution.[782,783] They found that the CdS activity was enormously increased by loading with MoS_2, even higher than that of Pt-loaded CdS under the same reaction conditions. The better coupling between the structures and electronic configurations of MoS_2 and CdS together, and the formation of junctions between CdS and MoS_2, improved the charge separation and were mainly responsible for the high activity of this MoS_2/CdS catalyst. MoS_2 nanoparticles cocatalysts were also found to be effective in H_2 evolution over CdSe nanoribbons.[784] The MoS_2 activated the photocatalyst by reducing the electrochemical proton reduction overpotential.[784] Li and co-workers found that the photocatalytic activity of CdS could be enhanced significantly by loading a small amount of a noble metal sulfide (PdS, Rh_2S_3, Ru_2S_3), as well as a noble metal (Pt, Pd, Ru, Rh).[733,785] Moreover, codeposition of Pt with other noble metal sulfides on CdS demonstrated further enhanced photoactivity in hydrogen production; the photocatalytic activity of CdS codeposited with Pt and PdS was greater than those of Pt/CdS and PdS/CdS. This synergistic effect between the Pt and PdS cocatalysts could be explained by the fact that the two cocatalysts may facilitate separation of the photogenerated electrons and holes on the photocatalyst.

Tabata et al. found that dispersion of transition metal sulfides such as NiS, FeS, Ru_2S_3, Ag_2S, CoS, and PdS, into

the $CuGa_3S_5$ photocatalyst solution also increased the photocatalytic activity.[498] The transition metal sulfides were believed to accept electrons from the excited state of $CuGa_3S_5$ and reduce H^+ into H_2 when transition metal sulfides and $CuGa_3S_5$ particles collided with each other. Jang et al. proved that tungsten carbide (WC) had potential as an alternative cocatalyst for photocatalytic hydrogen production.[786] Under visible-light irradiation, the WC/CdS photocatalyst showed excellent photocatalytic activity for hydrogen production from water, comparable to that of conventional Pt/CdS. This was because WC provided active sites for hydrogen evolution and promoted fast migration of the photogenerated electrons from CdS to WC. This resulted in efficient charge separation and enhanced photocatalytic activity.

5.2. Semiconductor Combinations

The semiconductor combination approach has been shown to be another effective method for improving photocatalytic activity through better photogenerated charge separation with a formation of a heterojunction structure.

As is well-known, CdS, which is a fascinating visible-light-driven photocatalyst for hydrogen production, is very unstable toward photocorrosion, as a result of serious self-oxidation by the photogenerated holes in the valence band. To improve its photocatalytic activity and stability, CdS has been embedded in different kinds of inert matrices,[787−793] as well as combined with other semiconductors of different band energies, such as TiO_2,[794,614] ZnO,[614,796−798] $LaMnO_3$,[799] and $KNbO_4$.[800,801] Among these composites, CdS-based semiconductor combination systems, CdS/TiO_2 has attracted the most extensive research.[802−810] Charge separation in a CdS/TiO_2 system, as shown in Figure 25,[811,812] has been investigated in several detailed studies.[614,811−814] Both the conduction and valence band edges of CdS are at more negative potentials than those of TiO_2. Under visible-light irradiation, the photogenerated electrons in the CdS particles quickly transfer to TiO_2 particles, whereas photogenerated holes stay in CdS. This facilitates the electron−hole separation and prevents the charge recombination, improving the photocatalytic activity.

Tada et al. developed an anisotropic CdS−Au−TiO_2 heterojunction, in which CdS, TiO_2, and the electron-transfer medium (Au) were all spatially fixed.[815] This three-component system exhibited a high photocatalytic activity, far exceeding those of the single- and two-component systems. This is a result of vectorial electron transfer driven by the two-step excitation of TiO_2 and CdS. Park et al. investigated the effects on visible-light-driven hydrogen production of varied combinations of CdS, TiO_2, and Pt in hybrid photocatalysts (Figure 26).[816] They found that direct particle-to-particle contact of CdS and TiO_2, and photodeposition of Pt on the TiO_2 particle surface, which resulted in the vectorial electron transfer of CdS → TiO_2 → Pt (Figure 26c), was necessary to achieve efficient charge separation and transfer and hence observed the highest photoactivity of the CdS/(Pt−TiO_2) hybrid catalyst.

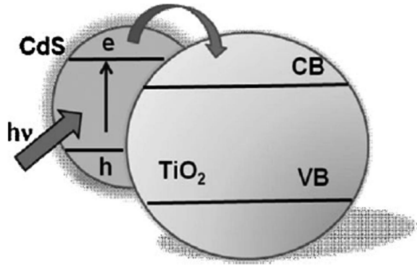

Figure 25. Charge separation in CdS/TiO_2 semiconductor combination system under visible-light irradiation. Reprinted with permission from ref 812. Copyright 2009 Wiley-VCH.

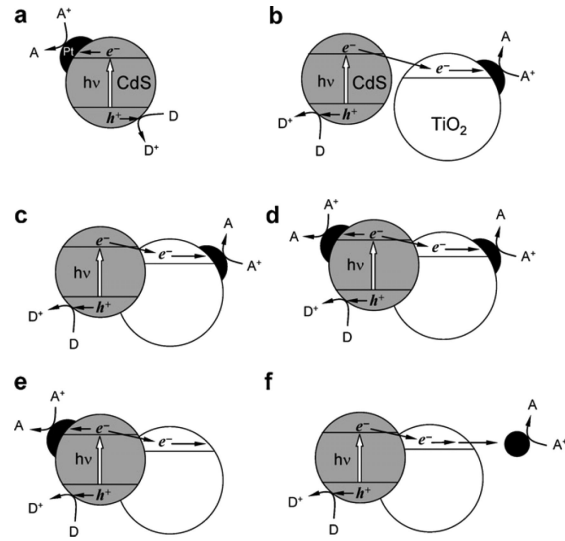

Figure 26. Illustrative diagrams of the electron transfers in the hybrid photocatalysts. (a) Pt−CdS; (b) CdS + Pt−TiO_2 (physically mixed); (c) CdS/(Pt−TiO_2); (d) Pt−(CdS/TiO_2); (e) TiO_2/(Pt−CdS); (f) CdS/TiO_2 + Pt. Reprinted with permission from ref 816. Copyright 2008 The Royal Society of Chemistry.

Because of the fact that the semiconductor combination has been proven to play a beneficial role in the improvement of photogenerated charge separation, many other different kinds of semiconductor combination systems have been developed for photocatalytic hydrogen production from water. Wang et al. developed a novel Zn-doped Lu_2O_3/Ga_2O_3 composite photocatalyst for stoichiometric water splitting.[255] It was proved to have great advantage over the individual precursor materials owing to its enhanced charge-separation ability. Similarly, the TiO_2/SnO_2 mixed oxide showed enhanced photocatalytic activity for hydrogen generation compared to pure TiO_2.[83] Guo and co-workers found that the $TiO_{2-x}N_x$−WO_3 composite photocatalyst showed higher hydrogen production activity under visible-light irradiation than either $TiO_{2-x}N_x$ or WO_3 alone.[817,818] Again this was attributed to the efficient charge separation of photogenerated electrons and holes.

Zou and co-workers reported a novel Cr-doped $Ba_2In_2O_5/In_2O_3$ system, which was properly bridged by an ohmic contact.[819] It turned out to be a novel composite photocatalyst with enhanced activity for water splitting when compared to the individual components. The photoinduced charge carrier separation and migration were promoted by the potential offsets between the band edges of individual materials Cr−$Ba_2In_2O_5$ and Cr−In_2O_3. On the basis of a similar electron transfer mechanism, $In_2O_3/NaNbO_3$ was also found to be advantageous for both photocatalytic H_2 evolution under visible-light irradiation and pure water splitting under UV irradiation.[820] Ou et al. successfully synthesized a visible-light-driven MWNT−TiO_2 composite catalyst using MWNTs dispersively grown on the surface of TiO_2.[821] In this system, efficient charge separation and effective photocatalytic H_2 evolution resulted when the photogenerated electrons of the MWNTs transferred quickly to the conduction band of the TiO_2 under visible-light irradiation. Similarly, in a Bi_2S_3/TiO_2 system, the enhanced photoactivity was

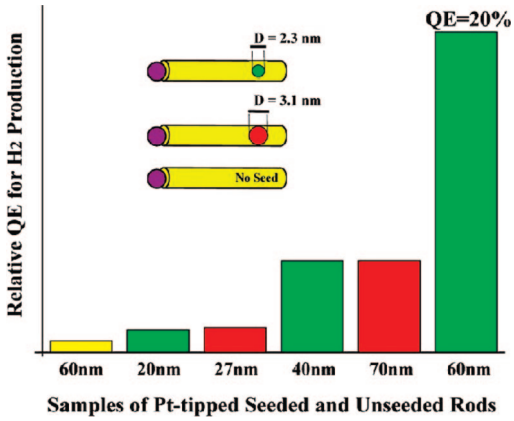

Figure 27. Relative quantum efficiency for hydrogen production, obtained from platinum-tipped unseeded CdS rods (yellow), and five different samples of platinum-tipped seeded rods, with seed diameters of 3.1 (red) or 2.3 nm (green). Underneath each bar is the corresponding average sample length. Reprinted with permission from ref 824. Copyright 2010 American Chemical Society.

ascribed to photoelectron transfer from the conduction band of Bi_2S_3 to the conduction band of TiO_2, resulting in water reduction.[822]

Silva et al. developed a novel Pt-interlinked hybrid composite of cubic-phase CdS (c-CdS) and hexagonal-phase CdS (hex-CdS).[823] In order to explain the relative order of photocatalytic activity found, c-CdS/Pt/hex-CdS > Pt/c-CdS/hex-CdS > Pt/hex-CdS > hex-CdS > c-CdS/hex-CdS > c-CdS, they concluded that the formation of a potential gradient at the interface between the cubic and hexagonal CdS, and the interlinkage of quantum-sized cubic CdS and bulk-phase hexagonal CdS with Pt, were necessary to achieve the efficient charge separation and transfer. This was quite similar to the CdS/Pt/TiO_2 semiconductor combination system investigated in their previous study.[816]

Recently, Amirav and Alivisatos designed a multicomponent nanoheterostructure for efficient photocatalytic hydrogen production composed of a Pt-tipped CdS rod with an embedded CdSe seed.[824] In such structures, holes were three-dimensionally confined to the CdSe seed, whereas the delocalized electrons were transferred to the metal tip. Consequently, the electrons were separated from the holes over three different components and by the tunable physical length of the CdS rod. By tuning the nanorod heterostructure length and the seed size, as shown in Figure 27, the hydrogen production activity was significantly increased compared to that of the unseeded rods. This structure was found to be highly active for hydrogen production, with an apparent quantum yield of 20% at 450 nm. There was also a demonstrated improved stability compared to CdS rods without CdSe seeding.

The incorporation of a guest semiconductor into the interlayers of a lamellar compound for fabricating an intercalated composite semiconductor has been considered as a promising method for the enhancement of the photocatalytic activity. The idea is that in this guest−host semiconductor combination system, the recombination between the photoinduced charge carriers is effectively suppressed due to the quick charge transfer from the guest to the host semiconductor.[825−829] In the past few years, some transition metal oxides with semiconducting host layers have been shown to be generally promising candidates for use as intercalation hosts in photocatalysts.[830−834] Wu and co-workers reported the intercalation of nanosized oxides (i.e., Fe_2O_3 or TiO_2) into the interlayer of various layered metal oxides (i.e., $H_4Nb_6O_{17}$, HNb(Ta)WO_6, or $HLaNb_2O_7$).[835−838] When compared to the unintercalated materials, these intercalated composite semiconductors possessed higher photocatalytic activities for hydrogen production in the presence of methanol as a sacrificial agent under UV or even visible-light irradiation. This was ascribed to an effective separation of the photogenerated electrons and holes by electron transfer from guest semiconductor to the host layer. Subsequently, Jang et al. intercalated nanosized Fe_2O_3 particles into the interlayers of $HTiNbO_5$ and $HTiTaO_5$ using successive intercalation reactions.[839] They found that the strong electronic interaction between the guest nanoparticles and the host layers, which was derived from the high electron deficiency of the nanosized Fe_2O_3 particles, could work favorably for photocatalysis because of an efficient electron−hole separation. However, in contrast to the results of Wu et al.,[838] this Fe_2O_3-intercalated layered composite semiconductor did not lead to photocatalytic H_2 production from water reduction but instead to a high activity for oxygen production from water oxidation under visible-light irradiation.

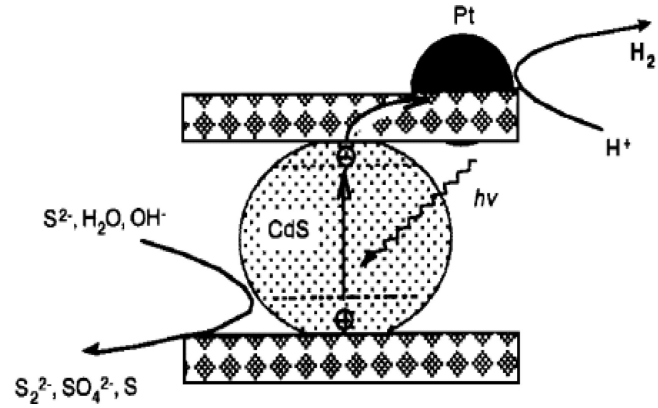

Figure 28. Mechanism of photocatalytic H_2 evolution on CdS-intercalated layered composites loaded with Pt. Photogenerated electrons in CdS quickly transferred to host layers through the nanostructure, and the recombination between the photoinduced electrons and holes was effectively suppressed. Reprinted with permission from ref 842. Copyright 2007 IOP Publishing Ltd.

To improve their photocatalytic stability and photoactivity, sulfides, such as CdS, have also been intercalcated into the interlayers of some layered metal oxides. Shangguan et al. prepared a series of CdS-intercalated metal oxides using direct Cd^{2+} exchange followed by a sulfurization process.[840−842] They found that the photocatalytic activities for hydrogen evolution of such CdS-intercalated composites were superior to those of CdS alone or to a physical mixture of CdS and the metal oxides. This activation effect was attributed to the quick transfer of the photogenerated electrons from CdS to the metal oxides through the layered nanostructure, as shown in Figure 28. The photogenerated charge recombination was effectively suppressed. Sato and co-workers investigated the photocatalytic activities of intercalated materials based on layered metal oxides (i.e., $Ca_{2-x}La_xNb_3O_{10}$, $HNbWO_6$, or $HLaNb_2O_7$) as the host and $Cd_{0.8}Zn_{0.2}S$ as the guest.[843−845] Fabrication involved successive intercalation and exchange reactions. Under visible-light irradiation, the hydrogen production activities of these $Cd_{0.8}Zn_{0.2}S$-intercalated composite photocatalysts were superior to those of unsupported $Cd_{0.8}Zn_{0.2}S$. They were further enhanced by the coincorporation of Pt. Clearly efficient charge separation resulted from the heterogeneous electron transfer from guest $Cd_{0.8}Zn_{0.2}S$

to host oxide layers, and this played an important role in the enhancement of the photocatalytic activity for hydrogen evolution.

It has also been noted that the encapsulation of guest semiconductors into the micro/mesostructured semiconducting host materials is effective for photogenerated charge separation and thus leads to the improved photocatalytic activity of such semiconductor combination systems. Using ion-exchange and sulfurization processes, Guan and co-workers successfully incorporated CdS nanoparticles into the microchannels of ETS-4 and ETS-10, which have the photocatalytically active −Ti−O−Ti− quantum wires in their frameworks.[846,847] The resulting CdS/ETS composite system showed better photocatalytic activity and stability than CdS nanoparticles for hydrogen production under visible-light irradiation. This was interpreted in terms of more efficient charge separation due to the transfer of the photogenerated electrons from the CdS nanopaticles to the −Ti−O−Ti−O− nanowires. Similarly, Shen and Guo encapsulated CdS and In_2S_3 nanoparticles into the mesopores of Ti-MCM-41.[848,849] Under visible-light irradiation, the composite materials exhibited greater and more stable photocatalytic activity for hydrogen evolution than either bulk CdS or In_2S_3. Jing and Guo reported the deposition of quantum-sized WS_2 onto the channel surface of crystalline mesoporous TiO_2.[850] It was postulated that under visible light only electrons transferred from nanosized WS_2 to the TiO_2 host. This resulted in the effective charge separation of electrons and holes photogenerated in the WS_2, and thus the efficient photocatalytic activity for hydrogen production on the WS_2/TiO_2 semiconductor combination system. Shortly afterward, they developed a novel composite CdS/meoporous zirconium titanium phosphate (ZTP) photocatalyst for working under visible light by a two-step thermal sulfidation procedure. In this system, the conduction band of ZTP could be continuously adjusted by choosing different Zr/Ti ratios. Therefore, by adjusting the conduction band of the photoactive ZTP to achieve an optimal optical match between the CdS guest and the ZTP host, highly efficient charge separation and hydrogen production were achieved over the designed CdS/ZTP composite photocatalyst. The highest quantum yield for this composite photocatalyst (with a Zr/Ti ratio of 1:3 in the ZTP host) at 420 nm as measured in experiments reached 27.2%.[851]

Narrow band gap semiconductors, such as CdS[852−854] and Cr_2O_3,[855] have also been incorporated into the nanotubular semiconducting host, generally titanate nanotubes (TiO_2NTs), to develop high-efficiency composite photocatalysts for hydrogen production. Among them, the CdS/TiO_2NTs composite photocatalyst, in which homogeneously distributed CdS was incorporated inside the TiO_2NTs, showed a high photoactivity for hydrogen production from water containing sulfide and sulfite ions as hole scavengers under visible-light irradiation, with the apparent quantum yield of ~43.4% at ~420 nm. The potential gradient at the interface between the CdS nanoparticles and TiO_2NTs helped to facilitate the photoelectron diffusion from CdS particles toward the TiO_2NTs and led to high photocatalytic activity of hydrogen production.[854]

It has been demonstrated that, in both photovoltaic and photoelectrochemical (PEC) cells, improved performance and higher conversion efficiency can be obtained by using diode structures. These were combined from suitable n-type photoanodes and p-type photocathodes[856−858] and led to efficient electron−hole separation with the suppression of energy-wasteful charge recombination.[859−866] A p-Cu_2O/n-WO_3 coupling system was developed by Hu et al. with a view to avoiding back-reactions of the photoinduced charges.[867] It resulted in higher photocatalytic hydrogen production. The reaction scheme of photoinduced water splitting over coupled p-type Cu_2O and n-type WO_3 photocatalysts in a suspension system is shown in Figure 29.

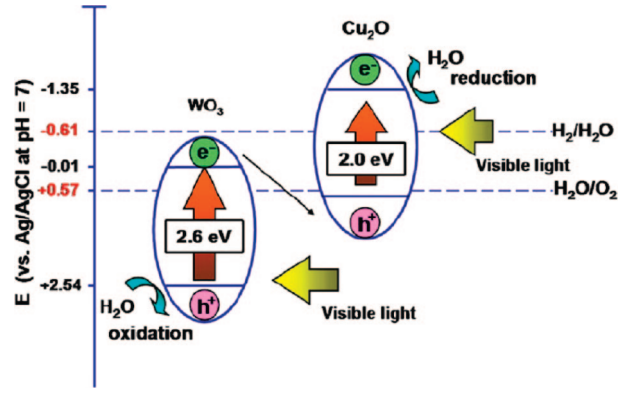

Figure 29. Reaction scheme of the photoinduced water splitting over the coupled p-type Cu_2O and n-type WO_3 photocatalysts in a suspension system. Reprinted with permission from ref 867. Copyright 2008 Elsevier.

Trari and co-workers synthesized a series of p−n heterojunction for use under visible-light irradiation, such as p-$CuMO_2$/n-Cu_2O (M = Mn, Cr),[868,869] p-$CuAlO_2$/n-TiO_2,[870] p-$CuFeO_2$/n-SnO_2,[871] and p-$ZnFe_2O_4$/n-$SrTiO_3$,[872] for photocatalytic hydrogen production from aqueous solutions containing hole scavengers. In these p−n semiconductor systems, photogenerated electrons and holes separated efficiently and were involved in photocatalytic reduction and oxidation, respectively. Jang and co-workers successfully fabricated p/n-typed photocatalytic diodes, n-CdS/p-$AgGaS_2$,[873] p-$AgGaS_2$/n-TiO_2,[874] and p-$CaFe_2O_4$/n-$MgFe_2O_4$.[875] All of these p/n photocatalysts exhibited higher visible-light activities for hydrogen production than the single p- or n-component. This was mainly due to efficient charge separation, which was caused by the rectification of photogenerated electrons and holes.

Kim et al. reported that photocatalytic nanodiodes formed from p-$CaFe_2O_4$/n-$PbBi_2Nb_{0.9}W_{0.1}O_9$ yielded greatly enhanced and stable photocatalytic activity for water oxidation under visible light compared to the single-component photocatalyst.[876] In this p−n photocatalytic nanodiode, enhanced and stable photocatalytic activity was achieved because, under the influence of the internal electric field, the photogenerated holes moved to the p-$CaFe_2O_4$ side and the electrons moved to the n-$PbBi_2Nb_{1.9}W_{0.1}O_9$ side, leading to more efficient charge-carriers separation. In a later study, the authors adopted the concept of a p-type/n-type diode structure with an Ohmic junction and fabricated the p-semiconductor/metal/n-semiconductor structured composite photocatalyst n-WO_3/W/p-$PbBi_2Nb_{1.9}Ti_{0.1}O_9$ for more efficient utilization of visible-light photons.[877] This nanocomposite photocatalyst showed unprecedented high activity for the photocatalytic oxidation of water under visible-light irradiation, with quantum yield estimated to be ca. 41%. Figure 30 shows the working principle of WO_3/W/$PbBi_2Nb_{1.9}Ti_{0.1}O_9$ nanocomposite photocatalyst. It had efficient electron−hole separation and higher net photon energies available for redox reactions through creation of the metal W layer needed to separate the p-type and n-type

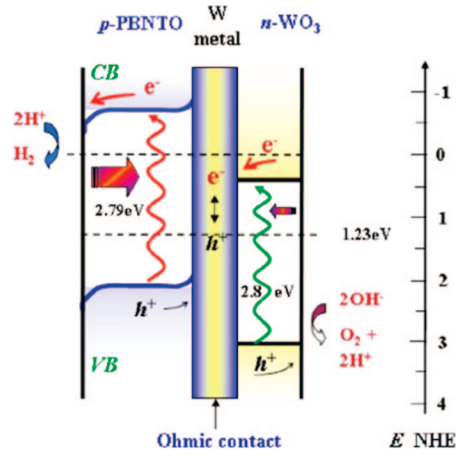

Figure 30. Working principle of n-WO_3/W/p-$PbBi_2Nb_{1.9}Ti_{0.1}O_9$ nanocomposite photocatalyst. Reprinted with permission from ref 877. Copyright 2006 American Institute of Physics.

semiconductors to yield an Ohmic contact in between. This led to more efficient photocatalytic activity than the p-type/n-type junction structure lacking this Ohmic layer.[877]

5.3. Modification of Crystal Structure and Morphology

In general, charge separation and transfer of photogenerated electrons and holes are strongly affected by the crystal structural features of the materials, namely, crystallinity, defects, and any crystal structure distortion. Additionally, surface properties such as particle size, surface area, surface structure, and active reaction sites, which are mainly related to the morphology of the materials, are also important. Thus, a respectable research effort has been dedicated to both the modification of crystal structure and morphology of the photocatalysts with the view to improve more efficient charge separation. This has had great success in the enhancement of photocatalytic activity for water splitting.

5.3.1. Modification of Crystal Structure

It has been well demonstrated that the crystal structure of TiO_2 plays a significant role in photocatalysis.[795,878−882] In photocatalysis, for pure-phase TiO_2, the anatase phase was considered to be more active than the rutile phase.[795,878] In anatase TiO_2, the photoexcited electrons could be trapped in oxygen vacancies of the anatase structure.[72] This made them easier to transfer to an electron trap, such as Pt particles on the surface, to participate in the photocatalytic reaction, preventing electron−hole recombination in photocatalysis. On the other hand, the poor photoactivity of rutile TiO_2 was due to the fact the electrons are trapped within intrinsic defects of the rutile structure where they were deexcited by near-infrared emission.[72] Meanwhile, enhanced activity was observed on mixed-phase TiO_2 photocatalysts relative to the corresponding pure phases.[73,883−887] Taking an anatase/rutile mixed-phase TiO_2 as an example, Figure 31 reveals a junction structure formed between the anatase and rutile phases. The migration of electrons across a phase junction (as shown in Figure 32) was beneficial for charge separation, thereby enhancing the photocatalytic activity for hydrogen evolution.[73,888] Furthermore, the high crystallinity of anatase TiO_2, which had fewer lattice defects, was reported to have a positive effect on the photocatalytic activity for H_2 production. Good crystallinity led to significant enhancement

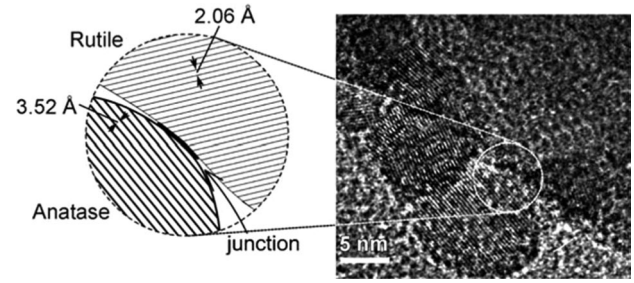

Figure 31. Junction structure formed between the anatase and rutile phase. Reprinted with permission from ref 73. Copyright 2008 Wiley-VCH.

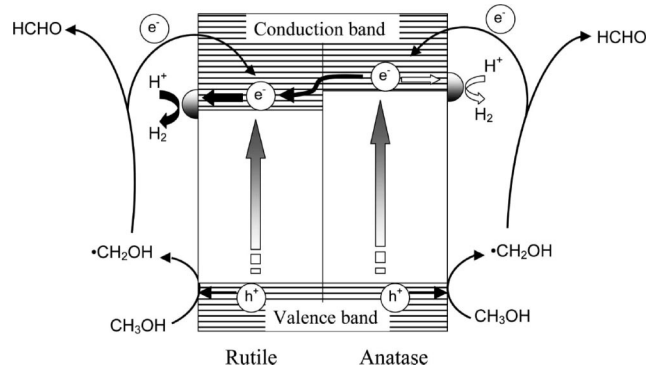

Figure 32. Proposed pathway of electrons during photocatalytic H_2 evolution over a mixture of anatase and rutile TiO_2 nanoparticles. The amount of electron transfer proceeds predominantly in the order of solid thick arrow > thin solid arrow > unfilled arrow. Note: For simplicity, the formation of hydroxymethyl radicals (•CH_2OH) by hydroxyl radicals (•OH) is represented by the hole oxidation step. Reprinted with permission from ref 888. Copyright 2010 American Chemical Society.

of the electron transport properties, whereas lattice defects behaved as recombination centers for the photoinduced electron/hole pairs with a concomitant decrease in the photocatalytic activity.[889,890]

Fu et al. studied the In_2S_3 samples with different crystal structures.[891] Their results showed that the indium vacancy-ordered tetragonal In_2S_3 was inactive for hydrogen generation, whereas the vacancy-disordered cubic In_2S_3 exhibited stable photoactivity under visible light.[891] Amano et al. reported that, owing to the suppression of the fast recombination of electron−hole pairs, the photocatalytic activity of visible-light-responsive Bi_2WO_6 was greatly enhanced by crystallizaiton under a hydrothermal treatment, when compared to the negligible photocatalytic activity of amorphous Bi_2WO_6.[892] Noda et al. demonstrated that the high photocatalytic activity of crystallized mesoporous Ta_2O_5, for overall water splitting, was attributable to the efficient transfer of the excited electrons and holes from inside the catalyst to the surface through the thin-walled crystalline phase.[893]

Domen and co-workers found that high-pressure treatment of β-Ge_3N_4 and Ta_3N_5 under ammonia was effective for reducing the defect sites and/or structural imperfections both in the bulk and on the surface, resulting in enhanced photocatalytic activities for water splitting.[278,279,894] Postcalcination at moderate temperatures was found to be effective for improving the activities of $(Ga_{1-x}Zn_x)(N_{1-x}O_x)$ and $(Zn_{1+x}Ge)(N_2O_x)$ as visible-light-driven photocatalysts for overall water splitting. This was also attributed to a reduction in the density of lattice defects in the catalyst materials, which in return reduced the number of sites available for the

recombination of the photogenerated electrons and holes.[575,579] A H_2S post-treatment was applied by Jang and co-workers for the synthesis of pure sulfide-type photocatalysts, with high crystallinities. Because of the suppressed charge recombination, the obtained $AgGaS_2$ exhibited high photocatalytic activity for hydrogen production under visible light.[496]

Good crystallinity and fewer crystal defects were also discovered to benefit bulk electron−hole separation as well as the efficient photocatalytic activity of CdS.[895] Li et al. found that suitable photoetching could notably increase photocatalytic activity of Pt/CdS for hydrogen evolution by removing selectively grain boundary defects that were the recombination centers for photoinduced electron−hole pairs.[896] Maeda et al. found that Ta_3N_5 nanoparticles with a lower density of defect sites exhibited enhanced photocatalytic activity for H_2 evolution.[472] They also reported the positive effect of a monoclinic-ZrO_2 modification on the photocatalytic H_2 evolution activity of TaON under visible-light irradiation. Both prior incorporation of a zirconium species into $Zr_xTa_{1-x}O_{1+x}N_{1-x}$ solid solutions and surface modification of TaON with monoclinic-ZrO_2 suppressed the formation of surface defects by inhibiting tantalum reduction during nitridation even though the ZrO_2 component itself did not undergo nitridation.[897,898]

The photocatalytic performance of semiconducting nanocrystals is also highly dictated by their crystal planes. For TiO_2, different groups have reported the tailored synthesis of anatase single crystals with a high percentage of the highly reactive {001} facets. These showed superior photoreactivity compared to P25 as a benchmarking material.[899−905] Wu et al.[905] and Li and Xu[906] reported that nanostructured anatase TiO_2 with a large percentage of other exposed high-energy facets, {010} and {100}, respectively, exhibited much higher activities than that of commercial anatase powders. Pt/TiO_2 nanosheets with exposed (001) facets fabricated by a hydrothermal treatment of tetrabutyl titanate and hydrofluoric acid mixture were shown to exhibit a much higher photocatalytic activity for H_2 evolution than Degussa P-25 TiO_2 and pure TiO_2 nanoparticles because of the synergistic effect of surface fluorination and exposed (001) facets.[907]

Zhao et al. prepared WO_3 octahedra with {111} surface facets, which were covered and stabilized with a thin tungstic acid layer.[908] The as-prepared octahedra exhibited high visible-light-driven photocatalytic activity for oxidation of H_2O to O_2. This was due to the high adsorption capacity of the tungstic acid sheath for Ag^+ as the electron acceptor and the efficient water oxidation at the high-energy {111} facets. Nian et al. succeeded in controlling the crystalline texture of Cu_2O by varying the electrodeposition conditions.[909] The Cu_2O grown with a [111] out-of-plane texture had a better photocatalytic performance in water splitting for hydrogen production than that with a [110] texture, due to the large exposure area of {111} facets of Cu_2O crystalline.[910,911] As shown in Figure 33, Xi and Ye deemed that the exposed {001} facets of the monoclinic $BiVO_4$ nanoplates led to a remarkable enhancement of the visible-light photocatalytic oxidation of water for O_2 generation.[912]

Yin et al. found evidence for the possible role of lattice vibrations in the photocatalytic H_2 production activity of $BaM_{1/3}N_{2/3}O_3$ (M = Ni, Zn; N = Nb, Ta).[178] They found that the lower photocatalytic activity resulted from the deviation of the bond angle M−O−N from 180°. This change increased the migration energy of the charge carriers, thus hindering their migration of the charge carriers and leading to a higher possibility of recombination between the photogenerated electrons and holes.

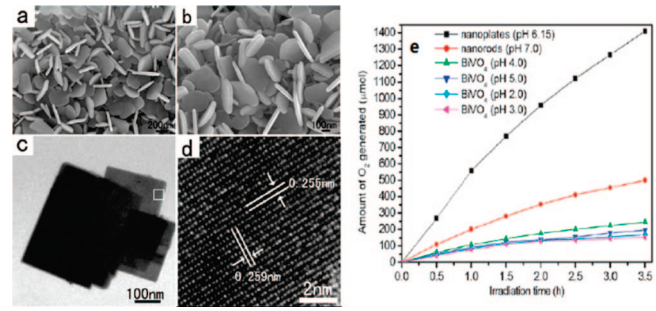

Figure 33. (a, b) Low- and high-magnification field emission scanning electron microscopy (FESEM) image of the m-$BiVO_4$ nanoplates. (c) Low-magnification transmission electron microscopy (TEM) image of the m-$BiVO_4$ nanoplates. (d) High-resolution TEM (HRTEM) image of the m-$BiVO_4$ nanoplate. (e) Photocatalytic O_2 evolution from an aqueous $AgNO_3$ solution (0.05 M, 270 mL) under visible-light irradiation ($\lambda > 420$ nm) over various photocatalysts (0.1 g). Reprinted with permission from ref 912. Copyright 2010 The Royal Society of Chemistry.

Similarly, in the study of Kudo et al.,[21] $Sr_2Ta_2O_7$ displayed a higher photocatalytic activity for water splitting than $Sr_2Nb_2O_7$. As the bond angle of O−Ta−O in $Sr_2Ta_2O_7$ was closer to 180° than that of O−Nb−O in $Sr_2Nb_2O_7$, the charge carriers in $Sr_2Ta_2O_7$ moved more easily than those in $Sr_2Nb_2O_7$. On the other hand, $Sr_2Nb_2O_7$ was also active for the water splitting even if it was a niobate. This was due to a dipole moment along the perovskite layers resulting from the distortion of NbO_6 octahedra, which, it was suggested, could enhance the charge separation of the photogenerated electrons and holes in $Sr_2Nb_2O_7$. In fact, a dipole moment of this type, due to the distortion of TiO_6 octahedra in some titanates such as $BaTi_4O_9$, was reported previously by Inoue and co-workers as being important for the charge separation in photocatalytic water splitting.[101,913,914] In their later studies,[258−260,263,265] the prominent effect of crystal structure distortion on photocatalytic activity was also reported for other metal oxide photocatalysts: Zn_2GeO_4, MIn_2O_4 (M = Ca, Sr), $M_2Sb_2O_7$ (M = Ca, Sr), and $AInO_2$ (A = Li, Na). It was demonstrated that the metal oxides consisting of distorted structural units with dipole moments were all photocatalytically active in water decomposition, whereas distortion-free oxides exhibited negligible activity. Structure distortion was clearly effective for charge separation. Figure 34 compares the correlation between photocatalytic activity and dipole moment.

Recently, Shen et al. found that, in hydrogen evolution, the photocatalytic activity for $ZnIn_2S_4$ was greatly affected by the crystal plane space along the *c*-axis; the increasing *d* (001) space greatly improved its photocatalytic activity of $ZnIn_2S_4$.[377,915] They concluded that the structural distortion of $ZnIn_2S_4$ induced a dipole moment through increasing the *d* (001) space. Since the internal fields caused by the dipole moment were considered to be useful for the charge separation of the photogenerated electrons and holes, this in turn proved effective in promoting the photocatalytic activity.

5.3.2. Modification of Size and Morphology

It is well-known that particle size is a crucial factor in the dynamics of electron/hole recombination (including bulk recombination and surface recombination) processes, especially in semiconductor nanomaterials, and that the move-

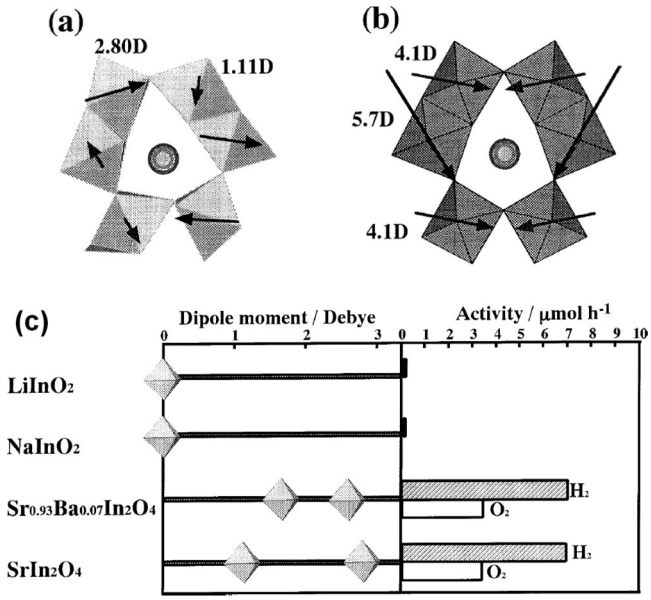

Figure 34. Dipole moments in (a) $SrIn_2O_4$ and (b) $BaTi_4O_9$, and (c) correlation between photocatalytic activity and dipole moment. The octahedral structures represent InO_6 units. The indates with dipole moments are photocatalytically active, whereas the distortion-free indates exhibited negligible activity. Reprinted with permission from ref 260. Copyright 2003 American Chemical Society.

ment of electrons and holes is primarily governed by the well-known quantum confinement.[300] Generally, a decrease in particle size could be expected to lead to a higher efficiency in photocatalysis.[163,916−920] This was because the bulk charge recombination of photogenerated electrons and holes, dominant in the well-crystallized large semiconductor particles, was reduced by decreasing particle size. Reduction in particle size could also lead to a larger surface area and increased the available surface active sites.[209,921,922] Lee et al. reported that the smaller particle size and higher surface area of $NaTaO_3$ led to its high photocatalytic activity in overall water splitting.[209] They proposed that this was due to the increased probability of surface reactions between the electrons and holes rather than recombination in the bulk. Sathish et al.[923] found that CdS nanoparticles showed a higher photocatalytic activity for hydrogen evolution compared to bulk CdS. This was correlated well with the particle size and surface area. Lunawat et al. also found that, compared to bulk CdS, its nanocrystallites dispersed into the channels of mesoporous silicate SBA-15 exhibited enhanced photocatalytic activity for water splitting under visible light.[924] This result illustrated the fact that the smaller particle size was capable of enhancing the photocatalytic activity of a semiconducting material. However, the photocatalytic activity does not monotonically increase but even decreases with the decreasing particle size. This is because surface charge recombination can become an important process. When particle size of the nanocrystalline semiconductor becomes extremely small, this in return can offset the benefits of the ultrahigh surface area of the nanocrystalline particles.[921,925]

Wang et al. showed that there existed an optimal particle size for the pure nanocrystalline TiO_2 photocatalyst used in the photocatalytic reaction of chloroform decomposition.[926] A similar phenomenon for $K_2Ta_2O_6$[219] and CdS nanocrystals[927,928] was also reported. It was found that the optimal particle size was important to achieve the high photocatalytic activity for water splitting. Neither the smallest nor the largest nanocrystals showed the highest photocatalytic activity for hydrogen evolution. The smallest nanocrystals suffered more from the charge recombination on the surface, whereas, to some extent, the largest nanocrystals suffered from the same disadvantages as large-size particles. Hong et al. investigated the effects of crystal size on photoanode materials based on WO_3 in both a particulate suspension (PS) system and a photoelectrochemical (PEC) film system.[929] In the PS system, the large crystals showed higher photoactivity because of a well-developed space charge layer and high crystallinity, whereas in the PEC system, the smaller crystals performed better because of the reduced hole diffusion length. These different behaviors were attributed to different charge-separation mechanisms in the two systems. Balázs and co-workers investigated the effect of particle shape on the activity of nanocrystalline TiO_2 photocatalysts in phenol decomposition.[930−932] They found that the average particle diameter of the best photocatalysts was in the range of 50−70 nm, and the photocatalyst containing only polyhedral nanocrystals displayed better photocatalytic performance than those containing both spherical and polyhedral nanocrystals.

Since the first report on the ordered mesoporous silica material MCM-41,[933] inorganic materials with controlled porosity have been widely exploited in photocatalysis.[934−940] These mesoporous photocatalysts possess two major beneficial characteristics. The first is the high specific surface area, which provides more reactive sites at the surface for photocatalytic reaction to occur. The second is the nanoscale channel wall of mesopores, which can facilitate the transfer of photogenerated electrons and holes to the surface, thus avoiding their recombination in the bulk.[80,158,202] For example, different kinds of mesoporous TiO_2-based photocatalysts have been previously reported as being promising candidates for efficient charge separation and transport, leading to higher efficiency in photocatalysis for water splitting.[80,889,941−946] The mesoporous-assembled $SrTiO_3$ nanocrystal photocatalysts also exhibited much higher photocatalytic activity than the nonmesoporous-assembled commercial $SrTiO_3$ photocatalysts.[947,948] Domen and co-workers reported that, although the inorganic phases are amorphous, the photocatalytic activities for overall water decomposition over mesoporous Ta_2O_5 and Mg−Ta oxide are much higher than over crystallized Ta_2O_5 and $MgTa_2O_6$, respectively.[202,204] This high activity was due to the thin walls of the mesopores, which provided a shorter distance for the excited electrons and holes to travel to the surface.

Chen et al. found that the photocatalytic activity of mesoporous Nb_2O_5 was 20 times higher than the bulk, which lacks porosity.[158] It was proposed that the positive effect of mesoporosity on the photocatalytic activity was abscribed to the oriented movement and efficient separation of electrons and holes, as shown in Figure 35. The mesoporous In−Nb mixed-oxide catalyst also showed photocatalytic activity for water splitting. This was attributed to the synergistic effects of a high surface area and the well-dispersed indium species intercalated into the mesoporous structure.[159]

Sang and co-workers synthesized the complex oxide $InVO_4$ with a mesoporous wormhole-like structure.[949,950] It had a highly efficient photocatalytic activity due to the low recombination rate of the photoexcited electrons and holes. Ta_3N_5 with a crystalline mesoporous framework showed the photocatalytic performance for hydrogen evolution greatly superior to that of conventional bulk Ta_3N_5. The thin-wall structure promoted charge transfer to active surface sites.[951] Wang and co-workers suggested that the efficiency of

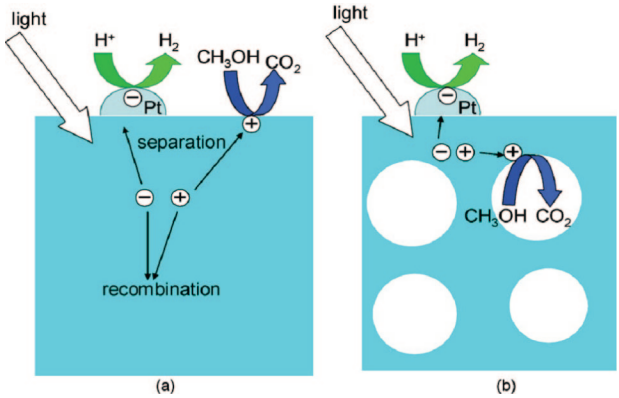

Figure 35. Model of photocatalytic H_2 evolution on a bulk photocatalyst (a) and a mesoporous photocatalyst (b). Reprinted with permission from ref 158. Copyright 2007 Elsevier.

hydrogen production could be improved by about an order of magnitude through the introduction of mesoporosity into polymeric C_3N_4.[952,953] Bao et al. prepared nanoporous CdS nanostructures using a two-step aqueous route, which displayed very high photocatalytic efficiency for hydrogen production under visible-light irradiation.[732] The quantum yield was found to be ~60.34% at 420 nm. This high activity was due the fact that the fast transport of the photogenerated carriers to the surface of the CdS by traveling only a short distance through the nanopore wall was so advantageous. It greatly decreased the bulk charge recombination, increased the quick surface charge separation and fast interfacial charge carrier transfer, and ensured the fast photochemical reaction at the CdS/electrolyte interface. Feng and co-workers developed a series of porous chalcogenides with open-framework construction as efficient photocatalysts for the reduction of water: $Na_{14}In_{17}Cu_3S_{35}\cdot xH_2O$, $Cu_8Ge_5S_{16}^{4-}$.[954−956] It was demonstrated that the open-framework construction helped not only to increase the number of active reaction sites owing to a high surface area but also to reduce the rate of charge recombination of the electron−hole pair.

Kudo's group was the first to report the positive effect of the ordered surface structure on the photocatalytic activity for water splitting. The photocatalytic activity of La-doped $NaTaO_3$ with an ordered surface nanostep structure was 9 times higher than that of nondoped $NaTaO_3$. This was mainly because the ordered surface nanostep structure created by La doping (as shown in Figure 36) contributed to the separation of the photoactive sites in avoiding surface charge recombination and back-reactions.[20,216] A similar effect of the surface nanostructure was also observed on some sulfide photocatalysts, such as $(AgIn)_{0.22}Zn_{1.56}S_2$[537] and $AgGa_{0.9}In_{0.1}S_2$[544] solid solution. It was proposed that such nanostructured surface edges improved the photocatalytic properties because the incident photon was not shielded and the photogenerated electrons could more easily migrate to the edge of the nanostructured step. Hence, both compounds had enhanced photocatalytic activity for hydrogen evolution under visible-light irradiation. Jing and Guo prepared a highly stable and active CdS photocatalyst through thermal sulfidation of a CdO precursor.[957] The special nanostep structure was also observed at the surface of the sulfide photocatalyst, which further supported the premise that the nanostep surface was crucial for the remarkable enhancement of photocatalytic hydrogen production through active sites in suppressing the surface-charge recombination of photogenerated electrons and holes.

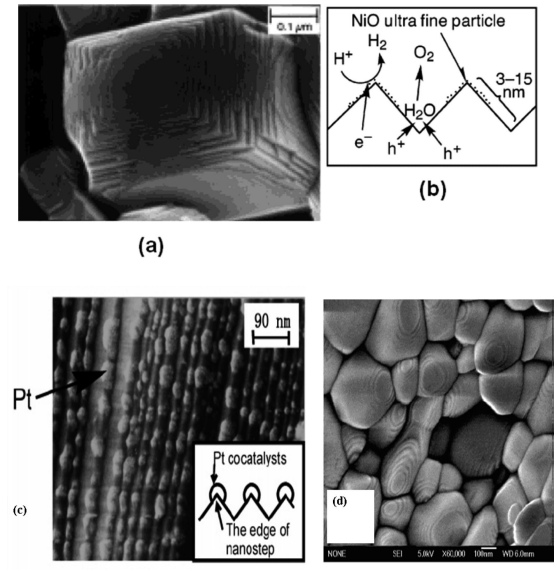

Figure 36. Ordered surface nanostep structure of $NiO/NaTaO_3$: La (a), and mechanism of highly efficient photocatalytic water splitting over $NiO/NaTaO_3$:La photocatalysts (b). Reprinted with permission from ref 20. Copyright 2003 American Chemical Society. Ordered surface nanostep structure of $Pt/(AgIn)_{0.22}Zn_{1.56}S_2$ (c) and CdS (d). (c) Reprinted with permission from ref 537. Copyright 2004 American Chemical Society. (d) Reprinted with permission from ref 957. Copyright 2006 American Chemical Society.

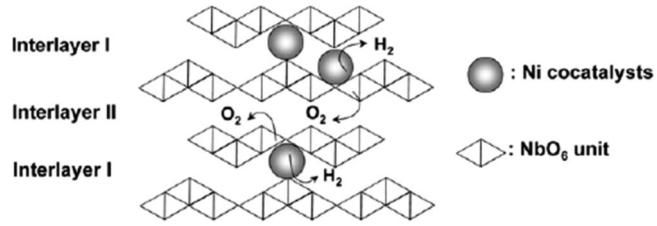

Figure 37. Schematic structure of the active $NiO-K_4Nb_6O_{17}$ photocatalyst and the reaction mechanism of H_2O decomposition into H_2 and O_2. Reprinted with permission from ref 55. Copyright 2009 The Royal Society of Chemistry.

Some ion-exchangeable layered oxides have been shown to be highly active photocatalysts with several distinct advantages compared to the so-called "bulk" type photocatalysts such as TiO_2 or $SrTiO_3$.[135,162,164,171,231,958−960] Because of their unique structural characteristics, such layered photocatalysts utilize the intercalated water molecules as reactants to produce hydrogen and oxygen.[135,164] $K_4Nb_6O_{17}$ has an ion-exchangeable layered structure with two different kinds of alternating interlayer spaces, i.e., interlayers I and II, as shown in Figure 37, which are the active sites for the production of hydrogen and oxygen, respectively.[164] It was proposed that the electrostatic gradient in the niobate sheet caused by the different locations of the K^+ and H^+ cations between interlayer I and II could drive the electrons and holes to move to different active sites, giving rise to efficient charge separation. Domen and co-workers found that a Ni-loaded ion-exchangeable layered oxide $K_2La_2Ti_3O_{10}$ showed high photocatalytic activity for water splitting.[23,135,139] $K_2La_2Ti_3O_{10}$ had only one type of interlayer space, and most of the loaded Ni existed at the external surface. It was proposed that H_2 evolved on the Ni particles at the external surface and O_2 evolved in the interlayer space. This again indicated efficient charge separation and suppression of back-reaction were achieved due to the layered structure.

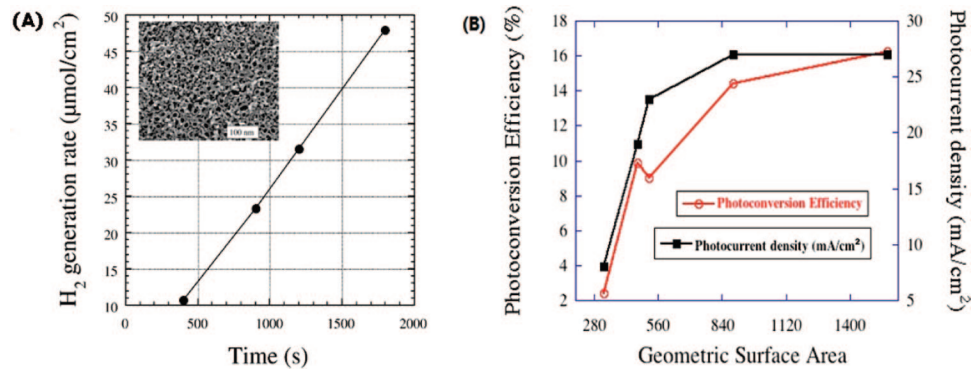

Figure 38. (A) Hydrogen photoproduction in a photoelectrochemical cell consisting of titania nanotube array photoanode and Pt mesh cathode. (inset) FESEM images of titania nanotube arrays. Reprinted with permission from ref 977. Copyright 2005 American Chemical Society. (B) Photoconversion efficiency during water photolysis and maximum photocurrent obtained using TiO_2 nanotube-array photoanode as a function of the geometric roughness factor of the nanotube arrays. Reprinted with permission from ref 980. Copyright 2007 IOP Publishing Ltd.

Yoshimura et al. found that different H_2 evolution sites in the layered structure led to quite different photocatalytic activities for hydrogen production.[959] $Pt/HPb_2Nb_3O_{10}$ with Pt in the interlayer space exhibited much higher activity than that with Pt only on the external surface. For the latter case, the electrons had to transfer a long distance through a two-dimensional niobate sheet to reduce H^+ on the external Pt. There was a short distance for electrons to transfer to the intercalated Pt, and the possibility of charge recombination was largely reduced. They also found that the intercalation of water or hydronium ion into the interlayer space was a key factor in increasing the photocatalytic activity of layered oxides for hydrogen evolution. The intercalation resulted in a dramatic increase in reaction sites for water decomposition along with efficient charge separation.[959,961] Moreover, pillared layered photocatalyts showed a marked increase in hydrogen production activities compared with the original layered oxides.[98,189] This may be due to the increase of surface area[98,962] and/or interlayer spacing,[189] which facilitated the reaction between photogenerated charges and reactant molecules and suppressed charge recombination.

Various architectures with nanometer- and micrometer-sized dimensions have been found to play an important role in achieving fast charge transfer and efficient charge separation for the improvement of photocatalytic activity.[963] One-dimensional (1D) nanostructures, such as nanowires,[730,964,965] nanotubes,[99,966−969] and nanorods/nanoribbons,[970−974,177] have all displayed great potential in environmental/energy photocatalysis applications. Jitputti and co-workers reported that TiO_2 nanowires with high crystallinity and surface area could promote higher H_2 evolution than commercial TiO_2 nanoparticles.[964,975] It was proposed that the unique 1D structure might facilitate the electron transport for reacting with water molecules adsorbed at the TiO_2 surface along the 1D structure. Additionally, TiO_2 nanofibers prepared by electrospinning techniques showed enhanced crystallinity, surface area, and photocatalytic activity for hydrogen evolution compared to nanofibers prepared by hydrothermal method.[975] Li and Lu demostrated that one apparent advantage of $Na_2Ti_2O_4(OH)_2$ nanotubes for photocatalytic hydrogen production over TiO_2 particles was their one-dimensional tubular structure, which was favorable for electron transfer and thus reduced the recombination of electron−hole pairs.[649]

Grimes and co-workers examined the use of titania nanotube arrays for the photocleavage of water into hydrogen and oxygen under UV irradiation.[976−982] The nanotubular architecture gave rise to superior electron lifetimes and, hence, more efficient charge separation.[977,983] On a per-watt basis, the hydrogen generation rate obtained of 24 mL/(h W) was among the highest reported for a titania-based photoelectrochemical cell, as shown in Figure 38A.[977] They also claimed that TiO_2 nanotube-array photoanodes could generate H_2 by water photolysis with a photoconversion efficiency of 16.5% under UV light illumination (Figure 38B).[980] A three-step electrochemical anodization was demonstrated to contribute to the formation of highly ordered TiO_2 nanotube arrays and then greatly enhance the photoelectrochemical and hydrogen evolution activities.[984]

Cho et al. found that single-crystalline $SrNb_2O_6$ nanotubes with rhombic cross sections exhibited superior photocatalytic activity for the H_2 evolution from pure water compared to their bulk counterparts.[985] This was attributed to the higher surface area and the smaller diffusion length of the charge carriers resulting from the morphological characteristics of the material. It was reported that the photocatalytic activity enhancement of TiO_2 nanorods could be attributed to the larger surface area,[970,973] which promoted the probability of a surface reaction between the electrons and holes rather than recombination in the bulk.[209] Chen and Ye found that, under UV irradiation, nanorod-like $SrSnO_3$ had a photoactivity 10 times greater than the particles prepared by a solid-state reaction.[268] Porous nanorod-structured $ZnFe_2O_4$ showed effective H_2 evolution from methanol aqueous solution under visible light. The nanorod shapes and their intraparticle porous structures were proven to be beneficial for more quickly transferring the photogenerated carriers onto the surfaces, which in return favored the efficient charge separation.[986] The high electron mobility in 1D nanostructured nanorods also partially contributed to the high photocatalytic hydrogen yield of the $(Cd_{0.8}Zn_{0.2})S$ nanorods.[987] A device physics model for radial p−n junction nanorod solar cells was developed by Kayes et al.[988] Densely packed nanorods were oriented with the rod axis parallel to the incident light direction. The study indicated that high-aspect-ratio (length/diameter) nanorods allowed the use of a sufficient thickness of material to obtain good optical absorption while simultaneously providing short collection lengths for excited carriers in a direction normal to the light absorption. The design of the radial p−n junction nanorod device could provide large improvements in efficiency relative to a conventional planar geometry.

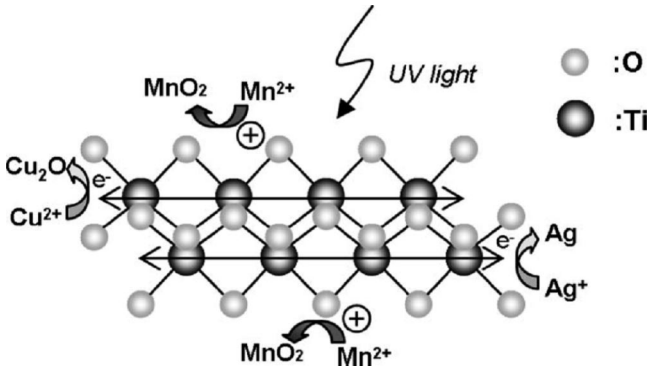

Figure 39. Model of the movements of the photoproduced electron and hole at the TiO_x nanosheet with a lepidocrosite-type structure. The electron moves in the 3d CB consisting of the Ti^{4+} network in the nanosheet and then reduces Ag^+ and Cu^{2+} at the edge, whereas the hole exists at the 2p VB consisting of the O^{2-} surface and oxidizes Mn^{2+} on the surface. Reprinted with permission from ref 993. Copyright 2008 American Chemical Society.

Two-dimensional (2D) nanostructures such as nanobelts,[989−991] nanosheets,[992−994] and nanoplates[995,996] also favor the transfer of electrons and holes generated inside the crystal to the surface and promote the charge separation, which helps to enhance the photocatalytic activity to some degree.[991,997−1001] Sun et al. found that the photocatalytic properties of ZnO nanobelt arrays was better than that found for ZnO film or the rod-/comblike ZnO nanostructures under identical conditions.[989] Ultrathin nanosheets of brookite TiO_2 displayed high phtocatalytic activity. The atomic scale thickness and large surface area allowed shorter migration time of carriers, suppressed bulk recombination and more electrons and holes on the surface.[1002] Jitputti et al. reported that nanosheet TiO_2 exhibited higher photocatalytic activity for hydrogen evolution than that of commercial TiO_2 anatase powder.[1003] Matsumoto et al. observed the separate photocatalytic active sites on the TiO_x nanosheets by photodepositing metal and metal oxide.[993] As shown in Figure 39, the photogenerated electrons mainly reacted at the edge of the nanosheets, whereas the photogenerated holes reacted all over the surface. Thus, the recombination of electrons and holes in the TiO_x nanosheets was to some extent impeded. Osterloh and coworkers developed a modular approach to the synthesis of nanostructured catalysts for photochemical water-splitting catalysts based on exfoliated, semiconducting niobate nanosheets.[188,1004−1007] These could be integrated into two-component nanostructures with separate sites for water reduction and oxidation. Zhang and Zhu revealed that Bi_2WO_6 nanoplates had a special advantage in photocatalytic reactions, because the nanoplate structure not only had a larger surface area but also promoted the efficiency of the electron−hole separation.[996]

Self-assembly of nanoscale building blocks into three-dimensional (3D) complex structures is another research hot spot in photocatalysis.[1008−1013] Song and Gao found that hollow NiO microspheres showed a significantly more enhanced photocatalytic activity than NiO rods.[1008] The increasing number of surface active sites and surface charge carrier transfer rate in the photocatalysis of the hollow NiO microspheres proved advantageous. Lu et al. reported that quite a good photocatalytic performance was obtained on a novel ZnO hierarchical micro/nanoarchitecture with dense nanosheet-built networks standing on hexagonal−pyramid-like microcrystals.[1009] This was because the special structural features of the micro/nanoarchitectured ZnO promoted electrons transfer from the nanosheets with high electric-potential to the core micropyramid with low electric-potential. The probability of photogenerated electron/hole pair recombination was thus reduced. Kale et al. reported that $CdIn_2S_4$ nanostructures with a marigold-like morphology composed of numerous nanosized petals displayed high photocatalytic activity for solar production of hydrogen from H_2S in KOH aqueous solution.[1010]

6. Photocatalytic Hydrogen Generation Systems

The tremendous effort put into the synthesis and modification of photocatalysts to adjust their band structures and increase the probabilty of photogenerated charge separation has resulted in the progressive development of high-efficiency visible-light-driven photocatalysts. Meanwhile, it is widely believed that the construction of appropriate and efficient photocatalytic hydrogen generation systems (solution/semiconductor suspensions) based on different kinds of photocatalysts is an indispensable step to achieving high performance for photocatalytic hydrogen generation.

6.1. Hydrogen Generation Systems Containing Sacrificial Reagents

The basic principle of photocatalytic reactions for hydrogen/oxygen generation using electron donors/acceptors as the sacrificial reagents is depicted schematically in Figure 40.[51] When the system is constructed in the presence of an electron donor, the photogenerated holes irreversibly oxidize the reducing electron donors instead of H_2O. If the bottom of the conduction band of the photocatalyst is located at a more negative potential than the water reduction potential, this then facilitates water reduction by the photogenerated electrons in the conduction band.[51,300] The different kinds of typical sacrificial reagents are shown in Table 3.

6.1.1. Inorganic Sacrificial Reagent Systems

6.1.1.1. S^{2-}/SO_3^{2-} System. Since S^{2-} and SO_3^{2-} could be oxidized by photogenerated holes to S_n^{2-} and SO_4^{2-}, respectively, they can thus act independently as sacrificial reagents for photocatalytic hydrogen generation.[848,849,1014−1017] However, the oxidation of S^{2-} ions to yellow polysulfides S_n^{2-} leads to a decrease in H_2 formation over time. This is due to the high light absorption of the yellow polysulfide S_n^{2-} in the visible region and then to the competitive reduction of S_n^{2-} with H_2O.[1014,1018−1020] Fortunately, SO_3^{2-} could act as S_n^{2-}-regenerating agent and maintain the solution colorless.[1021] Therefore, the S^{2-}/SO_3^{2-} mixture is most widely used as electron donors and added to the water/semiconductor suspension to improve the photocatalytic activity and stability

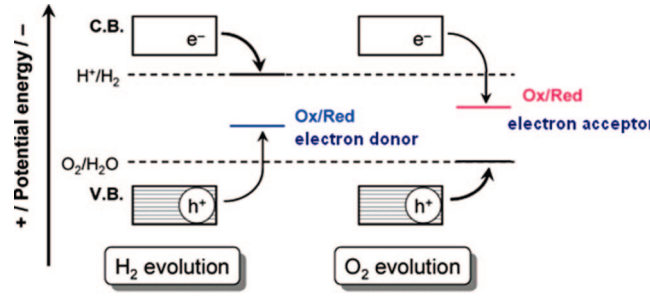

Figure 40. Basic principle of photocatalytic reactions in the presence of sacrificial reagents. Reprinted with permission from ref 51. Copyright 2007 American Chemical Society.

Table 3. Typical Sacrificial Reagent Contained Photocatalytic Hydrogen Production System

photocatalyst	mass (g)	sacrificial reagent	light Source	rate of hydrogen evolution (μmol·h^{-1}·g^{-1})	quantum yield (%)	reference
Pt−PdS/CdS	0.3	S^{2-}/SO_3^{2-}	300-W Xe (>420 nm)	29 233	93 (420 nm)	733
$Pt/WS_2/TiO_2$	0.2	S^{2-}	350-W Xe (>430 nm)	890		850
Pt/CdS/Ti-MCM-41	0.2	SO_3^{2-}	350-W Xe (>430 nm)	76	2.6 (420 nm)	849
$ZnFe_2O_4/SrTiO_3$	0.25	$S_2O_3^{2-}$	600-W W	410 688		872
Pt−PdS/CdS	0.025	H_2S	300-W Xe (>420 nm)	~94 000	30 (420 nm)	785
MoS_2/CdS	0.1	lactic acid	300-W Xe (>420 nm)	~5300		782
$RuO_2/K_2La_2Ti_3O_{10}$:Zn	1	I^-	250-W Xe	55.5		140
Pt/TiO_2	0.1	Br^-	500-W Hg	~550		1051
$KBi_3PbTi_5O_{16}$	1	Ce^{3+}	450-W Hg	35.21		146
$Pt/SrTiO_3$:Rh	0.1	Fe^{2+}	300-W Xe (>420 nm)	169		1046
NiO/TiO_2	0.2	CN^-	450-W Hg	1500	0.32	1052
$Pt/H_2LaNb_2O_7$:In	1	methanol	100-W Hg (>290 nm)	5268	1.54 (>290 nm)	183
Pt−Ru/$Y_2Ta_2O_5N_2$	0.3	ethanol	300-W Xe (>420 nm)	833		393
NiO_x/CdS/$KNbO_3$	0.2	isopropanol	500-W Hg−Xe (>400 nm)	203.5	8.8 (>400 nm)	800, 801
Pt/TiO_2	0.08	1-propanol	500-W Xe	~150		1066
Pt/TiO_2	0.08	1-butanol	500-W Xe	~75		1066
Pt/Cu_2O	0.01	formic acid	H (>420 nm)	155		1075
Pt/TiO_2	0.1	acetic acid	300-W Hg	28 380		1064
Ni−$La_2O_2CO_3$	0.1	formaldehyde	125-W Xe (>400 nm)	36		1065
Pt/TiO_2	0.08	acetaldehyde	500-W Xe	45.3		1066
DPt/TiO_2	0.02	oxalic acid	250-W Hg	2800		1056
Pt/TiO_2:Gd	0.1	glycol	1200-W Ultra-Vitalux	13 775		82
Wells−Dawson heteropoly blue/Pt/TiO_2	0.05	glycerol	300-W H (>420 nm)	~62.5	20.0 (670 nm)	637, 638
$H_4Nb_6O_{17}$/Pt/Ru(bpy)$_2$(4,4′-$(PO_3H_2)_2$bpy)$^{2+}$	0.005	EDTA	300-W Xe (>420 nm)	4320	22 (450 nm)	623, 624
Pd/TiO_2	0.05	glucose	125-W Hg	4580		1085
Pt/TiO_2:B,N	0.05	sucrose	300-W Xe	~2500		455
TiO_2/Rh/Eosin-Y	0.02	diethanolamine	200-W H (>420 nm)	1185.5	10.27 (>420 nm)	647
TiO_2/Pt/Fe^{3+}-Eosin-Y	0.1	TEA	400-W H (>420 nm)	2750	19.1 (>420 nm)	654
MoS_2/CdS	0.1	lactic acid	300-W Xe (>420 nm)	5400		782
Pt/TiO_2	0.3	*n*-pentane	500-W Xe	28		1070
Pt/TiO_2	0.3	*n*-heptane	500-W Xe	36.7		1070
Pt/TiO_2	0.3	isooctane	500-W Xe	31.3		1070
Pt/TiO_2	0.3	*n*-paraffin	500-W Xe	7.7		1070
Pt/TiO_2	0.3	polyethylene	500-W Xe	13		1070
Pt/TiO_2	0.3	benzene	500-W Xe	120		1070
Pt/TiO_2	0.3	phenol	500-W Xe	110		1070
Pt/TiO_2	0.3	pyridine	500-W Xe	103.3		1070
Pt/TiO_2	0.3	coal	500-W Xe	30		1070
Pt/TiO_2	0.3	tar sand	500-W Xe	33.3		1070
Pt/TiO_2	0.3	pitch	500-W Xe	33.3		1070
Pt/TiO_2	0.08	Acid Orange 7	500-W Xe	~502.5		1071
Pt/TiO_2	0.08	Basic Red 46	500-W Xe	~187.5		1071
Pt/TiO_2	0.08	Basic Blue 41	500-W Xe	~112.5		1071
Pt/TiO_2	0.04	monochloroacetic acid	250-W Hg	375		1073
Pt/TiO_2	0.04	dichloroacetic acid	250-W Hg	197		1073
Pt/TiO_2	0.04	trichloroacetic acid	250-W Hg	trace		1073
Pt/TiO_2	0.02	monoethanolamine	200-W Hg	191.7		1074
Pt/TiO_2	0.01	hydrazine dihydrochloride	500-W Hg	~8370		1076
WO_x/TiO_2	0.16	2,4-dichlorophenoxyacetic acid	250-W Na[a]	~0.036		1082
WO_x/TiO_2	0.16	4-chlorophenol	250-W Na	~0.005		1082
Pt/TiO_2	0.3	Polyvinyl alcohol	500-W Xe	28.7	~0.66 (380 nm)	1083

Table 3. Continued

photocatalyst	mass (g)	sacrificial reagent	light Source	rate of hydrogen evolution (μmol·h^{-1}·g^{-1})	quantum yield (%)	reference
Pt/TiO$_2$	0.3	polyvinylchloride	500-W Xe	15	~0.35 (380 nm)	1083
Pt/TiO$_2$	0.3	Teflon	500-W Xe	1.17	~0.027 (380 nm)	1083
Pt/TiO$_2$	0.3	trichlorobenzene	500-W Xe	16	~0.37 (380 nm)	1083
Pt/TiO$_2$	0.3	trichloroethylene	500-W Xe	18.3	~0.42 (380 nm)	1083
Pt/TiO$_2$	0.3	sugar	500-W Xe	306.7	~7 (380 nm)	1083
Pt/TiO$_2$	0.3	starch	500-W Xe	80	~1.8 (380 nm)	1083
Pt/TiO$_2$	0.05	microwave treated soluble starch	125-W Hg	~1857		1085
Pt/TiO$_2$	0.3	cellulose (filter paper)	500-W Xe	13.3	~0.3 (380 nm)	1083
Pt/TiO$_2$	0.3	glycine	500-W Xe	73.3	~1.7 (380 nm)	1083
Pt/TiO$_2$	0.3	glutamic acid	500-W Xe	42	~0.97 (380 nm)	1083
Pt/TiO$_2$	0.3	proline	500-W Xe	43.3	~1 (380 nm)	1083
Pt/TiO$_2$	0.3	gelatin	500-W Xe	23.7	~0.55 (380 nm)	1083
Pt/TiO$_2$	0.3	stearic acid	500-W Xe	29.3	~0.68 (380 nm)	1083
Pt/TiO$_2$	0.3	olive oil	500-W Xe	10.7	~0.25 (380 nm)	1083
Pt/TiO$_2$	0.3	Chlorella	500-W Xe	90	~2.1 (380 nm)	1083
Pt/TiO$_2$	0.3	Laver	500-W Xe	110.7	~2.6 (380 nm)	1083
Pt/TiO$_2$	0.3	rice plant	500-W Xe	58.3	~1.35 (380 nm)	1083
Pt/TiO$_2$	0.3	turf	500-W Xe	32.7	~0.75 (380 nm)	1083
Pt/TiO$_2$	0.3	cockroach	500-W Xe	28.7	~0.66 (380 nm)	1083
Pt/TiO$_2$	0.3	human (urine, feces)	500-W Xe	58.7	~1.43 (380 nm)	1083
Pt/TiO$_2$	0.3	cow dung	500-W Xe	66	~1.52 (380 nm)	1083

[a] Sodium lamp.

for hydrogen evolution from water.[732,733,1022−1027] For example, a quamtum yield of ~93% at 420 nm has recently been reported for the Pt−PdS/CdS photocatalyst, the highest photocatalytic activity so far achieved for hydrogen production in the presence of sacrificial reagents of S^{2-}/SO_3^{2-} under visible-light irradiation.[733] The reaction mechanism in the presence of S^{2-}/SO_3^{2-} as sacrificial reagent is described by eqs 6−11.[732]

$$\text{photocatalyst} + h\nu \rightarrow h^+ + e^- \quad (6)$$

$$2e^- + 2H_2O \rightarrow H_2 + 2OH^- \quad (7)$$

$$SO_3^{2-} + 2OH^- + 2h^+ \rightarrow SO_4^{2-} + 2H^+ \quad (8)$$

$$2S^{2-} + 2h^+ \rightarrow S_2^{2-} \quad (9)$$

$$S_2^{2-} + SO_3^{2-} \rightarrow S_2O_3^{2-} + S^{2-} \quad (10)$$

$$SO_3^{2-} + S^{2-} + 2h^+ \rightarrow S_2O_3^{2-} \quad (11)$$

Since $S_2O_3^{2-}$ could be oxidized to SO_3^{2-} and subsequently to SO_4^{2-} by photogenerated holes, it has also been occasionally used as a sacrificial reagent for photocatalytic hydrogen generation.[870,871,1028−1030]

6.1.1.2. H_2S-Splitting System. A particularly meaningful system from the point of view of energy conservation and environmental protection is the photocatalytic hydrogen generation from H_2S dissolved in water or alkali solution.[398,785,806,1010,1031−1041] This approach via H_2S could have practical applications using waste gas H_2S from chemical industries such as natural gas utilization and desulfurization process in petrochemical plants.[56,1042] When H_2S is dissolved in alkaline aqueous solution, sulfide ions are formed and henceforth can play the role of sacrificial reagent. As described by eqs 6 and 12−14, the overall process corresponds to H_2S splitting by two photons of visible light. This requires 39.3 kJ/mol.[1043,1044]

$$H_2S + OH^- \rightarrow HS^- + H_2O \quad (12)$$

$$2HS^- + 2h^+ \rightarrow S_2^{2-} + 2H^+ \quad (13)$$

$$2H^+ + 2e^- \rightarrow H_2 \quad (14)$$

Recently, Li and co-workers developed a nonaqueous ethanolamine solution as the solvent and reaction medium for the direct splitting of H_2S into H_2 and S on a CdS-based photocatalyst under visible-light irradiation.[785] The potential of H_2S splitting in ethanolamine was greatly lowered, and the photogenerated electrons could be fully used to reduce protons for hydrogen production. The quantum efficiency was as high as 30% under visible-light irradiation. They also investigated hydrogen generation using gas−solid-phase photocatalytic H_2S splitting on semiconductor photocatalysts.[1045] However, performance under gas−solid-phase conditions was substantially lower than that under liquid−solid-phase conditions.

6.1.1.3. Other Inorganic Sacrificial Reagent Systems. Other inorganic ions, such as Fe^{2+},[274,752,1046,1047] Ce^{3+},[146,1048,1049] I^-,[140,351,613,625,626,642−644,1050] Br^-,[1051] and CN^-,[1052] have also been used as sacrificial reagents for hydrogen generation. These inorganic ions were easily oxidized by the photoge-

nerated holes to Fe^{3+}, Ce^{4+}, I_3^- (or IO_3^-), Br_2, and OCN^-, respectively. The result is hydrogen generation via water reduction by photogenerated electrons. Taking I^- as an example of an inorganic sacrificial reagent, the photocatalytic mechanism for hydrogen generation is described as eq 6 and eqs 15 and 16.[1050]

$$2H^+ + 2e^- \rightarrow H_2 \quad (15)$$

$$\left.\begin{array}{l} 3I^- + 2h^+ \rightarrow I_3^- \text{ (in acidic solution)} \\ I^- + 6OH^- + 6h^+ \rightarrow IO_3^- + 3H_2O \text{ (in basic solution)} \end{array}\right\} \quad (16)$$

Some photooxided species, such as Fe^{3+}, Ce^{4+}, and IO_3^-, could be easily reduced by photogenerated electrons back to Fe^{2+},[269,336,764,1053] Ce^{3+},[269,1049] and I^-,[1054] respectively. Thus, they could act as electron acceptors for photocatalytic oxygen generation from aqueous solution. Fe^{2+}/Fe^{3+}, Ce^{3+}/Ce^{4+}, and I^-/IO_3^- have therefore been used as redox mediators to construct a suitable system for overall water splitting using the Z-scheme system shown in section 6.2.2.

6.1.2. Organic Sacrificial Reagent System

Organic compounds, such as alcohols (methanol, ethanol, isopropanol, etc.),[82,91,1054−1061] organic acids (formic acid, acetic acid, etc.),[91,938,1062−1064] and aldehydes (formaldehyde, acetaldehyde, etc.)[91,1056,1065,1066] have all been used as electron donors for photocatalytic hydrogen generation. Among them, methanol was most widely used, and the hydrogen generation process is described as eq 6 and eqs 17−21:[183,184,1067]

$$h^+ + H_2O \rightarrow \cdot OH + H^+ \quad (17)$$

$$CH_3OH + \cdot OH \rightarrow \cdot CH_2OH + H_2O \quad (18)$$

$$\cdot CH_2OH \rightarrow HCHO + H^+ + e^- \quad (19)$$

$$2H_2O + 2e^- \rightarrow H_2 + 2OH^- \quad (20)$$

$$\text{overall reaction:} \quad CH_3OH \xrightarrow{h\nu,\text{catalyst}} HCHO + H_2 \quad (21)$$

The product, formaldehyde (HCHO), could be further oxidized to methanoic acid HCOOH and subsequently to CO_2 together with hydrogen generation via eqs 22 and 23:[1054,1068,1069]

$$HCHO + H_2O \xrightarrow{h\nu,\text{catalyst}} HCOOH + H_2 \quad (22)$$

$$HCOOH \xrightarrow{h\nu,\text{catalyst}} CO_2 + H_2 \quad (23)$$

In these photocatalytic systems, organic compounds are oxidized and decomposed by the photogenerated holes. Meanwhile, the remaining photogenerated electrons reduce water to hydrogen. Thus, it can be envisaged that a bifunctional photocatalytic system could be constructed, in which organic pollutants will be used to act as electron donors that achieve photocatalytic production of hydrogen from polluted water and simultaneous degradation of organic pollutants.[91,1066] Hashimoto et al. pioneered the work on photocatalytic H_2 generation from fossil fuels and hydrocarbons with water with powdered Pt/TiO_2 catalyst suspended in solution.[1070] The mechanism for photocatalytic H_2 generation from aqueous solutions of hydrocarbons could be explained by eq 6 and eqs 24−30.[1070]

$$H_2O + h^+ \rightarrow \cdot OH + H^+ \quad (24)$$

$$H^+ + e^- \rightarrow 1/2H_2 \quad (25)$$

$$RCH_2CH_3 + 2\cdot OH \rightarrow RCH_2CH_2OH + H_2O \quad (26)$$

$$RCH_2CH_2OH \rightarrow RCH_2CHO + H_2 \quad (27)$$

$$RCH_2CHO + H_2O \rightarrow RCH_2COOH + H_2 \quad (28)$$

$$\text{photo-Kolbe reaction:} \quad RCH_2COOH \rightarrow RCH_3 + CO_2 \quad (29)$$

$$\text{overall reaction:} \quad RCH_2CH_3 + 2H_2O \xrightarrow{h\nu,\text{catalyst}} RCH_3 + 3H_2 + CO_2 \quad (30)$$

To date, different kinds of model pollutants (azo-dyes, oxalic acid, formic acid, formaldehyde, chloroacetic acids, acetic acid, EDTA, dithiothreitol, TEA, hydrazine, dichlorophenoxyacetic acid, chlorophenol, etc.) were used as electron donors to construct the bifunctional photocatalytic systems. The photocatalytic decomposition of organic pollutants happened synchronously with efficient hydrogen generation.[649,1056,1064,1071−1082] Furthermore, it has been suggested that the photocatalytic reforming of biomass, which serves as the energy resource in plants and animals, may be anthor promising way of producing hydrogen from water. Kawai and Sakata constructed a water splitting system based on TiO_2 catalyst for photocatalytic hydrogen production involving decomposition of protein, algae, dead insects, and excrement with CO_2 as the only byproduct.[1083,1084] Carbohydrates, such as starch, cellulose, glycerol, glucose, and sucrose, were used as the sacrificial electron donors to construct water-splitting system for hydrogen generation by photocatalytic reforming of biomass over metal-loaded TiO_2 catalysts as well.[455,755,1084−1089] A probable mechanism for the photocatalytic reforming of glucose for hydrogen generation over Pt/TiO_2 was proposed by Fu et al.[1085] The reactions involved in the mechanism are summarized by eqs 31−37 and Figure 41.

$$Pt/TiO_2 + h\nu \rightarrow e^- + h^+ \quad (31)$$

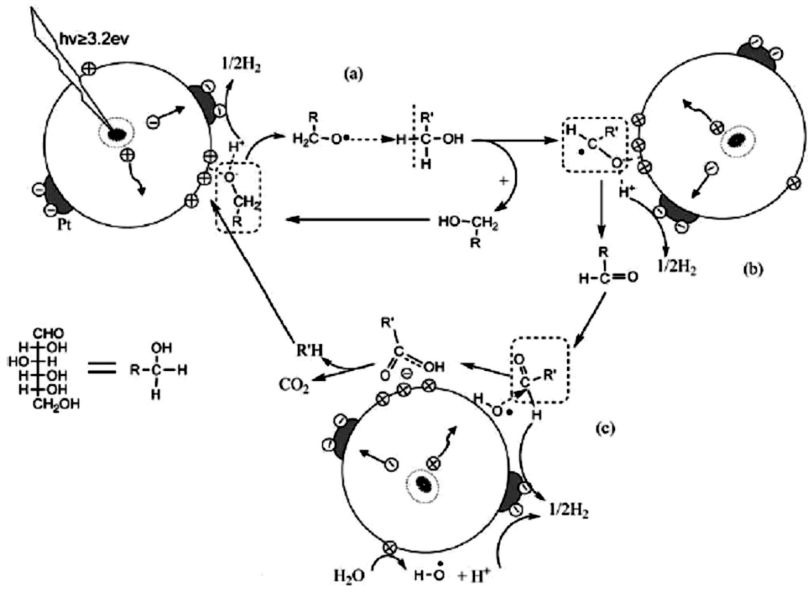

Figure 41. Proposed mechanism of the photocatalytic reforming of glucose on Pt/TiO_2. Reprinted with permission from ref 1085. Copyright 2008 Elsevier.

$$h^+ + H_2O \rightarrow H^+ + \cdot OH \quad (32)$$

$$H^+ + e^- \rightarrow 1/2H_2 \quad (33)$$

$$\left.\begin{array}{l}(RCH_2OH{=}C_6H_{12}O_6) + RCH_2OH \rightarrow H^+ + RCH_2O^- \\ \left\{\begin{array}{l}H^+ + e^- \rightarrow 1/2H_2 \\ RCH_2O^- + h^+ \rightarrow RCH_2O\cdot\end{array}\right. \\ RCH_2O\cdot + R'CH_2OH \rightarrow R'\dot{C}HOH + RCH_2OH\end{array}\right\} \quad (34)$$

$$\begin{array}{l}R'\dot{C}H_2OH + h^+ \rightarrow H^+ + R'\dot{C}HO\cdot \rightarrow R'CHO \\ H^+ + e^- \rightarrow 1/2H_2\end{array} \quad (35)$$

$$\begin{array}{l}R'CHO + \cdot OH \rightarrow [R'COOH]^- + H^+ \\ H^+ + e^- \rightarrow 1/2H_2 \\ [R'COOH]^- + h^+ \rightarrow R'H + CO_2\end{array} \quad (36)$$

$$\text{overall reaction:} \quad C_6H_{12}O_6 + 6H_2O \xrightarrow{h\nu,\text{catalyst}} 6CO_2 + 12H_2 \quad (37)$$

In spite of the limited work in this special area, the results are encouraging and promising for the construction of photocatalytic systems involving efficient hydrogen generation as well as pollutant decomposition or biomass reforming.

6.2. Overall Water-Splitting Systems

6.2.1. Pure Water-Splitting System

As illustrated in Figure 3, the photocatalyst acts as two roles, H_2 generators and O_2 generators in the overall pure water-splitting system. Over the past several decades, a number of photocatalysts have been successfully developed to construct an overall water-splitting system for simultaneous hydrogen and oxygen generation in the absence of sacrificial reagents.[20,22,24,51,353,1090] Among them, $(Ga_{1-x}Zn_x)(N_{1-x}O_x)$ has been proven as the most promising photocatalyst for overall water splitting.[575] Steady and stoichiometric H_2 and O_2 evolutions were found to evolve with a quantum yield of 5.9% in the range of 420−440 nm.[575]

6.2.2. Biomimetic Z-Scheme Water-Splitting System

The biomimetic Z-schem system mechanism using reversible redox mediators has been investigated with a view to constructing a photocatalytic system for overall water splitting into H_2 and O_2. For example, Arakawa and co-workers constructed an artificial Z-scheme system for overall water splitting using WO_3 photocatalyst and a Fe^{2+}/Fe^{3+} redox mediator.[1091,1092] Kozlova et al. investigated the overall water splitting over a Pt/TiO_2 catalyst with a Ce^{3+}/Ce^{4+} shuttle charge transfer system.[1048] However, in these studies, the photocatalytic activities for O_2 and H_2 production were low, due to the back-reaction and the interactional reaction characteristics. Fujihara et al. constructed a Z-scheme water-splitting system using a TiO_2-rutile photocatalyst and two redox mediators (Br_2/Br^- and Fe^{3+}/Fe^{2+}) in a two-compartment cell.[1051] As the production of H_2 and O_2 were carried out in separated compartments, the reversible reactions on photocatalysts, which often suffered from the effects of back-reactions, were largely prevented.

Abe et al. used an innovatively designed Z-scheme system for overall water splitting into H_2 and O_2 using a two-step photoexcitation.[1093] It was composed of an IO_3^-/I^- shuttle redox mediator and two different photocatalysts: Pt-loaded anatase TiO_2 for H_2 evolution and rutile TiO_2 for O_2 evolution. The proposed photocatalytic reaction mechanism for the Z-scheme water-splitting system is depicted schematically in Figure 42. Under UV irradiation, simultaneous gas evolution of H_2 (180 μmol/h) and O_2 (90 μmol/h) was observed from a basic (pH = 11) NaI aqueous suspension of these two different TiO_2 photocatalysts. The overall water splitting proceeded by the redox cycle between IO_3^- and I^- under basic conditions as follows: (a) water reduction to H_2 and I^- oxidation to IO_3^- over $Pt-TiO_2$-anatase and (b) IO_3^- reduction to I^- and water oxidation to O_2 over TiO_2-rutile. IO_3^- reduction to I^- over $Pt-TiO_2$-anatase was an undesirable side reaction. If this reaction was suppressed, the total water-splitting reaction took place more efficiently. The

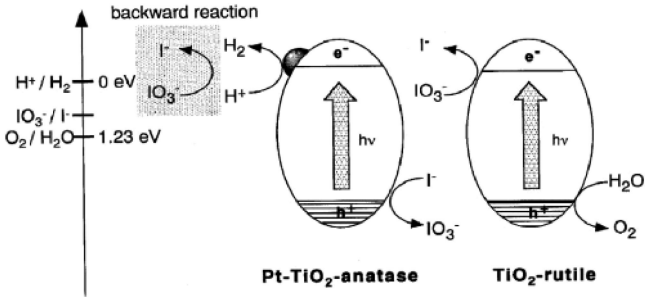

Figure 42. Proposed photocatalytic reaction mechanism for Z-scheme water-splitting system using an IO_3^-/I^- redox mediator and a mixture of Pt−TiO_2-antase and TiO_2-rutile photocatalysts. Reprinted with permission from ref 1093. Copyright 2001 Elsevier.

advantage of this system was that H_2 gas was evolved only over the Pt−TiO_2-anatase photocatalyst and that O_2 gas was evolved over the TiO_2-rutile photocatalyst only, even from a mixture of IO_3^- and I^- in a basic aqueous solution. Therefore, another undesirable backward reaction, H_2O formation from H_2 and O_2 on Pt particles, was suppressed.[1093]

In the later studies, a series of Z-scheme overall water-splitting systems active under visible-light irradiation were constructed, such as (Pt/$ATaO_2N$ (A = Ca, Sr, Ba))−(Pt/WO_3)−(IO_3^-/I^-),[395,1094] (Pt/TaON)−(Pt/WO_3)−(IO_3^-/I^-),[471] (Pt/$SrTiO_3$:Cr/Ta)−(Pt/WO_3)−(IO_3^-/I^-),[345,1095,1096] (Pt/ZrO_2−TaON)−(Pt/WO_3)−(IO_3^-/I^-),[897,1097] (Pt/TaON)−(RuO_2/TaON)−(IO_3^-/I^-),[1098] (Ru/$SrTiO_3$:Rh)−($BiVO_4$)−(Fe^{3+}/Fe^{2+}),[752] (Pt/$SrTiO_3$:Rh)−(Bi_2MoO_6)−(Fe^{3+}/Fe^{2+}),[1046] (Pt/$SrTiO_3$:Rh)−(WO_3)−(Fe^{3+}/Fe^{2+}),[1046,1047] (Pt/$SrTiO_3$:Rh)−($BiVO_4$)−(Fe^{3+}/Fe^{2+}),[1046] (Pt/ZrO_2−TaON)−(Ir/Ta_3N_5−TiO_2)−(IO_3^-/I^-),[1099] and (coumarin-dye-adsorbed Pt/$H_4Nb_6O_{17}$)−(IrO_2−Pt/WO_3)−(IO_3^-/I^-).[1100] These are summarized in Table 4. Of these, the (Pt/ZrO_2−TaON)−(Pt/WO_3)−(IO_3^-/I^-) system showed the highest photocatalytic activity for overall water splitting with a quantum efficiency of ca. 6.3% at 420.5 nm. In this Z-scheme overall water-splitting system, the H_2 and IO_3^- production proceeded over the Pt/ZrO_2−TaON photocatalyst; meanwhile, the IO_3^- reduction and water oxidation to O_2 took place over Pt−WO_3 under visible-light irradiation.[1097] In general, a redox mediator (such as IO_3^-/I^- and Fe^{3+}/Fe^{2+}) is required for the construction of a Z-scheme photocatalytic system. Undesirable side effects such as backward reactions to form water from the H_2 and O_2 evolved can occur.

Recently, Kudo et al. had a surprising success in fabricating an overall water-splitting system driven by a Z-scheme interparticle electron transfer between H_2- and O_2-photocatalysts (Ru/$SrTiO_3$:Rh-$BiVO_4$) without a redox mediator.[1101] This is shown in Figure 43, in which the undesirable reactions and negative effects by an electron mediator were excluded. Although the activity of a Z-scheme overall water-splitting system is quite low and only a little higher than that achieved by conventional pure water-splitting systems using one single photocatalyst, these results provided a promising approach to constructing efficient overall water-splitting systems.

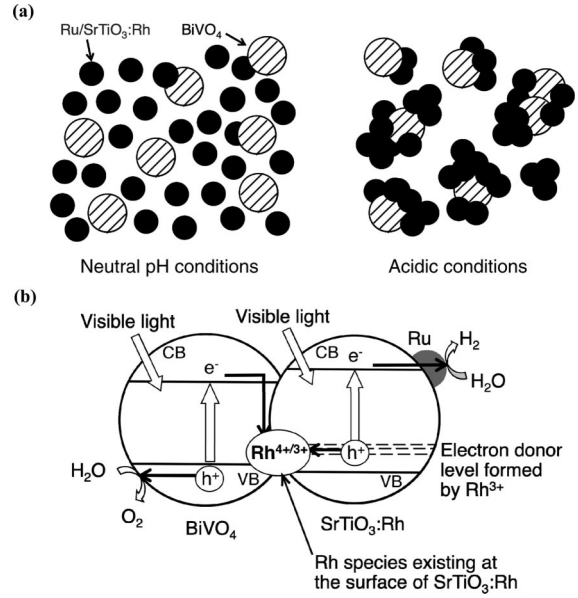

Figure 43. Mechanism of water splitting using the Z-scheme photocatalysis system driven by electron transfer between H_2- and O_2-photocatalysts. (a) Suspension of Ru/$SrTiO_3$:Rh and $BiVO_4$ at neutral and acidic conditions. (b) Scheme of photocatalytic water splitting. Reprinted with permission from ref 1101. Copyright 2009 American Chemical Society.

7. Summary and Prospects

So far, the sacrificial reagent-containing water-splitting systems constructed based on the Pt/CdS,[732] Pt−PdS/CdS,[733] and Zn/Cr layered double hydroxide[667] photocatalysts demonstrated the best performance for hydrogen production and oxygen production, with the highest quantum yields of ca. 60.35%, 93%, and 60.1%, respectively, at 420 nm. However, the efficiency of an overall water-splitting system based on visible-light-driven photocatalysts has been still quite low, with the maximum quantum efficiency of ca. 5.9% over $Rh_{2-y}Cr_yO_3$/GaN−ZnO in the range of 420−440 nm.[575] This is still far from the quantum efficiency (ca. 30% at 600 nm) designated the initial starting point for practical applications[51,56]

Table 4. Z-Schematic Photocatalytic System for Water Splitting to Hydrogen and Oxygen under Visible-Light Irradiation

H_2 photocatalyst	O_2 photocatalyst	mediator	light source	incident light	activity (μmol·h^{-1}·g^{-1}) H_2	activity (μmol·h^{-1}·g^{-1}) O_2	QY	ref
Pt/TaON (0.2 g)	Pt/WO_3 (0.2 g)	IO_3^-/I^-	300-W Xe	>420 nm	120	60	0.4 (420 nm)	471
Pt/$CaTaO_2N$ (0.1 g)	Pt/WO_3 (0.1 g)	IO_3^-/I^-	300-W Xe	>420 nm	43	21		395
Pt/$BaTaO_2N$ (0.1 g)	Pt/WO_3 (0.1 g)	IO_3^-/I^-	300-W Xe	>420 nm	67	33	0.1 (420−440 nm)	395
Pt/$SrTiO_3$:Cr/Ta (0.2 g)	Pt/WO_3 (0.325 g)	IO_3^-/I^-	300-W Xe	>420 nm	80	24.6	1 (420 nm)	345, 1095, 1096
Pt/ZrO_2−TaON (0.025 g)	Pt/WO_3 (0.05 g)	IO_3^-/I^-	300-W Xe	>420 nm	1040	266	6.3 (420.5 nm)	897, 1097
Pt/TaON (0.05 g)	RuO_2/TaON (0.05 g)	IO_3^-/I^-	300-W Xe	>420 nm	60	30	0.1−0.2	1098
Ru/$SrTiO_3$:Rh (0.05 g)	$BiVO_4$ (0.05 g)	Fe^{3+}/Fe^{2+}	300-W Xe	>420 nm	378	179	0.3 (420 nm)	752
Pt/$SrTiO_3$:Rh (0.02 g)	Bi_2MoO_6 (0.02 g)	Fe^{3+}/Fe^{2+}	300-W Xe	>420 nm	950	445	0.2 (440 nm)	1046
Pt/$SrTiO_3$:Rh (0.02 g)	WO_3 (0.02 g)	Fe^{3+}/Fe^{2+}	300-W Xe	>420 nm	390	200	0.2 (440 nm)	1046
Pt/$SrTiO_3$:Rh (0.02 g)	$BiVO_4$ (0.02 g)	Fe^{3+}/Fe^{2+}	300-W Xe	>420 nm	750	360	0.3 (440 nm)	1046
Pt/ZrO_2−TaON (0.05 g)	Ir/TiO_2/Ta_3N_5 (0.05 g)	IO_3^-/I^-	300-W Xe	>400 nm	~45	~22		1099
coumarin/Pt/$H_4Nb_6O_{17}$ (0.05 g)	IrO_2−Pt/WO_3 (0.1 g)	IO_3^-/I^-	300-W Xe	>400 nm	48.3	12.1	<0.1 (500 nm)	1100
Ru/$SrTiO_3$:Rh	$BiVO_4$		300-W Xe	>400 nm	400	190	1.7 (420 nm)	1101

or the critical conversion efficiency of light energy to hydrogen from photocatalytic water decomposition (15%).[1102] Therefore, more efficient visible-light-driven photocatalysts need to be developed to construct the necessay high-efficiency and cost-effective water-splitting systems.

To develop more efficient visible-light-driven photocatalysts, it is necessary to narrow the band gaps to harvest visible light in the longer-wavelength regions and enhance the photogenerated charge separation in photocatalysis. Thus, factors such as electronic properties, chemical composition, structure and crystallinity, surface states, and morphology, all of which determine the photocatalytic activity of such materials, need to be further elucidated in great detail. Band gap engineering for the modification of the band structure of semiconductor photocatalysts using ion doping, semiconductor sensitization, or solid solution all present significant opportunities to render such materials active in the visible-light region. Computational prediction based on first-principle calculations could not only provide an efficient way to identify a candidate but also suggest useful processing and production conditions. The crystallinity and crystal structure, surface structure, and morphology of photocatalysts on a nanometric scale need to be investigated systematically and modified to optimize the preparation methods and refine the materials for maximizing efficiency. These are the properties that have a major impact on charge separation, mobility, and the lifetime of the photogenerated electrons and holes. The loading of cocatalysts on the surface of the host photocatalysts has been shown to be rather effective in inhibiting charge recombination. Alternative more economical cocatalysts, such as the non-noble metals and other derived metal-based compounds, also need to be tested as possible substitutes for the most frequently used noble metals such as Pt, which although very efficient is expensive. Additionally, new insights are needed into the water-splitting mechanism, particularly with regards to identification of any thermodynamic and kinetic bottlenecks. This would facilitate the design of the most effective photocatalytic water-splitting systems.

Presently, the available efficiency for overall water (or natural water[1103−1105]) splitting systems for simultaneous hydrogen and oxygen production under visible-light irradiation is still quite low due to fast charge recombination and backward reactions. To achieve enhanced and sustainable hydrogen production, the continual addition of electron donors is required to make up half of the water-splitting reaction to reduce H_2O to H_2. These sacrificial electron donors can irreversibly consume photogenerated holes, thus prohibiting undesirable charge recombination. Taking into account the lowering cost for solar-to-H_2 energy conversion, polluting byproduct from industries and low-cost renewable biomass from animals or plants are preferential sacrificial electron donors in water-splitting systems. At little or no cost, they could be exploited to accomplish both the tasks of hydrogen production and waste treatment and biomass reforming simultaneously. The molecular mechanisms and reaction kinetics need to be considered carefully when designing such photocatalytic hydrogen production systems. Nevertheless, such an admirable goal for the practical application of water-splitting systems is especially interesting in light of worldwide energy and environmental concerns.

The current lack of industrial applications of the semiconductor-based photocatalytic hydrogen generation is largely due to two reasons: the low photocatalytic efficiency and the lack of extensive studies for a successful scale-up of the laboratory setup into an industrially relevant scale. To directly utilize solar light in the open air, a compound parabolic concentrator (CPC)-based photocatalytic hydrogen production reactor was recently designed by Jing et al.[1106] Efficient photocatalytic hydrogen production under direct solar light was accomplished by coupling a tubular reactor with the CPC concentrator. This demonstration drew attention for further studies in this promising direction. Nevertheless, both for material and reactor design, reduction of cost will have to be given special priority, before the final utilization of semiconductor-based photocatalytic hydrogen generation.[1107]

8. Acknowledgments

The authors thank Mr. Dale Parry and the Editorial Office of Chemical Reviews for assistance in editing the manuscript.

9. References

(1) Züttel, A.; Borgschulte, A.; Schlapbach, L. *Hydrogen as a Future Energy Carrier*; Wiley-VCH: Weinheim, Germany, 2008.
(2) Muradov, N. Z.; Veziroğlu, T. N. *Int. J. Hydrogen Energy* **2008**, *33*, 6804.
(3) U.S. Energy Information Administration. The Impact of Increased Use of Hydrogen on Petroleum Consumption and Carbon Dioxide Emissions. Report #: SR-OIAF-CNEAF/2008-04. http://www.eia.doe.gov/oiaf/servicerpt/hydro/hydrogen.html.
(4) Coughlin, R. W.; Farooque, M. *Nature* **1979**, *279*, 301.
(5) Wang, D.; Czernik, S.; Montane, D.; Mann, M.; Chornet, E. *Ind. Eng. Chem. Res.* **1997**, *36*, 1507.
(6) Sato, S.; Lin, S.; Suzuki, Y.; Hatano, H. *Fuel* **2003**, *82*, 561.
(7) Cortright, R. D.; Davda, R. R.; Dumesic, J. A. *Nature* **2002**, *418*, 964.
(8) Lu, Y. J.; Guo, L. J.; Ji, C. M.; Zhang, X. M.; Hao, X. H.; Yan, Q. H. *Int. J. Hydrogen Energy* **2006**, *31*, 822.
(9) Hao, X. H.; Guo, L. J.; Mao, X.; Zhang, X. M.; Chen, X. J. *Int. J. Hydrogen Energy* **2003**, *28*, 55.
(10) Navarro, R. M.; Pea, M. A.; Fierro, J. L. G. *Chem. Rev.* **2007**, *107*, 3952.
(11) Sand, H. J. S. *Philos. Mag.* **1901**, *1*, 45.
(12) Damen, K.; Troost, M.; Faaij, A.; Turkenburg, W. *Prog. Energy Combust. Sci.* **2006**, *32*, 215.
(13) Cormos, C. C.; Starr, F.; Tzimas, E.; Peteves, S. *Int. J. Hydrogen Energy* **2008**, *33*, 1286.
(14) Cobden, P. D.; van Beurden, P.; Reijers, H. T. J.; Elzinga, G. D.; Kluiters, S. C. A.; Dijkstra, J. W.; Jansen, D.; van den Brink, R. W. *Int. J. Greenhouse Gas Control* **2007**, *1*, 170.
(15) Wang, Y. G.; Li, H. Q.; He, P.; Zhou, H. S. *ChemSusChem* **2010**, *3*, 571.
(16) Rajeshwar, K.; McConnell, R.; Licht, S. *Solar Hydrogen Generation*; Springer: New York, 2008.
(17) Guo, L. J.; Zhao, L.; Jing, D. W.; Lu, Y. J.; Yang, H. H.; Bai, B. F.; Zhang, X. M.; Ma, L. J.; Wu, X. M. *Energy* **2009**, *34*, 1073.
(18) Fujishima, A.; Honda, K. *Nature* **1972**, *238*, 37.
(19) Mao, S. S.; Chen, X. *Int. J. Energy Res.* **2007**, *31*, 619.
(20) Kato, H.; Asakura, K.; Kudo, A. *J. Am. Chem. Soc.* **2003**, *125*, 3082.
(21) Kudo, A.; Kato, H.; Nakagawa, S. *J. Phys. Chem. B* **2000**, *104*, 571.
(22) Kim, H. G.; Hwang, D. W.; Bae, S. W.; Jung, J. H.; Lee, J. S. *Catal. Lett.* **2003**, *91*, 193.
(23) Ikeda, S.; Hara, M.; Kondo, J. N.; Domen, K.; Takahashi, H.; Okubo, T.; Kakihana, M. *Chem. Mater.* **1998**, *10*, 72.
(24) Maeda, K.; Saito, N.; Lu, D.; Inoue, Y.; Domen, K. *J. Phys. Chem. C* **2007**, *111*, 4749.
(25) Li, Y.; Zhang, J. Z. *Laser Photonic Rev.* **2010**, *4*, 517.
(26) Chen, Z.; Jaramillo, T. F.; Deutsch, T. G.; Kleiman-Shwarsctein, A.; Forman, A. J.; Gaillard, N.; Garland, R.; Takanabe, K.; Heske, C.; Sunkara, M.; McFarland, E. W.; Domen, K.; Miller, E. L.; A. Turner, J. A.; Dinh, H. N. *J. Mater. Res.* **2010**, *25*, 3.
(27) Minggu, L. J.; Daud, W. R. W.; Kassim, M. B. *Int. J. Hydrogen Energy* **2010**, *35*, 5233.
(28) van de Krol, R.; Liang, Y.; Schoonman, J. *J. Mater. Chem.* **2008**, *18*, 2311.
(29) Alexander, B. D.; Kulesza, P. J.; Rutkowska, I.; Solarska, R.; Augustynski, J. *J. Mater. Chem.* **2008**, *18*, 2298.
(30) Rajeshwar, K. *J. Appl. Electrochem.* **2007**, *37*, 765.

(31) Aroutiounian, V. M.; Arakelyan, V. M.; Shahnazaryan, G. E. *Sol. Energy* **2005**, *78*, 581.
(32) Nozik, J. *Annu. Rev. Phys. Chem.* **1978**, *29*, 189.
(33) Grätzel, M. *Acc. Chem. Res.* **1981**, *14*, 376.
(34) Grätzel, M. *Biochim. Biophys. Acta* **1982**, *683*, 221.
(35) Grätzel, M. *Energy Resources through Photochemistry and Catalysis*; Academic Press: New York, 1983.
(36) Serpone, N.; Pelizzetti, E. *Photocatalysis*; Wiley: New York, 1989.
(37) Bard, A. J.; Fox, A. M. *Acc. Chem. Res.* **1995**, *28*, 141.
(38) Domen, K.; Kondo, J. N.; Hara, M.; Takata, T. *Bull. Chem. Soc. Jpn.* **2000**, *73*, 1307.
(39) Domen, K.; Hara, M.; Kondo, J. N.; Takata, T.; Kudo, A.; Kobayashi, H.; Inoue, Y. *Korean J. Chem. Eng.* **2001**, *18*, 862.
(40) Kudo, A. *Catal. Surv. Asia* **2003**, *7*, 31.
(41) Zou, Z.; Arakawa, H. *J. Photochem. Photobiol., A* **2003**, *158*, 145.
(42) Yamasita, D.; Takata, T.; Hara, M.; Kondo, J. N.; Domen, K. *Solid State Ionics* **2004**, 172–591.
(43) Anpo, M.; Dohshi, S.; Kitano, M.; Hu, Y.; Takeuchi, M.; Matsuoka, M. *Annu. Rev. Mater. Res.* **2005**, *35*, 1.
(44) Lee, J. S. *Catal. Surv. Asia* **2005**, *9*, 217.
(45) Kudo, A. *Int. J. Hydrogen Energy* **2006**, *31*, 197.
(46) Maeda, K.; Teramura, K.; Saito, N.; Inoue, Y.; Kobayashi, H.; Domen, K. *Pure Appl. Chem.* **2006**, *78*, 2267.
(47) Matsuoka, M.; Kitano, M.; Takeuchi, M.; Tsujimaru, K.; Anpo, M.; Thomas, J. M. *Catal. Today* **2007**, *122*, 51.
(48) Shangguan, W. *Sci. Technol. Adv. Mater.* **2007**, *8*, 76.
(49) Kudo, A. *Pure Appl. Chem.* **2007**, *79*, 1917.
(50) Kudo, A. *Int. J. Hydrogen Energy* **2007**, *32*, 2673.
(51) Maeda, K.; Domen, K. *J. Phys. Chem. C* **2007**, *111*, 7851.
(52) Ekambaram, S. *J. Alloys Compd.* **2008**, *448*, 238.
(53) Laniecki, M. *Ceram. Eng. Sci. Proc.* **2008**, *28*, 23.
(54) Osterloh, F. E. *Chem. Mater.* **2008**, *20*, 35.
(55) Kudo, A.; Miseki, Y. *Chem. Soc. Rev.* **2009**, *38*, 253.
(56) Navarro, R. M.; Sánchez-Sánchez, M. C.; Álvarez-Galván, M. C.; del Valle, F.; Fierro, J. L. G. *Energy Environ. Sci.* **2009**, *2*, 35.
(57) Grimes, C.; Varghese, O. K.; Ranjan, S. *Light, Water, Hydrogen: The Solar Generation of Hydrogen by Water Photoelectrolysis*; Springer: New York, 2008.
(58) Kaneko, M.; Okura, I. *Photocatalysis: Science and technology*; Springer-Verlag: New York, 2002.
(59) Yerga, R. M. N.; Álvarez-Galván, M. C.; del Valle, F.; de la Mano, J. A. V.; Fierro, J. L. G. *ChemSusChem* **2009**, *2*, 471.
(60) Inoue, Y. *Energy Environ. Sci.* **2009**, *2*, 364.
(61) Zhu, J.; Zäch, M. *Curr. Opin. Colloid Interface Sci.* **2009**, *14*, 260.
(62) Wen, F.; Yang, J.; Zong, X.; Ma, Y.; Xu, Q.; Ma, B.; Li, C. *Prog. Chem.* **2009**, *21*, 2285.
(63) Bard, A. J. *J. Photochem.* **1979**, *10*, 59.
(64) Bard, A. J. *Science* **1980**, *207*, 139.
(65) Bard, A. J. *J. Phys. Chem.* **1982**, *86*, 172.
(66) Xu, Y.; Schoonen, M. A. A. *Am. Mineral.* **2000**, *85*, 543.
(67) Linsebigler, A. L.; Lu, G.; Yates, J. T. *Chem. Rev.* **1995**, *95*, 735.
(68) Serpone, N.; Sauvé, G.; Koch, R.; Tahiri, H.; Pichat, P.; Piccinini, P.; Pelizzetti, E.; Hidaka, H. *J. Photochem. Photobiol., A* **1996**, *94*, 191.
(69) Schrauzer, G. N.; Guth, T. D. *J. Am. Chem. Soc.* **1977**, *99*, 7189.
(70) Duonghong, D.; Borgarello, E.; Grätzel, M. *J. Am. Chem. Soc.* **1981**, *103*, 4685.
(71) Sayama, K.; Arakawa, H. *J. Chem. Soc., Faraday Trans.* **1997**, *93*, 1647.
(72) Shi, J.; Chen, J.; Feng, Z.; Chen, T.; Lian, Y.; Wang, X.; Li, C. *J. Phys. Chem. C* **2007**, *111*, 693.
(73) Zhang, J.; Xu, Q.; Feng, Z.; Li, M.; Li, C. *Angew. Chem., Int. Ed.* **2008**, *47*, 1766.
(74) Yamaguti, K.; Sato, S. *J. Chem. Soc., Faraday Trans. I* **1985**, *81*, 1237.
(75) Kudo, A.; Domen, K.; Maruya, K.; Onishi, T. *Chem. Phys. Lett.* **1987**, *133*, 517.
(76) Tabata, S.; Nishida, H.; Masaki, Y.; Tabata, K. *Catal. Lett.* **1995**, *34*, 245.
(77) Chen, X. *Chin. J. Catal.* **2009**, *30*, 839.
(78) Sayama, K.; Arakawa, H. *J. Photochem. Photobiol., A* **1994**, *77*, 243.
(79) Chae, J.; Lee, J.; Jeong, J. H.; Kang, M. *Bull. Korean Chem. Soc.* **2009**, *30*, 302.
(80) Jing, D.; Zhang, Y.; Guo, L. *Chem. Phys. Lett.* **2005**, *415*, 74.
(81) Sasikala, R.; Sudarsan, V.; Sudakar, C.; Naik, R.; Sakuntala, T.; Bharadwaj, S. R. *Int. J. Hydrogen Energy* **2008**, *33*, 4966.
(82) Zalas, M.; La, M. *Sol. Energy Mater. Sol. Cells* **2005**, *89*, 287.
(83) Sasikala, R.; Shirole, A.; Sudarsan, V.; Sakuntala, T.; Sudakar, C.; Naik, R.; Bharadwaj, S. R. *Int. J. Hydrogen Energy* **2009**, *34*, 3621.
(84) Yuan, Q.; Liu, Y.; Li, L. L.; Li, Z. X.; Fang, C. J.; Duan, W. T.; Li, X. G.; Yan, C. H. *Microporous Mesoporous Mater.* **2009**, *124*, 169.
(85) Xu, S.; Sun, D. D. *Int. J. Hydrogen Energy* **2009**, *34*, 6096.
(86) Xu, S.; Ng, J.; Zhang, X.; Bai, H.; Sun, D. D. *Int. J. Hydrogen Energy* **2010**, *35*, 5254.
(87) Choi, H. J.; Kang, M. *Int. J. Hydrogen Energy* **2007**, *32*, 3841.
(88) Park, J. W.; Kang, M. *Int. J. Hydrogen Energy* **2007**, *32*, 4840.
(89) Lalitha, K.; Reddy, J. K.; Sharma, M. V. P.; Kumari, V. D.; Subrahmanyam, M. *Int. J. Hydrogen Energy* **2010**, *35*, 3991.
(90) Park, M. S.; Kang, M. *Mater. Lett.* **2008**, *62*, 183.
(91) Zieliñska, B.; Borowiak-Palen, E.; Kalenczuk, R. J. *Int. J. Hydrogen Energy* **2008**, *33*, 1797.
(92) Moon, S. C.; Mametsuka, H.; Suzuki, E.; Anpo, M. *Chem. Lett.* **1998**, *27*, 117.
(93) Moon, S. C.; Mametsuka, H.; Tabata, S.; Suzuki, E. *Catal. Today* **2000**, *58*, 125.
(94) Liu, S. H.; Wang, H. P.; Huang, Y. J.; Sun, Y. M.; Lin, K. S.; Hsiao, M. C. *Energy Sources* **2003**, *25*, 591.
(95) Zhao, D.; Budhi, S.; Rodriguez, A.; Koodali, R. T. *Int. J. Hydrogen Energy* **2010**, *35*, 5276.
(96) Shibata, M.; Kudo, A.; Tanaka, A.; Domen, K.; Maruya, K.; Ohishi, T. *Chem. Lett.* **1987**, *16*, 1017.
(97) Allen, M. R.; Thibert, A.; Sabio, E. M.; Browning, N. D.; Larsen, D. S.; Osterloh, F. E. *Chem. Mater.* **2010**, *22*, 1220.
(98) Machida, M.; Ma, X. W.; Taniguchi, H.; Yabunaka, J.; Kijima, T. *J. Mol. Catal. A: Chem.* **2000**, *155*, 131.
(99) Jang, J. S.; Choi, S. H.; Kim, D. H.; Jang, J. W.; Lee, K. S.; Lee, J. S. *J. Phys. Chem. C* **2009**, *113*, 8990.
(100) Kudo, A.; Kondo, T. *J. Mater. Chem.* **1997**, *7*, 777.
(101) Ogura, S.; Kohno, M.; Sato, K.; Inoue, Y. *Appl. Surf. Sci.* **1997**, *121−122*, 521.
(102) Inoue, Y.; Kubokawa, T.; Sato, K. *J. Chem. Soc., Chem. Commun.* **1990**, *19*, 1298.
(103) Inoue, Y.; Kubokawa, T.; Sato, K. *J. Phys. Chem.* **1991**, *95*, 4059.
(104) Ogura, S.; Sato, K.; Inoue, Y. *Phys. Chem. Chem. Phys.* **2000**, *2*, 2449.
(105) Kohno, M.; Kaneko, T.; Ogura, S.; Sato, K.; Inoue, Y. *J. Chem. Soc., Faraday Trans.* **1998**, *94*, 89.
(106) Inoue, Y.; Niiyama, T.; Asai, Y.; Sato, K. *J. Chem. Soc., Chem. Commun.* **1992**, *7*, 579.
(107) Inoue, Y.; Asai, Y.; Sato, K. *J. Chem. Soc., Faraday Trans.* **1994**, *90*, 797.
(108) Yamashita, Y.; Yoshida, K.; Kakihana, M.; Uchida, S.; Sato, T. *Chem. Mater.* **1999**, *11*, 61.
(109) Domen, K.; Naito, S.; Soma, M.; Onishi, T.; Tamaru., K. *J. Chem. Soc., Chem. Commun.* **1980**, 543.
(110) Domen, K.; Naito, S.; Onishi, T.; Tamaru, K. *J. Phys. Chem.* **1982**, *86*, 3657.
(111) Domen, K.; Naito, S.; Onishi, T.; Tamaru, K. *Chem. Phys. Lett.* **1982**, *92*, 433.
(112) Domen, K.; Kudo, A.; Onishi, T. *J. Catal.* **1986**, *102*, 92.
(113) Kudo, A.; Tanaka, A.; Domen, K.; Onishi, T. *J. Catal.* **1988**, *111*, 296.
(114) Domen, K.; Kudo, A.; Onishi, T.; Kosugi, N.; Kuroda, H. *J. Phys. Chem.* **1986**, *90*, 292.
(115) Liu, Y.; Xie, L.; Li, Y.; Yang, R.; Qu, J.; Li, Y.; Li, X. *J. Power Sources* **2008**, *183*, 701.
(116) Qin, Y.; Wang, G.; Wang, Y. *Catal. Commun.* **2007**, *8*, 926.
(117) Takata, T.; Domen, K. *J. Phys. Chem. C* **2009**, *113*, 19386.
(118) Jeong, H.; Kim, T.; Kim, D.; Kim, K. *Int. J. Hydrogen Energy* **2006**, *31*, 1142.
(119) Ko, Y. G.; Lee, W. Y. *Catal. Lett.* **2002**, *83*, 157.
(120) Mizoguchi, H.; Ueda, K.; Orita, M.; Moon, S. C.; Kajihara, K.; Hirano, M.; Hosono, H. *Mater. Res. Bull.* **2002**, *37*, 2401.
(121) Sun, W.; Zhang, S.; Wang, C.; Liu, Z.; Mao, Z. *Catal. Lett.* **2007**, *119*, 148.
(122) Kim, A.; Hwang, D. W.; Bae, S. W.; Kim, Y. G.; Lee, J. S. *Korean J. Chem. Eng.* **2001**, *18*, 941.
(123) Kim, J.; Hwang, D. W.; Kim, H. G.; Bae, S. W.; Ji, S. M.; Lee, J. S. *Chem. Commun.* **2002**, *21*, 2488.
(124) Kim, H. G.; Ji, S. M.; Jang, J. S.; Bae, S. W.; Lee, J. S. *Korean J. Chem. Eng.* **2004**, *21*, 970.
(125) Kim, J.; Hwang, D. W.; Kim, H. G.; Bae, S. W.; Lee, J. S.; Li, W.; Oh, S. H. *Top. Catal.* **2005**, *35*, 295.
(126) Li, Z.; Chen, G.; Tian, X.; Li, Y. *Mater. Res. Bull.* **2008**, *43*, 1781.
(127) Hwang, D. W.; Lee, J. S.; Li, W.; Oh, S. H. *J. Phys. Chem. B* **2003**, *107*, 4963.
(128) Abe, R.; Higashi, M.; Zou, Z.; Sayama, K.; Abe, Y. *Chem. Lett.* **2004**, *33*, 954.
(129) Kakihana, M.; Domen, K. *MRS Bull.* **2000**, *25*, 27.
(130) Higashi, M.; Abe, R.; Sayama, K.; Sugihara, H.; Abe, Y. *Chem. Lett.* **2005**, *34*, 1122.
(131) Abe, R.; Higashi, M.; Sayama, K.; Abe, Y.; Sugihara, H. *J. Phys. Chem. B* **2006**, *110*, 2219.

(132) Uno, M.; Kosuga, A.; Okui, M.; Horisaka, K.; Yamanaka, S. *J. Alloys Compd.* **2005**, *400*, 270.
(133) Miseki, Y.; Kato, H.; Kudo, A. *Energy Environ. Sci.* **2009**, *2*, 306.
(134) Kim, H. G.; Hwang, D. W.; Kim, J.; Kim, Y. G.; Lee, J. S. *Chem. Commun.* **1999**, *12*, 1077.
(135) Takata, T.; Furumi, Y.; Shinohara, K.; Tanaka, A.; Hara, M.; Kondo, J. N.; Domen, K. *Chem. Mater.* **1997**, *9*, 1063.
(136) Huang, Y.; Wu, J.; Wei, Y.; Hao, S.; Huang, M.; Lin, J. *Scr. Mater.* **2007**, *57*, 437.
(137) Takata, T.; Tanaka, A.; Hara, M.; Kondo, J. N.; Domen, K. *Stud. Surf. Sci. Catal.* **2000**, *130*, 1943.
(138) Tai, Y. W.; Chen, J. S.; Yang, C. C.; Wan, B. Z. *Catal. Today* **2004**, *97*, 95.
(139) Takata, T.; Shinohara, K.; Tanaka, A.; Hara, M.; Kondo, J. N.; Domen, K. *J. Photochem. Photobiol., A* **1997**, *106*, 45.
(140) Yang, Y.; Chen, Q. Y.; Y, Z. L.; Li, J. *Appl. Surf. Sci.* **2009**, *255*, 8419.
(141) Huang, Y.; Wu, J.; Wei, Y.; Lin, J.; Huang, M. *J. Alloys Compd.* **2008**, *456*, 364.
(142) Takahashi, H.; Kakihan, M.; Yamashita, Y.; Yoshida, K.; Ikeda, S.; Hara, M.; Domen, K. *J. Alloys Compd.* **1999**, *285*, 77.
(143) Reddy, V. R.; Hwang, D. W.; Lee, J. S. *Catal. Lett.* **2003**, *90*, 39.
(144) Sekine, T.; Yoshimura, J.; Tanaka, A.; Domen, K.; Maruya, K.; Onishi, T. *Bull. Chem. Soc. Jpn.* **1990**, *63*, 2107.
(145) Kudo, A.; Hijii, S. *Chem. Lett.* **1999**, *28*, 1103.
(146) He, C. H.; Yang, O. B. *Ind. Eng. Chem. Res.* **2003**, *42*, 419.
(147) Sayama, K.; Arakawa, H. *J. Phys. Chem.* **1993**, *97*, 531.
(148) Sayarna, K.; Arakawa, H. *J. Photochem. Photobiol., A* **1996**, *94*, 67.
(149) Reddy, V. R.; Hwang, D. W.; Lee, J. S. *Korean J. Chem. Eng.* **2003**, *20*, 1026.
(150) Zou, J. J.; Liu, C. J.; Zhang, Y. P. *Langmuir* **2006**, *22*, 2334.
(151) Liu, S. H.; Wang, H. P. *Int. J. Hydrogen Energy* **2002**, *27*, 859.
(152) Yuan, Y.; Zhang, X.; Liu, L.; Jiang, X.; Lv, J.; Li, Z.; Zou, Z. *Int. J. Hydrogen Energy* **2008**, *33*, 5941.
(153) Yuan, Y. P.; Zhao, Z. Y.; Zheng, J.; Yang, M.; Qiu, L. G.; Li, Z. S.; Zou, Z. G. *J. Mater. Chem.* **2010**, *20*, 6772.
(154) Uno, M.; Kosuga, A.; Okui, M.; Horisaka, K.; Muta, H.; Kurosaki, K.; Yamanaka, S. *J. Alloys Compd.* **2006**, *420*, 291.
(155) Kapoor, M. P.; Inagaki, S.; Yoshida, H. *J. Phys. Chem. B* **2005**, *109*, 9231.
(156) Byrd, H.; Clearfield, A.; Poojary, D.; Reis, K. P.; Thompson, M. E. *Chem. Mater.* **1996**, *8*, 2239.
(157) Sayama, K.; Arakawa, H.; Domen, K. *Catal. Today* **1996**, *28*, 175.
(158) Chen, X.; Yu, T.; Fan, X.; Zhang, H.; Li, Z.; Ye, J.; Zou, Z. *Appl. Surf. Sci.* **2007**, *253*, 8500.
(159) Lin, H. Y.; Huang, H. C.; Wang, W. L. *Microporous Mesoporous Mater.* **2008**, *115*, 568.
(160) Domen, K.; Kudo, A.; Shibata, M.; Tanaka, A.; Maruya, K.; Onishi, T. *J. Chem. Soc., Chem. Commun.* **1986**, *23*, 1706.
(161) Domen, K.; Kudo, A.; Shinozaki, A.; Tanaka, A.; Maruya, K.; Onishi, T. *J. Chem. Soc., Chem. Commun.* **1986**, *4*, 356.
(162) Kudo, A.; Tanaka, A.; Domen, K.; Maruya, K.; Aika, K.; Onishi, T. *J. Catal.* **1988**, *111*, 67.
(163) Ikeda, S.; Tanaka, A.; Shinohara, K.; Hara, M.; Kondo, J. N.; Maruya, K.; Domen, K. *Microporous Mater.* **1997**, *9*, 253.
(164) Kudo, A.; Sayama, K.; Tanaka, A.; Asakura, K.; Domen, K.; Maruya, K.; Onishi, T. *J. Catal.* **1989**, *120*, 337.
(165) Domen, K.; Kudo, A.; Tanaka, A.; Onishi, T. *Catal. Today* **1990**, *8*, 77.
(166) Sayama, K.; Tanaka, A.; Domen, K.; Maruya, K.; Onishi, T. *Catal. Lett.* **1990**, *4*, 217.
(167) Iwase, A.; Kato, H.; Kudo, A. *Catal. Lett.* **2006**, *108*, 7.
(168) Sayama, K.; Tanaka, A.; Domen, K.; Maruya, K.; Onishi, T. *J. Phys. Chem.* **1991**, *95*, 1345.
(169) Sayama, K.; Yase, K.; Arakawa, H.; Asakura, K.; Tanaka, A.; Domen, K.; Onishi, T. *J. Photochem. Photobiol., A* **1998**, *114*, 125.
(170) Chung, K. H.; Park, D. C. *J. Mol. Catal. A: Chem.* **1998**, *129*, 53.
(171) Sayama, K.; Tanaka, A.; Domen, K.; Maruya, K.; Onishi, T. *J. Catal.* **1990**, *124*, 541.
(172) Li, G.; Kako, T.; Wang, D.; Zou, Z.; Ye, J. *J. Phys. Chem. Solids* **2008**, *69*, 2487.
(173) Ding, Q. P.; Yuan, Y. P.; Xiong, X.; Li, R. P.; Huang, H. B.; Li, Z. S.; Yu, T.; Zou, Z. G.; Yang, S. G. *J. Phys. Chem. C* **2008**, *112*, 18846.
(174) Zielińska, B.; Borowiak-Palen, E.; Kalenzuk, R. J. *J. Phys. Chem. Solids* **2008**, *69*, 236.
(175) Miseki, Y.; Kato, H.; Kudo, A. *Chem. Lett.* **2005**, *34*, 54.
(176) Ikeda, S.; Itani, T.; Nango, K.; Matsumura, M. *Catal. Lett.* **2004**, *98*, 229.
(177) Chen, D.; Ye, J. *Chem. Mater.* **2009**, *21*, 2327.
(178) Yin, J.; Zou, Z.; Ye, J. *J. Phys. Chem. B* **2004**, *108*, 8888.
(179) Yin, J.; Zou, Z.; Ye, J. *J. Phys. Chem. B* **2004**, *108*, 12790.
(180) Domen, K.; Yoshimura, J.; Sekine, T.; Tanaka, A.; Onishi, T. *Catal. Lett.* **1990**, *4*, 339.
(181) Li, Y.; Wu, J.; Huang, Y.; Huang, M.; Lin, J. *Int. J. Hydrogen Energy* **2009**, *34*, 7927.
(182) Huang, Y.; Xie, Y.; Fan, L.; Li, Y.; Wei, Y.; Lin, J.; Wu, J. *Int. J. Hydrogen Energy* **2008**, *33*, 6432.
(183) Wei, Y.; Li, J.; Huang, Y.; Huang, M.; Lin, J.; Wu, J. *Sol. Energy Mater. Sol. Cells* **2009**, *93*, 1176.
(184) Huang, Y.; Li, J.; Wei, Y.; Li, Y.; Lin, J.; Wu, J. *J. Hazard. Mater.* **2009**, *166*, 103.
(185) Huang, Y.; Wei, Y.; Fan, L.; Huang, M.; Lin, J.; Wu, J. *Int. J. Hydrogen Energy* **2009**, *34*, 5318.
(186) Ebina, Y.; Sasaki, T.; Harada, M.; Watanabe, M. *Chem. Mater.* **2002**, *14*, 4390.
(187) Ebina, Y.; Sakai, N.; Sasaki, T. *J. Phys. Chem. B* **2005**, *109*, 17212.
(188) Compton, O. C.; Carroll, E. C.; Kim, J. Y.; Larsen, D. S.; Osterloh, F. E. *J. Phys. Chem. C* **2007**, *111*, 14589.
(189) Ebina, Y.; Tanaka, A.; Kondo, J. N.; Domen, K. *Chem. Mater.* **1996**, *8*, 2534.
(190) Domen, K.; Ebina, Y.; Sekine, T.; Tanaka, A.; Kondo, J.; Hirose, C. *Catal. Today* **1993**, *16*, 479.
(191) Li, Y.; Wu, J.; Huang, Y.; Huang, M. *J. Alloys Compd.* **2008**, *453*, 437.
(192) Abe, R.; Higashi, M.; Zou, Z.; Sayama, K.; Abe, Y.; Arakawa, H. *J. Phys. Chem. B* **2004**, *108*, 811.
(193) Li, D.; Zheng, J.; Li, Z.; Fan, X.; Liu, L.; Zou, Z. *Int. J. Photoenergy* **2007**, 21860.
(194) Kudo, A.; Nakagawa, S.; Kato, H. *Chem. Lett.* **1999**, *28*, 1197.
(195) Li, Y.; Chen, G.; Zhang, H.; Lv, Z. *Int. J. Hydrogen Energy* **2010**, *35*, 2652.
(196) Luan, J.; Zheng, S.; Hao, X.; Luan, G.; Wu, X.; Zou, Z. *J. Braz. Chem. Soc.* **2006**, *17*, 1368.
(197) Zou, Z.; Ye, J.; Arakawa, H. *Chem. Phys. Lett.* **2001**, *333*, 57.
(198) Li, Y.; Chen, G.; Zhang, H.; Li, Z. *Mater. Res. Bull.* **2009**, *44*, 741.
(199) Zou, Z.; Ye, J.; Arakawa, H. *Top. Catal.* **2003**, *22*, 107.
(200) Zou, Z.; Ye, J.; Sayama, K.; Arakawa, H. *Chem. Phys. Lett.* **2001**, *343*, 303.
(201) Kato, H.; Kudo, A. *Chem. Phys. Lett.* **1998**, *295*, 487.
(202) Takahara, Y.; Kondo, J. N.; Takata, T.; Lu, D.; Domen, K. *Chem. Mater.* **2001**, *13*, 1194.
(203) Stodolny, M.; Laniecki, M. *Catal. Today* **2009**, *142*, 314.
(204) Kondo, J. N.; Uchida, M.; Nakajima, K.; Lu, D.; Hara, M.; Domen, K. *Chem. Mater.* **2004**, *16*, 4304.
(205) Takahara, Y.; Kondo, J. N.; Lu, D.; Domen, K. *Solid State Ionics* **2002**, *151*, 305.
(206) Kato, H.; Kudo, A. *J. Phys. Chem. B* **2001**, *105*, 4285.
(207) Kato, H.; Kudo, A. *Catal. Lett.* **1999**, *58*, 153.
(208) Kato, H.; Kudo, A. *Catal. Today* **2003**, *78*, 561.
(209) Lee, Y.; Watanabe, T.; Takata, T.; Hara, M.; Yoshimura, M.; Domen, K. *Bull. Chem. Soc. Jpn.* **2007**, *80*, 423.
(210) Liu, J. W.; Chen, G.; Li, Z. H.; Zhang, Z. G. *Int. J. Hydrogen Energy* **2007**, *32*, 2269.
(211) Hu, C. C.; Teng, H. *Appl. Catal., A* **2007**, *331*, 44.
(212) Mitsui, C.; Nishiguchi, H.; Fukamachi, K.; Ishihara, T.; Takita, Y. *Chem. Lett.* **1999**, *28*, 1327.
(213) Ishihara, T.; Nishiguchi, H.; Fukamachi, K.; Takita, Y. *J. Phys. Chem. B* **1999**, *103*, 1.
(214) Kudo, A.; Kato, H. *Chem. Phys. Lett.* **2000**, *331*, 373.
(215) Iwase, A.; Kato, H.; Okutomi, H.; Kudo, A. *Chem. Lett.* **2004**, *33*, 1260.
(216) Yamakata, A.; Ishibashi, T.; Kato, H.; Kudo, A.; Onishi, H. *J. Phys. Chem. B* **2003**, *107*, 14383.
(217) Maruyama, M.; Iwase, A.; Kato, H.; Kudo, A.; Onishi, H. *J. Phys. Chem. C* **2009**, *113*, 13918.
(218) Ikeda, S.; Fubuki, M.; Takahara, Y. K.; Matsumura, M. *Appl. Catal., A* **2006**, *300*, 186.
(219) Ishihara, T.; Baik, N. S.; Ono, N.; Nishiguchi, H.; Takita, Y. *J. Photochem. Photobiol., A* **2004**, *167*, 149.
(220) Kato, H.; Kudo, A. *Chem. Lett.* **1999**, *28*, 1207.
(221) Yoshioka, K.; Petrykin, V.; Kakihana, M.; Kato, H.; Kudo, A. *J. Catal.* **2005**, *232*, 102.
(222) Yoshino, M.; Kakihana, M.; Cho, W. S.; Kato, H.; Kudo, A. *Chem. Mater.* **2002**, *14*, 3369.
(223) Kato, H.; Kudo, A. *J. Photochem. Photobiol., A* **2001**, *145*, 129.
(224) Otsuka, H.; Kim, K.; Kouzu, A.; Takimoto, I.; Fujimori, H.; Sakata, Y.; Imamura, H.; Matsumoto, T.; Toda, K. *Chem. Lett.* **2005**, *34*, 822.
(225) Xu, B.; Zhang, W. F.; Liu, X. Y.; Ye, J. H.; Zhang, W. H.; Shi, L.; Wan, X. G.; Yin, J.; Liu, Z. G. *Phys. Rev. B* **2007**, *76*, 125109.
(226) Shimizu, K.; Tsuji, Y.; Hatamachi, T.; Toda, K.; Kodama, T.; Sato, M.; Kitayama, Y. *Phys. Chem. Chem. Phys.* **2004**, *6*, 1064.

(227) Shimizu, K.; Itoh, S.; Hatamachi, T.; Kodama, T.; Sato, M.; Toda, K. *Chem. Mater.* **2005**, *17*, 5161.
(228) Yao, W.; Ye, J. *Chem. Phys. Lett.* **2007**, *435*, 96.
(229) Mitsuyama, T.; Tsutsumi, A.; Hata, T.; Ikeue, K.; Machida, M. *Bull. Chem. Soc. Jpn.* **2008**, *81*, 401.
(230) Li, Y.; Chen, G.; Zhou, C.; Li, Z. *Catal. Lett.* **2008**, *123*, 80.
(231) Machida, M.; Miyazaki, K.; Matsushima, S.; Arai, M. *J. Mater. Chem.* **2003**, *13*, 1433.
(232) Machida, M.; Yabunaka, J.; Kijima, T. *Chem. Commun.* **1999**, *19*, 1939.
(233) Machida, M.; Yabunaka, J.; Kijima, T. *Chem. Mater.* **2000**, *12*, 812.
(234) Machida, M.; Yabunaka, J.; Kijima, T.; Matsushima, S.; Arai, M. *Int. J. Inorg. Mater.* **2001**, *3*, 545.
(235) Kudo, A.; Okutomi, H.; Kato, H. *Chem. Lett.* **2000**, *29*, 1212.
(236) Machida, M.; Murakami, S.; Kijima, T.; Matsushima, S.; Arai, M. *J. Phys. Chem. B* **2001**, *105*, 3289.
(237) Kudo, A.; Kato, H. *Chem. Lett.* **1997**, *26*, 867.
(238) Kurihara, T.; Okutomi, H.; Miseki, Y.; Kato, H.; Kudo, A. *Chem. Lett.* **2006**, *35*, 274.
(239) Luan, J. F.; Hao, X. P.; Zheng, S. R.; Luan, G. Y.; Wu, X. S. *J. Mater. Sci.* **2006**, *41*, 8001.
(240) Li, Y.; Chen, G.; Zhang, H.; Li, Z. *J. Phys. Chem. Solids* **2009**, *70*, 536.
(241) Li, Y.; Chen, G.; Zhang, H.; Li, Z.; Sun, J. *J. Solid State Chem.* **2008**, *181*, 2653.
(242) Kato, H.; Kobayashi, H.; Kudo, A. *J. Phys. Chem. B* **2002**, *106*, 12441.
(243) Hosogi, Y.; Tanabe, K.; Kato, H.; Kobayashi, H.; Kudo, A. *Chem. Lett.* **2004**, *33*, 28.
(244) Kadowaki, H.; Saito, N.; Nishiyama, H.; Kobayashi, H.; Shimodaira, Y.; Inoue, Y. *J. Phys. Chem. C* **2007**, *111*, 439.
(245) Saito, N.; Kadowaki, H.; Kobayashi, H.; Ikarashi, K.; Nishiyama, H.; Inoue, Y. *Chem. Lett.* **2004**, *33*, 1452.
(246) Kudo, A.; Steinberg, A.; Bard, A. J.; Campion, A.; Fox, M. A.; Mallouk, T. E.; Webber, S. E.; White, J. M. *Catal. Lett.* **1990**, *5*, 61.
(247) Kudo, A.; Kato, H. *Chem. Lett.* **1997**, *26*, 421.
(248) Kato, H.; Matsudo, N.; Kudo, A. *Chem. Lett.* **2004**, *33*, 1216.
(249) Nguyen, T. V.; Kim, K. J.; Yang, O. B. *J. Photochem. Photobiol., A* **2005**, *173*, 56.
(250) Wang, Y.; Zhang, Z.; Zhu, Y.; Li, Z.; Vajtai, R.; Ci, L.; Ajayan, P. M. *ACS Nano* **2008**, *2*, 1492.
(251) Luan, J.; Cai, H.; Zheng, S.; Hao, X.; Luan, G.; Wu, X.; Zou, Z. *Mater. Chem. Phys.* **2007**, *104*, 119.
(252) Luan, J.; Zheng, Z.; Cai, H.; Wu, X.; Luan, G.; Zou, Z. *Mater. Res. Bull.* **2008**, *43*, 3332.
(253) Yanagida, T.; Sakata, Y.; Imamura, H. *Chem. Lett.* **2004**, *33*, 726.
(254) Sakata, Y.; Matsuda, Y.; Yanagida, T.; Hirata, K.; Imamura, H.; Teramura, K. *Catal. Lett.* **2008**, *125*, 22.
(255) Wang, D.; Zou, Z.; Ye, J. *Chem. Phys. Lett.* **2004**, *384*, 139.
(256) Kudo, A.; Mikami, I. *J. Chem. Soc., Faraday Trans.* **1998**, *94*, 2929.
(257) Arai, N.; Saito, N.; Nishiyama, H.; Shimodaira, Y.; Kobayashi, H.; Inoue, Y.; Sato, K. *J. Phys. Chem. C* **2008**, *112*, 5000.
(258) Sato, J.; Kobayashi, H.; Saito, S.; Nishiyama, H.; Inoue, Y. *J. Photochem. Photobiol., A* **2003**, *158*, 139.
(259) Sato, J.; Saito, S.; Nishiyama, H.; Inoue, Y. *J. Phys. Chem. B* **2003**, *107*, 7965.
(260) Sato, J.; Kobayashi, H.; Inoue, Y. *J. Phys. Chem. B* **2003**, *107*, 7970.
(261) Sato, J.; Saito, N.; Nishiyama, H.; Inoue, Y. *J. Phys. Chem. B* **2001**, *105*, 6061.
(262) Sato, J.; Saito, N.; Nishiyama, H.; Inoue, Y. *Chem. Lett.* **2001**, *30*, 868.
(263) Sato, J.; Saito, S.; Nishiyama, H.; Inoue, Y. *J. Photochem. Photobiol., A* **2002**, *148*, 85.
(264) Ikarashi, K.; Sato, J.; Kobayashi, H.; Saito, N.; Nishiyama, H.; Inoue, Y. *J. Phys. Chem. B* **2002**, *106*, 9048.
(265) Sato, J.; Kobayashi, H.; Ikarashi, K.; Saito, N.; Nishiyama, H.; Inoue, Y. *J. Phys. Chem. B* **2004**, *108*, 4369.
(266) Kadowaki, H.; Sato, J.; Kobayashi, H.; Saito, N.; Nishiyama, H.; Simodaira, Y.; Inoue, Y. *J. Phys. Chem. B* **2005**, *109*, 22995.
(267) Zhang, W. F.; Tang, J. W.; Ye, J. H. *Chem. Phys. Lett.* **2006**, *418*, 174.
(268) Chen, D.; Ye, J. *Chem. Mater.* **2007**, *19*, 4585.
(269) Bamwenda, G. R.; Uesigi, T.; Abe, Y.; Sayama, K.; Arakawa, H. *Appl. Catal., A* **2001**, *205*, 117.
(270) Kadowaki, H.; Saito, N.; Nishiyama, H.; Inoue, Y. *Chem. Lett.* **2007**, *36*, 440.
(271) Reddy, J. K.; Suresh, G.; Hymavathi, C. H.; Kumari, V. D.; Subrahmanyam, M. *Catal. Today* **2009**, *141*, 89.
(272) Yuan, Y.; Zheng, J.; Zhang, X.; Li, Z.; Yu, T.; Ye, J.; Zou, Z. *Solid State Ionics* **2008**, *178*, 1711.
(273) Reber, J. F.; Meier, K. *J. Phys. Chem.* **1984**, *88*, 5903.
(274) Ohmori, T.; Mametsuka, H.; Suzuki, E. *Int. J. Hydrogen Energy* **2000**, *25*, 953.
(275) Maeda, K.; Teramura, K.; Saito, N.; Inoue, Y.; Domen, K. *Bull. Chem. Soc. Jpn.* **2007**, *80*, 1004.
(276) Arai, N.; Saito, N.; Nishiyama, H.; Inoue, Y.; Domen, K.; Sato, K. *Chem. Lett.* **2006**, *35*, 796.
(277) Sato, J.; Saito, N.; Yamada, Y.; Maeda, K.; Tsuyoshi, T.; Kondo, J. N.; Hara, M.; Kobayashi, H.; Domen, K.; Inoue, Y. *J. Am. Chem. Soc.* **2005**, *127*, 4150.
(278) Maeda, K.; Saito, N.; Inoue, Y.; Domen, K. *Chem. Mater.* **2007**, *19*, 4092.
(279) Lee, Y.; Watanabe, T.; Takata, T.; Hara, M.; Yoshimura, M.; Domen, K. *J. Phys. Chem. B* **2006**, *110*, 17563.
(280) Kakuta, N.; Goto, N.; Ohkita, H.; Mizushima, T. *J. Phys. Chem. B* **1999**, *103*, 5917.
(281) Matsumura, M.; Saho, Y.; Tsubomura, H. *J. Phys. Chem.* **1983**, *87*, 3807.
(282) Reber, J. F.; Meier, K. *J. Phys. Chem.* **1986**, *90*, 824.
(283) Darwent, J. R.; Mills, A. *J. Chem. Soc., Faraday Trans. 2* **1982**, *78*, 359.
(284) Erbs, W.; Desilvestro, J.; Borgarello, E.; Grätzel, M. *J. Phys. Chem.* **1984**, *88*, 4001.
(285) Miseki, Y.; Kusama, H.; Sugihara, H.; Sayama, K. *J. Phys. Chem. Lett.* **2010**, *1*, 1196.
(286) Meissner, D.; Memming, R.; Kastening, B. *J. Phys. Chem.* **1988**, *92*, 3476.
(287) Meissner, D.; Memming, R.; Kastening, B.; Bahnemann, D. *Chem. Phys. Lett.* **1986**, *127*, 419.
(288) Kalyanasundaram, K.; Borgarello, E.; Duonghong, D.; Grätzel, M. *Angew. Chem., Int. Ed.* **1981**, *20*, 987.
(289) Frank, A. J.; Honda, K. *J. Phys. Chem.* **1982**, *86*, 1933.
(290) Zhang, H.; Zhu, Y. F. *J. Phys. Chem. C* **2010**, *114*, 5822.
(291) Yan, X. X.; Liu, G.; Wang, L. Z.; Wang, Y.; Zhu, X. F.; Zou, J.; Lu, G. Q. *J. Mater. Res.* **2010**, *25*, 182.
(292) Torimoto, T.; Hashitani, M.; Konishi, T.; Okazaki, K. I.; Shibayama, T.; Ohtani, B. *J. Nanosci. Nanotechnol.* **2009**, *9*, 506.
(293) Solarska, R.; Alexander, B. D.; Braun, A.; Jurczakowski, R.; Fortunato, G.; Stiefel, M.; Graule, T.; Augustynski, J. *Electrochim. Acta* **2010**, *55*, 7780
(294) Gaillard, N.; Cole, B.; Kaneshiro, J.; Miller, E. L.; Marsen, B.; Weinhardt, L.; Bär, M.; Heske, C.; Ahn, K. S.; Yan, Y.; Al-Jassim, M. M. *J. Mater. Res.* **2010**, *25*, 45.
(295) Bär, M.; Weinhardt, L.; Marsen, B.; Cole, B.; Gaillard, N.; Miller, E.; Heske, C. *Appl. Phys. Lett.* **2010**, *96*, 032107.
(296) Augustynski, J.; Solarska, R.; Hagemann, H.; Santato, C. *Proc. SPIE* **2006**, *6340*, U140.
(297) Solarska, R.; Alexander, B. D.; Augustynski, J. *C. R. Chim.* **2006**, *9*, 301.
(298) Solarska, R.; Santato, C.; Jorand-Sartoretti, C.; Ulmann, M.; Augustynski, J. *J. Appl. Electrochem.* **2005**, *7*, 715.
(299) Solarska, R.; Alexander, B. D.; Augustynski, J. *J. Solid State Electrochem.* **2004**, *8*, 748.
(300) Chen, X.; Mao, S. S. *Chem. Rev.* **2007**, *107*, 2891.
(301) Ji, P. F.; Takeuchi, M.; Cuong, T. M.; Zhang, J. L.; Matsuoka, M.; Anpo, M. *Res. Chem. Intermed.* **2010**, *36*, 327.
(302) Leung, D. Y. C.; Fu, X. L.; Wang, C. F.; Ni, M.; Leung, M. K. H.; Wang, X. X.; Fu, X. Z. *ChemSusChem* **2010**, *3*, 681.
(303) Kato, H.; Kudo, A. *J. Phys. Chem. B* **2002**, *106*, 5029.
(304) Liu, J.; Chen, G.; Lia, Z.; Zhang, Z. *J. Solid State Chem.* **2006**, *179*, 3704.
(305) Hwang, D. W.; Kim, H. G.; Lee, J. S.; Li, W.; Oh, S. H. *J. Phys. Chem. B* **2005**, *109*, 2093.
(306) Kudo, A.; Sekizawa, M. *Catal. Lett.* **1999**, *58*, 241.
(307) Kudo, A.; Sekizawa, M. *Chem. Commun.* **2000**, *15*, 1371.
(308) Borgarello, E.; Kiwi, J.; Grätzel, M.; Pelizzetti, E.; Visca, M. *J. Am. Chem. Soc.* **1982**, *104*, 2996.
(309) Luo, Z.; Gao, Q. *J. Photochem. Photobiol., A* **1992**, *63*, 367.
(310) Tian, B.; Li, C.; Gu, F.; Jiang, H.; Hu, Y.; Zhang, J. *Chem. Eng. J.* **2009**, *151*, 220.
(311) Devi, L. G.; Kumar, S. G.; Murthy, B. N.; Kottam, N. *Catal. Commun.* **2009**, *10*, 794.
(312) Takaoka, G. H.; Nose, T.; Kawashita, M. *Vacuum* **2008**, *83*, 679.
(313) Fan, X.; Chen, X.; Zhu, S.; Li, Z.; Yu, T.; Ye, J.; Zou, Z. *J. Mol. Catal. A: Chem.* **2008**, *284*, 155.
(314) Kim, D. H.; Choi, D. K.; Kim, S. J.; Lee, K. S. *Catal. Commun.* **2008**, *9*, 654.
(315) Umebayashi, T.; Yamaki, T.; Itoh, H.; Asai, K. *J. Phys. Chem. Solids* **2002**, *63*, 1909.
(316) Nishikawa, T.; Shinohara, Y.; Nakajima, T.; Fujita, M.; Mishima, S. *Chem. Lett.* **1999**, *28*, 1133.
(317) Cao, Y.; Yang, W.; Zhang, W.; Liu, G.; Yue, P. *New J. Chem.* **2004**, *28*, 218.
(318) Klosek, S.; Raftery, D. *J. Phys. Chem. B* **2001**, *105*, 2815.

(319) Khan, M. A.; Woo, S. I.; Yang, O. B. *Int. J. Hydrogen Energy* **2008**, *33*, 5345.
(320) Dholam, R.; Patel, N.; Adami, M.; Miotello, A. *Int. J. Hydrogen Energy* **2009**, *34*, 5337.
(321) Eder, D.; Motta, M.; Windle, A. H. *Nanotechnology* **2009**, *20*, 055602.
(322) Anpo, M.; Kishiguchi, S.; Ichihashi, Y.; Takeuchi, M.; Yamashita, H.; Ikeue, K.; Morin, B.; Davidson, A.; Che, M. *Res. Chem. Intermed.* **2001**, *27*, 459.
(323) Anpo, M. *Pure Appl. Chem.* **2000**, *72*, 1787.
(324) Anpo, M. *Pure Appl. Chem.* **2000**, *72*, 1265.
(325) Anpo, M.; Takeuchi, M. *Int. J. Photoenergy* **2001**, *3*, 89.
(326) Anpo, M.; Takeuchi, M. *J. Catal.* **2003**, *216*, 505.
(327) Takeuchi, M.; Yamashita, H.; Matsuoka, M.; Anpo, M.; Hirao, T.; Itoh, N.; Iwamoto, N. *Catal. Lett.* **2000**, *67*, 135.
(328) Kim, S.; Hwang, S. J.; Choi, W. *J. Phys. Chem. B* **2005**, *109*, 24260.
(329) Rengaraj, S.; Li, X. Z. *J. Mol. Catal. A: Chem.* **2006**, *243*, 60.
(330) Choi, W. Y.; Termin, A.; Hoffmann, M. R. *J. Phys. Chem.* **1994**, *98*, 13669.
(331) Grätzel, M.; Howe, R. F. *J. Phys. Chem.* **1990**, *94*, 2566.
(332) Niishiro, R.; Konta, R.; Kato, H.; Chun, W. J.; Asakura, K.; Kudo, A. *J. Phys. Chem. C* **2007**, *111*, 17420.
(333) Niishiro, R.; Kato, H.; Kudo, A. *Phys. Chem. Chem. Phys.* **2005**, *7*, 2241.
(334) Ikeda, T.; Nomoto, T.; Eda, K.; Mizutani, Y.; Kato, H.; Kudo, A.; Onishi, H. *J. Phys. Chem. C* **2008**, *112*, 1167.
(335) Matsumoto, Y.; Unal, U.; Tanaka, N.; Kudo, A.; Kato, H. *J. Solid State Chem.* **2004**, *177*, 4205.
(336) Ohno, T.; Tanigawa, F.; Fujihara, K.; Izumi, S.; Matsumura, M. *J. Photochem. Photobiol., A* **1999**, *127*, 107.
(337) Khan, M. A.; Yang, O. B. *Catal. Today* **2009**, *146*, 177.
(338) Khan, M. A.; Akhtar, M. S.; Woo, S. I.; Yang, O. B. *Catal. Commun.* **2008**, *10*, 1.
(339) Sasikala, R.; Sudarsan, V.; Sudakar, C.; Naik, R.; Panicker, L.; Bharadwaj, S. R. *Int. J. Hydrogen Energy* **2009**, *34*, 6105.
(340) Kitano, M.; Takeuchi, M.; Matsuoka, M.; Thomas, J. M.; Anpo, M. *Catal. Today* **2007**, *120*, 133.
(341) Dholam, R.; Patel, N.; Adami, M.; Miotello, A. *Int. J. Hydrogen Energy* **2008**, *33*, 6896.
(342) Zuo, F.; Wang, L.; Wu, T.; Zhang, Z.; Borchardt, D.; Feng, P. *J. Am. Chem. Soc.* **2010**, *132*, 11856.
(343) Wang, D.; Ye, J.; Kako, T.; Kimura, T. *J. Phys. Chem. B* **2006**, *110*, 15824.
(344) Konta, R.; Ishii, T.; Kato, H.; Kudo, A. *J. Phys. Chem. B* **2004**, *108*, 8992.
(345) Sayama, K.; Mukasa, K.; Abe, R.; Abe, Y.; Arakawa, H. *Chem. Commun.* **2001**, *23*, 2416.
(346) Nishimoto, S.; Matsuda, M.; Miyake, M. *Chem. Lett.* **2006**, *35*, 308.
(347) Zhang, H.; Chen, G.; Li, Y.; Teng, Y. *Int. J. Hydrogen Energy* **2010**, *35*, 2713.
(348) Okazaki, Y.; Mishima, T.; Nishimoto, S.; Matsuda, M.; Miyake, M. *Mater. Lett.* **2008**, *62*, 3337.
(349) Hwang, D. W.; Kim, H. G.; Jang, J. S.; Bae, S. W.; Ji, S. M.; Lee, J. S. *Catal. Today* **2004**, *93*−*95*, 845.
(350) Wang, B.; Li, C.; Hirabayashi, D.; Suzuki, K. *Int. J. Hydrogen Energy* **2010**, *35*, 3306.
(351) Yang, Y.; Chen, Q.; Yin, Z.; Li, J. *J. Alloys Compd.* **2008**, *225*, 8419.
(352) Shah, P.; Bhange, D. S.; Deshpande, A. S.; Kulkarni, M. S.; Gupta, N. M. *Mater. Chem. Phys.* **2009**, *117*, 399.
(353) Zou, Z.; Ye, J.; Sayama, K.; Arakawa, H. *Nature* **2001**, *414*, 625.
(354) Zou, Z.; Ye, J.; Sayama, K.; Arakawa, H. *J. Photochem. Photobiol., A* **2002**, *148*, 65.
(355) Zou, Z.; Ye, J.; Arakawa, H. *Catal. Lett.* **2001**, *75*, 209.
(356) Zou, Z.; Ye, J.; Abe, R.; Sayama, K.; Arakawa, H. *Stud. Surf. Sci. Catal.* **2003**, *145*, 165.
(357) Zou, Z.; Ye, J.; Arakawa, H. *J. Phys. Chem. B* **2002**, *106*, 13098.
(358) Lin, H. Y.; Lee, T. H.; Sie, C. Y. *Int. J. Hydrogen Energy* **2008**, *33*, 4055.
(359) Zhang, H.; Chen, G.; Li, X.; Wang, Q. *Int. J. Hydrogen Energy* **2009**, *34*, 3631.
(360) Zhang, H.; Chen, G.; Li, X. *Solid State Ionics* **2009**, *180*, 1599.
(361) Iwase, A.; Saito, K.; Kudo, A. *Bull. Chem. Soc. Jpn.* **2009**, *82*, 514.
(362) Yang, M.; Huang, X.; Yan, S.; Li, Z.; Yu, T.; Zou, Z. *Mater. Chem. Phys.* **2010**, *121*, 506.
(363) Shimodaira, Y.; Kato, H.; Kobayashi, H.; Kudo, A. *Bull. Chem. Soc. Jpn.* **2007**, *80*, 885.
(364) Zeug, N.; Bücheler, J.; Kisch, H. *J. Am. Chem. Soc.* **1985**, *107*, 1459.
(365) Bang, J. H.; Helmich, R. J.; Suslick, K. S. *Adv. Mater.* **2008**, *9999*, 1.
(366) Ren, L.; Yang, F.; Deng, Y. R.; Yan, N. N.; Huang, S.; Lei, D.; Sun, Q.; Yu, Y. *Int. J. Hydrogen Energy* **2010**, *35*, 3297.
(367) Ikeue, K.; Shiiba, S.; Machida, M. *Chem. Mater.* **2010**, *22*, 743.
(368) Liu, G.; Zhao, L.; Ma, L.; Guo, L. *Catal. Commun.* **2008**, *9*, 126.
(369) Zhang, W.; Zhong, Z.; Wang, Y.; Xu, R. *J. Phys. Chem. C* **2008**, *112*, 17635.
(370) Wang, Y.; Wang, Y.; Xu, R. *Int. J. Hydrogen Energy* **2010**, *35*, 5245.
(371) Zhang, W.; Xu, R. *Int. J. Hydrogen Energy* **2009**, *34*, 8495.
(372) Subrahmanyam, M.; Supriya, V. T.; Reddy, P. R. *Int. J. Hydrogen Energy* **1996**, *21*, 99.
(373) Roy, A. M.; De, G. C. *J. Photochem. Photobiol., A* **2003**, *157*, 87.
(374) Zhang, X.; Jing, D.; Liu, M.; Guo, L. *Catal. Commun.* **2008**, *9*, 1720.
(375) Lei, Z.; You, W.; Liu, M.; Zhou, G.; Takata, T.; Hara, M.; Domen, K.; Li, C. *Chem. Commun.* **2003**, *17*, 2142.
(376) Shen, S.; Zhao, L.; Guo, L. *J. Phys. Chem. Solids* **2008**, *69*, 2426.
(377) Shen, S.; Zhao, L.; Guo, L. *Mater. Res. Bull.* **2009**, *44*, 100.
(378) Shen, S.; Zhao, L.; Zhou, Z.; Guo, L. *J. Phys. Chem. C* **2008**, *112*, 16148.
(379) Ni, M.; Leung, M. K. H.; Leung, D. Y. C.; Sumathy, K. *Renewable Sustainable Energy Rev.* **2007**, *11*, 401.
(380) Lindgren, T.; Mwabora, J. M.; Avendano, E.; Jonsson, J.; Hoel, A.; Granqvist, C. G.; Lindquist, S. E. *J. Phys. Chem. B* **2003**, *107*, 5709.
(381) Chen, X.; Burda, C. *J. Phys. Chem. B* **2004**, *108*, 15446.
(382) Gole, J. L.; Stout, J. D.; Burda, C.; Lou, Y.; Chen, X. *J. Phys. Chem. B* **2004**, *108*, 1230.
(383) Zaleska, A.; Grabowska, E.; Sobczak, J. W.; Gazda, M.; Hupka, J. *Appl. Catal., B* **2009**, *89*, 469.
(384) Wang, J.; Yin, S.; Komatsu, M.; Sato, T. *J. Eur. Ceram. Soc.* **2005**, *25*, 3207.
(385) Ohno, T.; Tsubota, T.; Nakamura, Y.; Sayama, K. *Appl. Catal., A* **2005**, *288*, 74.
(386) Paven-Thivet, C. L.; Ishikawa, A.; Ziani, A.; Gendre, L. L.; Yoshida, M.; Kubota, J.; Tessier, F.; Domen, K. *J. Phys. Chem. C* **2009**, *113*, 6156.
(387) Yan, J. H.; Zhu, Y. R.; Tang, Y. G.; Zheng, S. Q. *J. Alloys Compd.* **2009**, *472*, 429.
(388) Ito, S.; Thampi, K. R.; Comte, P.; Liska, P.; Grätzel, M. *Chem. Commun.* **2005**, *2*, 268.
(389) Lu, D.; Hitoki, G.; Katou, E.; Kondo, J. N.; Hara, M.; Domen, K. *Chem. Mater.* **2004**, *16*, 1063.
(390) Hara, M.; Hitoki, G.; Takata, T.; Kondo, J. N.; Kobayashi, H.; Domen, K. *Catal. Today* **2003**, *78*, 555.
(391) Yashima, M.; Lee, Y.; Domen, K. *Chem. Mater.* **2007**, *19*, 588.
(392) Hitoki, G.; Takata, T.; Kondo, J. N.; Hara, M.; Kobayashi, H.; Domen, K. *Electrochem.* **2002**, *70*, 463.
(393) Liu, M.; You, W.; Lei, Z.; Zhou, G.; Yang, J.; Wu, G.; Ma, G.; Luan, G.; Takata, T.; Hara, M.; Domen, K.; Li, C. *Chem. Commun.* **2004**, *19*, 2192.
(394) Liu, M.; You, W.; Lei, Z.; Takata, T.; Domen, K.; Li, C. *Chin. J. Catal.* **2006**, *27*, 556.
(395) Higashi, M.; Abe, R.; Teramura, K.; Takata, T.; Ohtani, B.; Domen, K. *Chem. Phys. Lett.* **2008**, *452*, 120.
(396) Mishima, T.; Matsuda, M.; Miyake, M. *Appl. Catal., A* **2007**, *324*, 77.
(397) Qiu, X.; Zhao, Y.; Burda, C. *Adv. Mater.* **2007**, *19*, 3995.
(398) Kanade, K. G.; Baeg, J. O.; Kale, B. B.; Lee, S. M.; Moon, S. J.; Kong, K. *Int. J. Hydrogen Energy* **2007**, *32*, 4678.
(399) Ji, S. M.; Borse, P. H.; Kim, H. G.; Hwang, D. W.; Jang, J. S.; Bae, S. W.; Lee, J. S. *Phys. Chem. Chem. Phys.* **2005**, *7*, 1315.
(400) Li, X.; Kikugawa, N.; Ye, J. *Adv. Mater.* **2008**, *20*, 3816.
(401) Shi, H.; Li, X.; Iwai, H.; Zou, Z.; Ye, J. *J. Phys. Chem. Solids* **2009**, *70*, 931.
(402) Matsumoto, Y.; Koinuma, M.; Iwanaga, Y.; Sato, T.; Ida, S. *J. Am. Chem. Soc.* **2009**, *131*, 6644.
(403) Burda, C.; Lou, Y.; Chen, X.; Samia, A. C. S.; Stout, J.; Gole, J. L. *Nano Lett.* **2003**, *3*, 1049.
(404) Sakatani, Y.; Ando, H.; Okusako, K.; Koike, H.; Nunoshige, J.; Takata, T.; Kondo, J. N.; Hara, M.; Domen, K. *J. Mater. Res.* **2004**, *19*, 2100.
(405) Choi, Y.; Umebayashi, T.; Yoshikawa, M. *J. Mater. Sci.* **2004**, *39*, 1837.
(406) Shen, M.; Wu, Z.; Huang, H.; Du, Y.; Zou, Z.; Yang, P. *Mater. Lett.* **2006**, *60*, 693.
(407) Ohno, T.; Mitsui, T.; Matsumura, M. *Chem. Lett.* **2003**, *32*, 364.
(408) Tesfamichael, T.; Will, G.; Bell, J. *Appl. Surf. Sci.* **2005**, *245*, 172.
(409) Gandhe, A. R.; Naik, S. P.; Fernandes, J. B. *Microporous Mesoporous Mater.* **2005**, *87*, 103.
(410) Zhao, Y.; Qiu, X.; Burda, C. *Chem. Mater.* **2008**, *20*, 2629.
(411) Zhang, G.; Ding, X.; Hu, Y.; Huang, B.; Zhang, X.; Qin, X.; Zhou, J.; Xie, J. *J. Phys. Chem. C* **2008**, *112*, 17994.
(412) Fang, J.; Wang, F.; Qian, K.; Bao, H.; Jiang, Z.; Huang, W. *J. Phys. Chem. C* **2008**, *112*, 18150.

(413) Gu, D.; Lu, Y.; Yang, B.; Hu, Y. *Chem. Commun.* **2008**, *21*, 2453.
(414) Chen, X.; Lou, Y.; Samia, A. C. S.; Burda, C.; Gole, J. L. *Adv. Funct. Mater.* **2005**, *15*, 41.
(415) Liu, Y.; Chen, X.; Li, J.; Burda, C. *Chemosphere* **2005**, *61*, 11.
(416) Liu, G.; Sun, C.; Yan, X.; Cheng, L.; Chen, Z.; Wang, X.; Wang, L.; Smith, S. C.; Lu, G. Q.; Cheng, H. M. *J. Mater. Chem.* **2009**, *19*, 2822.
(417) Chen, X.; Glans, P. A.; Qiu, X.; Dayal, S.; Jennings, W. D.; Smith, K. E.; Burda, C.; Guo, J. *J. Electron Spectrosc. Relat. Phenom.* **2008**, *162*, 67.
(418) Chen, X.; Burda, C. *J. Am. Chem. Soc.* **2008**, *130*, 5018.
(419) Asahi, R.; Morikawa, T.; Ohwaki, T.; Aoki, K.; Taga, Y. *Science* **2001**, *293*, 269.
(420) Braun, A.; Akurati, K. K.; Fortunato, G.; Reifler, F. A.; Ritter, A.; Harvey, A. S.; Vital, A.; Graule, T. *J. Phys. Chem. C* **2010**, *114*, 516.
(421) Yang, M. C.; Yang, T. S.; Wong, M. S. *Thin Solid Films* **2004**, *469−470*, 1.
(422) Suda, Y.; Kawasak, H. I.; Ueda, T. I.; Ohshima, T. *Thin Solid Films* **2004**, *453−454*, 162.
(423) Kobayakawa, K.; Murakami, K.; Sato, Y. *J. Photochem. Photobiol., A* **2004**, *170*, 177.
(424) Chen, S. Z.; Zhang, P. Y.; Zhuang, D. M.; Zhu, W. P. *Catal. Commun.* **2004**, *5*, 677.
(425) Torres, G. R.; Lindgren, T.; Lu, J.; Granqvist, C. G.; Lindquist, S. E. *J. Phys. Chem. B* **2004**, *108*, 5995.
(426) Jiang, Z.; Yang, F.; Luo, N.; Chu, B. T. T.; Sun, D.; Shi, H.; Xiao, T.; Edwards, P. P. *Chem. Commun.* **2008**, *47*, 6372.
(427) Huang, D.; Liao, S.; Quan, S.; Liu, L.; He, Z.; Wan, J.; Zhou, W. *J. Non-Cryst. Solids* **2008**, *354*, 3965.
(428) Mrowetz, M.; Balcerski, W.; Colussi, A. J.; Hoffmann, M. R. *J. Phys. Chem. B* **2004**, *108*, 17269.
(429) Mi, L.; Xu, P.; Wang, P. N. *Appl. Surf. Sci.* **2008**, *255*, 2574.
(430) Yuan, J.; Chen, M.; Shi, J.; Shangguan, W. *Int. J. Hydrogen Energy* **2006**, *31*, 1326.
(431) Lin, W. C.; Yang, W. D.; Huang, I. L.; Wu, T. S.; Chung, Z. J. *Energy Fuels* **2009**, *23*, 2192.
(432) Pillai, S. C.; Periyat, P.; George, R.; McCormack, D. E.; Seery, M. K.; Hayden, H.; Colreavy, J.; Corr, D.; Hinder, S. J. *J. Phys. Chem. C* **2007**, *111*, 1605.
(433) Padmanabhan, S. C.; Pillai, S. C.; Colreavy, J.; Balakrishnan, S.; McCormack, D. E.; Perova, T. S.; Gun'ko, Y.; Hinder, S. J.; Kelly, J. M. *Chem. Mater.* **2007**, *19*, 4474.
(434) Periyat, P.; Pillai, S. C.; McCormack, D. E.; Colreavy, J.; Hinder, S. J. *J. Phys. Chem. C* **2008**, *112*, 7644.
(435) Umebayashi, T.; Yamaki, T.; Itoh, H.; Asai, K. *Appl. Phys. Lett.* **2002**, *81*, 454.
(436) Umebayashi, T.; Yamaki, T.; Tanala, S.; Asai, K. *Chem. Lett.* **2003**, *32*, 330.
(437) Yu, J. C.; Ho, W. K.; Yu, J. G.; Yip, H. Y.; Wong, P. K.; Zhao, J. C. *Environ. Sci. Technol.* **2005**, *39*, 1175.
(438) Ho, W.; Yu, J. C.; Lee, S. *J. Solid State Chem.* **2006**, *179*, 1171.
(439) Takeshita, K.; Yamakata, A.; Ishibashi, T. A.; Onishi, H.; Nishijima, K.; Ohno, T. *J. Photochem. Photobiol., A* **2006**, *177*, 269.
(440) Nishijima, K.; Kamai, T.; Murakami, N.; Tsubota, T.; Ohno, T. *Int. J. Photoenergy* **2008**, 173943.
(441) Khan, S. U. M.; Al-Shahry, M.; Ingler, W. B., Jr. *Science* **2002**, *297*, 2243.
(442) Xu, C.; Shaban, Y. A.; Ingler, W. B., Jr.; Khan, S. U. M. *Sol. Energy Mater. Sol. Cells* **2007**, *91*, 938.
(443) Su, Y. L.; Zhang, X. W.; Han, S.; Chen, X. Q.; Lei, L. C. *Electrochem. Commun.* **2007**, *9*, 2291.
(444) Reyes-Garcia, E. A.; Sun, Y.; Raftery, D. *J. Phys. Chem. C* **2007**, *111*, 17146.
(445) Li, D.; Haneda, H.; Hishita, S.; Ohashi, N. *Chem. Mater.* **2005**, *17*, 2588.
(446) Li, D.; Haneda, H.; Hishita, S.; Ohashi, N. *Chem. Mater.* **2005**, *17*, 2596.
(447) Chen, X.; Su, Y.; Zhang, X.; Lei, L. *Chin. Sci. Bull.* **2008**, *53*, 1983.
(448) Lim, M.; Zhou, Y.; Wood, B.; Guo, Y.; Wang, L.; Rudolph, V.; Lu, G. *J. Phys. Chem. C* **2008**, *112*, 19655.
(449) Cong, Y.; Chen, F.; Zhang, J. L.; Anpo, M. *Chem. Lett.* **2006**, *35*, 800.
(450) Yang, J.; Bai, H.; Jiang, Q.; Lian, J. *Thin Solid Films* **2008**, *516*, 1736.
(451) Yu, J. G.; Zhou, M. H.; Cheng, B.; Zhao, X. J. *J. Mol. Catal. A: Chem.* **2006**, *246*, 176.
(452) Periyat, P.; McCormack, D. E.; Hinder, S. J.; Pillai, S. C. *J. Phys. Chem. C* **2009**, *113*, 3246.
(453) Sheng, Y.; Xu, Y.; Jiang, D.; Liang, L.; Wu, D.; Sun, Y. *Int. J. Photoenergy* **2008**, 563949.
(454) In, S.; Orlov, A.; Berg, R.; García, F.; Pedrosa-Jimenez, S.; Tikhov, M. S.; Wright, D. S.; Lambert, R. M. *J. Am. Chem. Soc.* **2007**, *129*, 13790.
(455) Luo, N.; Jiang, Z.; Shi, H.; Cao, F.; Xiao, T.; Edwards, P. P. *Int. J. Hydrogen Energy* **2009**, *34*, 125.
(456) Ozaki, H.; Iwamoto, S.; Inoue, M. *J. Mater. Sci.* **2007**, *42*, 4009.
(457) Sun, H.; Bai, Y.; Cheng, Y.; Jin, W.; Xu, N. *Ind. Eng. Chem. Res.* **2006**, *45*, 4971.
(458) Chen, X.; Zhang, X.; Su, Y.; Lei, L. *Appl. Surf. Sci.* **2008**, *254*, 6693.
(459) Luo, H.; Takata, T.; Lee, Y.; Zhao, J.; Domen, K.; Yan, Y. *Chem. Mater.* **2004**, *16*, 846.
(460) Nukumizu, K.; Nunoshige, J.; Takata, T.; Kondo, J. N.; Hara, M.; Kobayashi, H.; Domen, K. *Chem. Lett.* **2003**, *32*, 196.
(461) Maeda, K.; Shimodaira, Y.; Lee, B.; Teramura, K.; Lu, D.; Kobayashi, H.; Domen, K. *J. Phys. Chem. C* **2007**, *111*, 18264.
(462) Maeda, K.; Lee, B.; Lu, D.; Domen, K. *Chem. Mater.* **2009**, *21*, 2286.
(463) Fang, J.; Shi, F.; Bu, J.; Ding, J.; Xu, S.; Bao, J.; Ma, Y.; Jiang, Z.; Zhang, W.; Gao, C.; Huang, W. *J. Phys. Chem. C* **2010**, *114*, 7940.
(464) Liu, G.; Zhao, Y.; Sun, C.; Li, F.; Lu, G. Q.; Cheng, H. M. *Angew. Chem., Int. Ed.* **2008**, *47*, 4516.
(465) Li, Y.; Ma, G.; Peng, S.; Lu, G.; Li, S. *Appl. Surf. Sci.* **2008**, *254*, 6831.
(466) Azouani, R.; Tieng, S.; Chhor, K.; Bocquet, J. F.; Eloy, P.; Gaigneaux, E. M.; Klementiev, K.; Kanaev, A. V. *Phys. Chem. Chem. Phys.* **2010**, *12*, 11325.
(467) Chun, W. J.; Ishikawa, A.; Fujisawa, H.; Takata, T.; Kondo, J. N.; Hara, M.; Kawai, M.; Matsumoto, Y.; Domen, K. *J. Phys. Chem. B* **2003**, *107*, 1798.
(468) Hitoki, G.; Takata, T.; Kondo, J. N.; Hara, M.; Kobayashi, H.; Domen, K. *Chem. Commun.* **2002**, *16*, 1698.
(469) Hara, M.; Takata, T.; Kondo, J. N.; Domen, K. *Catal. Today* **2004**, *90*, 313.
(470) Hitoki, G.; Ishikawa, A.; Takata, T.; Kondo, J. N.; Hara, M.; Domen, K. *Chem. Lett.* **2002**, *31*, 736.
(471) Abe, R.; Takata, T.; Sugihara, H.; Domen, K. *Chem. Commun.* **2005**, *30*, 3829.
(472) Maeda, K.; Nishimura, N.; Domen, K. *Appl. Catal., A* **2009**, *370*, 88.
(473) Wang, J.; Yin, S.; Masakazu, K.; Zhang, Q.; Fumio, S.; Tsugio, S. *J. Photochem. Photobiol., A* **2004**, *165*, 149.
(474) Wang, J.; Li, H.; Li, H.; Yin, S.; Sato, T. *Solid State Sci.* **2009**, *11*, 182.
(475) Kasahara, A.; Nukumizu, K.; Hitoki, G.; Takata, T.; Kondo, J. N.; Hara, M.; Kobayashi, H.; Domen, K. *J. Phys. Chem. A* **2002**, *106*, 6750.
(476) Kasahara, A.; Nukumizu, K.; Takata, T.; Kondo, J. N.; Hara, M.; Kobayashi, H.; Domen, K. *J. Phys. Chem. B* **2003**, *107*, 791.
(477) Nishimura, N.; Raphael, B.; Maeda, K.; Le Gendre, L.; Abe, R.; Kubota, J.; Domen, K. *Thin Solid Films* **2010**, *518*, 5855.
(478) Hagiwara, H.; Kumagae, K.; Ishihara, T. *Chem. Lett.* **2010**, *39*, 498.
(479) Reyes-Gil, K. R.; Reyes-García, E. A.; Raftery, D. *J. Phys. Chem. C* **2007**, *111*, 14579.
(480) Sun, Y.; Murphy, C. J.; Reyes-Gil, K. R.; Reyes-García, E. A.; Lilly, J. P.; Raftery, D. *Int. J. Hydrogen Energy* **2008**, *33*, 5967.
(481) Ge, S.; Jia, H.; Zhao, H.; Zheng, Z.; Zhang, L. *J. Mater. Chem.* **2010**, *20*, 3052.
(482) Hisatomi, T.; Hasegawa, K.; Teramura, K.; Takata, T.; Hara, M.; Domen, K. *Chem. Lett.* **2007**, *36*, 558.
(483) Parida, K. M.; Martha, S.; Das, D. P.; Biswal, N. *J. Mater. Chem.* **2010**, *20*, 7144.
(484) Jiang, L.; Wang, Q.; Li, C.; Yuan, J.; Shangguan, W. *Int. J. Hydrogen Energy* **2010**, *35*, 7043.
(485) Ishikawa, A.; Takata, T.; Kondo, J. N.; Hara, M.; Kobayashi, H.; Domen, K. *J. Am. Chem. Soc.* **2002**, *124*, 13547.
(486) Ishikawa, A.; Yamada, Y.; Takata, T.; Kondo, J. N.; Hara, M.; Kobayashi, H.; Domen, K. *Chem. Mater.* **2003**, *15*, 4442.
(487) Yashima, M.; Ogisub, K.; Domen, K. *Acta Crystallogr.* **2008**, *B64*, 291.
(488) Ishikawa, A.; Takata, T.; Matsumura, T.; Kondo, J. N.; Hara, M.; Kobayashi, H.; Domen, K. *J. Phys. Chem. B* **2004**, *108*, 2637.
(489) Ogisu, K.; Ishikawa, A.; Teramura, K.; Toda, K.; Hara, M.; Domen, K. *Chem. Lett.* **2007**, *36*, 854.
(490) Ogisu, K.; Ishikawa, A.; Shimodaira, Y.; Takata, T.; Kobayashi, H.; Domen, K. *J. Phys. Chem. C* **2008**, *112*, 11978.
(491) Ikeue, K.; Ando, S.; Mitsuyama, T.; Ohta, Y.; Arayama, K.; Tsutsumi, A.; Machida, M. *Top. Catal.* **2008**, *47*, 175.
(492) Kobayakawa, K.; Teranishi, A.; Tsurumaki, T.; Sato, Y.; Fujishima, A. *Electrochim. Acta* **1992**, *37*, 465.
(493) Zheng, L.; Xu, Y.; Song, Y.; Wu, C.; Zhang, M.; Xie, Y. *Inorg. Chem.* **2009**, *48*, 4003.

(494) Fan, W. J.; Zhou, Z. F.; Xu, W. B.; Shi, Z. F.; Ren, F. M.; Ma, H. H.; Huang, S. W. *Int. J. Hydrogen Energy* **2010**, *35*, 6525.
(495) Shen, S.; Zhao, L.; Guo, L. *Int. J. Hydrogen Energy* **2010**, *35*, 10148.
(496) Jang, J. S.; Choi, S. H.; Shin, N.; Yu, C.; Lee, J. S. *J. Solid State Chem.* **2007**, *180*, 1110.
(497) Chen, D.; Ye, J. *J. Phys. Chem. Solids* **2007**, *68*, 2317.
(498) Tabata, M.; Maeda, K.; Ishihara, T.; Minegishi, T.; Takata, T.; Domen, K. *J. Phys. Chem. C* **2010**, *114*, 11215.
(499) Yokoyama, D.; Minegishi, T.; Maeda, K.; Katayama, M.; Kubota, J.; Yamada, A.; Konagai, M.; Domen, K. *Electrochem. Commun.* **2010**, *12*, 851.
(500) Kudo, A.; Nagane, A.; Tsuji, I.; Kato, H. *Chem. Lett.* **2002**, *31*, 882.
(501) Jang, J. S.; Yu, C. J.; Choi, S. H.; Ji, S. M.; Kim, E. S.; Lee, J. S. *J. Catal.* **2008**, *254*, 144.
(502) Xu, J.; Ao, Y.; Fu, D. *Appl. Surf. Sci.* **2009**, *256*, 884.
(503) Song, S.; Tu, J.; Xu, L.; Xu, X.; He, Z.; Qiu, J.; Ni, J.; Chen, J. *Chemosphere* **2008**, *73*, 1401.
(504) Liu, C.; Tang, X.; Mo, C.; Qiang, Z. *J. Solid State Chem.* **2008**, *181*, 913.
(505) Wei, C.; Tang, X.; Liang, J.; Tan, S. *J. Environ. Sci.* **2007**, *19*, 90.
(506) Tryba, B. *Int. J. Photoenergy* **2008**, 721824.
(507) Shen, X. Z.; Guo, J.; Liu, Z. C.; Xie, S. M. *Appl. Surf. Sci.* **2008**, *254*, 4726.
(508) Lv, K.; Zuo, H.; Sun, J.; Deng, K.; Liu, S.; Li, X.; Wang, D. *J. Hazard. Mater.* **2009**, *161*, 396.
(509) Wang, Y.; Wang, Y.; Meng, Y.; Ding, H.; Shan, Y.; Zhao, X.; Tang, X. *J. Phys. Chem. C* **2008**, *112*, 6620.
(510) Huang, Y.; Ho, W.; Ai, Z.; Song, X.; Zhang, L.; Lee, S. *Appl. Catal., B* **2009**, *89*, 398.
(511) Zhang, X.; Liu, Q. *Appl. Surf. Sci.* **2008**, *254*, 4780.
(512) Xia, H.; Zhuang, H.; Xiao, D.; Zhang, T. *J. Alloys Compd.* **2008**, *465*, 328.
(513) He, Z.; Xu, X.; Song, S.; Xie, L.; Tu, J.; Chen, J.; Yan, B. *J. Phys. Chem. C* **2008**, *112*, 16431.
(514) Liu, Z.; Zhou, Y.; Li, Z.; Wang, Y.; Ge, C. *Rare Met.* **2007**, *26*, 263.
(515) Xu, J.; Ao, Y.; Fu, D.; Yuan, C. *J. Colloid Interface Sci.* **2008**, *328*, 447.
(516) Long, R.; English, N. J. *Chem. Phys. Lett.* **2009**, *478*, 175.
(517) Li, J.; Xu, J.; Dai, W. L.; Li, H.; Fan, K. *Appl. Catal., B* **2008**, *82*, 233.
(518) Shen, Y.; Xiong, T.; Du, H.; Jin, H.; Shang, J.; Yang, K. *J. Sol-Gel Sci. Technol.* **2009**, *50*, 98.
(519) Huang, L. H.; Sun, C.; Liu, Y. L. *Appl. Surf. Sci.* **2007**, *253*, 7029.
(520) Miyauchi, M.; Takashio, M.; Tobimatsu, H. *Langmuir* **2004**, *20*, 232.
(521) Wang, J.; Yin, S.; Komatsu, M.; Sato, T. *J. Eur. Ceram. Soc.* **2005**, *25*, 3207.
(522) Wei, W.; Dai, Y.; Guo, M.; Yu, L.; Huang, B. *J. Phys. Chem. C* **2009**, *113*, 15046.
(523) Gai, Y.; Li, J.; Li, S. S.; Xia, J. B.; Wei, S. H. *Phys. Rev. Lett.* **2009**, *102*, 036402.
(524) Yin, W. J.; Tang, H. W.; Wei, S. H.; Al-Jassim, M. M.; Turner, J.; Yan, Y. F. *Phys. Rev B* **2010**, *82*, 045106.
(525) Sasikala, R.; Shirole, A. R.; Sudarsan, V.; Sudakar, C.; Naik, R.; Rao, R.; Bharadwaj, S. R. *Appl. Catal., A* **2010**, *377*, 47.
(526) Shet, S.; Ahn, K. S.; Deutsch, T.; Wang, H. L.; Nuggehalli, R.; Yan, Y. F.; Turner, J.; Al-Jassim, M. *J. Power Sources* **2010**, *195*, 5801.
(527) Tsuji, I.; Kudo, A. *J. Photochem. Photobiol., A* **2003**, *156*, 249.
(528) Lei, Z.; Ma, G.; Liu, M.; You, W.; Yan, H.; Wu, G.; Takata, T.; Hara, M.; Domen, K.; Li, C. *J. Catal.* **2006**, *237*, 322.
(529) Youn, H. C.; Baral, S.; Fendler, J. H. *J. Phys. Chem.* **1988**, *92*, 6320.
(530) Hetterich, W.; Kisch, H. *Photochem. Photobiol.* **1990**, *52*, 631.
(531) Li, W.; Li, D.; Chen, Z.; Huang, H.; Sun, M.; He, Y.; Fu, X. *J. Phys. Chem. C* **2008**, *112*, 14943.
(532) Wang, W.; Zhu, W.; Xu, H. *J. Phys. Chem. C* **2008**, *112*, 16754.
(533) Li, M. T.; Jiang, J. G.; Guo, L. J. *Int. J. Hydrogen Energy* **2010**, *35*, 7036.
(534) Kakuta, N.; Park, K. H.; Finlayson, M. F.; Ueno, A.; Bard, A. J.; Campion, A.; Fox, M. A.; Webber, S. E.; White, J. M. *J. Phys. Chem.* **1985**, *89*, 732.
(535) Xing, C. J.; Zhang, Y. J.; Yan, W.; Guo, L. J. *Int. J. Hydrogen Energy* **2006**, *31*, 2018.
(536) Zhang, K.; Jing, D.; Xing, C.; Guo, L. J. *Int. J. Hydrogen Energy* **2007**, *32*, 4685.
(537) Tsuji, I.; Kato, H.; Kobayashi, H.; Kudo, A. *J. Am. Chem. Soc.* **2004**, *126*, 13406.
(538) Tsuji, I.; Kato, H.; Kobayashi, H.; Kudo, A. *J. Phys. Chem. B* **2005**, *109*, 7323.
(539) Torimoto, T.; Adachi, T.; Okazaki, K.; Sakuraoka, M.; Shibayama, T.; Ohtani, B.; Kudo, A.; Kuwabata, S. *J. Am. Chem. Soc.* **2007**, *129*, 12388.
(540) Tsuji, I.; Kato, H.; Kudo, A. *Angew. Chem., Int. Ed.* **2005**, *44*, 3565.
(541) Tsuji, I.; Kato, H.; Kobayashi, H.; Kudo, A. *Chem. Mater.* **2006**, *18*, 1969.
(542) Tsuji, I.; Shimodaira, Y.; Kato, H.; Kobayashi, H.; Kudo, A. *Chem. Mater.* **2010**, *22*, 1042.
(543) Kaga, H.; Saito, K.; Kudo, A. *Chem. Commun.* **2010**, *46*, 3779.
(544) Jang, J. S.; Borse, P. H.; Lee, J. S.; Choi, S. H.; Kim, H. G. *J. Chem. Phys.* **2008**, *128*, 154717.
(545) Li, Y.; Chen, G.; Zhou, C.; Sun, J. *Chem. Commun.* **2009**, *15*, 2020.
(546) Li, X.; Chen, G.; Wang, Q.; Wang, X.; Zhou, A.; Shen, Z. *Adv. Funct. Mater.* **2010**, *20*, 3390.
(547) Li, Y.; Ma, G.; Peng, S.; Lu, G.; Li, S. *Appl. Catal., A* **2009**, *363*, 180.
(548) Hirano, M.; Ito, T. *Mater. Res. Bull.* **2008**, *43*, 2196.
(549) Li, G.; Kako, T.; Wang, D.; Zou, Z.; Ye, J. *J. Solid State Chem.* **2007**, *180*, 2845.
(550) Muktha, B.; Madras, G.; Row, T. N. G. *J. Photochem. Photobiol., A* **2007**, *187*, 177.
(551) Zou, Z.; Ye, J.; Arakawa, H. *Solid State Commun.* **2001**, *119*, 471.
(552) Luan, J.; Zou, Z.; Lu, M.; Chen, Y. *Mater. Chem. Phys.* **2006**, *98*, 434.
(553) Yi, Z. G.; Ye, J. H. *Appl. Phys. Lett.* **2007**, *91*, 254108.
(554) Yao, W.; Ye, J. *J. Phys. Chem. B* **2006**, *110*, 11188.
(555) Yao, W.; Ye, J. *Chem. Phys. Lett.* **2008**, *450*, 370.
(556) Li, Z.; Wang, Y.; Liu, J.; Chen, G.; Li, Y.; Zhou, C. *Int. J. Hydrogen Energy* **2009**, *34*, 147.
(557) Wang, D.; Kako, T.; Ye, J. *J. Am. Chem. Soc.* **2008**, *130*, 2724.
(558) Wang, D.; Kako, T.; Ye, J. *J. Phys. Chem. C* **2009**, *113*, 3785.
(559) Liu, H.; Yuan, J.; Shangguan, W.; Teraoka, Y. *J. Phys. Chem. C* **2008**, *112*, 8521.
(560) Wang, Q.; Liu, H.; Jiang, L.; Yuan, J.; Shangguan, W. *Catal. Lett.* **2009**, *131*, 160.
(561) Cheviré, F.; Tessier, F.; Marchand, R. *Eur. J. Inorg. Chem.* **2006**, *6*, 1223.
(562) Luo, W.; Li, Z.; Jiang, X.; Yu, T.; Liu, L.; Chen, X.; Ye, J.; Zou, Z. *Phys. Chem. Chem. Phys.* **2008**, *10*, 6717.
(563) Maeda, K.; Takata, T.; Hara, M.; Saito, N.; Inoue, Y.; Kobayashi, H.; Domen, K. *J. Am. Chem. Soc.* **2005**, *127*, 8286.
(564) Maeda, K.; Teramura, K.; Lu, D.; Takata, T.; Saito, N.; Inoue, Y.; Domen, K. *Nature* **2006**, *440*, 295.
(565) Yashima, M.; Maeda, K.; Teramura, K.; Takata, T.; Domen, K. *Mater. Trans.* **2006**, *47*, 295.
(566) Yashima, M.; Maeda, K.; Teramura, K.; Takata, T.; Domen, K. *Chem. Phys. Lett.* **2005**, *416*, 225.
(567) Maeda, K.; Teramura, K.; Masuda, H.; Takata, T.; Saito, N.; Inoue, Y.; Domen, K. *J. Phys. Chem. B* **2006**, *110*, 13107.
(568) Hirai, T.; Maeda, K.; Yoshida, M.; Kubota, J.; Ikeda, S.; Matsumura, M.; Domen, K. *J. Phys. Chem. C* **2007**, *111*, 18853.
(569) Maeda, K.; Teramura, K.; Takata, T.; Hara, M.; Saito, N.; Toda, K.; Inoue, Y.; Kobayashi, H.; Domen, K. *J. Phys. Chem. B* **2005**, *109*, 20504.
(570) Maeda, K.; Hashiguchi, H.; Masuda, H.; Abe, R.; Domen, K. *J. Phys. Chem. C* **2008**, *112*, 3447.
(571) Sun, X.; Maeda, K.; Faucheur, M. L.; Teramura, K.; Domen, K. *Appl. Catal., A* **2007**, *327*, 114.
(572) Maeda, K.; Domen, K. *Chem. Mater.* **2010**, *22*, 612.
(573) Yashima, M.; Yamada, H.; Maeda, K.; Domen, K. *Chem. Commun.* **2010**, *14*, 2379.
(574) Hisatomi, T.; Maeda, K.; Takanabe, K.; Kubota, J.; Domen, K. *J. Phys. Chem. C* **2009**, *113*, 21458.
(575) Maeda, K.; Teramura, K.; Domen, K. *J. Catal.* **2008**, *254*, 198.
(576) Maeda, K.; Masuda, H.; Domen, K. *Catal. Today* **2009**, *147*, 173.
(577) Lee, Y.; Terashima, H.; Shimodaira, Y.; Teramura, K.; Hara, M.; Kobayashi, H.; Domen, K.; Yashima, M. *J. Phys. Chem. C* **2007**, *111*, 1042.
(578) Lee, Y.; Teramura, K.; Hara, M.; Domen, K. *Chem. Mater.* **2007**, *19*, 2120.
(579) Wang, X.; Maeda, K.; Lee, Y.; Domen, K. *Chem. Phys. Lett.* **2008**, *457*, 134.
(580) Tessier, F.; Maillard, P.; Lee, Y.; Bleugat, C.; Domen, K. *J. Phys. Chem. C* **2009**, *113*, 8526.
(581) Kamata, K.; Maeda, K.; Lu, D.; Kako, Y.; Domen, K. *Chem. Phys. Lett.* **2009**, *470*, 90.
(582) Gerischer, H. *Photochem. Photobiol.* **1972**, *16*, 243.
(583) Gerischer, H. J. *J. Electroanal. Chem.* **1977**, *82*, 133.
(584) Anderson, S.; Constable, E. C.; Dareedwards, M. P.; Goodenough, J. B.; Hamnett, A.; Seddon, K. R.; Wright, R. D. *Nature* **1979**, *280*, 571.
(585) Hara, K.; Sugihara, H.; Tachibana, Y.; Islam, A.; Yanagida, M.; Sayama, K.; Arakawa, H. *Langmuir* **2001**, *17*, 5992.

(586) Nakade, S.; Kanzaki, T.; Kubo, W.; Kitamura, T.; Wada, Y.; Yanagida, S. *J. Phys. Chem. B* **2005**, *109*, 3480.
(587) Wang, P.; Dai, Q.; Zakeeruddin, S. M.; Forsyth, M.; MacFarlane, D. R.; Grätzel, M. *J. Am. Chem. Soc.* **2004**, *126*, 13590.
(588) Kim, S. L.; Jang, S. R.; Vittal, R.; Lee, J.; Kim, K. J. *J. Appl. Electrochem.* **2006**, *36*, 1433.
(589) Chen, C. Y.; Wu, S. J.; Li, J. Y.; Wu, C. G.; Chen, J. G.; Ho, K. C. *Adv. Mater.* **2007**, *19*, 3888.
(590) Kuang, D.; Klein, C.; Zhang, Z.; Ito, S.; Moser, J. E.; Zakeeruddin, S. M.; Grätzel, M. *Small* **2007**, *3*, 2094.
(591) Robertson, N. *Angew. Chem., Int. Ed.* **2008**, *47*, 1012.
(592) Borgarello, E.; Kiwi, J.; Pelizzetti, E.; Visca, M.; Grätzel, M. *J. Am. Chem. Soc.* **1981**, *103*, 6324.
(593) Chen, F.; Deng, Z.; Li, X.; Zhang, J.; Zhao, J. *Chem. Phys. Lett.* **2005**, *415*, 85.
(594) Yao, K. S.; Wang, D. Y.; Chang, C. Y.; Weng, K. W.; Yang, L. Y.; Lee, S. J.; Cheng, T. C.; Hwang, C. C. *Surf. Coat. Technol.* **2007**, *202*, 1329.
(595) Nguyen, T. V.; Wu, J. C. S.; Chiou, C. H. *Catal. Commun.* **2008**, *9*, 2073.
(596) O'Regan, B.; Grätzel, M. *Nature* **1991**, *353*, 737.
(597) Nazeeruddin, M. K.; Angelis, F. D.; Fantacci, S.; Selloni, A.; Viscardi, G.; Liska, P.; Ito, S.; Bessho, T.; Grätzel, M. *J. Am. Chem. Soc.* **2005**, *127*, 16835.
(598) Wang, Z. S.; Yamaguchi, T.; Sugihara, H.; Arakawa, H. *Langmuir* **2005**, *21*, 4272.
(599) Chiba, Y.; Islam, A.; Komiya, R.; Koide, N.; Han, L. *Appl. Phys. Lett.* **2006**, *88*, 223505.
(600) Nazeeruddin, M. K.; Bessho, T.; Cevey, L.; Ito, S.; Klein, C.; Angelis, F. D.; Fantacci, S.; Comte, P.; Liska, P.; Imai, H.; Grätzel, M. *J. Photochem. Photobiol., A* **2007**, *185*, 331.
(601) Yum, J. H.; Chen, P.; Grätzel, M.; Nazeeruddin, M. K. *ChemSusChem* **2008**, *1*, 699.
(602) Grätzel, M. *Chem. Lett.* **2005**, *34*, 8.
(603) Moser, J.; Grätzel, M. *J. Am. Chem. Soc.* **1984**, *106*, 6557.
(604) Maeda, K.; Eguchi, M.; Youngblood, W. J.; Mallouk, T. E. *Chem. Mater.* **2008**, *20*, 6770.
(605) Kiwi, J.; Borgarello, E.; Pelizzetti, E.; Visca, M.; Grätzel, M. *Angew. Chem., Int. Ed.* **1980**, *19*, 647.
(606) Borgarello, E.; Kiwi, J.; Pelizzetti, E.; Visca, M.; Grätzel, M. *Nature* **1981**, *289*, 158.
(607) Dung, D. H.; Serpone, N.; Grätzel, M. *Helv. Chim. Acta* **1984**, *67*, 1012.
(608) Nakahira, T.; Inoue, Y.; Iwasaki, K.; Tanigawa, H.; Kouda, Y.; Iwabuchi, S.; Kojima, K. *Makromol. Chem. Rapid Commun.* **1988**, *9*, 13.
(609) Furlong, D. N.; Wells, D.; Sasse, W. H. F. *J. Phys. Chem.* **1986**, *90*, 1107.
(610) Hirano, K.; Suzuki, E.; Ishikawa, A.; Moroi, T.; Shiroishi, H.; Kaneko, M. *J. Photochem. Photobiol., A* **2000**, *136*, 157.
(611) Dhanalakshmi, K. B.; Latha, S.; Anandan, S.; Maruthamuthu, P. *Int. J. Hydrogen Energy* **2001**, *26*, 669.
(612) Bae, E.; Choi, W.; Park, J.; Shin, H. S.; Kim, S. B.; Lee, J. S. *J. Phys. Chem. B* **2004**, *108*, 14093.
(613) Abe, R.; Sayama, K.; Sugihara, H. *J. Sol. Energy Eng.* **2005**, *27*, 413.
(614) Peng, T.; Dai, K.; Yi, H.; Ke, D.; Cai, P.; Zan, L. *Chem. Phys. Lett.* **2008**, *460*, 216.
(615) Peng, T.; Ke, D.; Cai, P.; Dai, K.; Ma, L.; Zan, L. *J. Power Sources* **2008**, *180*, 498.
(616) Kim, W.; Tachikawa, T.; Majima, T.; Choi, W. *J. Phys. Chem. C* **2009**, *113*, 10603.
(617) Park, J.; Yi, J.; Tachikawa, T.; Majima, T.; Choi, W. *J. Phys. Chem. Lett.* **2010**, *1*, 1351.
(618) Reisner, E.; Powell, D. J.; Cavazza, C.; Fontecilla-Camps, J. C.; Armstrong, F. A. *J. Am. Chem. Soc.* **2009**, *131*, 18457.
(619) Gurunathan, K.; Maruthamuthu, P.; Sastri, M. V. C. *Int. J. Hydrogen Energy* **1997**, *22*, 57.
(620) Furube, A.; Shiozawa, T.; Ishikawa, A.; Wada, A.; Domen, K.; Hirose, C. *J. Phys. Chem. B* **2002**, *106*, 3065.
(621) Unal, U.; Matsumoto, Y.; Tamoto, N.; Koinuma, M.; Machida, M.; Izawa, K. *J. Solid State Chem.* **2006**, *179*, 33.
(622) Youngblood, W. J.; Lee, S. H. A.; Maeda, K.; Mallouk, T. E. *Acc. Chem. Res.* **2009**, *42*, 1966.
(623) Maeda, K.; Eguchi, M.; Lee, S. H. A.; Youngblood, W. J.; Hata, H.; Mallouk, T. E. *J. Phys. Chem. C* **2009**, *113*, 7962.
(624) Maeda, K.; Eguchi, M.; Youngblood, W. J.; Mallouk, T E. *Chem. Mater.* **2009**, *21*, 3611.
(625) Kim, Y. I.; Atherton, S. J.; Brigham, E. S.; Mallouk, T. E. *J. Phys. Chem.* **1993**, *97*, 11802.
(626) Kim, Y. I.; Salim, S.; Huq, M. J.; Mallouk, T. E. *J. Am. Chem. Soc.* **1991**, *113*, 9561.
(627) Zakharenko, V. S.; Bulatov, A. V.; Parmon, V. N. *React. Kinet. Catal. Lett.* **1988**, *36*, 295.
(628) Jarosz, P.; Du, P.; Schneider, J.; Lee, S. H.; McCamant, D.; Eisenberg, R. *Inorg. Chem.* **2009**, *48*, 9653.
(629) Malinka, E. A.; Khutornoi, A. M.; Vodzinskii, S. V.; Zhilina, Z. I.; Kamalov, G. L. *React. Kinet. Catal. Lett.* **1988**, *36*, 407.
(630) Malinka, E. A.; Kamalov, G. L.; Vodzinskii, S. V.; Melnik, V. I.; Zhilina, Z. I. *J. Photochem. Photobiol., A* **1995**, *90*, 153.
(631) Shimidzu, T.; Iyoda, T.; Koide, Y.; Kanda, N. *Nouv. J. Chim.* **1983**, *7*, 21.
(632) Nada, A. A.; Hamed, H. A.; Barakat, M. H.; Mohamed, N. R.; Veziroglu, T. N. *Int. J. Hydrogen Energy* **2008**, *33*, 3264.
(633) Hagiwara, H.; Ono, N.; Inoue, T.; Matsumoto, H.; Ishihara, T. *Angew. Chem., Int. Ed.* **2006**, *45*, 1420–1422.
(634) Rayalu, S. S.; Dubey, N.; Labhsetwar, N. K.; Kagne, S.; Devotta, S. *Int. J. Hydrogen Energy* **2007**, *32*, 2776.
(635) Dubey, N.; Rayalu, S. S.; Labhsetwar, N. K.; Devotta, S. *Int. J. Hydrogen Energy* **2008**, *33*, 5958.
(636) Chatti, R. V.; Dubey, N.; Joshi, M. V.; Labhsetwar, N. K.; Joshi, P. N.; Rayalu, S. S. *Int. J. Hydrogen Energy* **2010**, *35*, 1911.
(637) Fu, N.; Lu, G. *Chem. Commun.* **2009**, *24*, 3591.
(638) Fu, N.; Lu, G. *Appl. Surf. Sci.* **2008**, *255*, 4378.
(639) Houlding, V. H.; Grätzel, M. *J. Am. Chem. Soc.* **1983**, *105*, 5695.
(640) Chatterjee, D. *Catal. Commun.* **2010**, *11*, 336.
(641) Ikeda, S.; Abe, C.; Torimoto, T.; Ohtani, B. *J. Photochem. Photobiol., A* **2003**, *160*, 61.
(642) Abe, R.; Sayama, K.; Arakawa, H. *Chem. Phys. Lett.* **2002**, *362*, 441.
(643) Abe, R.; Sayama, K.; Arakawa, H. *J. Photochem. Photobiol., A* **2004**, *166*, 115.
(644) Abe, R.; Sayama, K.; Arakawa, H. *Chem. Phys. Lett.* **2003**, *379*, 230.
(645) Shimidzu, T.; Iyoda, T.; Koide, Y. *J. Am. Chem. Soc.* **1985**, *107*, 35.
(646) Abe, R.; Hara, K.; Sayama, K.; Domen, K.; Arakawa, H. *J. Photochem. Photobiol., A* **2000**, *137*, 63.
(647) Jin, Z.; Zhang, X.; Lu, G.; Li, S. *J. Mol. Catal. A: Chem.* **2006**, *259*, 275.
(648) Jin, Z.; Zhang, X.; Li, Y.; Li, S.; Lu, G. *Catal. Commun.* **2007**, *8*, 1267.
(649) Li, Q.; Lu, G. *J. Mol. Catal. A: Chem.* **2007**, *266*, 75.
(650) Li, Y.; Xie, C.; Peng, S.; Lu, G.; Li, S. *J. Mol. Catal. A: Chem.* **2008**, *282*, 117.
(651) Zhang, X.; Jin, Z.; Lib, Y.; Li, S.; Lu, G. *Appl. Surf. Sci.* **2008**, *254*, 4452.
(652) Li, Q.; Jin, Z.; Peng, Z.; Li, Y.; Li, S.; Lu, G. *J. Phys. Chem. C* **2007**, *111*, 8237.
(653) Li, Q.; Lu, G. *J. Power Sources* **2008**, *185*, 577.
(654) Li, Y.; Guo, M.; Peng, S.; Lu, G.; Li, S. *Int. J. Hydrogen Energy* **2009**, *34*, 5629.
(655) Zhang, X.; Jin, Z.; Li, Y.; Li, S.; Lu, G. *J. Power Sources* **2007**, *166*, 74.
(656) Li, Q.; Chen, L.; Lu, G. *J. Phys. Chem. C* **2007**, *111*, 11494.
(657) Yin, J.; Zou, Z.; Ye, J. *Chem. Phys. Lett.* **2003**, *378*, 24.
(658) Wang, D.; Zou, Z.; Ye, J. *Chem. Phys. Lett.* **2003**, *373*, 191.
(659) Ouyang, S.; Li, Z.; Ouyang, Z.; Yu, T.; Ye, J.; Zou, Z. *J. Phys. Chem. C* **2008**, *112*, 3134.
(660) Lv, J.; Zhao, Z.; Li, Z.; Ye, J.; Zou, Z. *J. Alloys Compd.* **2009**, *485*, 346.
(661) Ye, J.; Zou, Z.; Matsushita, A. *Int. J. Hydrogen Energy* **2003**, *28*, 651.
(662) Yao, W.; Ye, J. *Catal. Lett.* **2006**, *110*, 139.
(663) Yao, W.; Huang, C.; Ye, J. *Chem. Mater.* **2010**, *22*, 1107.
(664) Li, D.; Zheng, J.; Zou, Z. *J. Phys. Chem. Solids* **2006**, *67*, 801.
(665) Wang, D.; Zou, Z.; Ye, J. *Chem. Phys. Lett.* **2005**, *411*, 285.
(666) Wang, D.; Ye, J.; Kitazawa, H.; Kimura, T. *J. Phys. Chem. C* **2007**, *111*, 12848.
(667) Silva, C. G.; Bouizi, Y.; Fornés, V.; García, H. *J. Am. Chem. Soc.* **2009**, *131*, 13833.
(668) Ye, J.; Zou, Z.; Oshikiri, M.; Matsushita, A.; Shimoda, M.; Imai, M.; Shishido, T. *Chem. Phys. Lett.* **2002**, *356*, 221.
(669) Kudo, A.; Ueda, K.; Kato, H.; Mikami, I. *Catal. Lett.* **1998**, *53*, 229.
(670) Kudo, A.; Omori, K.; Kato, H. *J. Am. Chem. Soc.* **1999**, *121*, 11459.
(671) Yu, J.; Zhang, Y.; Kudo, A. *J. Solid State Chem.* **2009**, *182*, 223.
(672) Ke, D.; Peng, T.; Ma, L.; Cai, P.; Dai, K. *Inorg. Chem.* **2009**, *48*, 4685.
(673) Ke, D.; Peng, T.; Ma, L.; Cai, P.; Jiang, P. *Appl. Catal., A* **2008**, *350*, 111.
(674) Li, M. T.; Zhao, L.; Guo, L. J. *Int. J. Hydrogen Energy* **2010**, *35*, 7127.
(675) Wang, D.; Zou, Z.; Ye, J. *Catal. Today* **2004**, *93−95*, 891.
(676) Wang, D.; Tang, J.; Zou, Z.; Ye, J. *Chem. Mater.* **2005**, *17*, 5177.

(677) Weifeng, Y.; Jinhua, Y. *Catal. Today* **2006**, *116*, 18.
(678) Liu, H.; Nakamura, R.; Nakato, Y. *ChemPhysChem* **2005**, *6*, 2499.
(679) Liu, H.; Nakamura, R.; Nakato, Y. *Electrochem. Solid-State Lett.* **2006**, *9*, G187.
(680) Yin, J.; Zou, Z.; Ye, J. *J. Phys. Chem. B* **2003**, *107*, 4936.
(681) Yin, J.; Zou, Z.; Ye, J. *J. Mater. Sci.* **2006**, *41*, 1131.
(682) Sun, S.; Wang, W.; Xu, H.; Zhou, L.; Shang, M.; Zhang, L. *J. Phys. Chem. C* **2008**, *112*, 17835.
(683) Wang, Y. X.; Wang, Y. Q.; Gao, Y. T. *React. Kinet. Mech. Catal.* **2010**, *99*, 485.
(684) Konta, R.; Kato, H.; Kobayashi, H.; Kudo, A. *Phys. Chem. Chem. Phys.* **2003**, *5*, 3061.
(685) Tang, J.; Zou, Z.; Ye, J. *J. Phys. Chem. B* **2003**, *107*, 14265.
(686) Maruyama, Y.; Irie, H.; Hashimoto, K. *J. Phys. Chem. B* **2006**, *110*, 23274.
(687) Hosogi, Y.; Kato, H.; Kudo, A. *J. Mater. Chem.* **2008**, *18*, 647.
(688) Li, X.; Ouyang, S.; Kikugawa, N.; Ye, J. *Appl. Catal., A* **2008**, *334*, 51.
(689) Tang, J.; Zou, Z.; Katagiri, M.; Kako, T.; Ye, J. *Catal. Today* **2004**, *93*−*95*, 885.
(690) Tang, J.; Zou, Z.; Ye, J. *Chem. Mater.* **2004**, *16*, 1644.
(691) Zou, Z.; Ye, J.; Arakawa, H. *Mater. Res. Bull.* **2001**, *36*, 1185.
(692) Zhang, L.; Djerdj, I.; Cao, M.; Antonietti, M.; Niederberger, M. *Adv. Mater.* **2007**, *19*, 2083.
(693) Chiou, Y. C.; Kumar, U.; Wu, J. C. S. *Appl. Catal., A* **2009**, *357*, 73.
(694) Scaife, D. E. *Sol. Energy* **1980**, *25*, 41.
(695) Zhou, J.; Zou, Z.; Ray, A. K.; Zhao, X. S. *Ind. Eng. Chem. Res.* **2007**, *46*, 745.
(696) Tang, J.; Zou, Z.; Ye, J. *Angew. Chem.* **2004**, *116*, 4563.
(697) Solarska, R.; Heel, A.; Ropka, J.; Braun, A.; Holzer, L.; Ye, J.; Graule, T. *Appl. Catal., A* **2010**, *382*, 190.
(698) Zhang, C.; Zhu, Y. *Chem. Mater.* **2005**, *17*, 3537.
(699) Fu, H.; Zhang, L.; Yao, W.; Zhu, Y. *Appl. Catal., B* **2006**, *66*, 100.
(700) Shimodaira, Y.; Kato, H.; Kobayashi, H.; Kudo, A. *J. Phys. Chem. B* **2006**, *110*, 17790.
(701) Lin, X. P.; Huang, F. Q.; Wang, W. D.; Zhang, K. L. *Appl. Catal., A* **2006**, *307*, 257.
(702) Zou, Z.; Ye, J.; Arakawa, H. *Mater. Sci. Eng.* **2001**, *B79*, 83.
(703) Zou, Z.; Ye, J.; Arakawa, H. *Int. J. Hydrogen Energy* **2003**, *28*, 663.
(704) Kako, T.; Zou, Z.; Katagiri, M.; Ye, J. *Chem. Mater.* **2007**, *19*, 198.
(705) Li, X.; Kako, T.; Ye, J. *Appl. Catal., A* **2007**, *326*, 1.
(706) Li, X.; Ye, J. *J. Phys. Chem. C* **2007**, *111*, 13109.
(707) Kim, H. G.; Becker, O. S.; Jang, J. S.; Ji, S. M.; Borse, P. H.; Lee, J. S. *J. Solid State Chem.* **2006**, *179*, 1214.
(708) Kim, H. G.; Hwang, D. W.; Lee, J. S. *J. Am. Chem. Soc.* **2004**, *126*, 8912.
(709) Hosogi, Y.; Kato, H.; Kudo, A. *Chem. Lett.* **2006**, *35*, 578.
(710) Hosogi, Y.; Shimodaira, Y.; Kato, H.; Kobayashi, H.; Kudo, A. *Chem. Mater.* **2008**, *20*, 1299.
(711) Hosogi, Y.; Kato, H.; Kudo, A. *J. Phys. Chem. C* **2008**, *112*, 17678.
(712) Cho, I. S.; Kwak, C. H.; Kim, D. W.; Lee, S.; Hong, K. S. *J. Phys. Chem. C* **2009**, *113*, 10647.
(713) Zou, Z.; Ye, J.; Arakawa, H. *J. Phys. Chem. B* **2002**, *106*, 517.
(714) Tian, M.; Shangguan, W.; Yuan, J.; Jiang, L.; Chen, M.; Shi, J.; Ouyang, Z.; Wang, S. *Appl. Catal., A* **2006**, *309*, 76.
(715) Tang, X.; Ye, H.; Liu, H.; Ma, C.; Zhao, Z. *J. Solid State Chem.* **2010**, *183*, 192.
(716) Tang, X. D.; Ye, H. Q.; Liu, H.; Ma, C. X.; Zhao, Z. *Chem. Phys. Lett.* **2009**, *484*, 48.
(717) Yi, Z.; Ye, J.; Kikugawa, N.; Kako, T.; Ouyang, S.; Stuart-Williams, H.; Yang, H.; Cao, J.; Luo, W.; Li, Z.; Liu, Y.; Withers, R. L. *Nat. Mater.* **2010**, *9*, 559.
(718) Ji, F.; Li, C.; Zhang, J. *ACS Appl. Mater. Interface* **2010**, *2*, 1674.
(719) Ritterskamp, P.; Kuklya, A.; Wüstkamp, M. A.; Kerpen, K.; Weidenthaler, C.; Demuth, M. *Angew. Chem., Int. Ed.* **2007**, *46*, 7770.
(720) Wang, X.; Maeda, K.; Thomas, A.; Takanabe, K.; Xin, G.; Carlsson, J. M.; Domen, K.; Antonietti, M. *Nat. Mater.* **2008**, *8*, 76.
(721) Liu, G.; Niu, P.; Sun, C.; Smith, S. C.; Chen, Z.; Lu, G. Q.; Cheng, H. M. *J. Am. Chem. Soc.* **2010**, *132*, 11642.
(722) Zhang, J.; Chen, X.; Takanabe, K.; Maeda, K.; Domen, K.; Epping, J. D.; Fu, X.; Antonietti, M.; Wang, X. *Angew. Chem., Int. Ed.* **2010**, *49*, 441.
(723) Yeh, T. F.; Syu, J. M.; Cheng, C.; Chang, T. H.; Teng, H. *Adv. Funct. Mater.* **2010**, *20*, 2255.
(724) Kudo, A.; Mikami, I. *Chem. Lett.* **1998**, *27*, 1027.
(725) Ikuma, Y.; Bessho, H. *Int. J. Hydrogen Energy* **2007**, *32*, 2689.
(726) Kiwi, J.; Gratzel, M. *J. Phys. Chem.* **1984**, *88*, 1302.
(727) Sobczynski, A.; Yildiz, A.; Bard, A. J.; Campion, A.; Fox, M. A.; Mallouk, T.; Webber, S. E.; White, J. M. *J. Phys. Chem.* **1988**, *92*, 2311.
(728) Jang, J. S.; Joshi, U. A.; Lee, J. S. *J. Phys. Chem. C* **2007**, *111*, 13280.
(729) Bessekhouad, Y.; Mohammedi, M.; Trari, M. *Sol. Energy Mater. Sol. Cells* **2002**, *73*, 339.
(730) Bao, N.; Shen, L.; Takata, T.; Lu, D.; Domen, K. *Chem. Lett.* **2006**, *35*, 318.
(731) Xiao, W.; Yuan, J.; Zhang, Y.; Shangguan, W. *Mater. Chem. Phys.* **2007**, *105*, 6.
(732) Bao, N.; Shen, L.; Takata, T. *Chem. Mater.* **2008**, *20*, 110.
(733) Yan, H.; Yang, J.; Ma, G.; Wu, G.; Zong, X.; Lei, Z.; Shi, J.; Li, C. *J. Catal.* **2009**, *266*, 165.
(734) Chiarello, G. L.; Selli, E.; Forni, L. *Appl. Catal., B* **2008**, *84*, 332.
(735) Sreethawong, T.; Yoshikawa, S. *Catal. Commun.* **2005**, *6*, 661.
(736) Bae, E.; Choi, W. *Environ. Sci. Technol.* **2003**, *37*, 147.
(737) Arabatzis, M.; Stergiopoulos, T.; Andreeva, D.; Kitova, S.; Neophytides, G. S.; Falaras, P. *J. Catal.* **2003**, *220*, 127.
(738) Bamwenda, G. R.; Tshbota, S.; Nakamura, T.; Haruta, M. *J. Photochem. Photobiol., A* **1995**, *89*, 177.
(739) Tai, Y. W.; Chen, J. S.; Yang, C. C.; Wan, B. Z. *Catal. Today* **2004**, *97*, 95.
(740) Hara, M.; Nunoshige, J.; Takata, T.; Kondo, J. N.; Domen, K. *Chem. Commun.* **2003**, *24*, 3000.
(741) Navarro, R. M.; del Valle, F.; Fierro, J. L. G. *Int. J. Hydrogen Energy* **2008**, *33*, 4265.
(742) Ranjit, K. T.; Varadarajan, T. K.; Viswanathan, B. *J. Photochem. Photobiol., A* **1995**, *89*, 67.
(743) Sano, T.; Kutsuna, S.; Negishi, N.; Takeuchi, K. *J. Mol. Catal. A: Chem.* **2002**, *189*, 263.
(744) Wang, X.; He, Z.; Zhong, S.; Xiao, X. *J. Nat. Gas Chem.* **2007**, *16*, 173.
(745) Jin, S.; Shiraishi, F. *Chem. Eng. J.* **2004**, *97*, 203.
(746) Ke, D.; Peng, T.; Ma, L.; Cai, P.; Jiang, P. *Appl. Catal., A* **2008**, *350*, 111.
(747) Georgekutty, R.; Seery, M. K.; Pillai, S. C. *J. Phys. Chem. C* **2008**, *112*, 13563.
(748) Lu, W.; Gao, S.; Wang, J. *J. Phys. Chem. C* **2008**, *112*, 16792.
(749) Anandan, S.; Kumar, P. S.; Pugazhenthiran, N.; Madhavan, J.; Maruthamuthu, P. *Sol. Energy Mater. Sol. Cells* **2008**, *92*, 929.
(750) Hou, X. G.; Huang, M. D.; Wu, X. L.; Liu, A. D. *Chem. Eng. J.* **2009**, *146*, 42.
(751) Pal, B.; Ikeda, S.; Kominami, H.; Kera, Y.; Ohtani, B. *J. Catal.* **2003**, *217*, 152.
(752) Sasaki, Y.; Iwase, A.; Kato, H.; Kudo, A. *J. Catal.* **2008**, *259*, 133.
(753) Pal, B.; Torimoto, T.; Okazaki, K.; Ohtani, B. *Chem. Commun.* **2007**, *5*, 483.
(754) Naito, S. *Can. J. Chem.* **1986**, *64*, 1795.
(755) Wu, G.; Chen, T.; Zhou, G.; Zong, X.; Li, C. *Sci. China, Ser. B* **2008**, *51*, 97.
(756) Korzhak, A. V.; Ermokhina, N. I.; Stroyuk, A. L.; Bukhtiyarov, V. K.; Raevskaya, A. E.; Litvin, V. I.; Kuchmiy, S. Y.; Ilyin, V. G.; Manorik, P. A. *J. Photochem. Photobiol., A* **2008**, *198*, 126.
(757) Gurunathan, K. *Int. J. Hydrogen Energy* **2004**, *29*, 933.
(758) Mizukoshi, Y.; Sato, K.; Konno, T. J.; Masahashi, N. *Appl. Catal., B* **2010**, *94*, 248.
(759) Arai, N.; Saito, N.; Nishiyama, H.; Domen, K.; Kobayashi, H.; Sato, K.; Inoue, Y. *Catal. Today* **2007**, *129*, 407.
(760) Ebina, Y.; Sakai, N.; Sasaki, T. *J. Phys. Chem. B* **2005**, *109*, 17212.
(761) Sreethawong, T.; Suzuki, Y.; Yoshikawa, S. *Int. J. Hydrogen Energy* **2005**, *30*, 1053.
(762) Lin, H.; Chen, Y.; Chen, Y. *Int. J. Hydrogen Energy* **2007**, *32*, 86.
(763) Maeda, K.; Wang, X.; Nishihara, Y.; Lu, D.; Antonietti, M.; Domen, K. *J. Phys. Chem. C* **2009**, *113*, 4940.
(764) Abe, T.; Suzuki, E.; Nagoshi, K.; Miyashita, K.; Kaneko, M. *J. Phys. Chem. B* **1999**, *103*, 1119.
(765) Ma, B.; Yang, J.; Han, H.; Wang, J.; Zhang, X.; Li, C. *J. Phys. Chem. C* **2010**, *114*, 12818.
(766) Kiwi, J.; Borgarello, E.; Pelizzetti, E.; Visca, M.; Gratzel, M. *Angew. Chem., Int. Ed.* **1980**, *19*, 646.
(767) Teramura, K.; Maeda, K.; Saito, T.; Takata, T.; Saito, N.; Inoue, Y.; Domen, K. *J. Phys. Chem. B* **2005**, *109*, 21915.
(768) Maeda, K.; Teramura, K.; Lu, D.; Takata, T.; Saito, N.; Inoue, Y.; Domen, K. *J. Phys. Chem. B* **2006**, *110*, 13753.
(769) Maeda, K.; Teramura, K.; Saito, N.; Inoue, Y.; Domen, K. *J. Catal.* **2006**, *243*, 303.
(770) Maeda, K.; Teramura, K.; Domen, K. *Catal. Surv. Asia* **2007**, *11*, 145.
(771) Maeda, K.; Lu, D.; Teramura, K.; Domen, K. *J. Mater. Chem.* **2008**, *18*, 3539.
(772) Hisatomi, T.; Miyazaki, K.; Takanabe, K.; Maeda, K.; Kubota, J.; Sakata, Y.; Domen, K. *Chem. Phys. Lett.* **2010**, *486*, 144.

(773) Maeda, K.; Teramura, K.; Lu, D.; Saito, N.; Inoue, Y.; Domen, K. *Angew. Chem., Int. Ed.* **2006**, *45*, 7806.
(774) Maeda, K.; Teramura, K.; Lu, D.; Saito, N.; Inoue, Y.; Domen, K. *J. Phys. Chem. C* **2007**, *111*, 7554.
(775) Maeda, K.; Lu, D.; Teramura, K.; Domen, K. *Energy Environ. Sci.* **2010**, *3*, 471.
(776) Maeda, K.; Sakamoto, N.; Ikeda, T.; Ohtsuka, H.; Xiong, A.; Lu, D.; Kanehara, M.; Teranishi, T.; Domen, K. *Chem.—Eur. J.* **2010**, *16*, 7750.
(777) Maeda, K.; Xiong, A.; Yoshinaga, T.; Ikeda, T.; Sakamoto, N.; Hisatomi, T.; Takashima, M.; Lu, D.; Kanehara, M.; Setoyama, T.; Teranishi, T.; Domen, K. *Angew. Chem., Int. Ed.* **2010**, *49*, 4096.
(778) Kudo, A.; Sayama, K.; Tanaka, A.; Asakura, K.; Domen, K.; Maruya, K.; Onishi, T. *J. Catal.* **1989**, *120*, 337.
(779) Tian, M.; Shangguan, W.; Yuan, J.; Wang, S.; Ouyang, Z. *Sci. Technol. Adv. Mater.* **2007**, *8*, 82.
(780) Hwang, D. W.; Kim, H. G.; Kim, J.; Cha, K. Y.; Kim, Y. G.; Lee, J. S. *J. Catal.* **2000**, *193*, 40.
(781) Thaminimulla, C. T. K.; Takata, T.; Hara, M.; Kondo, J. N.; Domen, K. *J. Catal.* **2000**, *196*, 362.
(782) Zong, X.; Yan, H.; Wu, G.; Ma, G.; Wen, F.; Wang, L.; Li, C. *J. Am. Chem. Soc.* **2008**, *130*, 7176.
(783) Zong, X.; Wu, G.; Yan, H.; Ma, G.; Shi, J.; Wen, F.; Wang, L.; Li, C. *J. Phys. Chem. C* **2010**, *114*, 1963.
(784) Frame, F. A.; Osterloh, F. E. *J. Phys. Chem. C* **2010**, *114*, 10628.
(785) Ma, G.; Yan, H.; Shi, J.; Zong, X.; Lei, Z.; Li, C. *J. Catal.* **2008**, *260*, 134.
(786) Jang, J. S.; Ham, D. J.; Lakshminarasimhan, N.; Choi, W.; Lee, J. S. *Appl. Catal., A* **2008**, *346*, 149.
(787) Peng, S.; Xie, D.; Li, Y.; Lu, G.; Li, S. *React. Kinet. Catal. Lett.* **2008**, *95*, 185.
(788) Ke, D.; Liu, S.; Dai, K.; Zhou, J.; Zhang, L.; Peng, T. *J. Phys. Chem. C* **2009**, *113*, 16021.
(789) Hirai, T.; Bando, Y.; Komasawa, I. *J. Phys. Chem. B* **2002**, *106*, 8967.
(790) Deshpande, A.; Shah, P.; Gholap, R. S.; Gupta, N. M. *J. Colloid Interface Sci.* **2009**, *333*, 263.
(791) Sahu, N.; Upadhyay, S. N.; Sinha, A. S. K. *Int. J. Hydrogen Energy* **2009**, *34*, 130.
(792) Lunawat, P. S.; Senapati, S.; Kumar, R.; Gupta, N. M. *Int. J. Hydrogen Energy* **2007**, *32*, 2784.
(793) Zhang, Y.; Zhang, L. *Appl. Surf. Sci.* **2009**, *255*, 4863.
(794) Jang, J. S.; Li, W.; Oh, S. H.; Lee, J. S. *Chem. Phys. Lett.* **2006**, *425*, 278.
(795) Spanhel, L.; Weller, H.; Henglein, A. *J. Am. Chem. Soc.* **1987**, *109*, 6632.
(796) Nayak, J.; Sahu, S. N.; Kasuya, J.; Nozaki, S. *Appl. Surf. Sci.* **2008**, *254*, 7215.
(797) Wang, X.; Liu, G.; Chen, Z.; Li, F.; Wang, L.; Lu, G.; Cheng, H. *Chem. Commun.* **2009**, *23*, 3452.
(798) Wang, X.; Liu, G.; Lu, G.; Cheng, H. *Int. J. Hydrogen Energy* **2010**, *35*, 8199.
(799) Kida, T.; Guan, G.; Yoshida, A. *Chem. Phys. Lett.* **2003**, *371*, 563.
(800) Ryu, S. Y.; Choi, J.; Balcerski, W.; Lee, T. K.; Hoffmann, M. R. *Ind. Eng. Chem. Res.* **2007**, *46*, 7476.
(801) Choi, J.; Ryu, S. Y.; Balcerski, W.; Lee, T. K.; Hoffmann, M. R. *J. Mater. Chem.* **2008**, *18*, 2371.
(802) Hirai, T.; Suzuki, K.; Komasawa, I. *J. Colloid Interface Sci.* **2001**, *244*, 262.
(803) Jang, J. S.; Ji, S. M.; Bae, S. W.; Son, H. C.; Lee, J. S. *J. Photochem. Photobiol., A* **2007**, *188*, 112.
(804) Fujii, H.; Ohtaki, M.; Eguchi, K.; Arai, H. *J. Mol. Catal. A: Chem.* **1998**, *129*, 61.
(805) Jang, J. S.; Kim, H. G.; Joshi, U. A.; Jang, J. W.; Lee, J. S. *Int. J. Hydrogen Energy* **2008**, *33*, 5975.
(806) Jang, J. S.; Kim, H. G.; Borse, P. H.; Lee, J. S. *Int. J. Hydrogen Energy* **2007**, *32*, 4786.
(807) Yu, J. C.; Wu, L.; Lin, J.; Lia, P.; Li, Q. *Chem. Commun.* **2003**, *13*, 1552.
(808) Bessekhouad, Y.; Robert, D.; Weber, J. *J. Photochem. Photobiol., A* **2004**, *163*, 569.
(809) Srinivasan, S. S.; Wade, J.; Stefanakos, E. K. *J. Nanomater.* **2006**, 87326.
(810) Prabakar, K.; Takahashi, T.; Nezuka, T.; Takahashi, K.; Nakashima, T.; Kubota, Y.; Fujishima, A. *J. Vac. Sci. Technol.* **2007**, *A25*, 1188.
(811) Santz, P. A.; Kamat, P. V. *Phys. Chem. Chem. Phys.* **2002**, *4*, 198.
(812) Baker, D. R.; Kamat, P. V. *Adv. Funct. Mater.* **2009**, *19*, 805.
(813) Gopidas, K. R.; Bohorquez, M.; Kamat, P. V. *J. Phys. Chem.* **1990**, *94*, 6435.
(814) Evans, J. E.; Springer, K. W.; Zhang, J. Z. *J. Chem. Phys.* **1994**, *101*, 6222.
(815) Tada, H.; Mitsui, T.; Kiyonaga, T.; Akita, T.; Tanaka, K. *Nat. Mater.* **2006**, *5*, 782.
(816) Park, H.; Choi, W.; Hoffmann, M. R. *J. Mater. Chem.* **2008**, *18*, 2379.
(817) Liu, Y.; Guo, L.; Yan, W.; Liu, H. *J. Power Sources* **2006**, *159*, 1300.
(818) Yang, H.; Guo, L.; Yan, W.; Liu, H. *J. Power Sources* **2006**, *159*, 1305.
(819) Wang, D.; Zou, Z.; Ye, J. *Chem. Mater.* **2005**, *17*, 3255.
(820) Lv, J.; Kako, T.; Li, Z.; Zou, Z.; Ye, J. *J. Phys. Chem. C* **2010**, *114*, 6157.
(821) Ou, Y.; Lin, J.; Fang, S.; Liao, D. *Chem. Phys. Lett.* **2006**, *429*, 199.
(822) Brahimi, R.; Bessekhouad, Y.; Bouguelia, A.; Trari, M. *Catal. Today* **2007**, *122*, 62.
(823) Silva, L. A.; Ryu, S. Y.; Choi, J.; Choi, W.; Hoffmann, M. R. *J. Phys. Chem. C* **2008**, *112*, 12069.
(824) Amirav, L.; Alivisatos, A. P. *J. Phys. Chem. Lett.* **2010**, *1*, 1051.
(825) Sato, T.; Masaki, K.; Sato, K. *J. Chem. Technol. Biotechnol.* **1996**, *67*, 339.
(826) Tawkaew, S.; Fujishiro, Y.; Yin, S.; Sato, T. *Colloids Surf., A* **2001**, *179*, 139.
(827) Yin, S.; Maeda, D.; Ishitsuka, M.; Wu, J. H.; Sato, T. *Solid State Ionics* **2002**, *151*, 377.
(828) Shimizu, K.; Murayama, H.; Nagai, A.; Shimada, A. *Appl. Catal., B* **2005**, *55*, 141.
(829) Liu, S.; Yang, J.; Choy, J. *J. Photochem. Photobiol., A* **2006**, *179*, 75.
(830) Palacin, M. R.; Lira, M.; Garcia, J. L. *Mater. Res. Bull.* **1996**, *31*, 217.
(831) Shangguan, W.; Inoue, K.; Yoshida, A. *Chem. Commun.* **1998**, *7*, 779.
(832) Shangguan, W.; Yoshida, A. *J. Mater. Sci.* **2001**, *36*, 4989.
(833) Hata, H.; Kobayashi, Y.; Bojan, V.; Youngblood, W. J.; Mallouk, T. E. *Nano Lett.* **2008**, *8*, 794.
(834) Ma, R.; Kobayashi, Y.; Youngblood, W. J.; Mallouk, T. E. *J. Mater. Chem.* **2008**, *18*, 5982.
(835) Wu, J.; Uchida, S.; Fujishiro, Y.; Yin, S.; Sato, T. *Int. J. Inorg. Mater.* **1999**, *1*, 253.
(836) Wu, J.; Uchida, S.; Fujishiro, Y.; Yin, S.; Sato, T. *J. Photochem. Photobiol., A* **1999**, *128*, 129.
(837) Tawkaew, S.; Yin, S.; Sato, T. *Int. J. Inorg. Mater.* **2001**, *3*, 855.
(838) Wu, J.; Cheng, Y.; Lin, J.; Huang, Y.; Huang, M.; Hao, S. *J. Phys. Chem. C* **2007**, *111*, 3624.
(839) Jang, J. S.; Kim, H. G.; Reddy, V. R.; Bae, S. W.; Ji, S. M.; Lee, J. S. *J. Catal.* **2005**, *231*, 213.
(840) Shangguan, W.; Yoshida, A. *Sol. Energy Mater. Sol. Cells* **2001**, *69*, 189.
(841) Shangguan, W.; Yoshida, A. *J. Phys. Chem. B* **2002**, *106*, 12227.
(842) Shangguan, W. *Sci. Technol. Adv. Mater.* **2007**, *8*, 76.
(843) Wu, J.; Lin, J.; Yin, S.; Sato, T. *J. Mater. Chem.* **2001**, *11*, 3343.
(844) Sato, T.; Fukugami, Y.; Shu, Y. *Scr. Mater.* **2001**, *44*, 1905.
(845) Wu, J.; Cheng, Y.; Lin, J.; Huang, Y.; Huang, M.; Li, Y.; Yin, S.; Sato, T. *Sci. China, Ser. B* **2007**, *50*, 514.
(846) Guan, G.; Kida, T.; Kusakabe, K.; Kimura, K.; Fang, X.; Abe, E.; Yoshida, A. *Chem. Phys. Lett.* **2004**, *385*, 319.
(847) Guan, G.; Kida, T.; Kusakabe, K.; Kimura, K.; Abe, E.; Yoshida, A. *Appl. Catal., A* **2005**, *295*, 71.
(848) Shen, S.; Guo, L. *J. Solid State Chem.* **2006**, *179*, 2629.
(849) Shen, S.; Guo, L. *Mater. Res. Bull.* **2008**, *43*, 437.
(850) Jing, D.; Guo, L. *Catal. Commun.* **2007**, *8*, 795.
(851) Jing, D.; Guo, L. *J. Phys. Chem. C* **2007**, *111*, 13437.
(852) Xing, C.; Jing, D.; Liu, M.; Guo, L. *Mater. Res. Bull.* **2009**, *44*, 442.
(853) Zhang, Y.; Wei, Y.; Yan, P.; Zhen, H. *Mater. Lett.* **2008**, *62*, 3846.
(854) Li, C.; Yuan, J.; Han, B.; Jiang, L.; Shangguan, W. *Int. J. Hydrogen Energy* **2010**, *35*, 7073.
(855) Zhang, Y.; Wang, Y.; Yan, W.; Li, T.; Li, S.; Hu, Y. R. *Appl. Surf. Sci.* **2009**, *255*, 9508.
(856) Nozik, A. J. *Appl. Phys. Lett.* **1976**, *29*, 150.
(857) Khaselev, O.; Turner, J. *Science* **1998**, *280*, 425.
(858) Grätzel, M. *Nature* **2001**, *414*, 338.
(859) Long, M.; Cai, W.; Cai, J.; Zhou, B.; Chai, X.; Wu, Y. *J. Phys. Chem. B* **2006**, *110*, 20211.
(860) Bessekhouad, Y.; Robert, D.; Weber, J. V. *Catal. Today* **2005**, *101*, 315.
(861) Yang, C.; Wang, W.; Huang, F. *J. Solid State Chem.* **2009**, *182*, 807.
(862) Ye, F.; Ohmoria, A.; Li, C. *Surf. Coat. Technol.* **2004**, *184*, 233.
(863) Kang, S.; Yang, Y.; Bu, W.; Mu, J. *J. Solid State Chem.* **2009**, *182*, 2972.
(864) Chen, S.; Zhao, W.; Liu, W.; Zhang, H.; Yu, X.; Chen, Y. *J. Hazard. Mater.* **2009**, *172*, 1415.
(865) Chen, S.; Zhao, W.; Liu, W.; Zhang, S. *Appl. Surf. Sci.* **2008**, *255*, 2478.

(866) Long, M.; Cai, W.; Kisch, H. *J. Phys. Chem. C* **2008**, *112*, 548.
(867) Hu, C. C.; Nian, J. N.; Teng, H. *Sol. Energy Mater. Sol. Cells* **2008**, *92*, 1071.
(868) Bessekhouad, Y.; Trari, M.; Doumerc, J. P. *Int. J. Hydrogen Energy* **2003**, *28*, 43.
(869) Saadi, S.; Bouguelia, A.; Trari, M. *Sol. Energy* **2006**, *80*, 272.
(870) Brahimi, R.; Bessekhouad, Y.; Bouguelia, A.; Trari, M. *J. Photochem. Photobiol., A* **2007**, *186*, 242.
(871) Derbal, A.; Omeiri, S.; Bouguelia, A.; Trari, M. *Int. J. Hydrogen Energy* **2008**, *33*, 4274.
(872) Boumaza, S.; Boudjemaa, A.; Bouguelia, A.; Bouarab, R.; Trari, M. *Appl. Energy* **2010**, *87*, 2230.
(873) Jang, J. S.; Hwang, D. W.; Lee, J. S. *Catal. Today* **2007**, *120*, 174.
(874) Jang, J. S.; Hong, S. J.; Kim, J. Y.; Lee, J. S. *Chem. Phys. Lett.* **2009**, *475*, 78.
(875) Kim, H. G.; Borse, P. H.; Jang, J. S.; Jeong, E. D.; Jung, O. S.; Suh, Y. J.; Lee, J. S. *Chem. Commun.* **2009**, *39*, 5889.
(876) Kim, H. G.; Borse, P. H.; Choi, W.; Lee, J. S. *Angew. Chem., Int. Ed.* **2005**, *44*, 4585.
(877) Kim, H. G.; Jeong, E. D.; Borse, P. H.; Jeon, S.; Yong, K.; Lee, J. S.; Li, W.; Oh, S. H. *Appl. Phys. Lett.* **2006**, *89*, 064103.
(878) Bickley, R. I.; Gonzalez-Carreno, T.; Lee, J. S.; Palmisano, L.; Tilley, R. J. D. *J. Solid State Chem.* **1991**, *92*, 178.
(879) Karakitsou, K. E.; Verykios, X. E. *J. Phys. Chem.* **1993**, *97*, 1184.
(880) Zhu, J.; Zheng, W.; He, B.; Zhang, J.; Anpo, M. *J. Mol. Catal. A: Chem.* **2004**, *216*, 35.
(881) Ding, Z.; Liu, G. Q.; Greenfield, P. F. *J. Phys. Chem. B* **2000**, *104*, 4815.
(882) Ohno, T.; Sarukawa, K.; Matsumura, M. *J. Phys. Chem. B* **2001**, *105*, 2417.
(883) Bickley, R. J. *J. Solid State Chem.* **1991**, *92*, 178.
(884) Yu, J. C.; Zhang, L. Z.; Yu, J. G. *Chem. Mater.* **2002**, *14*, 4647.
(885) Xu, H.; Zhang, L. *J. Phys. Chem. C* **2009**, *113*, 1785.
(886) Rosseler, O.; Shankar, M. V.; Du, M. K.; Schmidlin, L.; Keller, N.; Keller, V. *J. Catal.* **2010**, *269*, 179.
(887) Kandiel, T. A.; Feldhoff, A.; Robben, L.; Dillert, R.; Bahnemann, D. W. *Chem. Mater.* **2010**, *22*, 2050.
(888) Kho, Y. K.; Iwase, A.; Teoh, W. Y.; Mädler, L.; Kudo, A.; Amal, R. *J. Phys. Chem. C* **2010**, *114*, 2821.
(889) Jitputti, J.; Pavasupree, S.; Suzuki, Y.; Yoshikawa, S. *J. Solid State Chem.* **2007**, *180*, 1743.
(890) Oekermann, T.; Zhang, D.; Yoshida, T.; Minoura, H. *J. Phys. Chem. B* **2004**, *108*, 2227.
(891) Fu, X.; Wang, X.; Chen, Z.; Zhang, Z.; Li, Z.; Leung, D. Y. C.; Wu, L.; Fu, X. *Appl. Catal., B* **2010**, *95*, 393.
(892) Amano, F.; Yamakata, A.; Nogami, K.; Osawa, M.; Ohtani, B. *J. Am. Chem. Soc.* **2008**, *130*, 17650.
(893) Noda, Y.; Lee, B.; Domen, K.; Kondo, J. N. *Chem. Mater.* **2008**, *20*, 5361.
(894) Lee, Y.; Nukumizu, K.; Watanabe, T.; Takata, T.; Hara, M.; Yoshimura, M.; Domen, K. *Chem. Lett.* **2006**, *35*, 352.
(895) Muruganandham, M.; Kusumoto, Y.; Okamoto, C.; Muruganandham, A.; Abdulla-Al-Mamun, M.; Ahmmad, B. *J. Phys. Chem. C* **2009**, *113*, 19506.
(896) Li, Y.; Du, J.; Peng, S.; Xie, D.; Lu, G.; Li, S. *Int. J. Hydrogen Energy* **2008**, *33*, 2007.
(897) Maeda, K.; Terashima, H.; Kase, K.; Higashi, M.; Tabata, M.; Domen, K. *Bull. Chem. Soc. Jpn.* **2008**, *81*, 927.
(898) Maeda, K.; Terashima, H.; Kase, K.; Domen, K. *Appl. Catal., A* **2009**, *357*, 206.
(899) Han, X.; Kuang, Q.; Jin, M.; Xie, Z.; Zheng, L. *J. Am. Chem. Soc.* **2009**, *131*, 3152.
(900) Yang, H. G.; Sun, C. H.; Qiao, S. Z.; Zou, J.; Liu, G.; Smith, S. C.; Cheng, H. M.; Lu, G. Q. *Nature* **2008**, *453*, 638.
(901) Yang, H. G.; Liu, G.; Qiao, S. Z.; Sun, C. H.; Jin, Y. G.; Smith, S. C.; Zou, J.; Cheng, H. M.; Lu, G. Q. *J. Am. Chem. Soc.* **2009**, *131*, 4078.
(902) Liu, G.; Yang, H. G.; Wang, X.; Cheng, L.; Lu, H.; Wang, L.; Lu, G. Q.; Cheng, H. M. *J. Phys. Chem. C* **2009**, *113*, 21784.
(903) Liu, G.; Yang, H. G.; Wang, X.; Cheng, L.; Pan, J.; Lu, G. Q.; Cheng, H. M. *J. Am. Chem. Soc.* **2009**, *131*, 12868.
(904) Liu, M.; Piao, L.; Zhao, L.; Ju, S.; Yan, Z.; He, T.; Zhou, C.; Wang, W. *Chem. Commun.* **2010**, *46*, 1664.
(905) Wu, B.; Guo, C.; Zheng, N.; Xie, Z.; Stucky, G. D. *J. Am. Chem. Soc.* **2008**, *130*, 17563.
(906) Li, J.; Xu, D. *Chem. Commun.* **2010**, *46*, 2301.
(907) Yu, J. G.; Qi, L. F.; Jaroniec, M. *J. Phys. Chem. C* **2010**, *114*, 13118.
(908) Zhao, Z. G.; Liu, Z. F.; Masahiro., M. *Chem. Commun.* **2010**, *19*, 3321.
(909) Nian, J. N.; Hu, C. C.; Teng, H. *Int. J. Hydrogen Energy* **2008**, *33*, 2897.
(910) Xu, H.; Wang, W.; Zhu, W. *J. Phys. Chem. B* **2006**, *110*, 13829.
(911) Huang, L.; Shengsen, Z.; Peng, F.; Wang, H.; Yu, H.; Yang, J.; Zhang, S.; Zhao, H. *Scr. Mater.* **2010**, *63*, 159.
(912) Xi, G.; Ye, J. *Chem. Commun.* **2010**, *46*, 1893.
(913) Inoue, Y.; Kohno, M.; Ogura, S.; Sato, K. *Chem. Phys. Lett.* **1997**, *267*, 72.
(914) Inoue, Y.; Kohno, M.; Ogura, S.; Sato, K. *J. Chem. Soc., Faraday Trans.* **1997**, *93*, 2433.
(915) Shen, S.; Zhao, L.; Guo, L. *Int. J. Hydrogen Energy* **2008**, *33*, 4501.
(916) Hidalgo, M. C.; Aguilar, M.; Maicu, M.; Navío, J. A.; Colón, G. *Catal. Today* **2007**, *129*, 50.
(917) Testino, A.; Bellobono, I. R.; Buscaglia, V.; Canevali, C.; D'Arienzo, M.; Polizzi, S.; Scotti, R.; Morazzoni, F. *J. Am. Chem. Soc.* **2007**, *129*, 3564.
(918) Datta, A.; Priyama, A.; Bhattacharyya, S. N.; Mukherjea, K. K.; Saha, A. *J. Colloid Interface Sci.* **2008**, *322*, 128.
(919) Chae, S. Y.; Park, M. K.; Lee, S. K.; Kim, T. Y.; Kim, S. K.; Lee, W. I. *Chem. Mater.* **2003**, *15*, 3326.
(920) Liu, G.; Sun, C.; Yang, H. G.; Smith, S. C.; Wang, L.; Lu, G. Q.; Cheng, H. M. *Chem. Commun.* **2010**, *46*, 755.
(921) Zhang, Z.; Wang, C. C.; Zakaria, R.; Ying, J. Y. *J. Phys. Chem. B* **1998**, *102*, 10871.
(922) Sun, W.; Zhang, S.; Liu, Z.; Wang, C.; Mao, Z. *Int. J. Hydrogen Energy* **2008**, *33*, 1112.
(923) Sathish, M.; Viswanathan, B.; Viswanath, R. P. *Int. J. Hydrogen Energy* **2006**, *31*, 891.
(924) Lunawat, P. S.; Kumar, R.; Gupta, N. *Catal. Lett.* **2008**, *121*, 226.
(925) Serpone, N.; Lawless, D.; Khaircutdinov, R.; Pelizzetti, E. *J. Phys. Chem.* **1995**, *99*, 16655.
(926) Wang, C. C.; Zhang, Z.; Ying, J. Y. *Nanostruct. Mater.* **1997**, *9*, 583.
(927) Bao, N.; Shen, L.; Takata, T.; Domen, K.; Gupta, A.; Yanagisawa, K.; Grimes, C. A. *J. Phys. Chem. C* **2007**, *111*, 17527.
(928) Deshpande, A.; Gupta, N. M. *Int. J. Hydrogen Energy* **2010**, *35*, 3287.
(929) Hong, S. J.; Jun, H.; Borse, P. H.; Lee, J. S. *Int. J. Hydrogen Energy* **2009**, *34*, 3234.
(930) Balázs, N.; Srankó, D. F.; Dombi, A.; Sipos, P.; Mogyorósi, K. *Appl. Catal., B* **2010**, *96*, 569.
(931) Balázs, N.; Mogyorósi, K.; Srankó, D. F.; Pallagi, A.; Alapi, T.; Oszkó, A.; Dombi, A.; Sipos, P. *Appl. Catal., B* **2008**, *84*, 356.
(932) Mogyorósi, K.; Balázs, N.; Srankó, D. F.; Tombácz, E.; Dékány, I.; Oszkó, A.; Sipos, P.; Dombi, A. *Appl. Catal., B* **2010**, *96*, 577.
(933) Kresge, C. T.; Leonowicz, M. E.; Roth, W. J. *Nature* **1992**, *359*, 710.
(934) Sreethawong, T.; Puangpetch, T.; Chavadej, S.; Yoshikawa, S. *J. Power Sources* **2007**, *165*, 861.
(935) Fei, H.; Liu, Y.; Li, Y.; Sun, P.; Yuan, Z.; Li, B.; Ding, D.; Chen, T. *Microporous Mesoporous Mater.* **2007**, *102*, 318.
(936) Ito, S.; Thampi, K. R.; Comte, P.; Liska, P.; Grätzel, M. *Chem. Commun.* **2005**, *2*, 268.
(937) Li, H.; Bian, Z.; Zhu, J.; Huo, Y.; Li, H.; Lu, Y. *J. Am. Chem. Soc.* **2007**, *129*, 4538.
(938) Shen, S.; Guo, L. *Catal. Today* **2007**, *129*, 414.
(939) Sathish, M.; Viswanath, R. P. *Catal. Today* **2007**, *129*, 421.
(940) Sivula, K.; Zboril, R.; Le Formal, F.; Robert, R.; Weidenkaff, A.; Tucek, J.; Frydrych, J.; Gratzel, M. *J. Am. Chem. Soc.* **2010**, *132*, 7436.
(941) Lakshminarasimhan, N.; Bae, E.; Choi, W. *J. Phys. Chem. C* **2007**, *111*, 15244.
(942) Zhang, Z.; Zuo, F.; Feng, P. *J. Mater. Chem.* **2010**, *20*, 2206.
(943) Bai, Y.; Li, W.; Liu, C.; Yang, Z.; Feng, X.; Lu, X.; Chan, K. Y. *J. Mater. Chem.* **2009**, *19*, 7055.
(944) Sreethawong, T.; Junbua, C.; Chavadej, S. *J. Power Sources* **2009**, *190*, 513.
(945) Sreethawong, T.; Laehsalee, S.; Chavadej, S. *Catal. Commun.* **2009**, *10*, 538.
(946) Hartmann, P.; Lee, D. K.; Smarsly, B. M.; Janek, J. *ACS Nano* **2010**, *4*, 3147.
(947) Puangpetch, T.; Sreethawong, T.; Yoshikawa, S.; Chavadej, S. *J. Mol. Catal. A: Chem.* **2009**, *312*, 97.
(948) Puangpetch, T.; Sreethawong, T.; Chavadej, S. *Int. J. Hydrogen Energy* **2010**, *35*, 6531.
(949) Sang, L.; Dai, H.; Sun, J.; Xu, L.; Wang, F.; Ma, C. *Int. J. Hydrogen Energy* **2010**, *35*, 7098.
(950) Xu, L.; Sang, L.; Ma, C.; Lu, Y.; Wang, F.; Li, Q.; Dai, H.; He, H.; Sun, J. *Chin. J. Catal.* **2006**, *27*, 100.
(951) Hisatomi, T.; Otani, M.; Nakajima, K.; Teramura, K.; Kako, Y.; Lu, D.; Takata, T.; Kondo, J. N.; Domen, K. *Chem. Mater.* **2010**, *22*, 3854.
(952) Wang, X.; Maeda, K.; Chen, X.; Takanabe, K.; Domen, K.; Hou, Y.; Fu, X.; Antonietti, M. *J. Am. Chem. Soc.* **2009**, *131*, 1680.
(953) Chen, X.; Jun, Y. S.; Takanabe, K.; Maeda, K.; Domen, K.; Fu, X.; Antonietti, M.; Wang, X. *Chem. Mater.* **2009**, *21*, 4093.

(954) Zheng, N.; Bu, X.; Vu, H.; Feng, P. *Angew. Chem.* **2005**, *117*, 5433.
(955) Zheng, N.; Bu, X.; Feng, P. *J. Am. Chem. Soc.* **2005**, *127*, 5286.
(956) Zhang, Z.; Zhang, J.; Wu, T.; Bu, X.; Feng, P. *J. Am. Chem. Soc.* **2008**, *130*, 15238.
(957) Jing, D.; Guo, L. *J. Phys. Chem. B* **2006**, *110*, 11139.
(958) Domen, K.; Yoshimura, J.; Sekine, T.; Tanaka, A.; Onishi, T. *Catal. Lett.* **1990**, *4*, 339.
(959) Yoshimura, J.; Ebina, Y.; Kondo, J.; Domen, K. *J. Phys. Chem.* **1993**, *97*, 1970.
(960) Miseki, Y.; Kato, H.; Kudo, A. *Chem. Lett.* **2006**, *35*, 1052.
(961) Takahashi, H.; Kakihana, M.; Yamashita, Y.; Yoshida, K.; Ikeda, S.; Hara, M.; Domen, K. *Phys. Chem. Chem. Phys.* **2000**, *2*, 4461.
(962) Hou, W.; Yan, Q.; Fu, X. *J. Chem. Soc., Chem. Commun.* **1994**, *11*, 1371.
(963) Kamat, P. V. *J. Phys. Chem. C* **2007**, *111*, 2834.
(964) Jitputti, J.; Suzuki, Y.; Yoshikawa, S. *Catal. Commun.* **2008**, *9*, 1265.
(965) Liu, H.; Yang, J.; Liang, J.; Huang, Y.; Tang, C. *J. Am. Ceram. Soc.* **2008**, *91*, 1287.
(966) Jitputti, J.; Pavasupree, S.; Suzuki, Y.; Yoshikawa, S. *Jpn. J. Appl. Phys.* **2008**, *47*, 751.
(967) Jiang, Z.; Yang, F.; Luo, N.; Chu, B. T. T.; Sun, D.; Shi, H.; Xiao, T.; Edwards, P. P. *Chem. Commun.* **2008**, *47*, 6372.
(968) Yu, J.; Yu, H.; Chenga, B.; Trapalis, C. *J. Mol. Catal. A: Chem.* **2006**, *249*, 135.
(969) Palmas, S.; Polcaro, A. M.; Ruiz, J. R.; Da Pozzo, A.; Mascia, M.; Vacca, A. *Int. J. Hydrogen Energy* **2010**, *35*, 6561.
(970) Jia, H.; Xiao, W. J.; Zhang, L.; Zheng, Z.; Zhang, H.; Deng, F. *J. Phys. Chem. C* **2008**, *112*, 11379.
(971) Wang, Y.; Zhang, L.; Deng, K.; Chen, X.; Zou, Z. *J. Phys. Chem. C* **2007**, *111*, 2709.
(972) Li, Y.; Hu, Y.; Peng, S.; Lu, G.; Li, S. *J. Phys. Chem. C* **2009**, *113*, 9352.
(973) Li, Y.; Sasaki, T.; Shimizu, Y.; Koshizaki, N. *J. Am. Chem. Soc.* **2008**, *130*, 14755.
(974) Frame, F. A.; Carroll, E. C.; Larsen, D. S.; Sarahan, M.; Browning, N. D.; Osterloh, F. E. *Chem. Commun.* **2008**, *19*, 2206.
(975) Chuangchote, S.; Jitputti, J.; Sagawa, T.; Yoshikawa, S. *ACS Appl. Mater. Interface* **2009**, *1*, 1140.
(976) Mor, G. K.; Prakasam, H. E.; Varghese, O. K.; Shankar, K.; Grimes, C. A. *Nano Lett.* **2007**, *7*, 2356.
(977) Mor, G. K.; Shankar, K.; Paulose, M.; Varghese, O. K.; Grimes, C. A. *Nano Lett.* **2005**, *5*, 191.
(978) Mor, G. K.; Varghese, O. K.; Paulose, M.; Shankar, K.; Grimes, C. A. *Mater. Res. Soc. Symp. Proc.* **2005**, *836*, 29.
(979) Varghese, O. K.; Paulose, M.; Shankar, K.; Mor, G. K.; Grimes, C. A. *J. Nanosci. Nanotechnol.* **2005**, *5*, 1158.
(980) Shankar, K.; Mor, G. K.; Prakasam, H. E.; Yoriya, S.; Paulose, M.; Varghese, O. K.; Grimes, C. A. *Nanotechnology* **2007**, *18*, 065707.
(981) Paulose, M.; Shankar, K.; Yoriya, S.; Prakasam, H. E.; Varghese, O. K.; Mor, G. K.; Latempa, T. A.; Fitzgerald, A.; Grimes, C. A. *J. Phys. Chem. B* **2006**, *110*, 16179.
(982) Mor, G. K.; Varghese, O. K.; Wilke, R. H. T.; Sharma, S.; Shankar, K.; Latempa, T. J.; Choi, K. S.; Grimes, C. A. *Nano Lett.* **2008**, *8*, 1906.
(983) Park, J. H.; Kim, S.; Bard, A. J. *Nano Lett.* **2006**, *6*, 24.
(984) Gong, J. J.; Lai, Y. K.; Lin, C. J. *Electrochim. Acta* **2010**, *55*, 4776.
(985) Cho, I. S.; Lee, S.; Noh, J. H.; Kim, D. W.; Lee, D. K.; Jung, H. S.; Kim, D. W.; Hong, K. S. *J. Mater. Chem.* **2010**, *20*, 3979.
(986) Lv, H.; Ma, L.; Zeng, P.; Ke, D.; Peng, T. *J. Mater. Chem.* **2010**, *20*, 3665.
(987) Wang, X.; Liu, G.; Chen, Z. G.; Li, F.; Lu, G. Q.; Cheng, H. M. *Electrochem. Commun.* **2009**, *11*, 1174.
(988) Kayes, B. M.; Atwater, H. A.; Lewis, N. S. *J. Appl. Phys.* **2005**, *97*, 114302.
(989) Sun, T.; Qiu, J.; Liang, C. *J. Phys. Chem. C* **2008**, *112*, 715.
(990) Wang, W. W.; Zhu, Y. J.; Yang, L. X. *Adv. Funct. Mater.* **2007**, *17*, 59.
(991) Xiong, S.; Xi, B.; Wang, C.; Xi, G.; Liu, X.; Qian, Y. *Chem.—Eur. J.* **2007**, *13*, 7926.
(992) Xu, T. G.; Zhang, C.; Shao, X.; Wu, K.; Zhu, Y. F. *Adv. Funct. Mater.* **2006**, *16*, 1599.
(993) Matsumoto, Y.; Ida, S.; Inoue, T. *J. Phys. Chem. C* **2008**, *112*, 11614.
(994) Carroll, E. C.; Compton, O. C.; Madsen, D.; Osterloh, F. E.; Larsen, D. S. *J. Phys. Chem. C* **2008**, *112*, 2394.
(995) Ye, C.; Bando, Y.; Shen, G.; Golberg, D. *J. Phys. Chem. B* **2006**, *110*, 15146.
(996) Zhang, C.; Zhu, Y. *Chem. Mater.* **2005**, *17*, 3537.
(997) Compton, O. C.; Osterloh, F. E. *J. Phys. Chem. C* **2009**, *113*, 479.
(998) Harada, M.; Sasaki, T.; Ebina, Y.; Watanabe, M. *J. Photochem. Photobiol., A* **2002**, *148*, 273.
(999) Zhang, L.; Chen, D.; Jiao, X. *J. Phys. Chem. B* **2006**, *110*, 2668.
(1000) Zhang, X.; Ai, Z.; Jia, F.; Zhang, L. *J. Phys. Chem. C* **2008**, *112*, 747.
(1001) Sarahan, M. C.; Carroll, E. C.; Allen, M.; Larsen, D. S.; Browning, N. D.; Osterloh, F. E. *J. Solid State Chem.* **2008**, *181*, 1678.
(1002) Xiang, G.; Li, T.; Zhuang, J.; Wang, X. *Chem. Commun.* **2010**, *46*, 6801.
(1003) Jitputti, J.; Rattanavoravipa, T.; Chuangchote, S.; Pavasupree, S.; Suzuki, Y.; Yoshikawa, S. *Catal. Commun.* **2009**, *10*, 378.
(1004) Kim, J. Y.; Osterloh, F. E.; Hiramatsu, H.; Dumas, R. K.; Liu, K. *J. Phys. Chem. B* **2005**, *109*, 11151.
(1005) Kim, J. Y.; Hiramatsu, H.; Osterloh, F. E. *J. Am. Chem. Soc.* **2005**, *127*, 15556.
(1006) Kim, J. Y.; Osterloh, F. E. *J. Am. Chem. Soc.* **2006**, *128*, 3868.
(1007) Compton, O. C.; Mullet, C. H.; Chiang, S.; Osterloh, F. E. *J. Phys. Chem. C* **2008**, *112*, 6202.
(1008) Song, X.; Gao, L. *J. Phys. Chem. C* **2008**, *112*, 15299.
(1009) Lu, F.; Cai, W.; Zhang, Y. *Adv. Funct. Mater.* **2008**, *18*, 1047.
(1010) Kale, B. B.; Baeg, J. O.; Lee, S. M.; Chang, H.; Moon, S. J.; Lee, C. W. *Adv. Funct. Mater.* **2006**, *16*, 1349.
(1011) Yao, W. T.; Yu, S. H.; Liu, S. J.; Chen, J. P.; Liu, X. M.; Li, F. Q. *J. Phys. Chem. B* **2006**, *110*, 11704.
(1012) Zhang, J.; Shi, F.; Lin, J.; Chen, D.; Gao, J.; Huang, Z.; Ding, X.; Tang, C. *Chem. Mater.* **2008**, *20*, 2937.
(1013) Zhou, J. K.; Lv, L.; Yu, J.; Li, H. L.; Guo, P. Z.; Sun, H.; Zhao, X. S. *J. Phys. Chem. C* **2008**, *112*, 5316.
(1014) Koriche, N.; Bouguelia, A.; Aider, A.; Trari, M. *Int. J. Hydrogen Energy* **2005**, *30*, 693.
(1015) Saadi, S.; Bouguelia, A.; Derbal, A.; Trari, M. *J. Photochem. Photobiol., A* **2007**, *187*, 97.
(1016) Boudjemaa, A.; Bouarab, R.; Saadi, S.; Bouguelia, A.; Trari, M. *Appl. Energy* **2009**, *86*, 1080.
(1017) Hirai, T.; Nomura, Y.; Komasawa, I. *J. Nanopart. Res.* **2003**, *5*, 61.
(1018) Saadi, S.; Bouguelia, A.; Trari, M. *Renewable Energy* **2006**, *31*, 2245.
(1019) Trari, M.; Bouguelia, A.; Bessekhouad, Y. *Sol. Energy Mater. Sol. Cells* **2006**, *90*, 190.
(1020) Younsi, M.; Saadi, S.; Bouguelia, A.; Aider, A.; Trari, M. *Sol. Energy Mater. Sol. Cells* **2007**, *91*, 1102.
(1021) Bessekhouad, Y.; Trari, M. *Int. J. Hydrogen Energy* **2002**, *27*, 357.
(1022) Inue, T.; Watanabe, T.; Fujishima, A.; Honda, K.; Kohayakawa, K. *J. Electrochem. Soc.* **1977**, *124*, 719.
(1023) Shen, S.; Guo, L.; Chen, X.; Ren, F.; Mao, S. S. *Int. J. Hydrogen Energy* **2010**, *35*, 7110.
(1024) Koriche, N.; Bouguelia, A.; Trari, M. *Int. J. Hydrogen Energy* **2006**, *31*, 1196.
(1025) Zhang, X.; Jing, D.; Guo, L. *Int. J. Hydrogen Energy* **2010**, *35*, 7051.
(1026) Zhang, K.; Jing, D.; Chen, Q.; Guo, L. *Int. J. Hydrogen Energy* **2010**, *35*, 2048.
(1027) Liu, H.; Zhang, K.; Jing, D.; Liu, G.; Guo, L. *Int. J. Hydrogen Energy* **2010**, *35*, 7080.
(1028) Younsi, M.; Aider, A.; Bouguelia, A.; Trari, M. *Sol. Energy* **2005**, *78*, 574.
(1029) Boumaza, S.; Bouarab, R.; Trari, M.; Bouguelia, A. *Energy Convers. Manage.* **2009**, *50*, 62.
(1030) Boumaza, S.; Bouguelia, A.; Bouarab, R.; Trari, M. *Int. J. Hydrogen Energy* **2009**, *34*, 4963.
(1031) Lu, G.; Li, S. *Int. J. Hydrogen Energy* **1992**, *17*, 767.
(1032) Gurunathan, K.; Baeg, J. O.; Lee, S. M.; Subramanian, E.; Moon, S. J.; Kong, K. J. *Int. J. Hydrogen Energy* **2008**, *33*, 2646.
(1033) Li, S. B.; Lu, G. X. *New J. Chem.* **1992**, *16*, 517.
(1034) Gurunathan, K.; Baeg, J. O.; Lee, S. M.; Subramanian, E.; Moon, S. J.; Kong, K. *Catal. Commun.* **2008**, *9*, 395.
(1035) Subramanian, E.; Baeg, J. O.; Lee, S. M.; Moon, S. J.; Kong, K. *Int. J. Hydrogen Energy* **2008**, *33*, 6586.
(1036) Barbeni, M.; Pelizzetti, E.; Borgarello, E.; Serpone, N.; Grätzel, M.; Balducci, L. *Int. J. Hydrogen Energy* **1985**, *10*, 249.
(1037) Buhler, N.; Meier, K.; Reber, J. P. *J. Phys. Chem.* **1984**, *88*, 3261.
(1038) De, G. C.; Roy, A. M.; Bhattacharya, S. S. *Int. J. Hydrogen Energy* **1995**, *20*, 127.
(1039) Naman, S. A.; Aliwi, S. M.; Al-emara, K. *Int. J. Hydrogen Energy* **1986**, *11*, 33.
(1040) Muradov, N. Z.; Rustamov, M. I.; Guseinova, A. D.; Bazhutin, Y. V. *React. Kinet. Catal. Lett.* **1987**, *33*, 279.
(1041) Linkous, C. A.; Muradov, N. Z.; Ramser, S. N. *Int. J. Hydrogen Energy* **1995**, *20*, 701.
(1042) Etiope, G.; Papatheodorou, G.; Christodoulou, D.; Favali, P.; Ferentinos, G. *TAO* **2005**, *16*, 897.
(1043) Tambwekar, S. V.; Subrahmanyam, M. *Int. J. Hydrogen Energy* **1997**, *22*, 959.

(1044) Grzyll, C. R.; Thomas, J. J.; Barile, R. G. *Int. J. Hydrogen Energy* **1989**, *14*, 647.
(1045) Ma, G.; Yan, H.; Zong, X.; Ma, B.; Jiang, H.; Wen, F.; Li, C. *Chin. J. Catal.* **2008**, *29*, 313.
(1046) Kato, H.; Hori, M.; Konta, R.; Shimodaira, Y.; Kudo, A. *Chem. Lett.* **2004**, *33*, 1348.
(1047) Bae, S. W.; Ji, S. M.; Hong, S. J.; Jang, J. W.; Lee, J. S. *Int. J. Hydrogen Energy* **2009**, *34*, 3243.
(1048) Kozlova, E. A.; Korobkina, T. P.; Vorontsov, A. V. *Int. J. Hydrogen Energy* **2009**, *34*, 138.
(1049) Kozlova, E. A.; Korobkina, T. P.; Vorontsov, A. V.; Parmon, V. N. *Appl. Catal., A* **2009**, *367*, 130.
(1050) Lee, K.; Nam, W. S.; Han, G. Y. *Int. J. Hydrogen Energy* **2004**, *29*, 1343.
(1051) Fujihara, K.; Ohno, T.; Matsumura, M. *J. Chem. Soc., Faraday Trans.* **1998**, *94*, 3705.
(1052) Lee, S. G.; Lee, S.; Lee, H. I. *Appl. Catal., A* **2001**, *207*, 173.
(1053) Ohno, T.; Tanigawa, F.; Fujihara, K.; Izumi, S.; Matsumura, M. *J. Photochem. Photobiol., A* **1998**, *118*, 41.
(1054) Galińska, A.; Walendziewski, J. *Energy Fuels* **2005**, *19*, 1143.
(1055) Bamwenda, G. R.; Tsubota, S.; Nakamura, T.; Haruta, M. P. *J. Photochem. Photobiol., A* **1995**, *89*, 177.
(1056) Li, Y. X.; Lu, G. X.; Li, S. B. *Chemosphere* **2003**, *52*, 843.
(1057) Wu, N. L.; Lee, M. S. *Int. J. Hydrogen Energy* **2004**, *29*, 1601.
(1058) Yi, H.; Peng, T.; Ke, D.; Ke, D.; Zan, L.; Yan, C. *Int. J. Hydrogen Energy* **2008**, *33*, 672.
(1059) Strataki, N.; Bekiari, V.; Kondarides, D. I.; Lianos, P. *Appl. Catal., B* **2007**, *77*, 184.
(1060) Daskalaki, V. M.; Kondarides, D. I. *Catal. Today* **2009**, *144*, 75.
(1061) Ohtani, B.; Kakimoto, M.; Nishimoto, S.; Kagiya, T. *J. Photochem. Photobiol., A* **1993**, *70*, 265.
(1062) Zhang, Y. J.; Zhang, L. *Desalination* **2009**, *249*, 1017.
(1063) Chen, T.; Wu, G.; Feng, Z.; Hu, G.; Su, W.; Ying, P.; Li, C. *Chin. J. Catal.* **2008**, *29*, 105.
(1064) Zheng, X.; Wei, L.; Zhang, Z.; Jiang, Q.; Wei, Y.; Xie, B.; Wei, M. *Int. J. Hydrogen Energy* **2009**, *34*, 9033.
(1065) Jia, L.; Li, J.; Fang, W. *J. Alloys Compd.* **2010**, *489*, L13.
(1066) Patsoura, A.; Kondarides, D. I.; Verykios, X. E. *Catal. Today* **2007**, *124*, 94.
(1067) Chiarello, G. L.; Forni, L.; Selli, E. *Catal. Today* **2009**, *144*, 69.
(1068) Chen, T.; Wu, G.; Feng, Z.; Hu, G.; Su, W.; Ying, P.; Li, C. *Chin. J. Catal.* **2008**, *29*, 105.
(1069) Kawai, T.; Sakata, T. *J. C. S. Chem. Commun.* **1980**, *15*, 694.
(1070) Hashimoto, K.; Kawai, T.; Sakata, T. *J. Phys. Chem.* **1984**, *88*, 4083.
(1071) Patsoura, A.; Kondarides, D. I.; Verykios, X. E. *Appl. Catal., B* **2006**, *64*, 171.
(1072) Li, Y.; Lu, G.; Li, S. *Appl. Catal., A* **2001**, *214*, 179.
(1073) Li, Y.; Xie, Y.; Peng, S.; Lu, G.; Li, S. *Chemosphere* **2006**, *63*, 1312.
(1074) Wu, Y. Q.; Lu, G. X.; Li, S. B. *Acta Phys. Chim. Sin.* **2004**, *20*, 755.
(1075) Kakuta, S.; Abe, T. *ACS Appl. Mater. Interface* **2009**, *1*, 2707.
(1076) Oosawa, Y. *J. Chem. Soc., Chem. Commun.* **1982**, *4*, 221.
(1077) Kim, Y. I.; Keller, S. W.; Krueger, J. S.; Yonemoto, E. H.; Saupe, G. B.; Mallouk, T. E. *J. Phys. Chem. B* **1997**, *101*, 2491.
(1078) Muradov, N. Z.; Bazhutin, Y. V.; Bezuglaya, A. G.; Izakovich, E. N.; Rustamov, M. I. *React. Kinet. Catal. Lett.* **1981**, *17*, 355.
(1079) Yang, H.; Yan, J.; Lu, Z.; Cheng, X.; Tang, Y. *J. Alloys Compd.* **2009**, *476*, 715.
(1080) Yan, J.; Yang, H.; Tang, Y.; Lu, Z.; Zheng, S.; Yao, M.; Han, Y. *Renewable Energy* **2009**, *34*, 2399.
(1081) Sobczynski, A.; Yildiz, A.; Bard, A. J.; Campion, A.; Fox, M. A.; Mallouk, T.; Webber, S. E.; White, J. M. *J. Phys. Chem.* **1988**, *92*, 2311.
(1082) Zhang, X.; Liu, H.; Li, W.; Cui, G.; Xu, H.; Han, K.; Long, Q. *Catal. Lett.* **2008**, *125*, 371.
(1083) Kawai, T.; Sakata, T. *Chem. Lett.* **1981**, *10*, 81.
(1084) Kawai, T.; Sakata, T. *Nature* **1980**, *286*, 474.
(1085) Fu, X.; Long, J.; Wang, X.; Leung, D. Y. C.; Ding, Z.; Wu, L.; Zhang, Z.; Li, Z.; Fu, X. *Int. J. Hydrogen Energy* **2008**, *33*, 6484.
(1086) Li, Y. X.; Xie, Y. Z.; Peng, S. Q. *Chem. J. Chin. Univ.* **2007**, *28*, 156.
(1087) Li, Y.; Wang, J.; Peng, S.; Lu, G.; Li, S. *Int. J. Hydrogen Energy* **2010**, *35*, 7116.
(1088) Enea, O. *Electrochim. Acta* **1986**, *31*, 405.
(1089) John, M. R. St.; Furgala, A. J.; Sammells, A. F. *J. Phys. Chem.* **1983**, *87*, 801.
(1090) Takata, T.; Tanaka, A.; Hara, M.; Kondo, J. N.; Domen, K. *Catal. Today* **1998**, *44*, 17.
(1091) Sayama, K.; Yoshida, R.; Kusama, H.; Okabe, K.; Abe, Y.; Arakawa, H. *Chem. Phys. Lett.* **1997**, *277*, 387.
(1092) Gratian, R.; Sayama, K.; Arakawa, H. *J. Photochem. Photobiol., A* **1999**, *122*, 175.
(1093) Abe, R.; Sayama, K.; Domen, K.; Arakawa, H. *Chem. Phys. Lett.* **2001**, *344*, 339.
(1094) Higashi, M.; Abe, R.; Takata, T.; Domen, K. *Chem. Mater.* **2009**, *21*, 1543.
(1095) Sayama, K.; Mukasa, K.; Abe, R.; Abe, Y.; Arakawa, H. *J. Photochem. Photobiol., A* **2002**, *148*, 71.
(1096) Abe, R.; Sayama, K.; Sugihara, H. *J. Phys. Chem. B* **2005**, *109*, 16052.
(1097) Maeda, K.; Higashi, M.; Lu, D.; Abe, R.; Domen, K. *J. Am. Chem. Soc.* **2010**, *132*, 5858.
(1098) Higashi, M.; Abe, R.; Ishikawa, A.; Takata, T.; Ohtani, B.; Domen, K. *Chem. Lett.* **2008**, *37*, 138.
(1099) Tabata, M.; Maeda, K.; Higashi, M.; Lu, D.; Takata, T.; Abe, R.; Domen, K. *Langmuir* **2010**, *26*, 9161.
(1100) Abe, R.; Shinmei, K.; Hara, K.; Ohtani, B. *Chem. Commun.* **2009**, *24*, 3577.
(1101) Sasaki, Y.; Nemoto, H.; Saito, K.; Kudo, A. *J. Phys. Chem. C* **2009**, *113*, 17536.
(1102) Feng, X.; Mao, W.; Yan, W. *Int. J. Hydrogen Energy* **2008**, *33*, 3644.
(1103) Domen, K.; Ebina, Y.; Sekine, T.; Tanaka, A.; Kondo, J.; Hirose, C. *Catal. Today* **1993**, *16*, 479.
(1104) Jin, Z. L.; Lu, G. X. *Energy Fuels* **2005**, *19*, 1126.
(1105) Ji, S. M.; Jun, H.; Jang, J. S.; Son, H. C.; Borse, P. H.; Lee, J. S. *J. Photochem. Photobiol., A* **2007**, *189*, 141.
(1106) Jing, D.; Liu, H.; Zhang, X.; Zhao, L.; Guo, L. *Energy Convers. Manage.* **2009**, *50*, 2919.
(1107) Jing, D.; Guo, L.; Zhao, L.; Zhang, X.; Liu, H.; Li, M.; Shen, S.; Liu, G.; Hu, X.; Zhang, X.; Zhang, K.; Ma, L.; Guo, P. *Int. J. Hydrogen Energy* **2010**, *35*, 7087.

CR1001645